QUANTIFICATION AND MOLECULAR CHARACTERIZATION OF ORGANO-MINERAL ASSOCIATIONS AS INFLUENCED BY REDOX OSCILLATIONS: RELEVANCE IN CARBON CYCLING AND STABILIZATION

by

Mohammad Zafar Afsar

A dissertation submitted to the Faculty of the University of Delaware in partial fulfillment of the requirements for the degree of Doctor of Philosophy in Plant and Soil Sciences

Summer 2020

QUANTIFICATION AND MOLECULAR CHARACTERIZATION OF ORGANO-MINERAL ASSOCIATIONS AS INFLUENCED BY REDOX OSCILLATIONS: RELEVANCE IN CARBON CYCLING AND STABILIZATION

by

Mohammad Zafar Afsar

Approved: _____
Eric Ervin, Ph.D.
Chair of the Department of Plant and Soil Sciences

Approved: _____
Mark Rieger, Ph.D.
Dean of the College of Agriculture and Natural Resources

Approved: _____
Douglas J. Doren, Ph.D.
Interim Vice Provost for Graduate and Professional Education and
Dean of the Graduate College

I certify that I have read this dissertation and that in my opinion it meets the academic and professional standard required by the University as a dissertation for the degree of Doctor of Philosophy.

Signed: _____

Yan Jin, Ph.D.
Professor in charge of dissertation

I certify that I have read this dissertation and that in my opinion it meets the academic and professional standard required by the University as a dissertation for the degree of Doctor of Philosophy.

Signed: _____

Bruce Vasilas, Ph.D.
Member of dissertation committee

I certify that I have read this dissertation and that in my opinion it meets the academic and professional standard required by the University as a dissertation for the degree of Doctor of Philosophy.

Signed: _____

Deb Jaisi, Ph.D.
Member of dissertation committee

I certify that I have read this dissertation and that in my opinion it meets the academic and professional standard required by the University as a dissertation for the degree of Doctor of Philosophy.

Signed: _____

Yu-Ping Chin, Ph.D.
Member of dissertation committee

ACKNOWLEDGMENTS

It is a great honor and pleasure to thank all of them without whom it would never be possible for me to accomplish the most challenging part of my life. First and foremost, I would like to thank the Almighty Allah whose blessings enabled me to complete this dissertation successfully. Countless salutations be upon the Holy Prophet MUHAMMAD (Salala-ho-alaihe Wa Sallam) who ordained us to yearn for knowledge from cradle to grave.

Very special thanks go to my advisor, Dr. Yan Jin for her never-ending support and insightful discussions during my whole Ph.D. program. As a great mentor, Dr. Jin always insists me to "think outside of the box" and take steps beyond my comfort zone. She provided conscientious guidance to take challenges to foster my professional skills and developments. I, personally, feel very relieve by talking to her whenever I face any frustrating and stressful situations not only in my academic activities but also in my social life. Her "open-door mentality" helped me a lot to solve any issues instantaneously. I am so lucky to be a part of her research team.

I would like to acknowledge my indebtedness and gratitude to the rest of my dissertation committee members: Dr. Bruce Vasilas, Dr. Deb Jaisi, and Dr. Yu-Ping Chin for their encouragement, thoughtful comments, and valuable insights to opt and complete this dissertation. A very special thanks for supporting me at different stages of my research works- from hands on training on field sampling to give permission and training on their own instruments. I really appreciate for the free access to the isotope ratio mass spectrometry and TOC analyzer.

My sincere thanks also go to Gerald Poirier, Director of the Advanced material Characterization lab, Karren Gartley from the Soil Testing Lab, Dr. Christopher Goodwin from the Surface Analytical Facility for their technical supports. My special thanks also go to the Delaware Environmental Institute (DENIN) and its Director Dr. Donald Sparks for awarding me financial support for two years as their environmental fellow and to the UD graduate office for awarding me the dissertation fellowship for another one year.

I thank all my fellow current and former lab mates in the Environmental Soil Physics Lab: Dr. Taozhu Sun, Dr. Jing Yan, Dr. Dengjun Wang, Dr. Volha Lazouskaya, Dr. Wenjuan Zheng, Saiqi Zeng, Shane Franklin, Fatema Kaniz, and Anna Jurusik for not only their professional skills and knowledge as scientists but also their understanding and consideration as friends.

I would like to thank my parents, Late Mohammad Zaker Hossain and Late Mosammad Rashida Hossain for their true inspiration and blessings to me. They always inspired me to dream big. I would also like to express my gratitude to my parents-in-law Md. Anwar Hussain Miazi and Puspa Begum for their spiritual support. To my elder brothers Dipu, Apu, Tipu, Mawla, and Mohiuddin and sisters Akhi, Tulee, and Moni, who always show support for me and believed in what I do, thank you for your care. I am so proud to have siblings like you. Today, I would also like to remember my lovely nephew/nieces: Shaima, Siyaam, and Zaisha.

Last but not the least, to my better-half Rifat Sultana and dearest son Rishad Afsar, for their dedication, love, and support. Without their support and encouragement, it could never be possible for me. Thank you for your comfort and standing through the years by my side. I am so proud of you.

TABLE OF CONTENTS

LIST OF TABLES x
LIST OF FIGURES xi
ABSTRACT xviii

Chapter

1 INTRODUCTION 1

1.1 Explanation of Problem 1
1.2 Soil Organic Matter: The Largest Organic C Pool on the Earth's Surface 3
1.3 Colloids- The Complex Mixture of Organic and Inorganic Entities 4
1.4 Factors Affective Mobilization of Colloids and Associated OC 6
1.5 Organo-Mineral Associations: Formation, Properties, and Significance in Terrestrial Environment 8
1.6 Persistence of SOM in the Natural Environment 9
1.7 Effect of Redox Oscillations on the Dynamics of Colloids and Associated OC 11
1.8 Broader Impacts 14

2 QUANTIFICATION AND MOLECULAR CHARACTERIZATION OF ORGANO-MINERAL ASSOCIATIONS AS INFLUENCED by REDOX OSCILLATIONS 16

2.1 Introduction 18
2.2 Materials and Methods 22

2.2.1 Study Site and Soil Sampling 22
2.2.2 Redox Oscillation Experiment 23
2.2.3 Sample Collection 24
2.2.4 IRMS Analyses 25
2.2.5 XPS Analyses 26
2.2.1 Statistics 27

2.3 Results and Discussion 28

2.3.1 Changes in Soil Solution Chemistry 28
2.3.2 Distribution of C and N in Size-fractionated Particles 30
2.3.3 Stable Isotopic ($\delta^{13}C$, $\delta^{15}N$) Signatures 34
2.3.4 Linking Surficial Elemental Composition of Soil Minerals to Associated Organic C and N 40
2.3.5 Speciation of Organic C and Selective Sorption on Mineral Surfaces 45
2.3.6 Size-Dependent Mineral-OC Interactions 48
2.3.7 Layer Thickness of Surficial OM 50
2.3.8 Relationship between Surface and Bulk C 53

2.4 Conclusions 54

3 REDOX OSCILLATIONS ENHANCE DESTABILIZATION AND MOBILIZATION OF PROTECTED COLLOIDAL SOIL ORGANIC CARBON 56

3.1 Introduction 58
3.2 Materials and Methods 61

3.2.1 Soil Description 61
3.2.2 Preparation of Soil Column 62
3.2.3 Redox Oscillation Experiment 63
3.2.4 Sample Analyses 66

3.2.4.1 Chemical Analyses 66
3.2.4.2 Spectrofluorometric Analyses 67
3.2.4.3 Isotope Ratio Mass Spectrometry (IRMS) Analyses 71

3.2.5 Statistics 71

3.3 RESULTS 71

3.3.1 Changes in Solution Chemistry 71
3.3.2 Mobilization of Colloids and OC 72
3.3.3 Changes in OC Properties 76

3.3.3.1 Optical and Fluorescence Properties 76
3.3.3.2 Isotope Signature 79

3.4 DISCUSSION 82

3.4.1 Dynamic Response of Soil Colloids to Redox Oscillations 82
3.4.2 Dynamic response of soil OC to redox oscillations 84

3.4.3 Mineral-SOM interactions as a function of redox oscillations.... 87
3.4.4 Stability of mineral-SOM complexes 89

3.5 CONCLUSIONS 91

4 COLLOIDAL ORGANIC CARBON HAS A KEY BUT ACCOUNTED ROLE IN CARBON DYNAMICS IN A DEPRESSIONAL WETLAND 92

4.1 Introduction 93
4.2 Materials and Methods 96

4.2.1 Field Site Selection, Monitoring, and Sample Collection 96

4.2.1.1 Site Description 96
4.2.1.2 Monitoring Well Installation 97
4.2.1.3 Piezometer Installation and Water Sample Collection 100

4.2.2 Sample Preparation and Analyses 101

4.2.2.1 Sample Size Fractionation 101
4.2.2.2 Sample Analyses 102

4.3 Results 104

4.3.1 Changes in Water-table 104
4.3.2 Pore Water Chemistry 106
4.3.1 Concentration of Soil Colloids in Pore Water 107
4.3.2 Size-fractionated SOC Concentrations in Pore Water..... 110
4.3.3 Surface and Bulk Molecular Composition of Size-fractionated Colloids and Associated COC 116

4.1 Discussion..... 120

4.1.1 Release of Soil Colloids and Associated OC 120
4.1.2 Significance of NNP and Fine Colloids 125
4.1.3 Size-fractionated OC Concentration and Formation of Organo-mineral complexes..... 126

4.2 Conclusion..... 129

5 EFFECT OF METAL:CARBON RATIOS ON THE MOBILITY OF ORGANIC CARBON IN A DEPRESSIONAL WETLAND..... 130

5.1 Introduction 132
5.2 Materials and Methods 134

5.2.1 Study Site Description 134
5.2.2 Monitoring Well and Piezometer Installation 135
5.2.3 Sample Preparation and Analyses 135
5.2.4 Calculation of the Concentration and Partition Coefficient of Different Elements 137
5.2.5 Distribution of Elements in the Dissolved, NNP, Fine Colloid, and Particulate Fractions 138
5.2.6 Ratios of Metals (Al, Fe) to OC and mobilization of Size-fractionated Organo-mineral Complexes 144

6 CONCLUSIONS 147

6.1 Summary of Research 147
6.2 Future Research 149

REFERENCES 151

Appendix

A LIST OF SYMBOLS AND ABBREVIATIONS 177
B CALCULATION OF CENTRIFUGATION TIME AND SPEED FOR DIFFERENTIAL CENTRIFUGATION 178
C DETERMINATION OF LAYER THICKNESS 179
D REPRINT PERMISSION LETTER 180

LIST OF TABLES

Table 2.1: Selected properties and general chemical composition of the soil sample 22

Table 2.2: Changes in C and particle concentration in different size factions along the redox oscillations 36

Table 2.3: Changes in stable C and N isotope signatures ($\delta^{13}C$, $\delta^{15}N$) in size-fractionated samples along the redox oscillations 37

Table 2.4: Two-way ANOVA test for isotope effects 37

Table 2.5: Two-way ANOVA test for variation in surface enrichment factor ($C_{surface}/C_{bulk}$) as a function of particle sizes and redox oscillations 54

Table 3.1: Optical and fluorescence indices used to characterize organic matter (OM) in this study. 70

Table 3.2: Redox potential changes along the soil columns. 72

Table 3.3: Organic C concentration (mg L^{-1}) in size-fractionated samples. 76

Table 4.1: Characteristics of soil profile in wetland, transition, and upland zones in the depressional wetland. 99

Table 4.2: Relative percentages of OC in the NNP, fine colloid, and particulate size fractions of samples collected on Feb. 2018 measured by using IRMS. 115

Table 4.3: Correlation (Pearson) between size-fractionated TOC concentration (ppm) and pH, pE, IS, soluble Fe^{2+} concentration of pore water samples (N = 42) 124

LIST OF FIGURES

Figure 1.1: (a) Processes affecting the dynamics of SOC. The blue upward arrows indicate the emission of CO_2 into the atmosphere (Lal, 2004), (b) Important factors controlling the main input and output of soil C (Davidson and Janssens, 2006)..... 2

Figure 1.2: Size distribution of particulate organic matter (POM) and dissolved organic matter (DOM). The size limit used to differentiate DOM from POM is operationally set to around 450 nm (Adopted from Docter et al., 2015)..... 4

Figure 1.3: Colloid and OC concentrations across different ecosystems, e.g., estuary, agriculture, forest stream, and wetland (Reprinted from Yan et al., 2018). 6

Figure 1.4: The role of DOM in the formation of organo-mineral associations. Figure reprinted from Markus Kleber et al. (2015), which was prepared based on the "partitioning model" of Hedges and Keil (1999). 9

Figure 1.5: Schematic representation of two potential preservation mechanisms (Adopted from Hemingway et al., 2019)..... 11

Figure 1.6: Effects of redox oscillations on the dynamics of colloids and associated OC (partially adopted from Kaiser and Kalbitz, 2012). 12

Figure 2.1**:** Schematic diagram of the batch incubation study. (a) Preparation of soil suspension using 2 mM NaCl electrolyte solution; (b) one complete redox oscillation consisted of 30 d reducing half-cycle (RHC) followed by 5 d oxidizing half-cycle (OHC) (a total of 3 complete redox oscillation cycles were carried out in this study); and (c) particle size fractionation using differential centrifugation processes. 24

Figure 2.2: A representative XPS survey spectrum with all elements. The spectrum was corrected to the aliphatic or aromatic C (C-C, C=C, C-H) at 284.6 eV. 29

Figure 2.3: High-resolution XPS C_{1s} spectrum (broken line) of Mineral-SOM complexes and the de-convoluted sub-peaks (solid lines) as assigned to different C components. 29

Figure 2.4: Changes in pH and pE along the redox oscillations. Both pH and PE measured (1) at time zero (0-day), (2) after 1st RHC (after 30-day), (3) after 1st RHC + OHC (after 35-day), (4) after 2nd RHC (after 65-day), (5) after 2nd RHC + OHC (after 70-day), (6) after 3rd RHC (after 100-day), and (7) after 3rd RHC + OHC (after 105-day). The error bar indicates standard deviation. 30

Figure 2.5: Changes in bulk (a) C ($[C]_{particle}$, g kg^{-1} size-fractionated particles) and (b) N concentrations ($[N]_{particle}$, g kg^{-1} size-fractionated particles) as a function of redox oscillations measured by IRMS equipped with EA. (c) Regression plot between C and N concentrations within 2.3-1000 nm size range. The error bars show standard deviations among replicates. 32

Figure 2.6: (a) Total mass of size-fractionated particles ($[M]_{particle}$, mg); (b) particle concentrations ($[particle]_{soil}$, g kg^{-1} soil); (c) total mass of C (M_C, mg); and (d) C concentrations ($[C]_{soil}$, mg kg^{-1} soil). Concentrations are calculated based on the oven-dry weight of soil suspension. The error bars indicate standard deviations among replicates. 33

Figure 2.7: Variation in isotope values of (a) C ($\delta^{13}C$, ‰) and (b) N ($\delta^{15}N$, ‰) in size-fractionated particles as a function of redox oscillations. The error bars represent standard deviations in stable isotope values among replicates. 35

Figure 2.8: (a) Isotope values of C ($\delta^{13}C$) vs N ($\delta^{15}N$) of size-fractionated colloid particles; (b) relationship between isotopes and concentration of C. 38

Figure 2.9: Variation in the atomic % of surficial (a) Al; (b) Si; (c) Fe; (d) C; and (e) N as a function of redox oscillations determined by XPS. 42

Figure 2.10: Regression plots of XPS-based surficial atomic % of Al, Fe, Si, Mg, and N with C atom %. Except Fe, all the relationships are significant at $p < 0.01$ level. Relationship between atom % of Fe and C was significant at $p < 0.05$. 43

Figure 2.11: High-resolution XPS N 1s spectra of mineral-SOM complexes and de-convoluted sub-peaks as assigned to different N components, (a) <2.3 nm and (b) 2.3-100 nm. 44

Figure 2.12: Regression plots of total mass of C (M_C, mg) with total mass of colloids ($M_{colloid}$, mg) at (a) 2.3-100 nm; (b) 100-450 nm; and (c) 450-100 nm size fractions. 44

Figure 2.13: Surface (a) Mg/Al and (b) Al/Si ratios as obtained from XPS analyses. 45

Figure 2.14: Different C functional groups as de-convoluted from C_{1s} XPS spectra. (a) aliphatic or aromatic C (C-C, C-H); (b) amines and/or alcohols like those in polysaccharides and amino acids (C-O, C-N); and (c) carbonyl/carboxyl C (C=O), each expressed by relative atom percent of the total C signal in size-fractionated samples (2.3-100 nm, 100-450 nm, and 450-1000 nm) as a function of redox oscillations. 47

Figure 2.15: Ratios of atomic % of different C functional groups in size-fractionated particles plotted by redox oscillations. The error bars represent standard deviations among replicates. 48

Figure 2.16: (a) Regression plots between the layer thickness (t, nm) of the SOM coatings on the mineral surfaces and the surface C (atom %) content in different size fractions measured by XPS; (b) relationship between surface C concentration ($C_{surface}$) measured by XPS and bulk C concentration (C_{bulk}) measured by IRMS; (c) variation in C surface enrichment factor ($C_{surface}/C_{bulk}$) in different size fractions as a function of redox oscillations. 52

Figure 3.1: Schematic diagram of the soil column. (a) Nylon mesh and porous plastic disk (pore size: ~ 2.0 mm in diameter), (b) three-way bulb and (c_1, c_2) peristaltic pumps. Tube A was dipped in DI water to remove excess air while 2.0 mM NaCl electrolyte solution was injected into the column using pump c_1 in up-flow mode. Tube B was used to flush the column with N_2 or O_2 gas. Column leachate samples were collected inside the anoxic glove bag using pump c_2. 63

Figure 3.2: The fitted EEMs data using the 13-component parallel factor (PARAFAC) model developed by Cory and McKnight (2005). 69

Figure 3.3: Changes in (a) pH, (b) pE (Eh), (c) IS (EC), (d) Fe^{2+} concentration (mM), and (e) colloid concentration ([colloid], mg L^{-1}) in leachate samples collected from oxic (control) soil column and after 1st and 2nd reducing half-cycle (RHC). Initial high colloid release at 0.1 pore volume (V/V_0) from oxic (control) column was shown separately using "▲" sign. The error bars represent the standard deviations among different PVs of samples collected from duplicate soil columns. Fe^{2+} concentration was below LOQ in leachates collected from oxic (control) columns. 73

Figure 3.4: Mean C concentration for bulk, >450 nm, 220-450 nm, 100-220 nm, 2.3-100 nm, and <2.3 nm size fractions in (a) oxic (control) column, (b) after 1st RHC, (c) after 2nd RHC, (d) after continuous oxic condition for 1 complete oscillation period, (e) after continuous anoxic condition for 1 complete oscillation period, (f) after continuous oxic condition for 2 complete oscillation period, and (g) after continuous oxic condition for 2 complete oscillation period. The left y-axis represents C concentration in mg L^{-1} and the right y-axis represents C concentration in relative percentages. The error bars represent the standard deviations in leachate C concentration at different PVs of samples collected from duplicate soil columns..... 75

Figure 3.5: Changes in specific UV absorbance ($SUVA_{254}$, L mgC^{-1} m^{-1}) and % aromatic C content in leachate samples collected from soil columns subjected to (a) oxic column (control), (b) after 1st reducing half-cycle, and (c) after 2nd reducing half-cycle at 0.18, 0.55 and 1.09 PV (V/V_0). Fig. (d) shows the changes in SUVA and % aromaticity for < 450 nm, < 220 nm, < 100 nm, and < 2.3 nm. 78

Figure 3.6: Changes in the fluorescence indices of the OC present in the column leachate samples. These indices include (a) humification index (HIX), (b) biological index (BIX) and (c) fluorescence index (FI), Cory and McKnight (2005) model components: (d) % C3, (e) % C5 and (f) % protein-like fluorescence. The error bars represent the standard deviations among different PVs of samples collected from duplicate soil columns. 79

Figure 3.7: Distribution of stable (a) C ($\delta^{13}C$, ‰) and (b) N ($\delta^{15}N$, ‰) isotopes in different size-fractionated samples collected after 1st and 2nd RHC. The error bars represent the standard deviations in stable isotope values among different pore volumes as collected from duplicate soil columns. 81

Figure 3.8: Correlation between colloid concentration [colloid] and pH of the column leachate samples. 83

Figure 3.9: Correlation between C concentration (mgL^{-1}) in size-fractionated samples and solution pH. Pearson's r values significant at $p < 0.01$ and $p < 0.001$ are denoted as ** and *** respectively. 85

Figure 4.1: (a) Sampling site located in the Blackbird state forest, (b, c) schematic diagram showing three hydrological zones and a cross-section of the wetland instrumented with piezometers at different zones. Letter A, B and C indicates three piezometers installed at 50 cm, 100, cm and 200 cm at the wetland, transition, and upland zones. 98

Figure 4.2: Schematic diagram of the monitoring wells and piezometers installed in the wetland, transition, and upland zones. 100

Figure 4.3: Seasonal dynamics of (a) daily average water table depth (cm) and (b) daily cumulative precipitation (cm) events for the hydrologic period between 2017 to 2019. Horizontal straight line indicates soil surface and vertical red dashed lines indicate sampling time. 105

Figure 4.4: Changes in (a) pH, (b) pE, (c) IS and (d) Fe^{2+} concentration (µM) in pore water samples along the redox gradients from upland to wetland zones and at different soil depths. 107

Figure 4.5: Distribution of Eh-pH values measured in pore water samples. Specific Eh/pH lines for oxygen and iron were drawn with the Eh values at pH 7 of + 0.35 V and + 0.12 V, respectively, adjusted with a slope of negative 60 for each pH value less than 7 (Hurt, 2013). The threshold limit for anaerobic condition was drawn as Eh = 595 – (60 x pH) (Vasilas and Vasilas, 2013). 108

Figure 4.6: Colloid concentration in NNP, fine colloid, and particulate fractions. There was no water in the piezometer at 50 cm depth in upland during Feb 21 and Nov 20, 2018 as the water table was below that level (indicated by "¶"). On Feb 02, 2019, the riser of piezometer installed at 200 cm depth was below the standing water in wetland (indicated by "*"). Very negligible amount of size-fractionated colloids was present at 200 cm depth in transition zone on Feb 05, 2019. 109

Figure 4.7: Linear relationship between size-fractionated colloid concentration to the total colloid concentration within 2.3-1000 nm range. 110

Figure 4.8: Organic C concentration in the dissolved, NNP, fine colloids, and particulate factions in pore water samples collected between Feb 21, 2018 to May 02, 2019 from wetland, transition and upland. There was no water in the piezometer at 50 cm depth in upland during Feb 21 and Nov 20, 2018 as the water table was below that level (indicated by "¶"). On Feb 02, 2019, the riser of piezometer installed at 200 cm depth was below the standing water in wetland (indicated by "*"). 112

Figure 4.9: Linear regression analyses between size fractionated OC (dissolved, NNP, fine colloid, and particulate) and total OC ($TOC_{<1000}$). Level of significance: * $p < 0.05$, ** $p < 0.01$, *** $p < 0.001$. No asterisk indicates not significant. 113

Figure 4.10: Relationship between operationally defined dissolved OC (<450 nm, $DOC_{<450}$) and total OC (<1000 nm, $TOC_{<1000}$)..... 114

Figure 4.11: Bulk C concentration (C_{bulk})of the size-fractionated COC measured by using IRMS..... 115

Figure 4.12: Surface atom percentages of different elements in size fractionated organo-mineral complexes as measured by XPS. Level of significance: * $p < 0.05$, ** $p < 0.01$, *** $p < 0.001$, no asterisk: not significant..... 116

Figure 4.13: Relative atom percentages of carbon functional groups in pore water samples collected on Feb 2018 as de-convoluted from C 1s XPS spectra. (a) aliphatic or aromatic C (C-C, C=C, C-H; at 284.6 eV); (b) amines and/or alcohols like those in polysaccharides and amino acids (C-O, C-N, at 286.5 ± 0.2 eV); and (c) carbonyl/carboxyl C (C=O; 288.6 ± 0.2) each expressed as the relative atom percent of the total C in size fractionated organo-mineral complexes. Level of significance: * $p < 0.05$, ** $p < 0.01$, *** $p < 0.001$, no asterisk: not significant..... 118

Figure 4.14: Variation in $\delta^{13}C$ in size-fractionated COC collected on 02.21.2018. The error bars represent standard deviations in stable isotope values among replicates..... 119

Figure 4.15: Linear relationship between bulk C ($[C]_{particle)}$ and N concentration ($[N]_{particle)}$ as measured by IRMS. 120

Figure 4.16: Transmission electron micrographs and energy dispersive X-ray spectroscopy of size-fractionated samples. 122

Figure 4.17: Linear relationship between the size-fractionated bulk C concentration (mg L^{-1}) to the colloid concentration (mg L^{-1}). 123

Figure 4.18: Relationship between bulk measured by IRMS (C_{IRMS}) and surface C concentration (C_{XPS}) measured by XPS of size-fractionated pore water samples collected on Feb 2018..... 127

Figure 5.1: Box plot of the mean, median and 1st and 3rd quartiles (25 and 75%) of the Al, Fe, Mn, and V concentrations in the respective dissolved, NNP, fine colloid, and particulate fractions. Statistical differences between element concentration in samples collected on Dec' 2018 and May' 2019 are marked with *p < 0.05, **p < 0.01, and ***p < 0.001..... 140

Figure 5.2: Box plot of the mean, median and 1st and 3rd quartiles (25 and 75%) of the Ga, Ti, and Zr concentrations in the respective dissolved, NNP, fine

colloid, and particulate fractions. Statistical differences between element concentration in samples collected on Dec' 2018 and May' 2019 are marked with *p < 0.05, **p < 0.01, and ***p < 0.001. 141

Figure 5.3: Box plot of the mean, median and 1st and 3rd quartiles (25 and 75%) of the Li, Na, K, Ca, Mg, Rb, Sr, Ba, and Co concentrations in the respective dissolved, NNP, fine colloid, and particulate fractions. Statistical differences between element concentration in samples collected on Dec' 2018 and May' 2019 are marked with *p < 0.05, **p < 0.01, and ***p < 0.001. 142

Figure 5.4: Distribution of Al, Fe, Mn, and V in the dissolved, NNP, fine colloid, and particulate fractions in different zones (wetland, transition, and upland zones) and at different depths (50 cm, 100 cm, and 200 cm). At each depth, the 1st and 2nd horizontal bars represent data for samples collected on Dec' 2018 and May' 2019, respectively..... 143

Figure 5.5: Box plot of the mean, median and 1st and 3rd quartiles (25 and 75%) of the Al-C and Fe-C ratios along the redox gradients from wetland-transition-upland zone (a, d), along the soil profile at 50 cm, 100 cm, and 200 cm depths (b, e), and in four different size fractions, i.e., dissolved, NNP, fine colloid, and particulate (c, f). 144

Figure 5.6: Box plot of the mean, median and 1st and 3rd quartiles (25 and 75%) of the specific UV absorbance at 254 nm ($SUVA_{254}$) and %Aromaticity for size fractionated samples..... 146

ABSTRACT

Redox-induced biogeochemical transformations are the key processes that control the fate and transport of soil organic carbon (SOC) via association with metal oxides in redox-sensitive wetlands. Given the particularly significant role of wetland soils in C storage (20-30% of terrestrial C) and cycling, the dynamics of soil colloids (1-1000 nm) and colloidal OC and their molecular composition remain a critical knowledge gap. Lack of such understanding limits our ability to predict the role that soil colloids play in C cycling in wetland soils and how colloidal interactions/processes may respond to climate change. Further, the question why some soil organic matter (SOM) persists for millennia whereas others decompose readily has motivated concerted efforts to improve our understanding of SOM stability. It is therefore important to investigate the fluxes and distribution of organo-mineral complexes in wetlands to better understand their role in the biogeochemical cycling of organic C and associated elements. My dissertation includes results from laboratory-based soil column and microcosm studies as well as field observations, focusing on (1) quantification of dissolved organic C and colloidal organic C (COC) loads, (2) identification of the molecular composition of colloids and associated OC in different size fractions, and (3) characterization of the influence of wetland hydrology on the concentration and composition of the organo-mineral complexes in a depressional wetland.

In Chapter 2, I present the results that addressed the dynamics of size-fractionated organo-mineral complexes by conducting redox oscillations in soil microcosms. Molecular composition of natural nanoparticle (NNP, 2.3-100 nm), fine colloid (100-450 nm), and particulate (450-1000 nm) fractions were measured using isotope ratio mass spectrometry (IRMS) and x-ray photoelectron spectroscopy (XPS). My findings clearly demonstrate an increase in colloid and OC concentrations and presence of more microbial-derived C in larger size fractions. It indicates that redox oscillations promote the formation of molecularly diverse organo-mineral associations within colloidal size range. In Chapter 3, I present the results of an investigation that studied the influence of redox oscillations on the mobilization of OC in soil columns. Results showed that bulk OC concentration in the mobile phase was increased by 425-1018% (121.55 ± 10.53 mg L^{-1}) and 311-830% (97.50 ± 5.36 mg L^{-1}) after respective 1st and 2nd reducing half-cycles (RHCs) in comparison to the oxic (control) soil column leachate (14.24 ± 5.43 mg L^{-1}) samples. Organic C in the leachate samples after the 1st RHC had greater contributions from NNP and dissolved fractions, higher aromatic C content, and was more biologically reactive than in the after the 2nd RHC. The observed OC release as influenced by their molecular composition and redox fluctuations provides a baseline for the size continuum of soil OC and its potential ecological and environmental roles. Chapter 4 shows the concentration and molecular composition of the dissolved, NNP, fine colloid, and particulate fractions in pore-waters collected from a Delmarva bay depressional wetland (divided into three zones: upland, transition, and wetland) located at Blackbird State Forest, Delaware, USA from Feb. 21, 2018 to May 01, 2019. Results reveal that (1) dissolved, NNP, fine colloid and particulate fractions comprise 45 ± 4%, 38 ± 4%, 8 ± 3% and 7 ± 3% of

the bulk OC (< 1000 nm) concentration, respectively, (2) organic C in the upland was more enriched in $\delta^{13}C$ stable isotopes than the transition and wetland zones, (3) NNP was more enriched in $\delta^{13}C$ than the fine colloid and particulate fractions, (4) and NNP fraction had a higher proportion of mostly oxidized OC ($p < 0.05$), while the particulate fraction has more aliphatic/aromatic OC functional groups. In Chapter 5, I discuss the concentrations of the major and trace elements in the pore water samples measured by the inductively coupled plasma mass spectrometry (ICP-MS). The samples were collected during water-table rising (Dec. 14, 2018) and declining (May 01, 2019) phases from the depressional wetland. My results revealed that the metal:C ratios were significantly higher in larger size fractions of the organo-mineral complexes, following the order: dissolved < NNP < fine colloid< particulate.

Overall, my findings clearly demonstrate significant new insights into the differences in the concentration and molecular composition of size-fractionated COC, which imply the importance of taking into consideration of the NNP and fine colloid fractions separately (as opposed to combining them into the “dissolved” fraction following the conventional definition of 450 nm) when assessing the cycling and transport of various elements and associated organic C in depressional wetlands.

Chapter 1

INTRODUCTION

1.1 Explanation of Problem

Soil organic matter (SOM), an important and complex component of the ecosystem, provides the substrate for microbial metabolism, facilitates transport of metals, and contributes to the emission of greenhouse gasses such as CH_4 and CO_2 (Lal, 2001). Soils comprise more than three times (2500 Gt) as much carbon (C) as is found in atmospheric and biotic C pools (Lal, 2004; Figure 1.1a). A large fraction of this soil C presents in the wetlands (500-700 Pg) and peatlands (~1700 Pg) (Ciais et al., 2013) which are very sensitive to any changes in the climate and local soil environments. This belowground C reservoir is controlled by the balance between the inputs and outputs of C depending on several biotic and abiotic environmental factors (Figure 1.1b, Davidson and Janssens, 2006). Thus, the stability of SOM is becoming an important issue as concerns for the impacts of climate change increase with interests for wetlands (Schmidt et al., 2011). Despite having only 8-10% of the world's land surface (Sahagian and Melack, 1998), wetlands are highly vulnerable to climate change due to their geographical locations and the large amount of organic matter (OM, 20-30% of terrestrial C) they contain (Mitsch et al., 2013). Further, soluble organic C exported from redox-sensitive wetlands contributes appreciably to the global C cycling as well as to the downstream aquatic ecosystems (Gurwick et al., 2008; Marín-Spiotta et al., 2014; Van Oost et al., 2012).

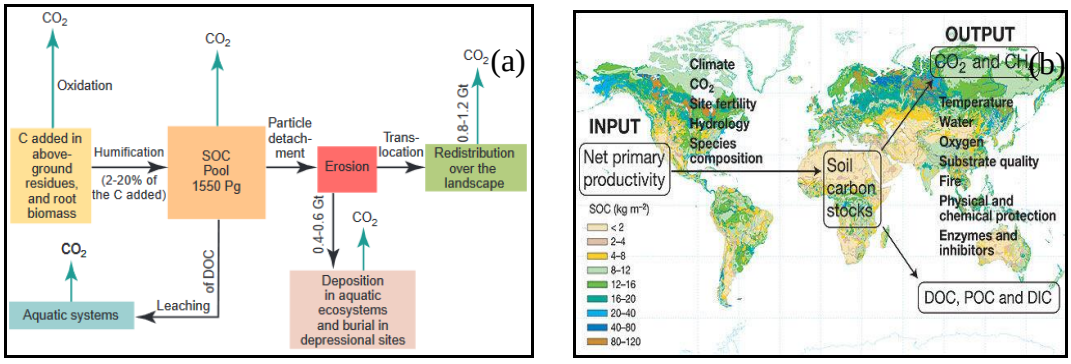

Figure 1.1: (a) Processes affecting the dynamics of SOC. The blue upward arrows indicate the emission of CO_2 into the atmosphere (Lal, 2004), (b) Important factors controlling the main input and output of soil C (Davidson and Janssens, 2006).

The question why some SOM persists for millennia whereas others decompose readily (Schmidt et al., 2011) has motivated concerted efforts to improve our understanding of SOM stability. Lack of such understanding limits our ability to predict the role that soils play in global C cycling and how soils will respond to climate change. Recent advances through analytical and experimental studies suggest that SOM is an ecosystem property in that SOM stability is not controlled by OM structure alone; rather, it is controlled by multiple environmental and biological factors (Schmidt et al., 2011). Among those factors, association of OM with soil minerals has been attracting increasing attention. The association of C with mineral phases, a major SOM stabilizing mechanism, depends on two main factors, 1) type (Kaiser et al., 2002) and surface area (Guggenberger and Kaiser, 2003) of the minerals and 2) the structural properties of the OM involved (Kalbitz et al., 2005; Mikutta et al., 2007). Therefore, molecular-level characterization of the nature and composition of organo-mineral complexes is necessary in addition to simple records of concentrations to study the stability of SOM (Kaiser and Kalbitz, 2012), the processes and dynamics

of soil carbon (C) (Tfaily et al., 2015), and the interactions with soil inorganic matrices.

Dissolved organic C (DOC) is ubiquitous in the terrestrial and aquatic ecosystems but represents only a small portion of the total SOM (McGill et al., 1986). For several decades, DOC has been operationally defined as "the organic carbon smaller than 450 nm in diameter" (Kalbitz et al., 2000). Owing to the very large specific surface areas, high reactive site densities, and mobility, colloids (1-1000 nm) can play an important role with respect to the organo-mineral complex formation. Therefore, there is a critical need to better understand quantitatively the partitioning and molecular composition of colloids and associated OC in size-fractionated particles. Such detailed characterization will enable us to explore the processes governing the accumulation and stabilization of SOM that otherwise would be impossible from simple records of concentration only. The following provides a literature review of the current state of knowledge on this topic.

1.2 Soil Organic Matter: The Largest Organic C Pool on the Earth's Surface

The total organic matter in terrestrial and aquatic ecosystems are operationally divided into two phases: particulate organic matter (POM) and dissolved organic matter (DOM) (Figure 1.2, Docter et al., 2015). Since C comprises approximately 58% of the organic matter, DOM is often quantified and referred as DOC. This "dissolved" fraction is ubiquitous in terrestrial and aquatic ecosystems (McGill et al., 1986) and is defined as that fraction of OC, which can pass through a 450 nm filter (Thurman, 1985; Zsolnay, 2003). It is now widely recognized that this mobile and actively cycling fraction can influence a myriad of biogeochemical processes in aquatic and

terrestrial environments, e.g., complexation with metals (Bartschat et al., 1992; Cabaniss and Shuman, 1987), binding of nonpolar organic compounds (Backhus and Gschwend, 1990; Chiou et al., 1986), and enhanced weathering of minerals (Hochella et al., 2008). Dynamic nature of DOM fraction additionally enables it to act as a sensitive indicator for any shifts in the ecological processes in terrestrial ecosystems. Globally, it has been estimated that 210 mt DOM and 170 Mt POM are transported from land to the oceans (Bolan et al., 2011).

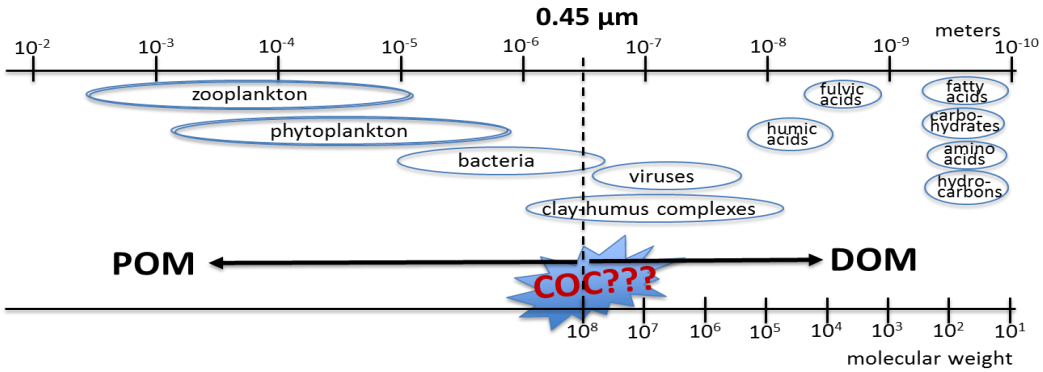

Figure 1.2: Size distribution of particulate organic matter (POM) and dissolved organic matter (DOM). The size limit used to differentiate DOM from POM is operationally set to around 450 nm (Adopted from Docter et al., 2015).

1.3 Colloids- The Complex Mixture of Organic and Inorganic Entities

Colloids are defined as inorganic and organic particles with sizes ranging from 1-1000 nm (Buffle, 1990) and is considered both as a reservoir and source of particle aggregation and disaggregation. In natural systems, colloids can be found as a multitude of compositions and conformations, e.g., clay minerals, oxides and oxyhydroxides of Fe, Mn, and Al, and various organic substances (Baalousha et al., 2011; Kretzschmar et al, 1999; Vold and Vold, 1983). As defined by (Sposito, 1989),

"The characteristic property of colloids is that they do not dissolved in water to form solutions, but instead remain as an identifiable solid phase in suspension."

According to the size-based definition, the colloidal phase is a critical transition zone between the dissolved phase and particulate phase, while nanoparticles describe a subset of the colloidal particles ranging from 1-100 nm (Christian et al., 2008). In soil, clay-humic-metal complexation is more dominant within the size range of 10 -1000 nm (Figure 1.2). Thus, the operational definition overestimates the actual "dissolved" phase by including colloidal and nanoparticles that are < 450 nm. Here, we need to ensure that the operational definition accurately differentiates the "dissolved" fraction from colloidal or particulate fractions, as only then we can advance our understanding about the significance of SOC in terrestrial ecosystems. Innovative development in separatory techniques, e.g., ultra-centrifugation, crossflow filtration, and filed-flow fractionation have extended our ideas about mineral-SOM interactions at the submicron levels. Colloids are naturally found in aquatic ecosystems including aquifers, rivers, oceans as a continuum of elements ranging from fully hydrated molecules to macroscopic flocs and grains (Schijf and Zoll, 2011). Very large specific surface areas, high reactive site densities, and mobility enable these colloidal particles to play an important role in binding nutrients, contaminants, and OM. Kleber et al. (2015) pointed that size fractionation becomes a minor component in mineral soil and is negligible in aquatic systems, where 1-2 kDa and 2-200 kDa fractions represent 50-70% and ~10% of the total organic compounds, respectively. However, this scenario might be different in redox fluctuating environments, where O_2 is periodically depleted. Much of the SOM which is stabilized via Fe-OM association becomes highly susceptible to any changes in the local environment. Dissolution of

Fe-minerals under reduced condition can ameliorate the dissociation of organo-mineral complexes. We would expect this mobile OC fraction to rapidly appear in the dissolved SOM pool. More recently, Yan et al. (2018) reported higher loading of colloids and OC in the wetlands compare to the agricultural, forestry, freshwater, and estuary ecosystems (**Figure 1.3**). Despite being an important vector for the transport of OC and inorganic elements, the contribution of these highly reactive colloids and nanoparticles in the retention and transport of SOM and contaminants has largely been ignored by including them with the dissolved fraction.

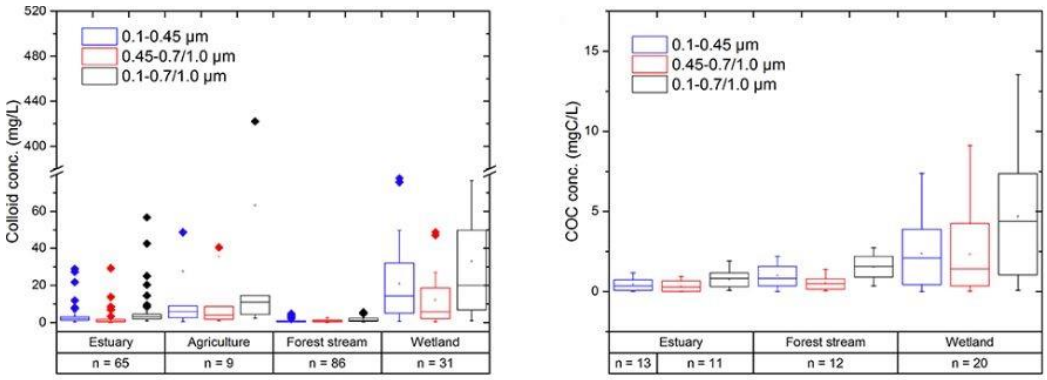

Figure 1.3: Colloid and OC concentrations across different ecosystems, e.g., estuary, agriculture, forest stream, and wetland (Reprinted from Yan et al., 2018).

1.4 Factors Affective Mobilization of Colloids and Associated OC

It is generally recognized that mobile organic and inorganic soil colloids play a major role in the fate and transport of the organic C, trace metals, radionuclides, bacteria, and viruses through the vadose zone (Afsar et al., 2020; de Jonge et al., 2004; Kjaergaard et al., 2004; Pédrot et al., 2008). Our knowledge about the colloid-facilitated transport of nutrients in riverine, estuarine, and ocean ecosystems has been rapidly improving, however, very little is still known for terrestrial ecosystem.

Colloids have been shown to contribute substantially to watershed fluxes of micronutrients from continents to oceans. Mobilization of these colloids is largely controlled by different environmental physicochemical factors, e.g., pH, redox potential, temperature, pressure, ionic strength, etc. (Grolimund and Borkovec, 1999; Ryan and Gschwend, 1994a; Thompson et al., 2006). The point of zero charge (PZC) of SOM, defined as the pH at which particle has no net charge, is typically less than three (Perdue and Lytle, 1983; Tombacz and Meleg, 1990). Deprotonation of surface functional groups of SOM results in negative charges at solution pH above its PZC. Colloid particles are negatively charged when pH is above the PZC value. An increase in pH diminished the positive surface charge of Fe and Al (hydr)oxides (PZC: ~ 6-9) and thus can mobilize the SOM into the aqueous phase. The pH-effect has been clearly demonstrated in an iron oxide-coated sand column study, where mobilization of clay colloids increased at pH > PZC (Ryan and Gschwend, 1994a). Increasing IS promotes colloid-colloid aggregation by decreasing the repulsive energy barrier between the particles (Ryan and Elimelech, 1996). In other word, decrease in IS facilitates colloid mobilization. In a column study using hematite colloids and quartz sand grains, Ryan and Gschwend (1994b) found an increase in the rate and extent of colloid release with decreasing IS. Similar results have been reported for natural sediments including studies on clay-containing Berea Sandstone (Khilar and Fogler, 1984; Kia et al., 1987; Vaidya and Fogler, 1990).

1.5 Organo-Mineral Associations: Formation, Properties, and Significance in Terrestrial Environment

Over the past three decades, the association between minerals and organic matter is receiving increasing attention as an important mechanism of the preservation and storage of SOM (Baldock and Skjemstad, 2000; Oades, 1988; Sollins et al., 1996; Torn et al., 1997). It is estimated that up to 90% of the organic matter is tightly associated with the minerals, particularly in deeper soil layers (Rumpel and Kögel-Knabner, 2011). Metal oxides, hydroxides, oxyhydroxides, phyllosilicates, and short-range ordered aluminosilicates are the dominant mineral components that interacts with SOM depending on the (1) type, abundance, and charges of the surface functional groups of both the minerals and OM, (2) size, shape, and surface topography of the mineral particles, and (3) degree of particle aggregation (Kögel-Knabner et al., 2008a). Carbon, nitrogen, phosphorus, and sulfur are central to all biogeochemical processes and is important to better understand any changes in the biosphere. Many laboratory and field investigations have found that colloids may influence nutrient movement, such as C (Buettner et al., 2014), P (Henderson et al., 2012; Rick and Arai, 2011), and trace elements (Doucet et al., 2007). Previous studies also confirmed that phosphorus sorption and desorption is strongly correlated with the Fe oxide and clay content of soils (Yousuf et al., 2018; Afsar, 2012a, 2012b, 2012c). **Figure 1.4** shows the general pathways to form organo-mineral associations. Depending on the environmental conditions and parent materials, mineral surfaces might be permanently noncharged, permanently charged, and variably (pH-dependent) charged. Size of the particles controls the ability of mineral surfaces to react with the SOM. The amount of reactive surfaces per unit mass of mineral that can interact with SOM generally increases with decreasing size of the particles due to an increase in the SSA.

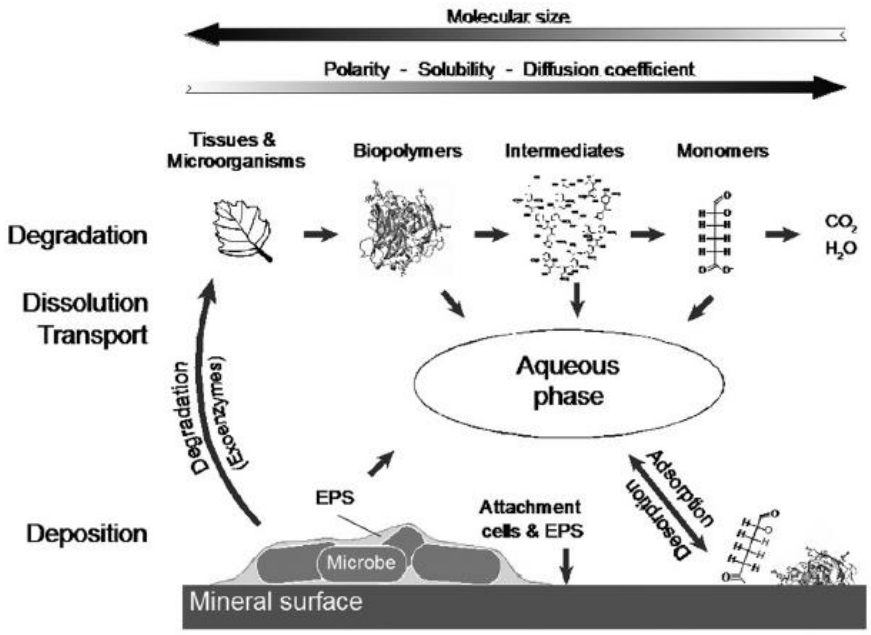

Figure 1.4: The role of DOM in the formation of organo-mineral associations. Figure reprinted from Markus Kleber et al. (2015), which was prepared based on the "partitioning model" of Hedges and Keil (1999).

1.6 Persistence of SOM in the Natural Environment

Despite very high sensitivity to changes in the climate or local environment, we have a poor understanding of the fate, stability, and persistence of SOM in the natural environment. Still, we are unable to answer how and to what time scale SOM will respond to such changes (Schmidt et al., 2011). Based on ^{14}C signatures, Kögel-Knabner et al. (2008) reported that the ages of SOM in forest soil ranges from < 50 to 3,840 years. The chemical composition controls the fate and reactivity of SOM (Sun et al., 1997). However, the composition depends on several biotic and abiotic factors in the terrestrial and aquatic ecosystems. Generally, two classes of mechanisms have been proposed to explain the persistence of SOM in natural environment- selectivity and protection (**Figure 1.5**, Hatcher et al., 1983; Mayer, 1994; Hedges and Keil, 1995;

Burdige, 2007). Selective preservation concept assumes that intrinsically bioavailable compounds (e.g., sugars, amino acids, etc.) are rapidly respired, while recalcitrant molecules (e.g., lignin) selectively preserved in the environment. In contrast, protection hypothesis relies on the mineral-SOM interactions regardless of the intrinsic recalcitrance SOM. Some aromatic SOM, previously assumed to persist in soil, have been found to be degraded relatively rapidly, while polysaccharide can last for decades (Amelung et al., 2008; Schmidt et al., 2011). Recent advances through analytical and experimental studies suggest that SOM is an ecosystem property in that SOM stability is not controlled by OM structure alone; rather, it is controlled by multiple environmental and biological factors (Schmidt et al., 2011). Among those factors, association of OM with soil minerals has been attracting increasing attention.

Interaction between soil minerals and OM is a major SOM stabilizing mechanism, which depends on three major factors: (1) the structural properties of SOM (Kalbitz et al., 2005; Mikutta et al., 2007), (2) type (Kaiser et al., 2002), and (3) surface area (Guggenberger and Kaiser, 2003) of the minerals involved. Interactions between organic and mineral particles lead to the formation of organo-mineral associations, which act as composite building units of soil micro aggregates (Kögel-Knabner et al., 2008; Lehmann et al., 2007). In a conceptual model of molecular soil C dynamics, Grandy and Neff (2008) argued that mineral-associated OC has distinct composition related more to microbial-derived C than to plant-derived C. In another study, Sollins et al. (2006) observed an increase in microbial C signature with increasing degree of mineral association, which can be stabilized via organo-mineral interactions (Baldock and Skjemstad, 2000; Kleber et al., 2015). Furthermore, Huygens et al. (2008) demonstrated microbial processing as an important step towards

SOM stabilization and observed high degree of microbial biomarkers in soil micro-aggregates.

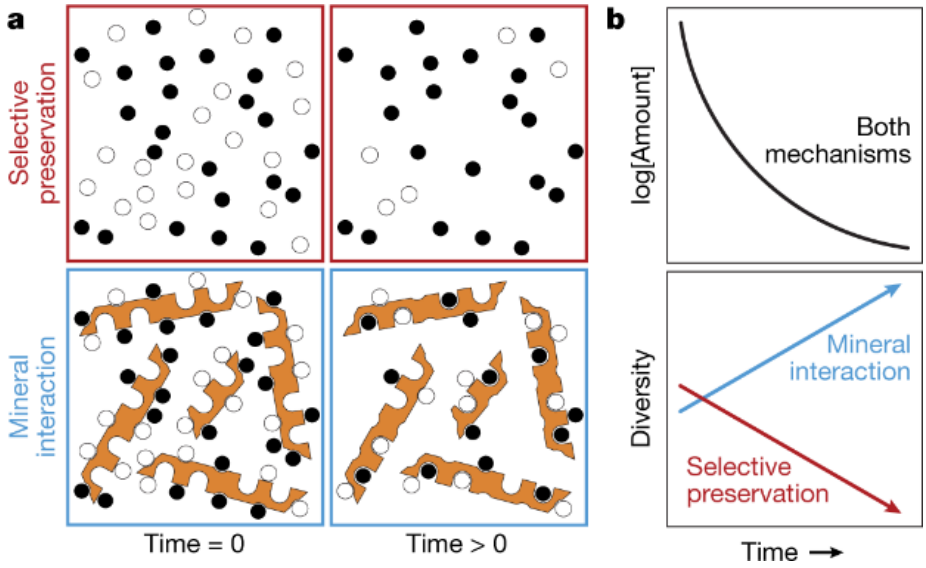

Figure 1.5: Schematic representation of two potential preservation mechanisms (Adopted from Hemingway et al., 2019).

1.7 Effect of Redox Oscillations on the Dynamics of Colloids and Associated OC

Reduction reactions in soil take place as a result of oxygen depletion from the ecosystems. Soil redox conditions are highly dynamic and changes with soil depth and saturation time. In contrast to the oxic condition when O_2 is the main terminal electron acceptor (TEA), other elements e.g., NO_3^-, Mn^{4+}, Fe^{3+}, SO_4^{2-}, CH_2O act as a TEA under facultatively anaerobic or anoxic conditions. In redox oscillating environments, much of the OC associated with redox-sensitive minerals, e.g., Fe and Al hydr(oxides), can be released to the dissolved pool through reductive dissolution of those minerals (Liptzin and Silver, 2009). In addition to regulating microbial/mineral

driven biogeochemical processes, redox oscillations can promote formation of new colloids (Thompson et al., 2006a) and thus the stability of associated OC (Figure 1.6). Thus, the redox oscillations have the potential to greatly influence the dynamics of colloids and associated OC in soils and sediments over that which might occur under strict anoxic or oxic conditions. De-Campos et al. (2009) reported that short term reducing conditions disintegrated soil aggregates and resulted in particle mobilization. Dissociation of colloids has also been observed in sediments and aquifers with high fluxes of DOM under reduced condition (Fuller and Davis, 1987; Magaritz et al., 1990; Ryan and Gschwend, 1990).

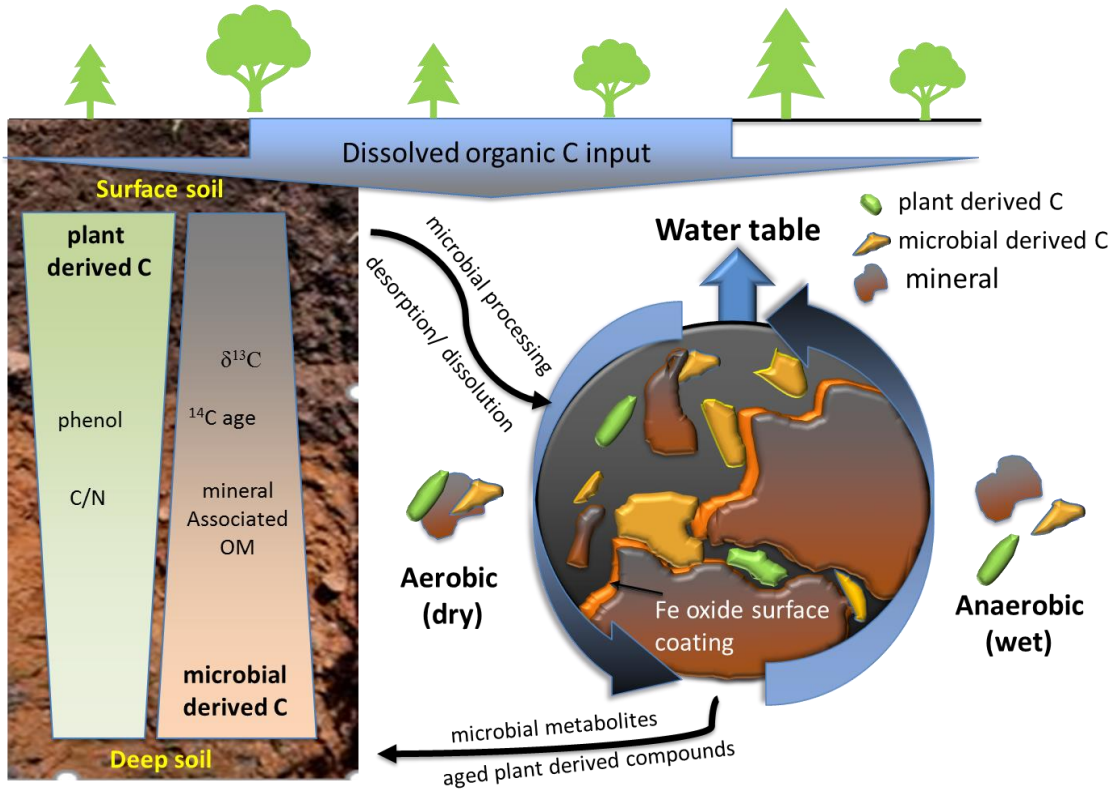

Figure 1.6: Effects of redox oscillations on the dynamics of colloids and associated OC (partially adopted from Kaiser and Kalbitz, 2012).

In wetlands, oscillations between reduction and oxidation events impact mobilization of mineral colloids and biogeochemical C cycling through dissolution of Fe minerals and accompanying shifts in pH. Colloids are ubiquitous in different environments, e.g., marine, riverine (Orlandini et al., 1990), and groundwater (McCarthy and Zachara, 1989) ecosystems as well as in soil pore waters (Chin and Gschwend, 1991). In uplands, Fe and Al (hydr)oxides protect OM from microbial decomposition and thereby contribute to C storage for centuries to millennia. In flooded soils such as wetlands, however, reductive dissolution of Fe(III) oxides and pH changes can lead to the mobilization of previously mineral-bound OC (Grybos et al., 2009). During water table dropdown, Fe(II) is either leached out from the profile or re-oxidized to Fe(III) oxides upon re-oxygenation of the soil. Despite the significance of colloid particles in such associations, we have very limited understanding on the size-dependent composition of colloidal mineral-OC complexes and colloidal organic carbon (COC), and their influence on the mobilization of soil C. Thus, the inaccurate differentiation of the colloids from the dissolved phase limits our ability to properly assess the biological functions and environmental fate and transport of colloid-associated-constituents such as OC.

Redox sensitive biogeochemical processes are significantly influenced by the hydrologic characteristics in redox dynamic wetlands. My overall hypothesis is that concentration and molecular composition of size-fractionated colloids and COC may vary widely within the colloidal size range. My overreaching research questions are:

- What is the contribution of COC to the operationally defined “dissolved” pool?
- How the molecular composition of colloids and associated OC varies among different size fractions?

- How wetland hydrology influences the composition of organo-mineral associations in depressional wetland?

My specific objectives are:

- To elucidate the mechanisms responsible for the release of colloid and OC under redox oscillating conditions,
- To investigate how the concentration and molecular composition of size-fractionated organo-mineral complexes vary as a function of redox oscillations, and
- To investigate the impacts of wetland's hydrologic condition (e.g., hydro-periods and hydro-dynamics) on the fate and release of SOC and other trace elements in a seasonally flooded wetland

To fulfill these objectives, I conducted laboratory-based soil column and microcosm studies as well as field observations, as discussed from Chapters 2-5.

Chapter 2: Quantification and molecular characterization of organo-mineral associations as influenced by redox oscillations

Chapter 3: Redox oscillations enhance destabilization and mobilization of protected colloidal soil organic carbon

Chapter 4: Colloidal organic carbon has a key but accounted role in carbon dynamics in a depressional wetland

Chapter 5: Effect of metal: carbon rations on the mobility of organic carbon in a depressional wetland

1.8 Broader Impacts

In my dissertation work, I systematically investigated the effects of redox oscillations on mineral-OM interactions at multiple scales, from molecular to field

level using a combination of traditional and contemporary research methods/tools. Small scale mechanistic knowledge is essential for interpreting the patterns of C stability and sequestration to a changing global climate at the large scale. Knowledge of mineral-OM association will contribute to improving our understanding of feedback between climate change and C cycling, better inform scientists, economists, coastal and wetland managers, and guide policymakers to make management decisions that are conducive to preserving the functions of wetlands in the changing environment.

Chapter 2

QUANTIFICATION AND MOLECULAR CHARACTERIZATION OF ORGANO-MINERAL ASSOCIATIONS AS INFLUENCED by REDOX OSCILLATIONS

[Afsar, M. Z., Goodwin, C., Beebe, T. P., Jaisi, D. P., and Jin, Y. (2020). Quantification and molecular characterization of organo-mineral associations as influenced by redox oscillations. *Science of the Total Environment*. 704, 135454]

Abstract

Organo-mineral association is one of the most important stabilization mechanisms of soil organic matter. However, few studies have been conducted to assess the retention, transformation, and transportation of colloids (1-1000 nm) and associated organic carbon (OC) in soil. Given the particularly significant role that wetland soils play in carbon storage and cycling, I quantified the dynamics of organo-mineral association within colloidal size range by conducting three consecutive 35-day redox (reduction-oxidation) oscillation experiments using a wetland soil. Molecular compositions of natural nanoparticle (NNP, 2.3-100 nm), fine colloid (100-450 nm), and particulate (450-1000 nm) fractions were measured using isotope ratio mass spectrometry (IRMS) and x-ray photoelectron spectroscopy (XPS). Results showed that NNP and fine colloids constituted up to 8.94 ± 0.50% and 22.19 ± 7.52% of bulk C concentration (2.3-1000 nm), respectively; indicating substantial contributions of these two fractions to the operationally defined "dissolved" (<450 nm) fraction. There was significant enrichment in heavier $\delta^{13}C$ isotopes ($p < 0.001$) with size: NNP (-

29.64 ± 0.32 ‰) < fine colloid (-28.81 ± 0.31 ‰) < particulate (-28.34 ± 0.25 ‰) fractions. NNP had the highest percentages of carbonyl/carboxyl C (C=O); while fine colloid and particulate fractions contained more reduced aromatic or aliphatic C (C-C, C=C, C-H). OC became more δ^{13}C-enriched (‰) in microbial-derived C with increasing particle size as well as with repeated redox oscillations. Our findings clearly demonstrate limitations of using the operationally defined "dissolved" fraction (<450 nm) to assess C cycling in ecosystems such as wetlands. Increase in colloid and OC concentrations and presence of more microbial-derived C in larger size fractions additionally imply that redox oscillations promote the formation of molecularly diverse sub-colloid sized organo-mineral associations. Being a composite unit of soil micro aggregates, organic-mineral associations can thus influence the overall stability of OC in wetland soils that undergo frequent redox oscillations.

2.1 Introduction

Soil organic matter (SOM), an important and complex component of the ecosystem, exists as a continuum from freshly produced plant residues to microbial-derived organic fractions (Lehmann and Kleber, 2015). Soil comprises at least 3 times more carbon (C, 2500 Gt) than the vegetative and atmospheric pools combined (Lal, 2004). SOM in wetlands is particularly important as concerns for climate change increase (Schmidt et al., 2011). Although wetlands cover only 8-10% of the world's land surface (Sahagian and Melack, 1998), their geographical location and high C content (20-30% of terrestrial C) make them highly vulnerable to climate change. Any changes in the frequency and duration of oxic and anoxic events can make wetlands biogeochemical "hotspots" for the (de)stabilization of SOM. The stability of SOM is largely controlled by the formation of organo-mineral associations that accounts for up to 90% of total soil C (Baldock and Skjemstad, 2000; Kleber et al., 2007; Wagai and Mayer, 2007). However, despite wetlands' recognized significance, comprehensive understanding of biogeochemical transformations of these associations resulting from redox (reduction-oxidation) oscillations remain inadequate.

The interactions between soil minerals and organic C (OC), are a major SOM stabilizing mechanism, which depend on three major factors: (1) the structural properties of SOM (Kalbitz et al., 2005; Mikutta et al., 2007), (2) type (Kaiser et al., 2002), and (3) surface area (Guggenberger and Kaiser, 2003) of the minerals involved. Interactions between organic and mineral particles lead to the formation of organo-mineral associations, which act as composite building units of soil micro aggregates (Kögel-Knabner et al., 2008a; Lehmann et al., 2007). There has been considerable evidence supporting the claim that the C incorporated onto mineral surfaces resembles microbial-derived C rather than plant-derived C. For example, in a conceptual model

of molecular soil C dynamics, Grandy and Neff (2008) argued that mineral-associated OC has distinct composition related more to microbial-derived C than to plant-derived C. In another study, Sollins et al. (2006) observed an increase in microbial C signature with increasing degree of mineral association, which can be stabilized via organo-mineral interactions (Baldock and Skjemstad, 2000; Kleber et al., 2015). Furthermore, Huygens et al. (2008) demonstrated microbial processing as an important step towards SOM stabilization and observed high degree of microbial biomarkers in soil micro-aggregates. Active contribution of microbial metabolites to the formation of organo-mineral associations additionally supports the conceptual three-dimensional functional view of C turnover dynamics as proposed by Kleber and Johnson (2010). According to this view, organo-mineral microstructures are formed around colloid to sub-colloid sized (discussed in the next paragraph) microbial cells rather than random attachment to the mineral surfaces. However, in redox oscillating environments, much of the OC associated with redox-sensitive minerals, e.g., Fe and Al hydr(oxides), can be released to the dissolved pool through reductive dissolution of those minerals (Liptzin and Silver, 2009). In addition to regulating microbial/mineral driven biogeochemical processes, redox oscillations can promote formation of new colloids (Thompson et al., 2006) and thus the stability of associated OC.

In soil, nano (1-100 nm) and colloid sized (1-1000 nm) (Everett, 2019; Guo and Santschi, 2007) organo-mineral associations are found in both immobile solid phase and colloidally dispersed mobile phase (Buettner et al., 2014; Fritzsche et al., 2016; Totsche et al., 2018). Mobile colloids are inorganic or organic entities and are the identifiable solid phase in the suspension (Sposito, 1989). Due to their large specific surface areas, high reactive site densities, and high mobility, colloids and

colloidal OC (COC), along with associated elements, can transport across long distances. They can also actively participate in the biogeochemical processes in both terrestrial and aquatic ecosystems (Kalbitz et al., 2000; Zsolnay, 2003). In aquatic and marine ecosystems, size-specific concentration and molecular composition of COC are widely used as indicators of environmental changes, however, those data are scarce for terrestrial ecosystems. Apart from the difficulty and labor-intensive nature of performing size-fractionated sample analysis, the scarcity is also due to the conventional technique to separate dissolved OC (DOC) from particulate OC (POC) using the cutoff size of 450 nm, which lumps COC with the dissolved fraction. DOC is a heterogeneous mixture of diverse organic matter (OM) that significantly contributes to the formation of organo-mineral associations (Kleber et al., 2015). The conventional practice also overestimates the contribution of actual dissolved phase to global C cycling by including colloids of diameter <450 nm in the dissolved fraction. For example, Yan et al. (2018) estimated that COC accounts for 8-19% of the operationally defined DOC pool (<450 nm) regardless of sampling source and location. This estimation corresponds to riverine flux of 13.6-32 TgC $year^{-1}$ of global DOC pool in global C cycle. Moreover, different cutoff size ranges are often used in different disciplines to define DOC fractions, e.g., <700 nm (DeVilbiss et al., 2016; Osburn et al., 2012), <450 nm (Kellerman et al., 2014; Poulin et al., 2014), or <200 nm (Chen et al., 2004). Such discrepancies make it more difficult to compare results in C behavior and processes between different ecosystems and environments.

A better understanding of both simple records of C concentration and molecular composition of sub-micron sized organo-mineral associations is thus necessary to make more accurate assessment of SOM stability (Kaiser and Kalbitz,

2012), the processes and dynamics of OC (Tfaily et al., 2015), and the interactions of OC with soil mineral matrices. During SOM decomposition, microbes preferentially respire the lighter C isotopes while they tend to incorporate the heavier $\delta^{13}C$ isotope into their biomass (Dijkstra et al., 2006; Emmerton et al., 2001). Thus, stable $\delta^{13}C$ values are a good indicator and correlate well with SOM composition, stability, and turnover processes during decomposition (Chen et al., 2005). Hence, I aimed to understand to what extent the concentration and molecular composition of organo-mineral associations vary (1) among different size fractions and (2) with redox oscillation cycles. I tested the hypothesis that concentration and composition of size-fractionated OC would vary widely within colloidal size range. I systematically induced redox oscillations in soil suspension in microcosms and analyzed the concentration and molecular composition of both colloids and associated OC in multiple size fractions including natural nanoparticle (NNP, 2.3-100 nm), fine colloid (100-450 nm), and particulate (450-1000 nm) fractions. Our comprehensive approach and the use of state-of-the-art spectroscopic techniques (isotope ratio mass spectrometry, IRMS; and x-ray photoelectron spectroscopy, XPS) yielded results that show size-specific molecular composition of organo-mineral associations and their response to redox oscillations. The results provide insights that improve the understanding of OC stability in redox-dynamic environments such as wetlands in response to climate change.

2.2 Materials and Methods

2.2.1 Study Site and Soil Sampling

Soil samples were collected from the top 0-15 cm layer in 2016 from the Devil's Hole wetland, a freshwater wetland, and a part of the White Clay Creek (WCC) watershed, Delaware, USA. Mean annual precipitation and water flow rate, respectively, are 105.4 cm and 50.8 cm per year (Corrozi et al., 2008). Over the last two decades, WCC watershed has experienced more frequent and intense floods and more severe droughts. Devil's Hole is defined as a permanently inundated and steady-state wetland and the hydroperiod of the wetland is "permanently saturated" (NTCHS, 2015). Water table fluctuates +/- 5 cm of the soil surface throughout the year and the wetland usually has no inundation during periods of drought. The soil is classified as fine-silty, active, mesic, Thapto-Histic Fluvaquents according to the U.S. Department of Agriculture (USDA) soil taxonomy (Soil Survey Staff, 2015). Soil samples were immediately transported to the lab and stored at 4^0C until they were used for the incubation study. A sub-set of the collected soil sample was air-dried and passed through a 2-mm sieve to study the basic characteristics of the soil. A summary of the soil physical and chemical composition is listed in **Table 2.1.**

Table 2.1: Selected properties and general chemical composition of the soil sample

Total concentration									
C (%)	N (%)	Al (g kg^{-1})	Ca (g kg^{-1})	Fe (g kg^{-1})	K (g kg^{-1})	Mg (g kg^{-1})	Na (g kg^{-1})	P (g kg^{-1})	S (g kg^{-1})
4.98	0.41	39.97	1.37	42.48	5.23	8.32	0.13	0.76	0.87

Textural class: Silt loam (Sand, silt, and clay is 5%, 72%, and 23%, respectively)
Cation exchange capacity (CEC) at pH 7.0 = 27.4 meq/100 g

2.2.2 Redox Oscillation Experiment

Moist soil samples were transferred from 4°C storage to a 95%:5% N_2:H_2 glovebox (Coy, Grass Lake, MI) and stored for 24 h to thoroughly equilibrate the samples with the gases to ensure anoxic conditions. Any visible plant debris and rocks were removed manually. Initially, soil was suspended in deoxygenated 2.0 mM NaCl solution at a soil: solution ratio of ~1:11 in the absence of light and without any supplemental C sources. Approximately 85 g (oven-dry weight) of soil was weighed into a 1 L microcosm; a total of 21 microcosms were prepared. The suspension was shaken for 5 min and then passed through a 1-mm sieve for several times (Thompson et al., 2006). The precise weight of the soil was determined by oven-drying (110 ^{0}C) 10 mL of the suspension. Microcosms were always capped with polypropylene screws fitted with Tygon tubing extended at the bottom of the jars. A complete redox oscillation was designated by 30-day of reducing half-cycle (RHC) followed by 5-day of oxidizing half-cycle (OHC). Microcosms were divided into 7 subsets to individually run (1) control (Initial soil, 0-day), (2) 1st RHC (30-day), (3) 1st RHC + OHC (1st redox oscillation, 35-day), (4) 2nd RHC (65-day), (5) 2nd RHC + OHC (2nd redox oscillation, 70-day), (6) 3rd RHC (100-day), and (7) 3rd RHC + OHC (3rd redox oscillation, 105-day), with 3 replicates for each treatment. The RHC was initiated by injecting nitrogen (N_2) gas intermittently for 2-h through Tygon tubing at the bottom of the soil suspension. Later, no N_2 gas was injected for the rest of the RHC period. During the OHC, microcosms were removed from the glove box and intermittently purged with O_2 gas (grade 4.7) at the bottom of the suspension. Microcosms were shaken for 5 min in every day to homogenize the soil suspension. Complete procedure for the redox oscillation study is outlined in **Figure 2.1**.

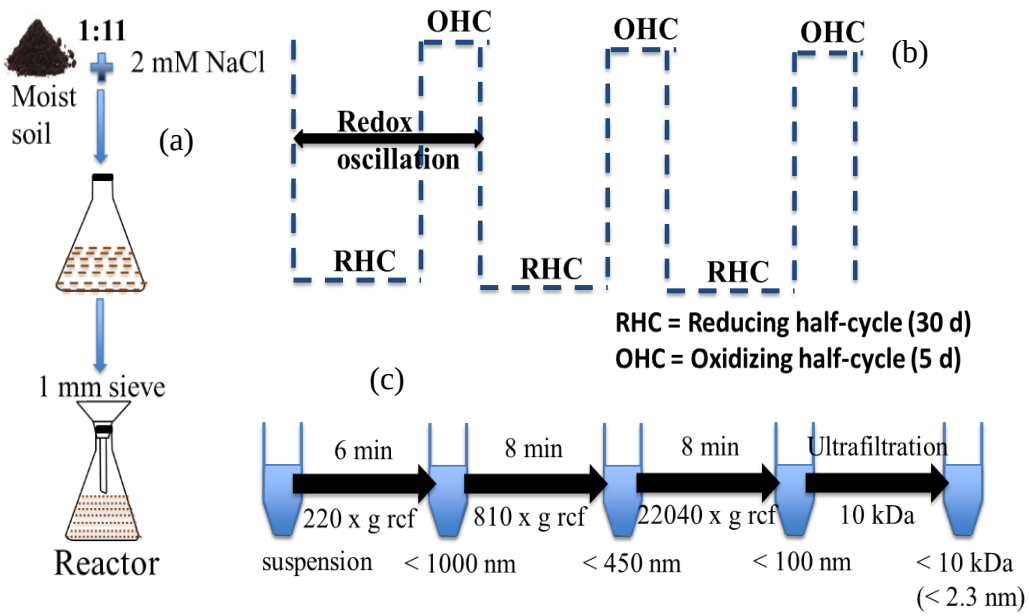

Figure 2.1**:** Schematic diagram of the batch incubation study. (a) Preparation of soil suspension using 2 mM NaCl electrolyte solution; (b) one complete redox oscillation consisted of 30 d reducing half-cycle (RHC) followed by 5 d oxidizing half-cycle (OHC) (a total of 3 complete redox oscillation cycles were carried out in this study); and (c) particle size fractionation using differential centrifugation processes.

2.2.3 Sample Collection

Soil suspension was destructively collected from triplicate microcosms after each treatment. Initially, microcosms were shaken for 5 min and allowed to settle for 2 h before supernatants were collected for size fractionation. The supernatants were transferred into four 250 ml centrifuge tubes and were fractionated into <1000 nm (6-min, 220 rcf), <450 nm (8-min, 810 rcf) and <100 nm (6-min, 22040 rcf) sized fractions using Sorvall centrifuge (Thermo Scientific) with a F14-6*250Y rotor. The centrifugation speed and time to achieve desired particle sizes were estimated from the

Stokes' law (Gimbert et al., 2005) assuming spherical particles and particle density of 2.65 g cm^{-3} (**Appendix B**), which is a typical value used for mineral soils (Murphy et al., 1993; Rozas et al., 2001; Taylor et al., 1992). Although the two assumptions do not consider heterogeneity in particle size and composition, I chose centrifugation over filtration for size fractionation (except at 2.3 nm) as it avoids the inaccuracies associated with filter/membrane filtration due to pore-clogging. Conventional filtration using 450 nm or 200 nm membrane filters can remove more soil particles than the corresponding centrifugation procedures particularly due to the influence of clogging of pores, particle shape (e.g., platey structure) and interactions between colloid particles and membrane surface (Gimbert et al., 2005). I acknowledge that organic materials having density <2.65 g cm^{-3} would likely remain in supernatants when mineral particles with the same size would settle at a given centrifugation speed, thus be underestimated. I passed the <100 nm fraction through an ultrafiltration system (Amicon® stirred cell) equipped with Ultracel® 10 kDa membrane ultrafiltration discs (EMD Millipore Corporation) to separate the dissolved, <10 kDa (~2.3 nm) fraction (Buettner et al., 2014; Guo and Santschi, 2007). The particulate, fine colloid and NNP fractions were collected from the precipitates at each centrifugation steps and freeze-dried. During the RHC events, Microcosms were kept and opened inside the glove box for all subsequent procedures. pH and Eh of the supernatants were measured using corresponding probes (Fisher Scientific, Hampton, NH).

2.2.4 IRMS Analyses

Stable $\delta^{13}C$ and $\delta^{15}N$ isotope values and total C and N concentrations of the freeze-dried, size-fractionated samples were determined using an IRMS (DELTA V plus, Thermo Fisher Scientific) equipped with an elemental analyzer (EA). Stable $\delta^{13}C$

or $\delta^{15}N$ values were calculated as (R_{sample}/ $R_{standard}$ -1) x 1000, where R is the ratio of heavier to lighter isotope ($^{13}C/^{12}C$, or $^{15}N/^{14}N$), and expressed in parts per thousand (‰) relative to their international standards Vienna-Pee Dee Belemnite (PDB) limestone and atmospheric N_2 standards. USGS-40 (L-glutamic acid, 40.8% C and 9.52% N) and USGS-41 (L-glutamic acid enriched in ^{13}C and ^{15}N, 41.9% C and 9.76% N) were used as reference materials. Because there was insufficient amount of samples at 2.3-100 nm after 1st and 2nd complete oscillations, replicate samples were combined to run the IRMS analyses.

2.2.5 XPS Analyses

The photoelectron spectra of the size-fractionated, freeze-dried samples were taken at the University of Delaware's Surface Analysis Facility (SAF) using a Thermo Scientific K-alpha+ XPS (East Grinstead, United Kingdom). Samples were dispersed uniformly on double-sided conducting tapes and affixed to a stainless-steel plug. The samples were excited with a monochromated aluminum Kα radiation (E_{exc} = 1486.6 eV) at an incident angle of 57.2° with a spot size of 100 μm wide ellipse; charge neutralization was carried out with a low energy electron flood gun. Elemental composition of soil minerals and their associated OC was measured by a survey scanning from 0 to 1200 eV using a 1 eV step size and 100 eV pass energy. The high-resolution scans for every element in the samples were obtained using a step size and pass energy of 0.1 eV and 20 eV, respectively. During operation, vacuum was maintained at $<3 \times 10^{-9}$ mbar. The chemical composition was revealed by deconvoluting C 1*s*, N 1*s*, Si 2*p*, Fe 2*p*3/2, Al 2*p*, Mn 2*p*, Mn 3*s*, O 1*s*, Mg 1*s*, Mg 2*p*, Ca 2*p*, Cl 2*p*, Na 1*s* peaks (**Figure 2.2**) into sub-peaks by fitting Gaussian-Lorentzian functions and Shirley background correction of the XPS spectra using the CasaXPS

version 2.3.16 (Teignmouth, UK). Molar fractions of the various elements were calculated from peak areas based on acquisition parameters and atomic sensitivity factors calculated from the electronic cross-section of each element and orbital (Scofield, 1976).

A typical C spectrum obtained by XPS (**Figure 2.3**) is deconvoluted into three components representing aliphatic and aromatic $C^{[0]}$ (C-C, C=C, C-H; at 284.6 eV), ether, alcohol, and amine C such as those in polysaccharides or amino acids, $C^{[+1]}$ (C-O, C-N; at 286.5±0.2 eV), and carbonyl and carboxyl C, $C^{[+2]}$ (C=O, at 288.6±0.2 eV), depending on the specific bonding environments or oxidation states (Gerin et al., 2003; Mikutta et al., 2009; Proctor and Sherwood, 1982). Though carbonyl/carboxyl C peaks are generally easily discerned, the effect of different counterions (H, Na, K) and low concentration might shift the peak position. Therefore, a combined peak shape was used for the fitting. Weight % of surface C ($C_{surface}$) was calculated by multiplying the molecular weight of all elements with their measured atom % assuming that hydrogen has negligible contribution (Arnarson and Keil, 2001, 2007).

2.2.1 Statistics

Statistical analyses were performed using R 3.3.1 (R core team, 2016). Two-way analysis of variance (ANOVA) was performed to test for redox oscillations and size effects on measured parameters using the Tukey's Honestly Significant Difference (HSD) test. Pearson's correlation coefficients between C and N concentration measured in IRMS and XPS analyses, and stable $\delta^{13}C$ and C concentrations were obtained using Origin (OriginLab, Northampton, MA). Regression plots of XPS-based surface atom % of Al, Fe, Si, Mg, and N with C atom

% and between OC and colloid mass were obtained using the Origin. Differences of means were significant at $p < 0.05$ unless otherwise noted.

2.3 Results and Discussion

2.3.1 Changes in Soil Solution Chemistry

Changes in solution pH and pE as a function of redox oscillations are summarized in **Figure 2.4**. As expected, RHCs were characterized by an increase in pH and decrease in pE, whereas OHCs exhibited opposite trends. These changes in solution chemistry are consistent with results from Thompson et al. (2006a), who studied colloid mobilization in wet tropical Hawaiian soils. Final pH of the suspension was decreased from 6.18 ± 0.40 after 1st RHC to 5.28 ± 0.31 after 3rd RHC. However, I did not observe wide variations in pE after 2nd and 3rd RHCs, which might be due to nitrate (NO_3^-) accumulation through ammonia oxidation during intermediate OHC periods. Being a terminal electron acceptor, NO_3^- produced under aerobic condition through ammonia oxidation tends to stabilize redox potential during successive reducing events (Reddy and Patrick, 1975).

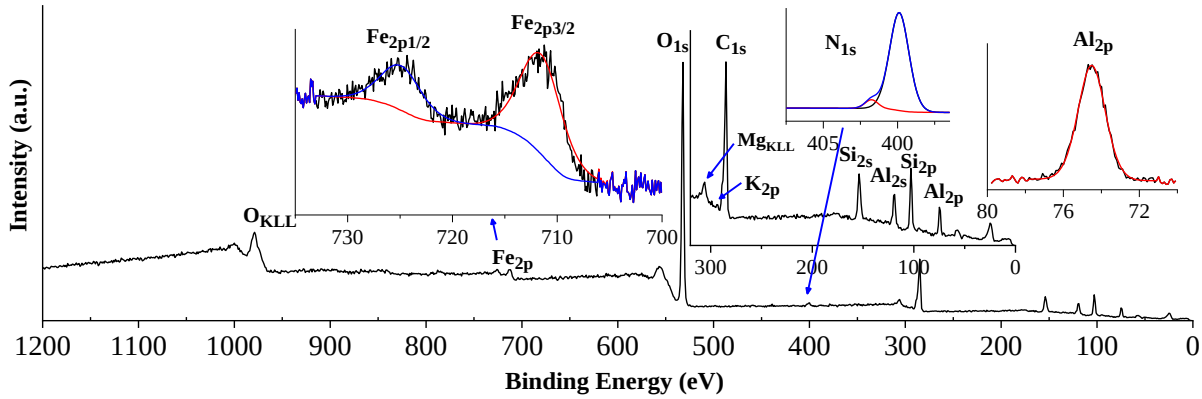

Figure 2.2: A representative XPS survey spectrum with all elements. The spectrum was corrected to the aliphatic or aromatic C (C-C, C=C, C-H) at 284.6 eV.

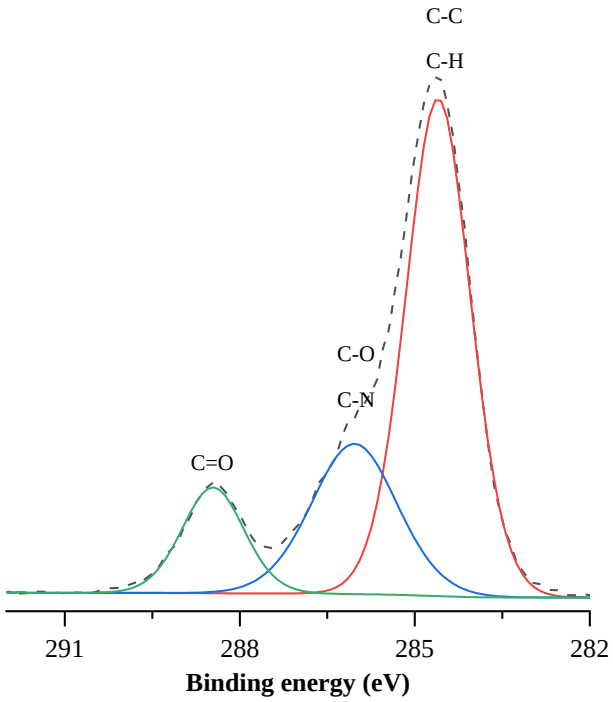

Figure 2.3: High-resolution XPS C_{1s} spectrum (broken line) of Mineral-SOM complexes and the de-convoluted sub-peaks (solid lines) as assigned to different C components.

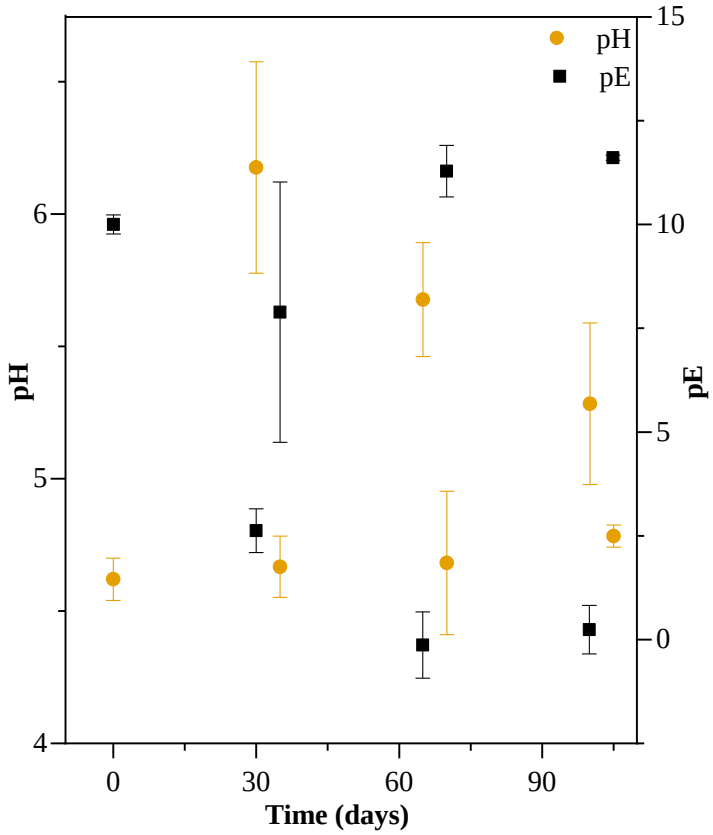

Figure 2.4: Changes in pH and pE along the redox oscillations. Both pH and PE measured (1) at time zero (0-day), (2) after 1st RHC (after 30-day), (3) after 1st RHC + OHC (after 35-day), (4) after 2nd RHC (after 65-day), (5) after 2nd RHC + OHC (after 70-day), (6) after 3rd RHC (after 100-day), and (7) after 3rd RHC + OHC (after 105-day). The error bar indicates standard deviation.

2.3.2 Distribution of C and N in Size-fractionated Particles

Total C and N concentrations ($[C]_{particle}$ and $[N]_{particle}$) of the size-fractionated particles based on their freeze-dry weight are shown in **Figure 2.5**. Both $[C]_{particle}$ and $[N]_{particle}$ values at NNP fractions dropped sharply after 1st RHC and fluctuated narrowly throughout the remaining redox oscillation events. Sharp drop in the concentrations after 1st RHC indicates that most of the labile OC was mineralized during that period. I also observed an overall decrease in redox-dependent fluctuation

in $[C]_{particle}$ and $[N]_{particle}$ with increasing particle size, following the order of NNP > fine colloid > particulate fractions (**Figure 2.5 a-b**). The smallest concentration changes in particulate size fraction indicates that OC in the larger size fractions is less redox-dependent. The higher $[C]_{particle}$ and $[N]_{particle}$ in the small size fractions might be due to (1) greater specific surface area, and/or (2) detachment/transformation of particulate OM (Guo and Santschi, 1997b) with decreasing size of the particles. In fact, Schulten and Leinweber (2000) also reported that OC and total N contents increased exponentially with decreasing particle sizes in soils with different clay and silt contents. Strong positive correlation between $[C]_{particle}$ and $[N]_{particle}$ at 2.3-1000 nm (**Figure 2.5c**; $r^2 = 0.97$, $p < 0.001$) additionally supports that they are mostly from soil organic matrices rather than from inorganic sources.

An opposite trend was observed in total mass and concentration when the size-fractionated particles and associated OC were expressed in per kg oven-dry soil (**Figure 2.6a-d** and Table A1 in appendix B). Among the different size fractions, least amount of C was partitioned at smaller size fractions; NNP (3 ± 1 to 54 ± 8 mg kg^{-1}), followed by fine colloid (17 ± 5 to 120 ± 50 mg kg^{-1}), and then particulate (49 ± 10 to 414 ± 32 mg kg^{-1}) (**Figure 2.6c-d**). The average percentages of NNP- and fine colloid-bound C were between $2.10 \pm 1.18\%$ to $8.94 \pm 0.50\%$ and $17.88 \pm 1.40\%$ to $22.19 \pm 7.52\%$ of the bulk C concentration (2.3-1000 nm), respectively, indicating substantial contributions of these two fractions to the operationally defined dissolved fraction (<450 nm).

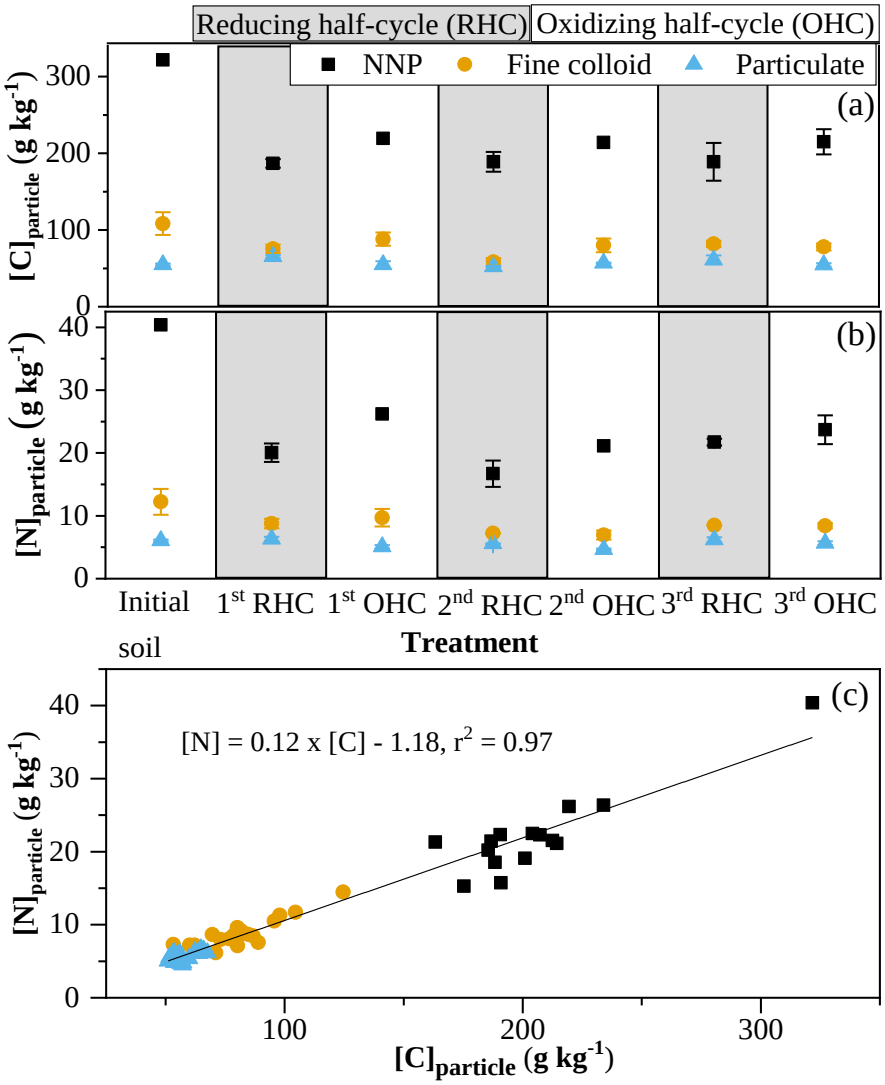

Figure 2.5: Changes in bulk (a) C ($[C]_{particle}$, g kg^{-1} size-fractionated particles) and (b) N concentrations ($[N]_{particle}$, g kg^{-1} size-fractionated particles) as a function of redox oscillations measured by IRMS equipped with EA. (c) Regression plot between C and N concentrations within 2.3-1000 nm size range. The error bars show standard deviations among replicates.

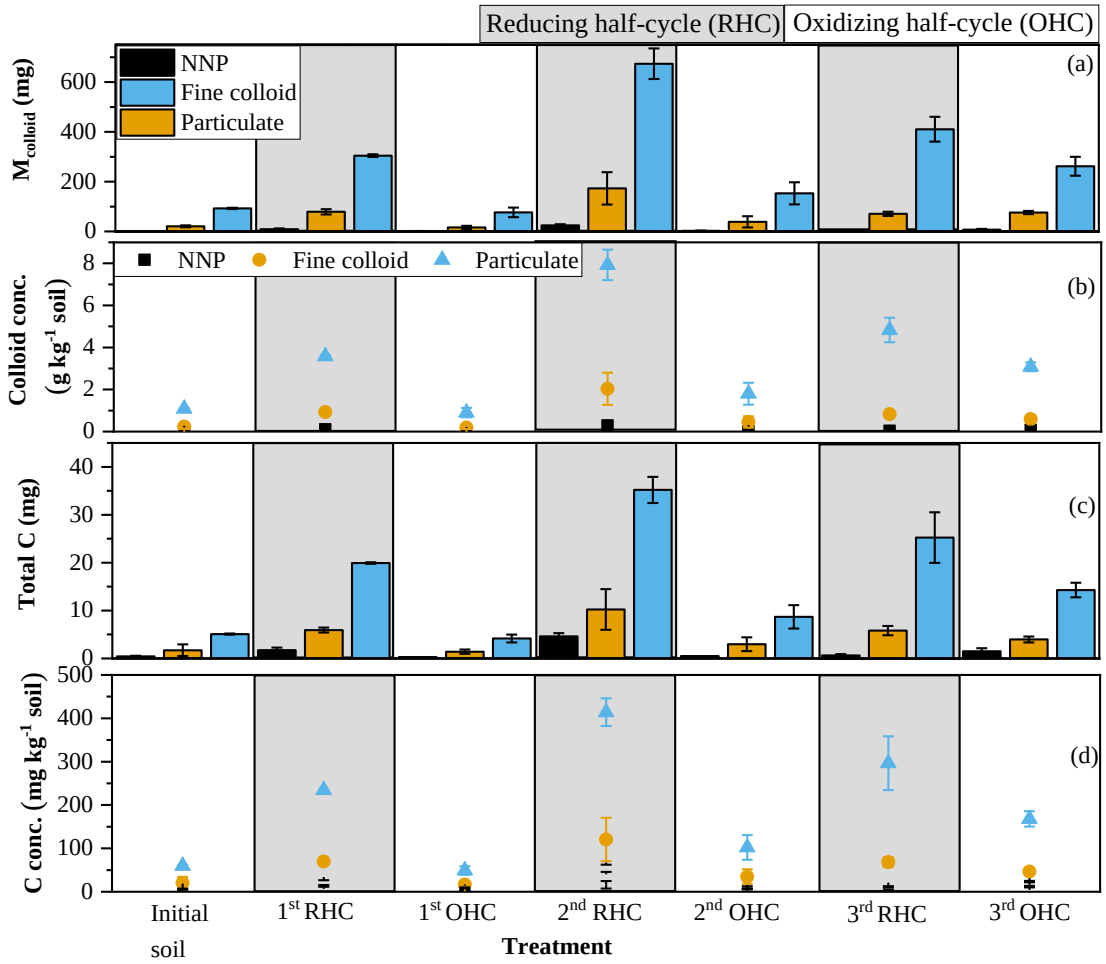

Figure 2.6: (a) Total mass of size-fractionated particles ($[M]_{particle}$, mg); (b) particle concentrations ($[particle]_{soil}$, g kg^{-1} soil); (c) total mass of C (M_C, mg); and (d) C concentrations ($[C]_{soil}$, mg kg^{-1} soil). Concentrations are calculated based on the oven-dry weight of soil suspension. The error bars indicate standard deviations among replicates.

Consistent with other studies (Grybos et al., 2009; F. Hagedorn et al., 2000; Olivie-Lauquet et al., 2001), RHC samples contained more C than the samples from complete oscillations (RHC + OHC). Under reduced condition, dissolution of Fe-oxide coatings and/or concomitant changes in pH can mobilize OC associated with the

minerals (Ryan and Gschwend, 1994a; Thompson et al., 2006). Until 2nd complete oscillation, RHC treated samples had 3-10 times more C than OHC. However, following the 3rd RHC, size-fractionated particles had only 1-2 times more C than the 3rd OHC. The changes in OC concentration along the redox oscillations might be due to the variation in redox potentials and possible de novo synthesis colloid particles with different surface charge properties. Microcosms had the lowest pE values after the 2nd RHC (-0.13 ± 0.8) compared to the 1st (2.62 ± 0.53) and the 3rd (0.24 ± 0.58) RHCs (**Figure 2.4**), which would favor Fe reduction and concomitant release of more colloids and OC during the 2nd RHC. In a closed system, Thompson et al. (2006b) repeated that redox oscillations could increase Fe crystallinity in soil by converting short-range ordered Fe minerals into less soluble, more crystalline Fe-oxides (e.g., goethite and hematite). Further, colloid and OC concentrations after each complete oscillation also increased, which might be due to the increase in colloid stability resulting from redox oscillations, as proposed by Thompson et al. (2006a). Overall, after the 3rd complete redox oscillation, C concentration in the respective NNP, fine colloid, and particulate fractions increased by 349±101%, 159±38%, and 281±33% relative to the concentration measured for the initial (control) soil (**Table 2.2**).

2.3.3 Stable Isotopic ($\delta^{13}C$, $\delta^{15}N$) Signatures

Stable isotopes of C ($\delta^{13}C$) and N ($\delta^{15}N$) values show the molecular heterogeneity among size-fractionated particles (**Figure 2.7** and **Table 2.3**). The $\delta^{13}C$ values enriched significantly ($p < 0.001$, **Table 2.4**) with increasing size: NNP (-29.64 ± 0.32 ‰) < fine colloid (-28.81 ± 0.31 ‰) < particulate (-28.34 ± 0.25 ‰). Similar trends were also observed in the $\delta^{15}N$ isotope signatures, ranging from 1.72 ± 0.56 ‰, 1.95 ± 0.69 ‰ and 2.81 ± 0.81 ‰ for NNP, fine colloid, and particulate size fractions,

respectively. Higher $\delta^{13}C$ and $\delta^{15}N$ values indicate enrichment of heavier isotopes (^{13}C and ^{15}N; Fry, 2006). Enrichment of heavier stable isotopes in larger size fractions is also consistent with results from (Guo and Macdonald, 2006), in which a consistent increase in $\delta^{13}C$ and $\delta^{15}N$ values was reported from colloid (1 kDa-450 nm) to particulate (>450 nm) OM fractions in samples from the upper Yukon River.

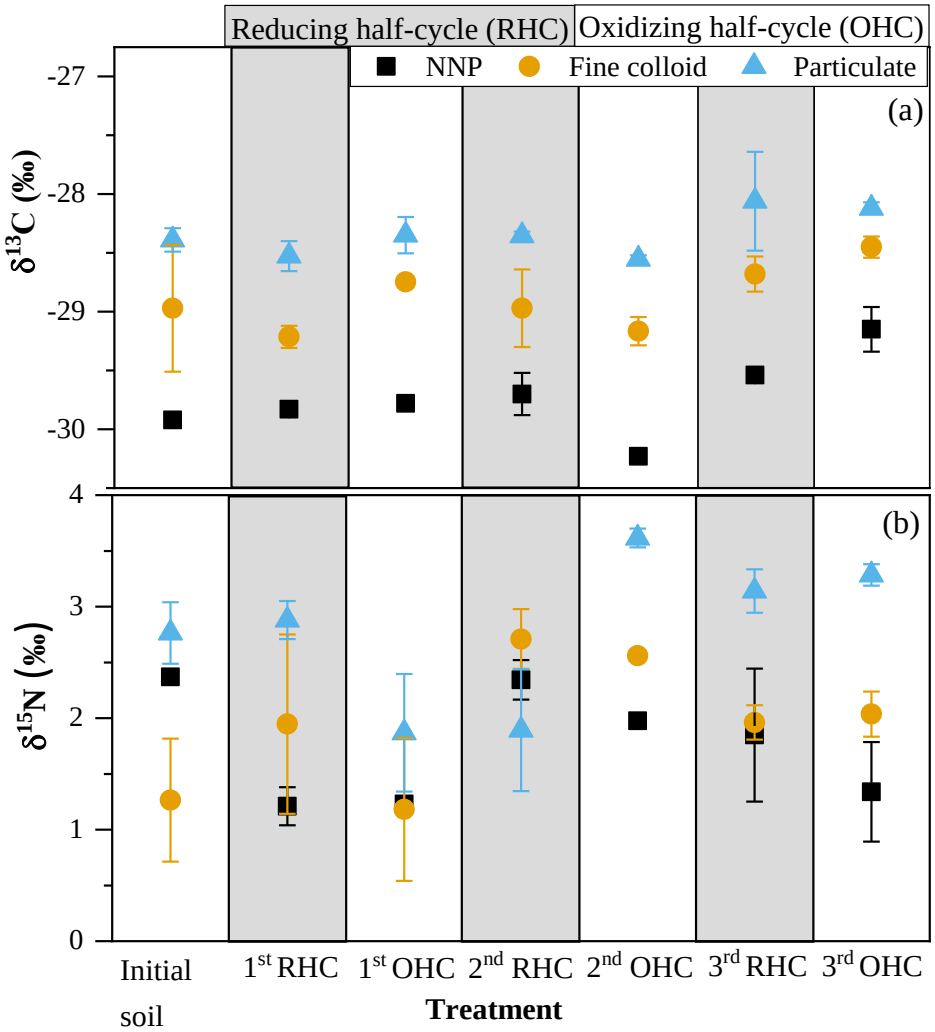

Figure 2.7: Variation in isotope values of (a) C ($\delta^{13}C$, ‰) and (b) N ($\delta^{15}N$, ‰) in size-fractionated particles as a function of redox oscillations. The error bars represent standard deviations in stable isotope values among replicates.

Table 2.2: Changes in C and particle concentration in different size factions along the redox oscillations

Cycle	Treatment	Size (nm)	Total C (mg)	C concentration ($mgkg^{-1}$ soil)	% of total C (2.3-1000 nm)	particle concentration (gkg^{-1} soil)	% of total particles	Normalized C concentration (in %)*
	Control	2.3-100	0.43±0.13	5.05±1.58	6±2	0.02±0.00	1±0.4	
		100-450	1.72±1.22	20.19±14.30	28±5	0.24±0.10	18±5.7	
		450-1000	5.09±0.12	59.91±1.42	67±5	1.09±0.00	81±5.7	
1	Reducing half-cycle	2.3-100	1.73±0.54	20.33±6.36	6±2	0.11±0.03	2±0.6	432±215
		100-450	5.93±0.51	69.77±5.96	21±1	0.93±0.12	20±1.8	239±62
		450-1000	19.93±0.17	234.47±1.99	72±3	3.58±0.07	78±2.3	391±8
	1^{st} redox oscillation	2.3-100	0.29±0.04	3.36±0.47	5±1	0.02±0.00	1±0.3	71±27
		100-450	1.41±0.45	16.63±5.31	24±3	0.19±0.07	17±3.6	55±10
		450-1000	4.16±0.83	48.99±9.73	71±2	0.90±0.23	81±3.4	82±16
2	Reducing half-cycle	2.3-100	4.60±0.69	54.09±8.14	9	0.29±0.05	3±0.4	1131±320
		100-450	10.24±4.25	120.45±50	20±6	2.04±0.77	19±4.8	412±172
		450-1000	35.20±2.72	414.06±32	71±6	7.92±0.72	78±5.0	691±54
	2^{nd} redox oscillation	2.3-100	0.51	6.00±0	4±1	0.03±0.00	1±0.8	126±36
		100-450	2.96±1.44	34.86±16.92	24±7	0.46±0.27	19±8.1	128±90
		450-1000	8.69±2.43	102.27±28.55	72±7	1.80±0.52	79±7.9	170±45
3	Reducing half-cycle	2.3-100	0.64±0.26	7.56±3.05	2±1	0.04±0.01	1±0.3	170±110
		100-450	5.81±0.98	68.40±11.52	18±2	0.83±0.10	15±0.5	240±99
		450-1000	25.24±5.27	296.97±62.04	79±3	4.83±0.59	85±0.8	494±94
	3^{rd} redox oscillation	2.3-100	1.50±0.65	17.64±7.64	7±3	0.08±0.04	2±0.9	349±101
		100-450	3.96±0.61	46.62±7.22	20±2	0.60±0.08	16±0.9	159±38
		450-1000	14.28±1.51	168.03±17.81	72±2	3.08±0.21	82±1.4	281±33

* Normalized C concentrations in each half cycle were calculated relative to the initial (control) C concentration in each size fraction.

Table 2.3: Changes in stable C and N isotope signatures ($\delta^{13}C$, $\delta^{15}N$) in size-fractionated samples along the redox oscillations

Cycle	Treatment	Size (nm)	Stable ^{13}C isotope ($\delta^{13}C$)	Stable ^{15}N isotope ($\delta^{15}N$)
	Initial soil (Control)	2.3-100 100-450 450-1000	-29.92 -28.97 ± 0.54 -28.39 ± 0.10	2.37 1.27 ± 0.55 2.76 ± 0.28
1	Reducing half-cycle	2.3-100 100-450 450-1000	-29.83 ± 0.06 -29.21 ± 0.09 -28.53 ± 0.13	1.21 ± 0.17 1.95 ± 0.80 2.88 ± 0.07
	1st redox oscillation	2.3-100 100-450 450-1000	-29.78 -28.75 ± 0.05 -28.35 ± 0.16	1.23 1.18 ± 0.64 1.87 ± 0.53
2	Reducing half-cycle	2.3-100 100-450 450-1000	-29.70 ± 0.18 -28.97 ± 0.33 -28.36 ± 0.04	2.34 ± 0.18 2.71 ± 0.27 1.89 ± 0.55
	2nd redox oscillation	2.3-100 100-450 450-1000	-30.23 -29.17 ± 0.12 -28.55 ± 0.03	1.98 2.56 ± 0.03 3.62 ± 0.08
3	Reducing half-cycle	2.3-100 100-450 450-1000	-29.54 ± 0.06 -28.68 ± 0.15 -28.06 ± 0.42	1.85 ± 0.60 1.96 ± 0.15 3.14 ± 0.19
	3rd redox oscillation	2.3-100 100-450 450-1000	-29.15 ± 0.19 -28.45 ± 0.09 -28.12 ± 0.05	1.34 ± 0.45 2.04 ± 0.20 3.28 ± 0.15

Table 2.4: Two-way ANOVA test for isotope effects

Treatment	Degree of freedom	Sum Sq.	Mean Sq.	F value
Redox oscillations	6	2.31	0.39	8.89***
Size	2	15.33	7.67	177.15***
Redox oscillations: size	10	0.42	0.04	0.81
Residuals	38	1.51	0.04	

Significant code: `***´ 0.001 level. There were 7 missing data.

Enrichment of heavier isotopes is often speculated to be due to greater microbial processed OC (Dijkstra et al., 2006; Ehleringer et al., 2000; Sollins et al., 2009). Microbes preferentially utilize ^{13}C-depleted molecules for respiration, while ^{13}C-enriched molecules tend to be used for the synthesis of microbial biomass and metabolites (Dijkstra et al., 2006; Emmerton et al., 2001). As a result, decomposition of SOM leads to an enrichment of $\delta^{13}C$ in microbial biomass and residual C pool. Gradual $\delta^{13}C$ enrichment (and analogously $\delta^{15}N$) from NNP to particulate fraction thus indicates presence of more microbial-derived C than plant-derived C in the larger size fractions. Previous studies have reported that plant-derived lignin compounds are usually depleted in heavier $\delta^{13}C$ isotopes than other types of SOM (Buettner et al., 2014; Schulten, 1999). Size-dependent heterogeneity in isotope signatures became more visible when $\delta^{13}C$ and $\delta^{15}N$ values were plotted in "isotope space" (**Figure 2.8a**).

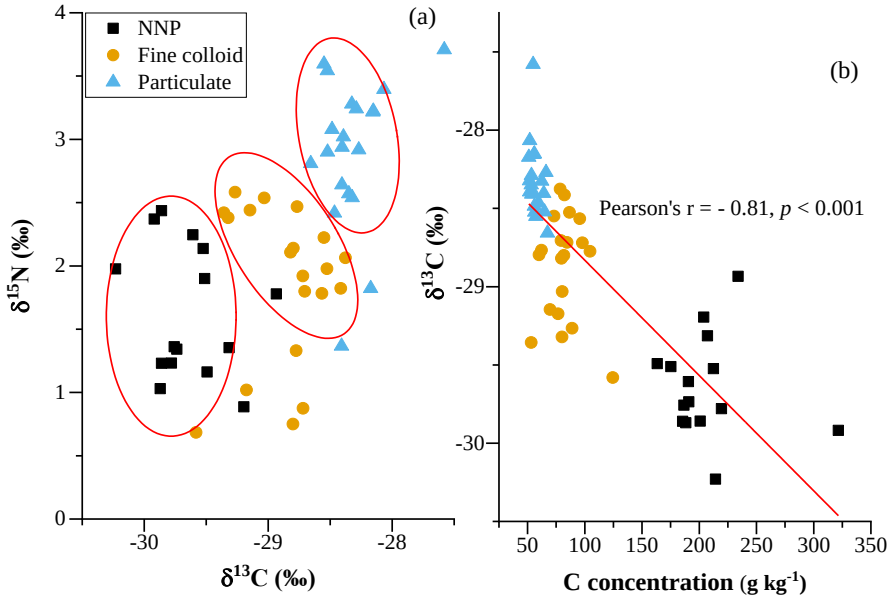

Figure 2.8: (a) Isotope values of C ($\delta^{13}C$) vs N ($\delta^{15}N$) of size-fractionated colloid particles; (b) relationship between isotopes and concentration of C.

With respect to the effects of redox oscillations, all size fractions became enriched in $\delta^{13}C$ values compared to the initial soil except the 2nd OHC, indicating an abundance of more microbial metabolites upon redox reactions. After 3rd redox oscillation, NNP, fine colloid, and particulate fractions became enriched in heaver $\delta^{13}C$ values by 0.77 ± 0.19 ‰, 0.53 ± 0.55 ‰, and 0.27 ± 0.11 ‰, respectively. However, anomalous trends were observed in $\delta^{15}N$ values along the redox oscillations, that is, $\delta^{15}N$ values decreased by ~1 ‰ during the 1st redox oscillation. Smaller particles responded more quickly to redox changes as shown by their early drop in $\delta^{15}N$ values. However, size-fractionated particles became enriched during the 2nd redox oscillation followed by a continuous drop in the heavier $\delta^{15}N$ isotopes. The changes in stable $\delta^{15}N$ values might be related to the biogeochemical cycling of organic N, however, I could not make any definite conclusion due to the lack of mass balance of total N. Further research is needed to investigate the size-specific biogeochemical cycling of organic-N under redox oscillation processes. Here, I posit that changes in $\delta^{15}N$ might reflect a shift from N assimilation to N dissimilation process, driven by respective higher C availability at the beginning and lower C availability at the later stages of our incubation study (Dijkstra et al., 2006). The observed depletion of $\delta^{15}N$ is consistent with the reported isotope fractionation range (-1.6 to +1 ‰) during N assimilation by microorganisms (Hübner, 1986). Other N transformation processes, e.g., NH_3 volatilization, nitrification and denitrification cause higher isotope fractionation than those associated with N assimilation and dissimilation (Kendall, 1998). It should also be noted that the C and N pool sizes can also influence the measured isotope values. If the C pool is small, isotope fractionation would trigger a bigger change in the $\delta^{13}C$ values due to the OC recycling. A

proportional recycling is possible but rare. Among the three size fractions, the least amount of C was partitioned at NNP, which had gradual $\delta^{13}C$ enrichment indicating the influence of OC pool sizes on final $\delta^{13}C$ values after cumulative redox oscillations.

To further examine dynamics of C under redox oscillations, I plotted the $\delta^{13}C$ values of size-fractionated OC against the logarithm of its concentration (**Figure 2.8b**). The regression plot was highly significant ($p < 0.001$) and the $\delta^{13}C$ values increased with decreasing C concentrations along a size continuum from NNP to particulate. Relatively large variations in $\delta^{13}C$ and $\delta^{15}N$ values thus confirm our hypothesis that NNP, fine colloid, and particulate fractions have widely diverse molecular compositions. Therefore, quantification and molecular characterization of size-specific organo-mineral associations are crucial for better understanding of the dynamics of OC in wetlands.

2.3.4 Linking Surficial Elemental Composition of Soil Minerals to Associated Organic C and N

Complement to the IRMS, XPS analyses provide information on surface composition of mineral matrices and functional groups of associated OC. Normalized atomic percentages of Al, Si, Fe, C, and N in size-fractionated particles are presented in **Figure 2.9**. Additionally, minor amounts of K, Mg, Mn, and Ca were also detected. Among the different size fractions, NNP had significantly ($p < 0.001$) the lowest % of Al, Si, and Fe and the highest % of C and N than the fine colloid and particulate fractions. The highest surface atomic % of C and N in NNP is also consistent to their bulk concentrations as determined from IRMS analyses. The strong negative correlations between C and other elements e.g., Al ($r^2 = 0.95$, $p < 0.01$), Fe ($r^2 = 0.32$, $p < 0.05$), Si ($r^2 = 0.93$, $p < 0.01$), and Mg ($r^2 = 0.58$, $p < 0.01$) indicate an overall

increase in surface coating of OC over the underlying mineral phases with increasing C concentration (**Figure 2.10**). Woche et al. (2017) found similar strong negative relationship between C and other elements during biogeochemical interface (BGI) formation. Additionally, strong positive relationship between C and N ($r^2 = 0.79$, $p < 0.01$) suggests that both C and N originated from organic fractions and agrees well with the values obtained from IRMS analyses ($r^2 = 0.97$, $p < 0.001$). The location of the deconvoluted N spectra confirms that SOM is the main source of the surface N within 2.3-1000 nm size range. N spectrum detected at a binding energy of 399-400 eV usually corresponds to organic-N, while mineral-N provides peaks at ~401.2 eV (NH_4^+) and 406-407 eV (NO_3^-) (Gerin et al., 2003). In our study, mineral-N was observed mostly at <2.3 nm size fraction (**Figure 2.11**). Size-dependent heterogeneity in the composition and reactivity of minerals is likely to play an important role in organo-mineral interactions. Strong linear regression between size-fractionated colloid particles and associated OC (**Figure 2.12**) points to the significance of organo-mineral associations to the sequestration of OC in soil that have been receiving increasing attention over the past three decades (Baldock and Skjemstad, 2000; Sollins et al., 1996). Due to sample scarcity, I was unable to run x-ray diffraction (XRD) analysis to investigate the mineralogical composition of different size fractions. However, XPS could compensate to some extent as it provides quantitative information of all surface elements (except H and He). For example, Mg/Al ratio (indicative of smectites) was the highest in NNP and decreased with increasing particle sizes (**Figure 2.13**), which suggests presence of less smectite minerals in larger size fractions. In soil, phyllosilicates, e.g., smectites are typically smaller than kaolinite and illite and are mostly concentrated in <100 nm size particles (Grim, 1953; Jepson, 1984; Muir et al.,

1957; Tsao et al., 2013). Consistent with previous studies (Arnarson and Keil, 2001; Barr et al., 1999) and based on measured Mg/Al ratios, it is likely that the smaller fractions are more abundant in Mg-smectites. Having a large specific surface area enables these minerals to have more OC attached to the NNPs (Bock and Mayer, 2000; Ransom et al., 1997).

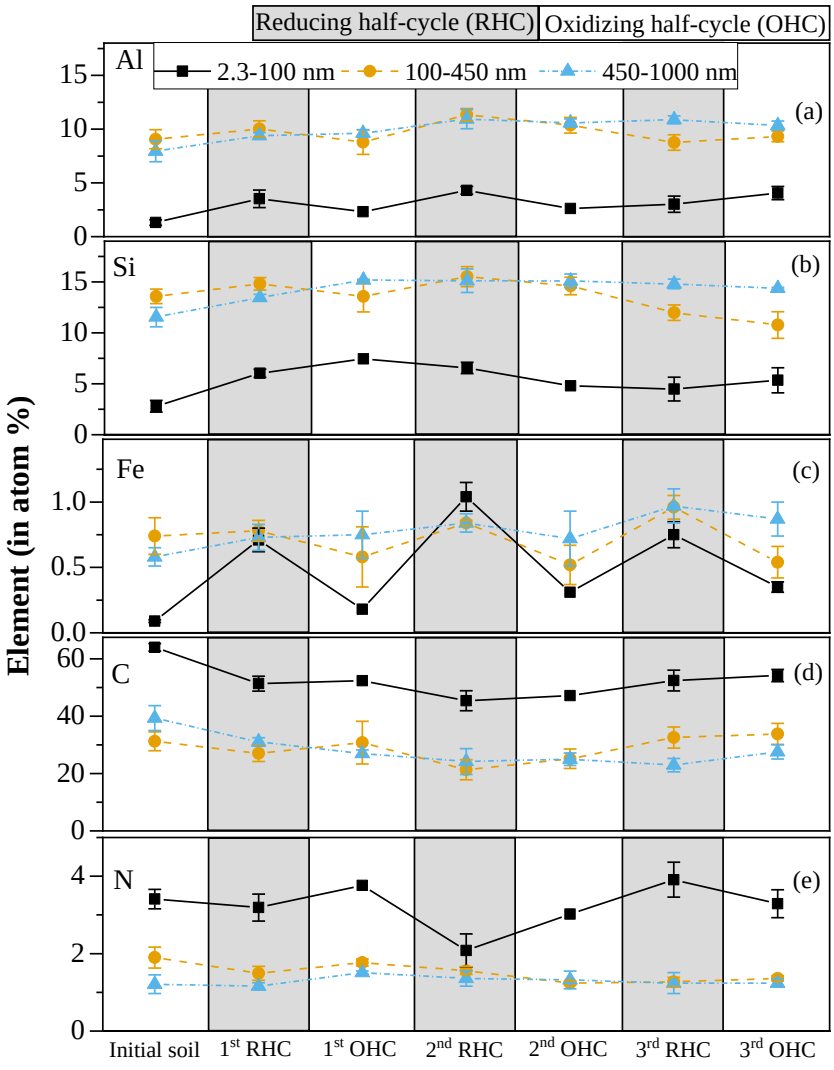

Figure 2.9: Variation in the atomic % of surficial (a) Al; (b) Si; (c) Fe; (d) C; and (e) N as a function of redox oscillations determined by XPS.

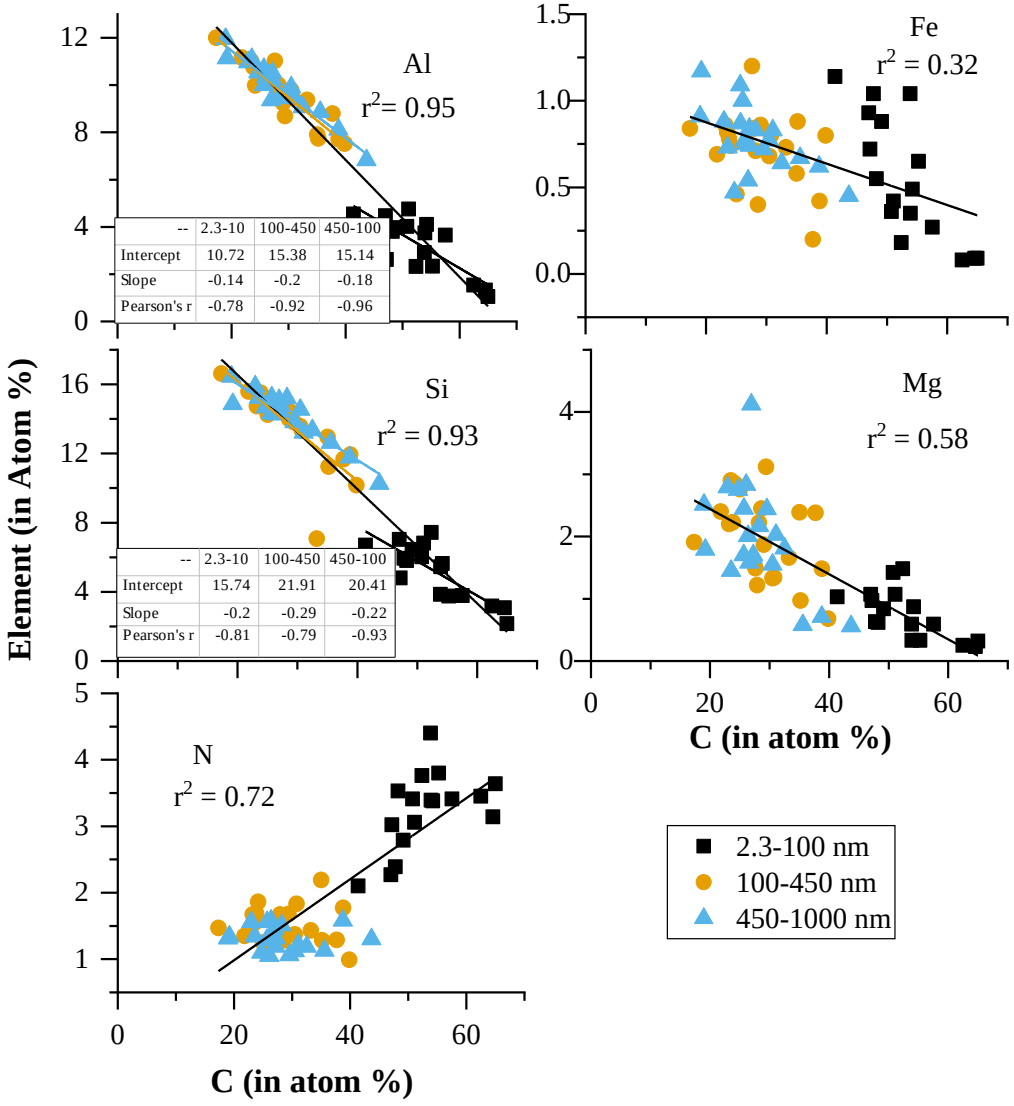

Figure 2.10: Regression plots of XPS-based surficial atomic % of Al, Fe, Si, Mg, and N with C atom %. Except Fe, all the relationships are significant at $p < 0.01$ level. Relationship between atom % of Fe and C was significant at $p < 0.05$.

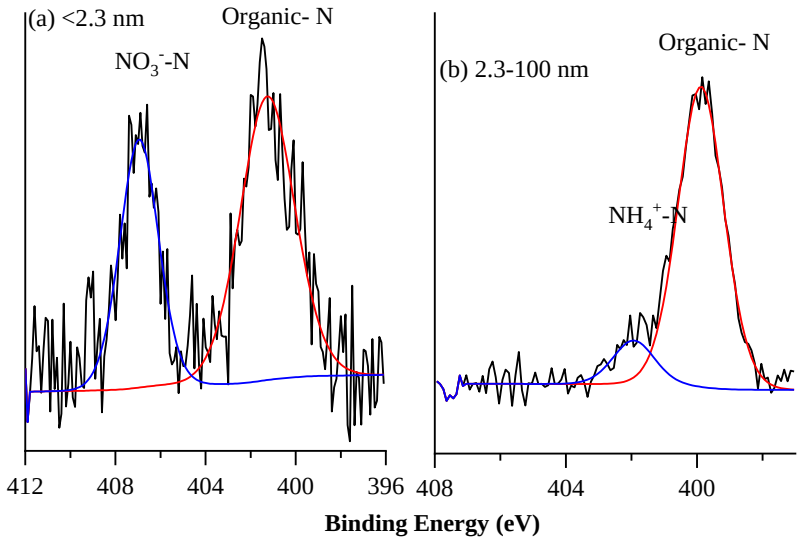

Figure 2.11: High-resolution XPS N 1s spectra of mineral-SOM complexes and de-convoluted sub-peaks as assigned to different N components, (a) <2.3 nm and (b) 2.3-100 nm.

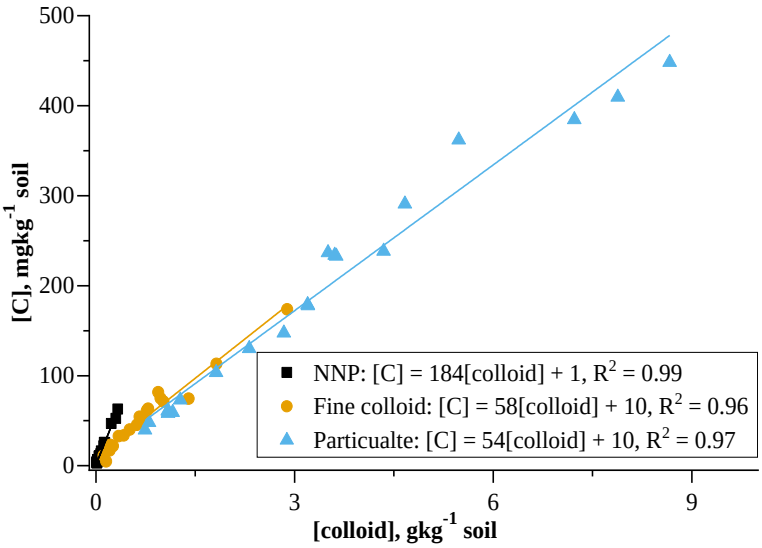

Figure 2.12: Regression plots of total mass of C (M_C, mg) with total mass of colloids ($M_{colloid}$, mg) at (a) 2.3-100 nm; (b) 100-450 nm; and (c) 450-100 nm size fractions.

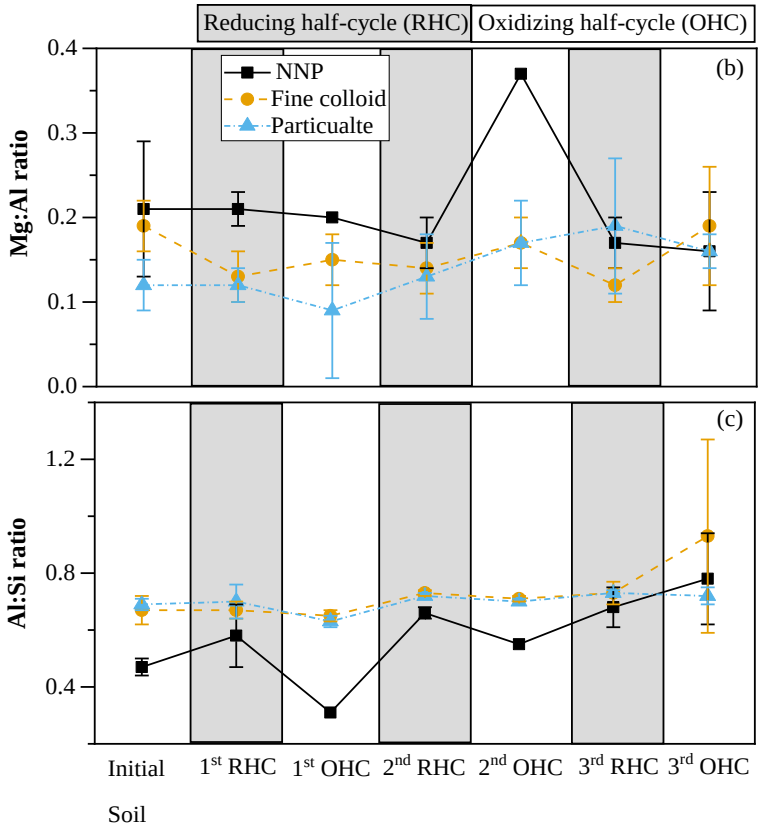

Figure 2.13: Surface (a) Mg/Al and (b) Al/Si ratios as obtained from XPS analyses.

2.3.5 Speciation of Organic C and Selective Sorption on Mineral Surfaces

The C 1*s* XPS spectrum was de-convoluted into 3 main peaks representing the most reduced (C-C, C-H) aliphatic or aromatic C (44.58%), the C-O/C-N peak that is indicative of amines and/or alcohols like those in polysaccharides and amino acids (28-34%) and the most oxidized (C=O) carbonyl/carboxyl C (12-33%) (**Figure 2.14**). Selective adsorption of reduced aliphatic and aromatic C over oxidized carbonyl/carboxyl C agrees well with Kothawala et al. (2012). However, considerable evidence suggested that the concentration and composition of dissolved organic matter (DOM) can influence the selectivity of OC functional groups to mineral surfaces. For

example, Avneri-Katz et al. (2017) studied adsorption of biosolid DOM on soil mineral surfaces and observed preferential sorption of hydrophobic DOM components on mineral surfaces relative to hydrophilic components at high DOM concentration. Hydrophobic DOM components include aromatic units associated with aliphatic moieties (Chefet et al., 1998). Young et al. (2018) demonstrated that the non-selective sorption of nitrogen-rich, biosolid DOM on Fe(III)-montmorillonite surfaces contributed substantially to the formation of organo-mineral association. The NNP fraction had a greater proportion of most oxidized C species than other larger size fractions, while the particulate fraction had higher proportion of aliphatic/aromatic C groups. Such size dependent heterogeneity in C functional groups clearly demonstrates the selective sorption of more degraded and highly oxidized C species in smaller size fractions. The ratios of aromatic or aliphatic C (most reduced) to alcohol/amine C and to carbonyl/carboxyl C (most oxidized) increased from NNP to particulate fractions (**Figure 2.15**). Together with the $\delta^{13}C$ and $\delta^{15}N$ stable isotope data, an increase in the reduced to oxidized form of C species suggest an increasing abundance of more stable, microbial-derived C in the larger size fractions. Based on XPS and solid-state C^{13}-nuclear magnetic resonance (NMR) spectroscopy analyses, Gentsch et al. (2015) also linked an increase in reduced to oxidized C species to the presence of more decomposed, microbial-derived C. Microbial-derived C has been recognized to form stable SOM (Gleixner et al., 1999; Huang et al., 1998; Knicker, 2011; Kögel-Knabner et al., 2008a). Microbes preferentially utilize more labile plant constituents, produce metabolites that serve as the main precursors of decomposition-resistant, stable SOM, and promote aggregation with soil matrix (Cotrufo et al., 2013). Stabilization of SOM is further favored by thermodynamic limitations of oxidation of highly reduced C

compounds under anoxic conditions (Boye et al., 2017). Our findings collectively suggest the significance of microbial-derived C to form organo-mineral and organo-metal oxide associations, which are considered as one of the important stabilization mechanisms of SOM (Baldock and Skjemstad, 2000; Kleber et al., 2015).

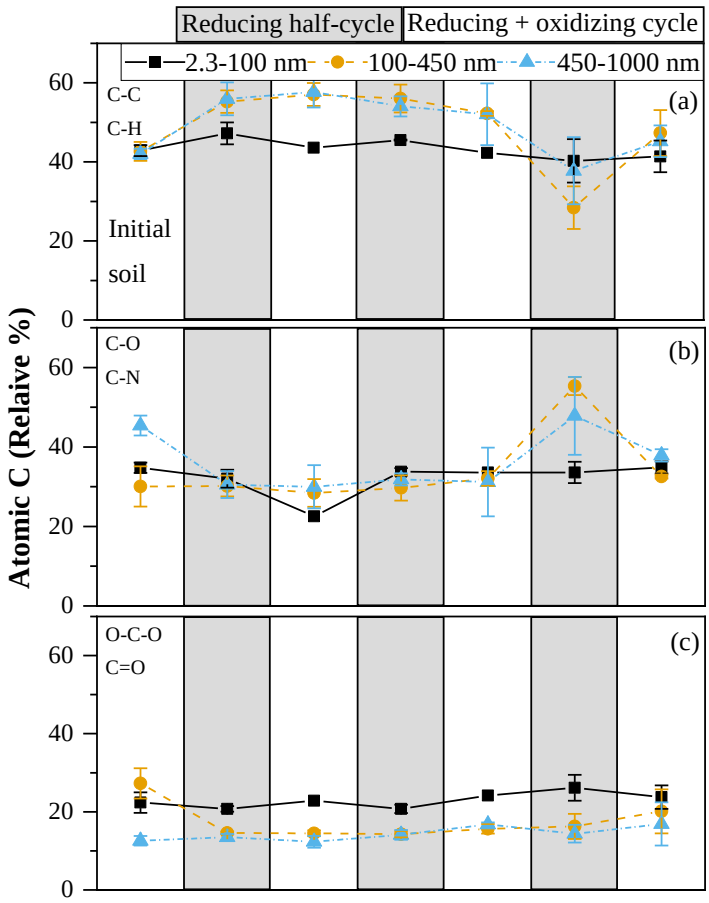

Figure 2.14: Different C functional groups as de-convoluted from C_{1s} XPS spectra. (a) aliphatic or aromatic C (C-C, C-H); (b) amines and/or alcohols like those in polysaccharides and amino acids (C-O, C-N); and (c) carbonyl/carboxyl C (C=O), each expressed by relative atom percent of the total C signal in size-fractionated samples (2.3-100 nm, 100-450 nm, and 450-1000 nm) as a function of redox oscillations.

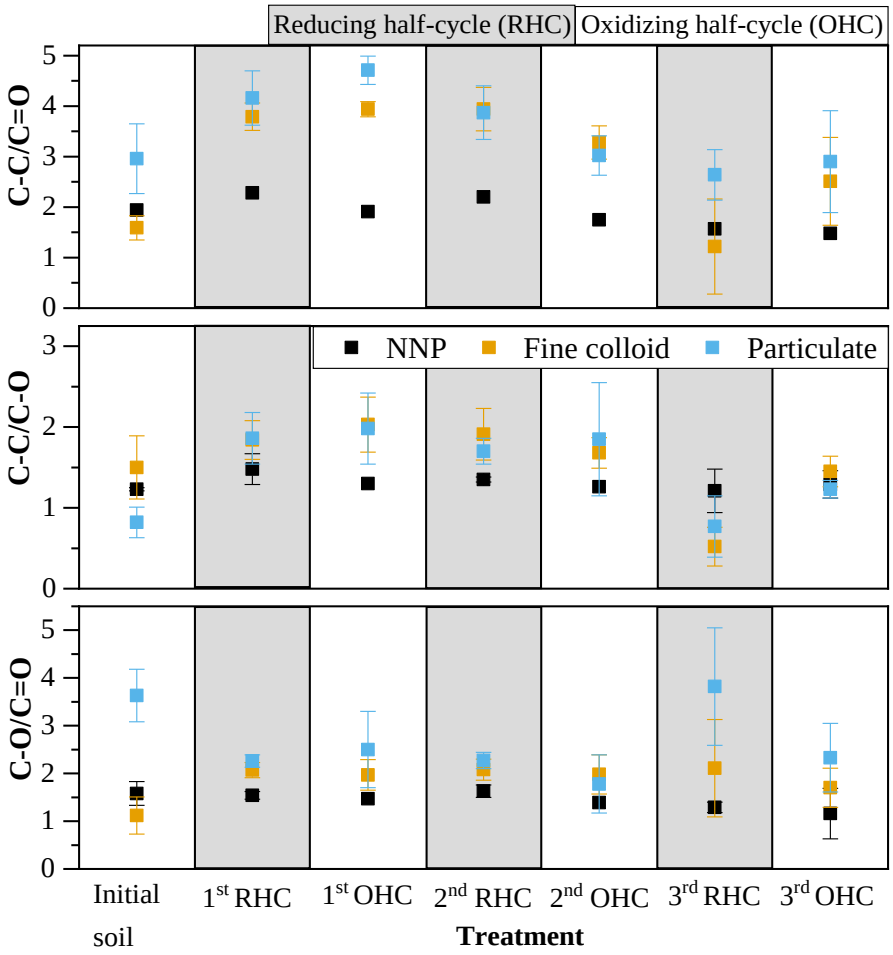

Figure 2.15: Ratios of atomic % of different C functional groups in size-fractionated particles plotted by redox oscillations. The error bars represent standard deviations among replicates.

2.3.6 Size-Dependent Mineral-OC Interactions

The assemblages of SOM to mineral surfaces may depend on the heterogeneity in the C and N bonding environment. The selective attachment and release of C to/from different mineral surfaces are controlled by their associated bonding mechanisms. For example, enrichment of oxidized C species (e.g., C-O, C=O) supports the significance of ligand exchange reaction and/or H-bonding with the

mineral matrices of NNPs. Phyllosilicate (e.g., smectite) dominated fraction was found to have the highest proportion of oxidized C species in protonated amide forms (Jones and Singh, 2014).

Here, the basal oxygen planes of smectite minerals can act as weak electron donors and form H-bonds with oxidized C species (Jones and Singh, 2014; Mortland, 1986). Additionally, Fe oxide minerals have higher affinity for highly oxidized, lignin-derived organic molecules (Kaiser et al., 1997; Mikutta et al., 2007) because ligand exchange reaction is the dominant bonding mechanism between SOM and iron oxides (Jones and Singh, 2014). Presence of more oxidized C species and higher Mg/Al ratios at NNP indicate greater degree of oxidative alteration and/or a stronger retention of OM components to mineral surfaces. Different from the NNP fraction, fine colloid and particulate fractions were enriched in aliphatic and aromatic C species. For soils with higher aliphatic C species, non-ionic lipids and ligand bonds are proposed to dominate the interactions between SOM and mineral surfaces (Gillabel et al., 2010; Jones and Singh, 2014; Kleber et al., 2015). Thus, organo-mineral associations might dominantly have ligand bonds at fine colloid and particulate size fractions that contain mostly microbial-derived C based on IRMS and XPS analyses.

Increase in soil particle and C concentrations (**Figure 2.6**) and presence of more microbial-derived C in NNP to particulate size fractions following redox oscillations are in good agreement with the three-dimensional conceptual view of C turnover dynamics as proposed by Kleber and Johnson (2010). Previously, the two-dimensional concept considered soil as a system composed of adsorbent (mineral surface) and adsorbate (SOM). This concept is now extended to the three-dimensional view assuming that colloid to sub-colloid sized organo-mineral associations are

considered as an important composite building units of soil micro aggregates (Kögel-Knabner et al., 2008a; Lehmann et al., 2007; Totsche et al., 2018). Based on the surface properties, SOM and minerals can adhere together to form the association and in contrast to the plant-derived C, microbial-derived C actively contribute to the formation of such stable nano and colloid sized organo-mineral associations (Asano and Wagai, 2015). Formation of organo-mineral associations are common in soil both in the mobile and immobile phases (Buettner et al., 2014; Totsche et al., 2018). Here I posit that microbial-derived C enhanced the formation of more nano and colloid sized organo-mineral associations as indicated from the increase in soil particle and C concentrations following the redox oscillations processes.

2.3.7 Layer Thickness of Surficial OM

Although XPS measurements do not provide information about the spatial distribution of adsorbed materials on mineral surfaces, layer thickness (t, nm) of surface SOM (Y) coating is often determined following a simplified model (Pantano and Wittberg, 1990; Woche et al., 2017). This approach ideally assumes a homogeneous and continuous coating of OM on mineral surfaces, although direct analyses by transmission electron microscopy and nano-scale secondary ion mass spectrometry (nanoSIMS) have shown that OM exists in patches on mineral surfaces (Heister et al., 2012; Vogel et al., 2014). Briefly, the thickness is calculated from the potential energy (PE) mean free path λ (nm) of an element X in the underlying minerals. The content of X is determined for both coated and non-coated surfaces. For a non-coated surface, the value of X is calculated from the regression analysis using a PE with similar λ of an element Y occurring in the coating (Appendix C). Here, I assumed that the roughness of all samples was the same on the scale of the x-ray spot

size and calculated mean layer thicknesses for all particle size fractions (n= 17 or 21). For simplicity, an additional assumption was made that there were only two layers to the material. The bottom layer was mainly Si (X_i; Si_{2p}, λ=3.2 nm; λ_{Si}) and Al (X_2; Al_{2p}; λ= 3 nm; λ_{Al}) and the surface layer was mostly OC (Y; C_{1s}; λ=3.0 nm) and the two layers did not overlap. The assumption is based on the highest atom % of Si and Al as revealed from XPS analyses (**Figure 2.9**). This model, of course, is an oversimplification for the non-ideal, heterogeneous soil particles. The rough soil surface can also emit electrons at many angles, and therefore may vary in the thickness of adsorbed components. Nevertheless, this model has been previously used (Gerin et al., 2003; Woche et al., 2017) to estimate an average thickness of OC attached to the mineral surfaces. The calculation revealed that the NNP had the highest mean layer thickness of surface OC coating (3.91 ± 1.25 nm), followed by fine colloid (1.55 ± 0.46 nm) and particulate (1.27 ± 0.36 nm) fractions. The significant relationships between mean layer thickness and atom C% in NNP (r^2 = 0.74), fine colloid (r^2 = 0.80), and particulate fractions (r^2 = 0.93) indicate SOM as the main coating component on mineral surfaces (**Figure 2.16**). The variations in the thickness of OM coating on mineral surfaces may be an indication that the associations between mineral and SOM surfaces vary at sub-micron size fractions, which is discussed further in the following section.

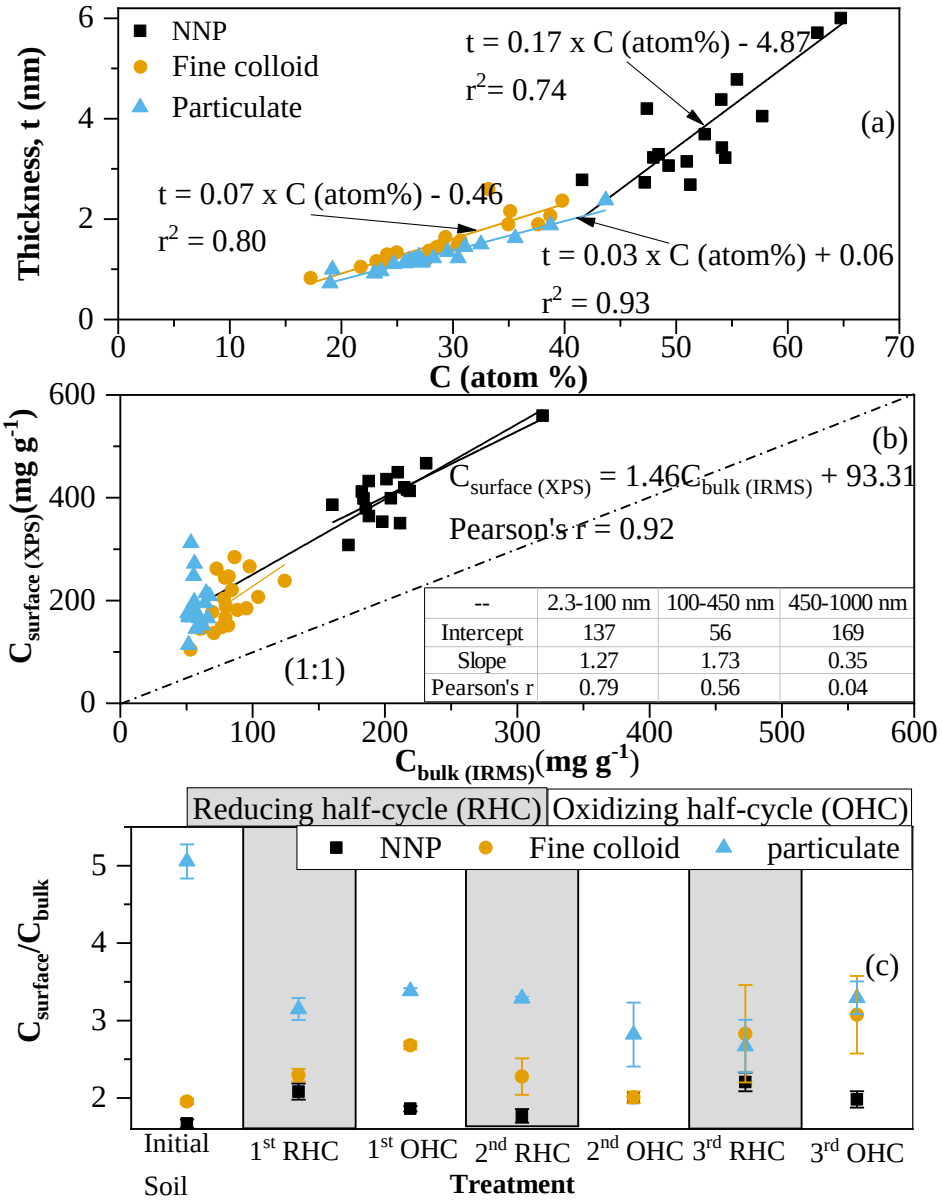

Figure 2.16: (a) Regression plots between the layer thickness (t, nm) of the SOM coatings on the mineral surfaces and the surface C (atom %) content in different size fractions measured by XPS; (b) relationship between surface C concentration ($C_{surface}$) measured by XPS and bulk C concentration (C_{bulk}) measured by IRMS; (c) variation in C surface enrichment factor ($C_{surface}/C_{bulk}$) in different size fractions as a function of redox oscillations.

2.3.8 Relationship between Surface and Bulk C

Figure 2.16b shows the surface C concentration ($C_{surface}$, measured by XPS) as a function of its bulk concentration (C_{bulk}, measured by IRMS) for different size fractions. The linear relationship between $C_{surface}$ vs C_{bulk} of NNPs deviated more from the 1:1 line than other size fractions, indicating that the surfaces of NNP are more enriched in C (Gerin et al., 2003). The C enrichment factors ($C_{surface}/C_{bulk}$) under alternating redox oscillation conditions for different size fractions show a significant increase in the surface C concentration relative to the bulk with increasing particle size and the values ranged from 1.92 ± 0.22, 2.47 ± 0.50, and 3.36 ± 0.66 for NNP, fine colloid, and particulate fractions, respectively (**Figure 2.16c** and **Table 2.5**). Repeated redox oscillations decreased the enrichment factor in the particulate size fraction while increased in other two size fractions. These observations indicate that OM primarily exists as coatings on minerals surfaces rather than being dispersed or incorporated into soil particle structures on larger size fractions while the smaller fractions are mostly organic materials with some minerals glued to them. Previous studies (Arnarson and Keil, 2007; Jones and Singh, 2014) also observed an increase in C enrichment factor from lighter to heavier fractions and suggested that the heavier fractions are mostly mineral aggregates with increasing C concentration on the mineral surfaces relative to the bulk C concentration.

Table 2.5: Two-way ANOVA test for variation in surface enrichment factor ($C_{surface}/C_{bulk}$) as a function of particle sizes and redox oscillations

Treatment	Degree of freedom	Sum Sq.	Mean Sq.	F value
Redox oscillations	6	1.51	0.25	4.06**
Size	2	21.40	10.70	172.11***
Redox oscillations: size	12	9.45	0.79	12.66***
Residuals	38	2.36	0.06	

Significant codes: `***´0.001, `**´ 0.01 level. There were 4 missing data.

2.4 Conclusions

Being a coastal state in the Northeast region of the United States, Delaware is already facing several challenges due to climate change, such as extreme precipitation, inundation, and sea-level rise (Melillo et al., 2014). Any changes in the frequency, duration and degree of reduced conditions in wetlands will have profound influence on soil biogeochemistry that can modify organo-mineral associations and hence the stability of SOM. Moreover, soluble C formed during anoxic events in wetlands has significant influence on biogeochemical cycles in terrestrial and downstream aquatic ecosystems. I designed our batch incubation study to evaluate how anoxic-oxic events would influence the organo-mineral associations within colloid size range. From this study, I observed that size-fractionated COC varied widely both in concentration and molecular composition. Our results clearly showed that NNP and fine-colloid fractions constituted up to 8.94 ± 0.50% and 22.19 ± 7.52% of bulk C concentration (2.3-1000 nm), respectively, that would be otherwise lumped as “dissolved fraction” (<450 nm) in the operational definition of DOM. The cutoff size range of DOM at 450 nm thus

can significantly overestimate the dissolved phase OC concentration, which can lead to inaccurate assessment of OC fate and transport behavior in the environment. Therefore, understanding of the size-specific molecular composition of COC could improve the accuracy in assessing the mobility, reactivity and environmental functions of OC in redox-sensitive wetlands. Stable $\delta^{13}C$ and $\delta^{15}N$ isotope signatures and XPS analyses demonstrated that microbial metabolites are the pervasive SOM components in fine colloid and particulate size fractions, while NNPs were enriched in plant-derived C. Size-specific, selective attachment and/or release of C to/from different mineral surfaces additionally give weight to the three-dimensional conceptual view of soil micro aggregates by incorporating the microbe-mineral interactions.

Chapter 3

REDOX OSCILLATIONS ENHANCE DESTABILIZATION AND MOBILIZATION OF PROTECTED COLLOIDAL SOIL ORGANIC CARBON

Abstract

In redox dynamic wetlands, the onset of oxic-anoxic events induces biogeochemical processes that may have profound influence on the fate and transport of soil organic carbon (OC). A laboratory soil column study was conducted to investigate the influence of two oxidation-reduction cycles (redox oscillations) on the mobilization of OC. Molecular characteristics of dissolved (< 2.3 nm), natural nanoparticle (NNP, 2.3-100 nm), fine colloid (100-450 nm), and particulate (> 450 nm) OC were examined through spectrofluorometric and stable carbon (C, $\delta^{13}C$) and nitrogen (N, $\delta^{15}N$) isotope analyses. Results showed that bulk OC concentration increased by 425-1018% (121.55 ± 10.53 mg L^{-1}) and 311-830% (97.50 ± 5.36 mg L^{-1}) after respective 1st and 2nd reducing half-cycles (RHCs) in comparison to the oxic (control) soil column leachate (14.24 ± 5.43 mg L^{-1}) samples. Organic C released after the 1st RHC (i.e., single) had greater contributions from NNP and dissolved fractions, higher aromatic C content, and was more biologically reactive than the 2nd RHC (i.e., cumulative). In contrast, OC released after the 2nd RHC had higher contributions from fine colloid and particulate size fractions, and was less aromatic, less biologically reactive, microbial-derived components than the 1st RHC. Our findings show that the less aromatic, microbial-derived C became highly mobile under redox-fluctuating conditions, which could explain the downward migration of this soil OC fraction. The

observed OC release as influenced by their molecular composition and redox fluctuations provides a baseline for the size continuum of soil OC and its potential ecological and environmental roles.

3.1 Introduction

Soil organic carbon (OC) is the most important and largest terrestrial C pool on earth (Lal, 2004). A significant portion of this pool exists in wetlands (535 Gt C, ~ 30% of terrestrial C) (Mitsch and Gosselink, 2007) and is highly vulnerable to hydrological perturbations, which can be exacerbated by climate change. Any changes in the stability and turnover of OC induced by geochemical and climatic factors will have significant impacts on global C cycles (Doetterl et al., 2015). Increasing evidence supports the idea that soil organic matter (SOM) is an ecosystem-level property (Schmidt et al., 2011) and SOM association with mineral phases is one of the key C stabilization mechanisms (Baldock and Skjemstad, 2000; Kleber et al., 2007; Wagai and Mayer, 2007). Thus, systematic studies of the stability and composition of mineral-SOM complexes in soil, particularly in redox-sensitive systems such as wetlands, are warranted.

Redox-induced biogeochemical transformations are among the key processes that control the stabilization of C stocks in soil; more than 90% of which reside in intimate association with minerals (Baisden et al., 2002; Basile-Doelsch et al., 2007; Crow et al., 2007). The stability of SOM-minerals association is influenced by their structural and chemical properties (Kalbitz et al., 2005), as well as by the chemistry of the porewater, e.g., pH, ionic strength (IS), and ionic composition (Bunn et al., 2002). Adsorption or coprecipitation of SOM with Fe- and Al- oxides and hydroxides and formation of bridging complexes with Ca (Mikutta et al., 2007; Weng et al., 2005) can alter particle size, structural order and reactivity of newly formed minerals (Eusterhues et al., 2014; Kleber et al., 2015; Shimizu et al., 2013). Especially minerals with large specific surface area (SSA) are important for OC stabilization. Mineral colloids have very large SSA and reactive site densities due to their small particle size (1 nm to1

μm; Vold and Vold, 1983). Based on soil biogeochemical processes, colloid particles can disperse in the soil solution and thus mobile so that they can facilitate the transport of associated OC through the vadose zone (de Jonge et al., 1998; Sprague et al., 2000; Villholth et al., 2000).

In redox-sensitive environments, colloid mobilization strongly depends on reductive dissolution of Mn- and Fe- oxyhydroxides, shifts in pH driven by redox reactions (Grybos et al., 2009; Thompson et al., 2006) and microbial decomposition of SOM (Guggenberger et al., 1998). Any alteration in soil solution properties, e.g., pE, pH, IS, and ionic composition can influence release and dispersion of colloids, through (i) dissolution of Fe-oxide cements that hold aggregates together, and (ii) pH-dependent changes in mineral surface charge resulting in inter-particle electrostatic repulsion by lowering IS between like-charged particles (Bunn et al., 2002; Heil and Sposito, 1993; Suarez et al., 1984). On the other hand, microorganisms contribute to the formation of organic solutes by releasing microbial metabolites in the soil environment. Based on size, colloids are a transition between dissolved phase and the bulk solid phase, while nanoparticles are a subset of colloid particles with sizes from 1-100 nm (Christian et al., 2008). Traditionally, dissolved organic matter (DOM) is operationally defined as the filtrate that passes through 450 nm filter. This separation overestimates the dissolved phase by including colloids of diameter < 450 nm in it and may lead to an inaccurate interpretation of biodegradability and mobility of OC. Moreover, different cutoff size ranges are often used in different disciplines to define DOC fractions that makes it difficult to compare results in C behavior and processes between different ecosystems and environments. Therefore, more detailed redox-dependent size delineation and characterization of mobile SOM are necessary.

In wetlands, mobile DOM can significantly influence the distribution and cycling of C within and between ecosystems (Kalbitz et al., 2000). In general, DOM is considered as having more plant-derived components in topsoil whereas most subsoil DOM is of microbial origin (Guggenberger and Zech, 1994; Klaus Kaiser et al., 2004; Kaiser and Kalbitz, 2012). In line with this view, surface-reactive C components (e.g., aromatic plant-derived components) are strongly retained by soil matrices and restrained from leaching through the soil profile (Guggenberger and Kaiser, 2003) and the sorbed OM is more recalcitrant to further biodegradation (Karsten Kalbitz et al., 2005). However, recent studies with new molecular and spectroscopic techniques revealed that some decomposition-resistant OM more closely resembles microbial biomass and metabolites (Amelung et al., 2008; Gleixner, 2013; Miltner et al., 2012) and is stabilized via organo-mineral complexation (Baldock and Skjemstad, 2000; Kleber et al., 2015). Grandy and Neff (2008) also reported that the C sorbed on mineral fractions resemble microbially processed OM more than plant-derived components. Thus, the fluxes and accumulation of DOM through soil profile is controlled by the continuous sorption and desorption, combined with microbial processing and subsequent desorption and dissolution (Kalbitz et al., 2000). However, despite the significance of mobile OC in downward cycling of OM through soil profile, a comprehensive view about the fluxes and molecular composition of OC in different size fractions has been elusive so far.

I conducted a soil column study to assess the influence of redox oscillations on the concentration and molecular composition of size-fractionated OC in leachates. I hypothesized that redox potential changes could cause wide shifts in the size-dependent mobilization and composition of aqueous OC in soil. Columns were

systematically maintained under alternate reducing-oxidizing events; leachate samples were collected at defined time intervals and were size-fractionated using differential centrifugation and ultrafiltration. The unique aspects of this work relative to prior studies include 1) redox oscillations were induced in column-flow mode rather than through batch incubation and 2) concentration and molecular composition of aqueous OC were quantified and characterized for multiple size fractions, i.e., dissolved (< 2.3 nm), natural nanoparticles (NNP, 2.3-100 nm), fine colloid (100-450 nm), and particulate (> 450 nm). Total OC concentration, UV-visible absorbance, fluorescence excitation-emission matrices (EEMs), and stable isotope ($\delta^{13}C$, $\delta^{15}N$) fingerprints were measured to elucidate size-dependent heterogeneity in the concentration and molecular composition of aqueous OC.

3.2 Materials and Methods

3.2.1 Soil Description

Soil samples were collected from the top 0-15 cm layer of a freshwater wetland located in the White Clay Creek (WCC) watersheds, Delaware, USA. It is one of the four major watersheds in the 1463 km^2 6^{th}-order Christina River Basin - a part of the larger 33,700 km^2 Delaware River Basin. The respective mean annual precipitation and water flow rates are 105.4 cm and 50.8 cm per year, indicating relatively plentiful groundwater recharge to stream base flow (Corrozi et al., 2008). In addition, Corrozi et al. (2008) noted that there have been more frequent and intense floods and more severe droughts over the last two decades in the WCC watersheds. Approximately 55% of the WCC watershed lies in Pennsylvania, 45% in Delaware and < 1% in Maryland. The creek and aquifers in the watersheds serve as a major drinking water

source for over 120,000 residents of northern Delaware. The watershed is fairly developed under 3 major land cover types: Developed land (37%), agriculture (33%), and natural areas (forest and wetlands 30%) (Narvaez and Homsey, 2016). The sampling site is located at the edge of the WCC floodplain and is bordered by cliffs on two sides. The soil in the wetland is classified as fine-silty, active, mesic Thapto-Histic Fluvaquents according to the U.S. Department of Agriculture (USDA) soil taxonomy (Soil Survey Staff, 2015). Hydroperiod class of the wetland is permanently inundated, where "saturation" is defined as saturation of micropores to the soil mineral surface (NTCHS, 2015). This wetland usually has no inundation during periods of drought. Multiple toeslope seeps are the primary source of hydrologic input. Air-dried soil samples were passed through a 2-mm sieve and stored in the dark until used for column preparation. A summary of the soil chemical composition is listed in Table 2.1 in Chapter 2.

3.2.2 Preparation of Soil Column

Columns were made of acrylic (wall thickness: 0.60 cm, inner diameter: 7.5 cm, length 35 cm), equipped with a nylon mesh (bubbling pressure: 40 mbar) and a porous plastic disk (pore size: ~ 2.0 mm in diameter) at the bottom to support the packed soil (**Figure 3.1**). Two replicate soil columns were prepared to induce redox oscillations and another set of duplicate oxic (control, not incubated) columns were prepared to collect leachate samples at time zero. Each soil column was packed by adding soil layer by layer in 1-cm increments while each layer was gently pressed to have a bulk density of ~1.23 g cm^{-3} (~1.3 kg of soil in each column to a total height of 24 cm), leaving a headspace of 11 cm. During column preparation, two platinum redox probes were installed horizontally in each column at 10 and 17 cm depths,

respectively, to monitor soil redox status continuously along the column for the entire duration of the experiments.

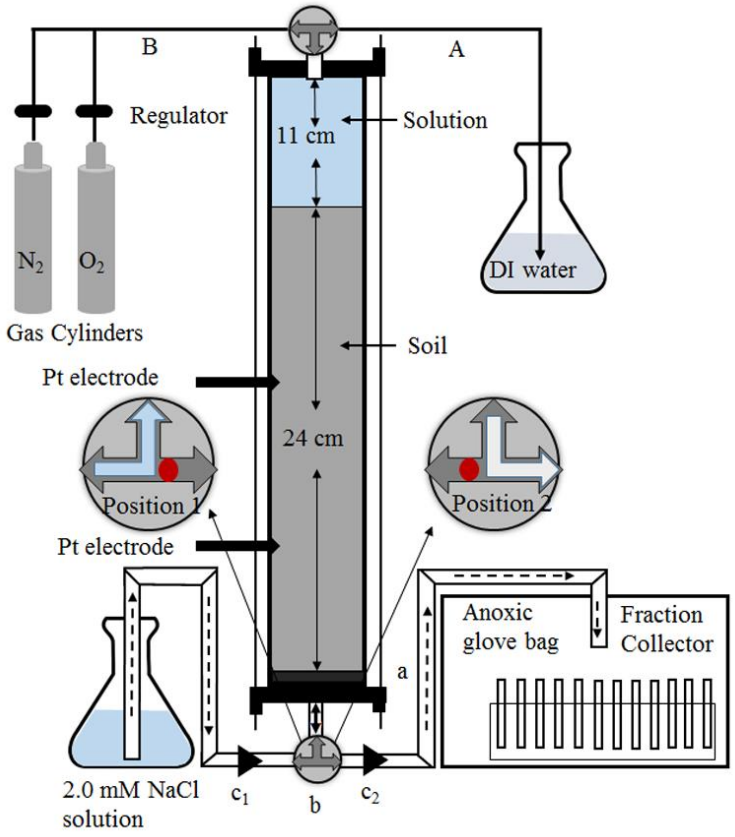

Figure 3.1: Schematic diagram of the soil column. (a) Nylon mesh and porous plastic disk (pore size: ~ 2.0 mm in diameter), (b) three-way bulb and (c_1, c_2) peristaltic pumps. Tube A was dipped in DI water to remove excess air while 2.0 mM NaCl electrolyte solution was injected into the column using pump c_1 in up-flow mode. Tube B was used to flush the column with N_2 or O_2 gas. Column leachate samples were collected inside the anoxic glove bag using pump c_2.

3.2.3 Redox Oscillation Experiment

Soil columns with redox oscillations were thoroughly flushed with nitrogen (N_2) gas, followed by addition of 2.0 mM NaCl electrolyte solution in an upward flow mode at a velocity of 1 mL min^{-1} for ~20 h using a peristaltic pump until the standing water height reached at 11 cm above the soil surface. The specific height of water

above the soil surface was chosen to ensure enough volume for collecting at least 1 pore volume (PV) of leachate. For the columns used in this study, 1 PV was calculated to be 573 mL assuming a particle density of 2.65 g cm^{-3} using the equation described by Singh and Kanwar (1991). Soil columns were incubated for two oxidation-reduction cycles and each complete oscillation was designated as 28 days of oxidizing half-cycle (OHC) followed by 35 days of reducing half-cycle (RHC). Columns were completely flushed out after 1^{st} RHC (single oscillation). After collection of the leachate samples at the end of the 1^{st} RHC, the columns were flushed intermittently with oxygen (O_2) gas for 28 days to maintain oxic conditions throughout the columns. During O_2 flushing, top lid of the acrylic tube was removed so the soil was exposed to drying. Finally, the columns were saturated again with the electrolyte solution, incubated and completely flushed out once again after 35 days (2^{nd} RHC, cumulative oscillation). Solution input was stopped when its height reached 11 cm above the soil surface for all columns. I have prepared separate soil columns that were maintained under continuous oxic and anoxic conditions without any redox oscillations, where leachate samples were collected after 63 days (28 + 35) and 126 days. The replicate oxic (control) soil columns were prepared in the same manner as the treatment columns, i.e., 2.0 mM NaCl was injected at 1 mL min^{-1} flow rate for ~20 h in an upward flow mode until water level reached at 11 cm above the soil surface. They were then immediately (time zero) flushed out and leachate samples were collected for analyses. Thus, the oxic (control) soil columns were not exposed to any redox oscillation events and leachates were solely gained once at the beginning of the experiment. All leachate samples were stored at 4^0C until analyzed. No supplemental C sources were added to the columns.

From columns with redox oscillations, leachate samples were collected sequentially (0.18, 0.36, 0.55, 0.82, and 1.09 PV) after each RHC using a fraction collector (Foxy Jr., Teledyne Isco, Lincoln, NE), which was placed inside a glove bag under continuous flushing with N_2. Four 10-mL leachate samples were transferred to 15-mL centrifuge tubes for targeted size fractionation using a Sorvall centrifuge (Thermo Scientific) with a F13s-14*50Y rotor into < 450 nm (7 min at 680 × *g* rcf or 2000 rpm), < 220 nm (10 min at 1860 × *g* rcf or 3300 rpm), < 100 nm (11 min at 8370 × *g* rcf or 7000 rpm), and < 2.3 nm (~10 kDa) fractions. The centrifugation speed and time to achieve desired particle sizes were calculated from the Stokes' law (Gimbert et al., 2005) assuming spherical particles and particle density of 2.65 g cm^{-3}. Although these two assumptions do not account for the heterogeneity of particle composition and size, this method avoids errors caused by pore-clogging associated with membrane filtration. However, in the case of particles composed of mostly organic materials thus having lower than 2.65 g cm^{-3} density, they would preferentially remain in the supernatant than mineral particles with the same size, thus be underestimated. The < 2.3 nm fraction was separated using an ultrafiltration system (Amicon® stirred cell) equipped with Ultracel® 10 kDa membrane ultrafiltration discs (EMD Millipore Corporation). The millipore ultrafiltration system was operated inside the glove bag to maintain anoxic conditions. In this study, the cutoff sizes of 450 nm, 100 nm, and 2.3 nm were chosen to represent fine colloid, NNP, and dissolved C fractions.

3.2.4 Sample Analyses

3.2.4.1 Chemical Analyses

pH, Eh, and electrical conductivity (EC) of the column leachate samples were measured with corresponding probes (Fisher Scientific, Hampton, NH). Ionic Strength values were calculated from measured EC values (Alva et al., 1991; Morrisson et al., 1990) using equation: IS = 0.013 x EC, where EC is the suspension electrical conductivity (ds m^{-1}).

Fe^{2+} concentration of the leachate samples (at < 2.3 nm size fraction) was measured following the ferrozine method (Stookey, 1970) using UV-visible spectrophotometer with a limit of quantification (LOQ) of 0.1 mg L^{-1}. Both Fe^{2+} and Fe^{3+} can form complexes with organic and inorganic compounds. However, Viollier et al. (2000) demonstrated that Fe complexation with the Suwannee river OM did not significantly underestimate the measured Fe content; even in organic-rich water (e.g., 25 mg L^{-1}). Total organic carbon (TOC) concentration in each size fraction (bulk, < 450 nm, < 220 nm, < 100 nm, and < 2.3 nm) was measured with a TOC analyzer (Apollo 9000 TOC analyzer, Tekmar, Dohrmann). Later, C concentrations in > 450 nm, 220-450 nm, 100-220 nm, and 2.3-100 nm size fractions were calculated from the difference in C concentration between different size fractions as measured using TOC analyzer. Turbidity of the leachate samples was determined using a nephelometer (HACH) in nephelometric turbidity units (NTU), which was then converted into colloid concentrations using the concentration-turbidity regression equation developed by Yan et al. (2017) (concentration = (0.94 ± 0.02) × Turbidity, R^2 = 0.86) from 37 soil samples for < 1.0 μm colloids.

3.2.4.2 Spectrofluorometric Analyses

Molar absorption spectra were measured with a double beam Shimadzu UV-mini spectrophotometer (Shimadzu Inc.) equipped with a 1 cm path-length quartz cuvette. The specific ultraviolet absorbance ($SUVA_{254}$) for each size fraction was calculated by normalizing the UV absorbance at 254 nm by their corresponding C concentration (Weishaar et al., 2003) and reported in units of L mg C^{-1} m^{-1}. Previous studies have shown that aqueous Fe (III) complexes (Stefánsson, 2007) and iron (III) oxyhydroxide colloids (Pullin and Cabaniss, 2003) can interfere the determination of UV absorbance at 254 nm wavelengths (Weishaar et al., 2003). However, in contrast to the linear relationship between Fe (III) concentration and $SUVA_{254}$, Fe (II) has negligible effects on it particularly at low pH condition (<4) (Doane and Horwáth, 2010; Poulin et al., 2014). Therefore, we immediately acidified the size-fractionated samples to reduce Fe oxidation. Three-dimensional DOM fluorescence scans were also performed with a Horiba Jobin Yvon Fluoromax-P Spectrofluorometer (Horiba Scientific, Edison, NJ, USA). Size-fractionated sample was transferred from sealed sample vial to quartz cuvette, immediately screwed to minimize direct exposure to air, and analyzed under anoxic conditions. Fluorescence EEMs spectra were measured with scanning emission (em) wavelengths from 300 to 550 nm at 2 nm increments by varying the excitation (ex) wavelengths from 270 to 450 nm at 5 nm intervals. The integration time for sample collection was set at 0.30 s. Results were normalized to the integrated intensity of the Raman scattering band of ultrapure water (Milli-Q, Milipore) at excitation wavelength of 350 nm (Cory and McKnight, 2005). Samples were diluted as necessary to avoid inner filter effects, i.e., reabsorption of fluorescence light (Green and Blough, 1994; Sainz Rozas et al., 2001). Fluorescence properties of the size-fractionated OM were assessed by determining three fluorescence indices:

humification index (HIX), biological index (BIX), and fluorescence index (FI). The EEMs scans were further fitted to a 13-component parallel factor (PARAFAC) model (**Figure 3.2**) developed by Cory and McKnight (2005). Four of the 13 components (Component 3, 5, 8, and 13) were studied in detail to elucidate molecular properties of the size-fractionated OM. Different optical and fluorescence indices used in this study are summarized and explained in Table 3.1.

Size (nm)	Oxic (control) column	1st reducing half-cycle	2nd reducing half-cycle
<450	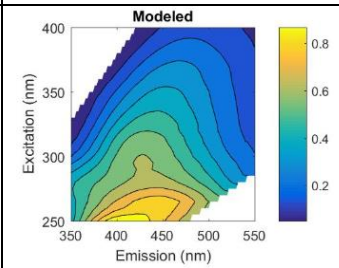	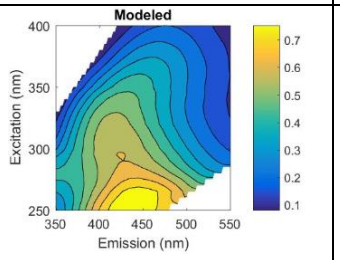	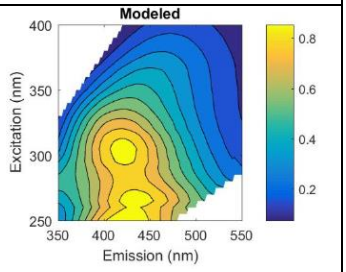
<220	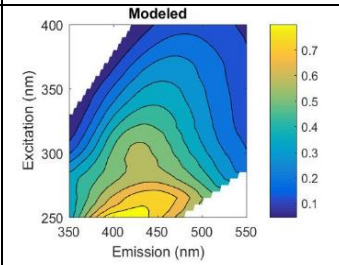	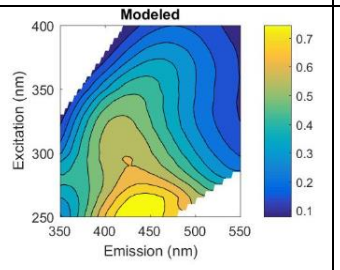	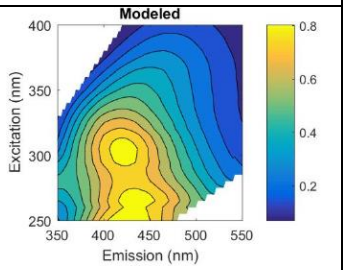
<100	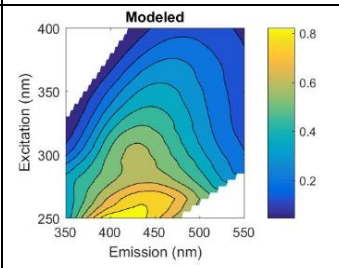	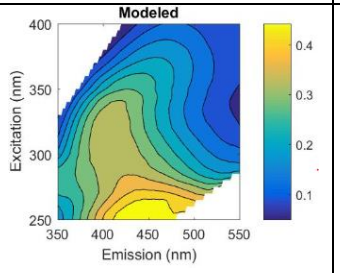	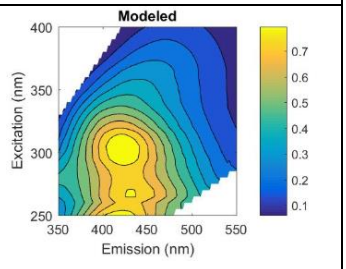
<2.3	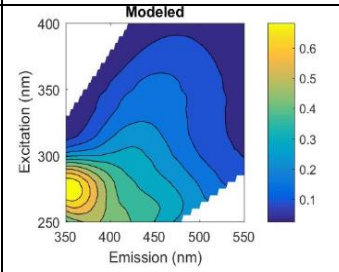	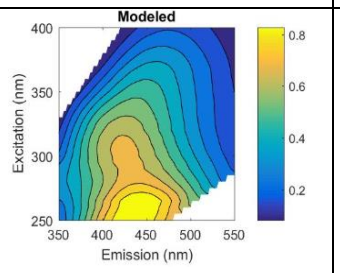	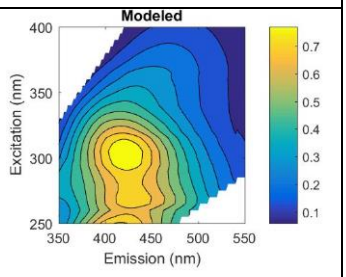

Figure 3.2: The fitted EEMs data using the 13-component parallel factor (PARAFAC) model developed by Cory and McKnight (2005).

Table 3.1: Optical and fluorescence indices used to characterize organic matter (OM) in this study.

Index	Definition and significance	Reference
Specific UV absorbance (SUVA$_{254}$)	UV absorbance at 254 nm (m^{-1}) normalized to the OM concentration. SUVA$_{254}$ is positively correlated with the aromaticity of the OM. Aromaticity = 6.52 x SUVA + 3.63)	Weishaar et al. (2003)
Humification index (HI)	Estimates the degree of humification/maturation of OM in soil. HIX value ranges from 0 to 1 with higher values indicate greater degree of humification HIX = $\sum I435\text{-}480/ (\sum I300\text{-}345 + \sum I435\text{-}480)$	Ohno (2002)
Fluorescence index (FI)	The ratio of emission intensities at 470 nm and 520 nm at an excitation wavelength of 370 nm. Widely used to differentiate between OM derived from higher vascular plants (FI: 1.2-1.5) versus microbial sources (FI: 1.7-2.0)	McKnight et al. (2001)
% C3	Represents OM of microbial origin	Cory and McKnight (2005)
% C5	Indicates higher plant-derived OM	Cory and McKnight (2005)
% protein-like fluorescence	Sum of % tyrosine (C13) and % tryptophan (C8) like compounds. This index is also an important indicator of bioavailable OM	Fellman et al. (2008a)

3.2.4.3 Isotope Ratio Mass Spectrometry (IRMS) Analyses

Abundance of stable isotopes ($\delta^{13}C$ and $\delta^{15}N$) were determined using an IRMS (DELTA V plus, Thermo Fisher Scientific) equipped with an elemental analyzer (EA) to further evaluate the molecular composition of size-fractionated OC. Stable C and N isotope ratios were calculated in terms of $\delta^{13}C$ and $\delta^{15}N$, $(R_{sample}/ R_{standard} -1) \times 1000$, where R is the ratio between heavier to lighter isotope ($^{13}C/^{12}C$, or $^{15}N/^{14}N$) in the samples relative to the Vienna-Pee Dee Belemnite (PDB) limestone standards. USGS-40 (L-glutamic acid, 40.8% C and 9.52% N) and USGS-41 (L-glutamic acid enriched in ^{13}C and ^{15}N, 41.9% C and 9.76% N) were used as reference materials. The precision and accuracy of $\delta^{13}C$ and $\delta^{15}N$ were ± 0.1‰ and ± 0.2‰, respectively, as determined from replicate analyses of the standards and samples. Size fractionated samples collected from oxic (control) soil columns were not enough to run for IRMS-EA analysis.

3.2.5 Statistics

Two-way ANOVA analysis was performed to identify statistical differences in measured parameters using the Tukey's Honestly Significant Difference (HSD) test. All statistical analyses were performed using the R 3.3.1 statistical software and the differences of means were considered significant at $p < 0.05$.

3.3 RESULTS

3.3.1 Changes in Solution Chemistry

Solution chemistry parameters for all column leachate samples are summarized in **Figure 3.3a-c**. Values of pH, pE and IS of the leachate samples from the oxic column (control, time zero) were 5.25 ± 0.10, 7.10 ± 0.41, and 3.30 ± 0.23 mM; they

changed to 7.52 ± 0.26, -1.94 ± 0.62, and 16.74 ± 0.40 mM after the 1st RHC and to 6.40 ± 0.20, 3.42 ± 0.33, and 5.72 ± 0.92 mM after the 2nd RHC, respectively. As expected, in comparison to the oxic (control) column, pH and IS increased and pE decreased during reducing conditions. However, changes in IS and pE compared to the oxic (control) columns were smaller after the 2nd RHC than after 1st RHC. Similarly, aqueous Fe^{2+} concentration was higher after 1st than 2nd RHC **(Figure 3.3d)**. Redox potential changes at 10 and 17 cm depths of the soil columns are presented in Table 3.2.

Table 3.2: Redox potential changes along the soil columns.

Depth (cm)	Redox potential (Eh, mV)			
	Oxic column (control)	1st RHC (35 d)	1st OHC (28 d)	2nd RHC (35 d)
10	328 ± 10	58 ± 15	480 ± 21	124 ± 17
17	331 ± 22	64 ± 12	465 ± 10	159 ± 25

RHC = Reducing half-cycle, OHC= Oxidizing half-cycle

3.3.2 Mobilization of Colloids and OC

Colloid concentration ([colloid]) in the leachate samples under different redox oscillation events are plotted in **Figure 3.3e**. The oxic (control) column had a rapid, high-concentration release of colloids at the beginning (79.5 mg L^{-1}) followed by a sharp decline to 4.08 ± 3.37 mg L^{-1}. Leachates from the redox-oscillating columns did not have any such sharp decline. After 1st RHC, the [colloid] rapidly increased at to 13.60 ± 7.04 mg L^{-1}; while after 2nd RHC, the concentration dropped at to 3.46 ± 2.69 mg L^{-1}.

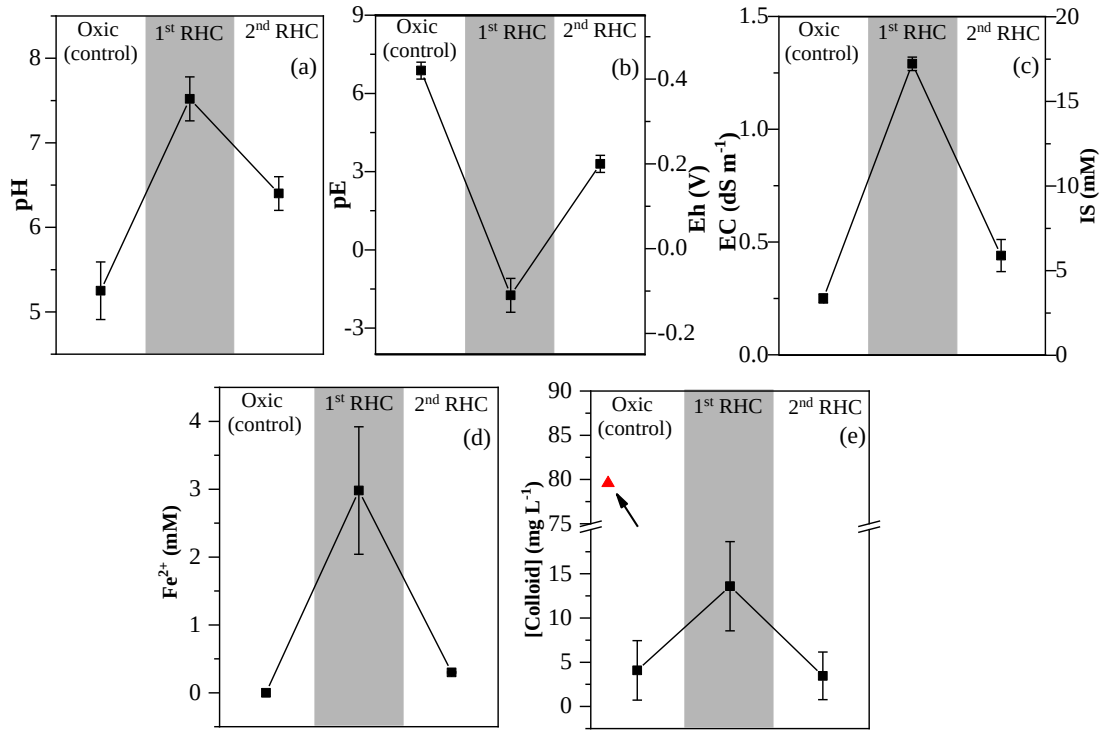

Figure 3.3: Changes in (a) pH, (b) pE (Eh), (c) IS (EC), (d) Fe^{2+} concentration (mM), and (e) colloid concentration ([colloid], mg L^{-1}) in leachate samples collected from oxic (control) soil column and after 1st and 2nd reducing half-cycle (RHC). Initial high colloid release at 0.1 pore volume (V/V_0) from oxic (control) column was shown separately using "▲" sign. The error bars represent the standard deviations among different PVs of samples collected from duplicate soil columns. Fe^{2+} concentration was below LOQ in leachates collected from oxic (control) columns.

Organic C concentrations of size-fractionated leachate samples are shown in **Figure 3.4** and **Table 3.3**. The highest bulk C concentration was observed after the 1st RHC (122 ± 11 mg L^{-1}), followed by the 2nd RHC (98 ± 5 mg L^{-1}) and then the oxic (control) column (14 ± 5 mg L^{-1}); the increase in concentration was 425-1018% (after 1st RHC) and 311-830% (after 2nd RHC) from that of the oxic (control) soil column. The TOC concentration varied significantly both as a function of redox oscillation ($p < 0.001$) and size ($p < 0.01$). Among size-fractionated samples, dissolved fraction had the highest C concentration irrespective of redox conditions. As shown in **Figure 3.4**,

dissolved and NNP fractions contributed 62 ± 4% and 32 ± 4% of total C content after 1st RHC and the values were respectively 49 ± 8% and 12 ± 5% after 2nd RHC. However, the percentages of particulate and fine colloid C fractions increased after 2nd RHC (25 ± 8% and 14 ± 5%) in compare to 1st RHC (2 ± 1 % and 4 ± 2 %). In the leachate from the control soil columns, the dissolved and NNP fractions contributed most to the total OC (55 ± 10.0%, 24 ± 9%, respectively).

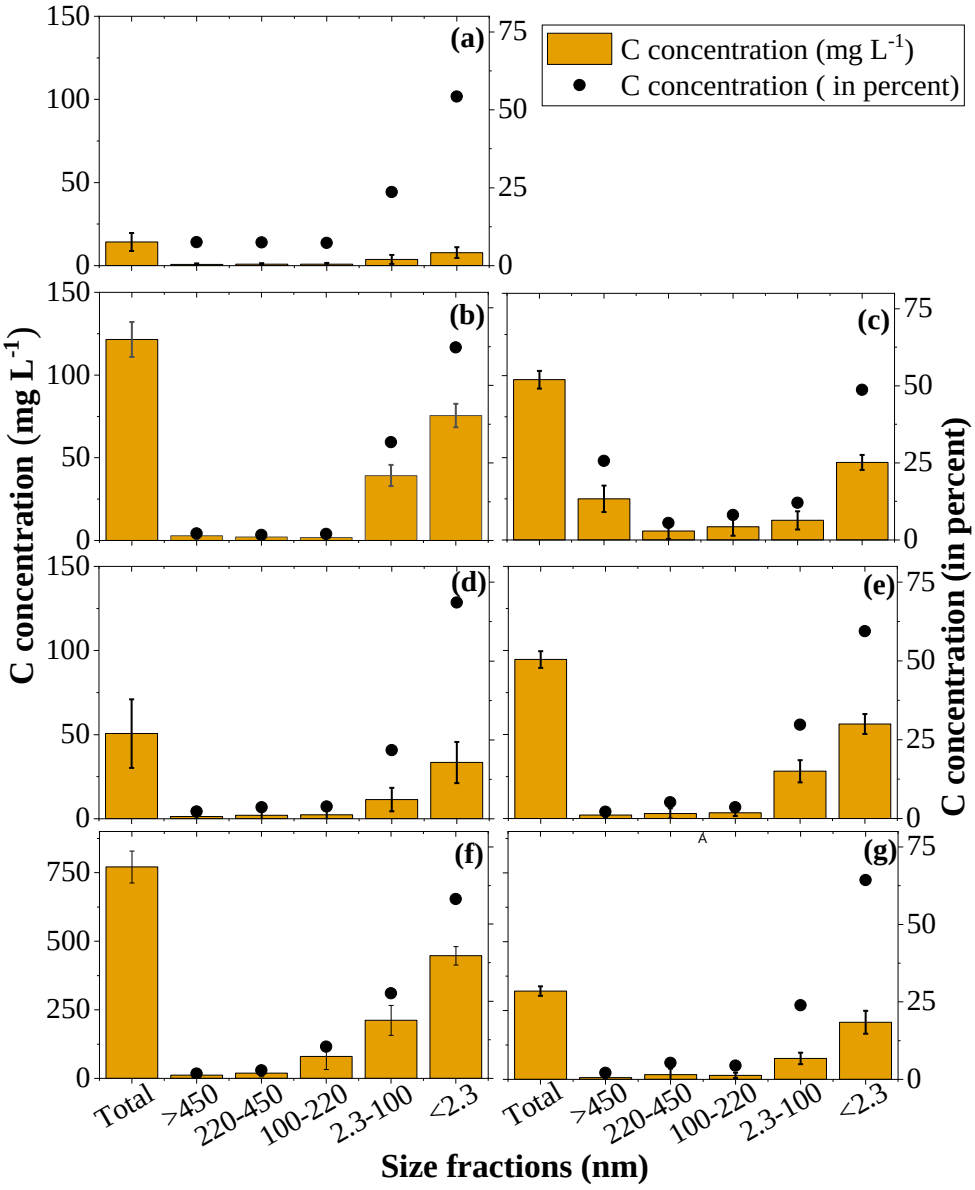

Figure 3.4: Mean C concentration for bulk, >450 nm, 220-450 nm, 100-220 nm, 2.3-100 nm, and <2.3 nm size fractions in (a) oxic (control) column, (b) after 1st RHC, (c) after 2nd RHC, (d) after continuous oxic condition for 1 complete oscillation period, (e) after continuous anoxic condition for 1 complete oscillation period, (f) after continuous oxic condition for 2 complete oscillation period, and (g) after continuous oxic condition for 2 complete oscillation period. The left y-axis represents C concentration in mg L^{-1} and the right y-axis represents C concentration in relative percentages. The error bars represent the standard deviations in leachate C concentration at different PVs of samples collected from duplicate soil columns.

Table 3.3: Organic C concentration (mg L^{-1}) in size-fractionated samples.

Size (nm)	C concentration (mg L^{-1})		
	Oxic column (control)	**1st reducing half-cycle**	**2nd reducing half-cycle**
> 450	0.80 ± 0.5 (6%) aA	2.85 ±1.9 (2%) aA	24.99 ± 8.0 (26%) bB
220-450	0.95 ± 0.5 (8%) aA	2.14 ± 1.3 (2%) aA	5.41 ± 4.8 (6%) aA
100-220	0.88 ± 0.7 (7%) aA	2.59 ± 1.5 (2%) aA	7.99 ± 5.4 (8%) aA
2.3-100	3.77 ± 3.0 (24%) bA	38.45 ± 5.5 (32%) bC	11.92 ± 5.4 (12%) aAB
< 2.3	7.87 ± 3.3 (55%) cA	75.52 ± 7.1 (62%) cC	47.18 ± 4.6 (49%) cB

Mean values ± standard deviations are calculated from leachate samples collected at different PVs from duplicate soil columns. The values in parenthesis (mean ± standard deviation) indicate percent contribution of each size fraction to the total C content in the column leachate samples.
Mean values in each vertical column followed by different lowercase letters indicate significant variation between different size fractions using Tukey's honestly significant difference (HSD) test at $p \leq 0.05$ level.
Mean values in each horizontal row followed by different uppercase letters indicate significant variation between different stages of redox oscillation cycles by the Tukey's HSD test at $p \leq 0.05$ level.

3.3.3 Changes in OC Properties

3.3.3.1 Optical and Fluorescence Properties

$SUVA_{254}$ values and % aromatic C contents as a function of PV and particle size fractions are summarized in **Figure 3.5a-c**. The $SUVA_{254}$ values of the oxic column leachate samples ranged from 0.65 to 2.3 L mg^{-1} C m^{-1} representing an aromatic C content of 8-19% and gradually decreased with increasing PV. In comparison, % aromatic C content was significantly higher following the 1st RHC ($p <$

0.001) than the 2nd RHC and the values were respectively, 40 ± 8%, 40 ± 12%, 36 ± 12%, and 30 ± 14% at < 450 nm, < 220 nm, < 100 nm, and < 2.3 nm size fractions (**Figure 3.5d**). Following the 2nd RHC, % aromatic C content decreased at 15 ± 1%, 16 ± 1%, 18 ± 4%, and 13 ± 2% at < 450 nm, < 220 nm, < 100 nm, and < 2.3 nm size fractions, respectively. In contrast to the oxic soil column, optical properties of the OC following the RHCs are characterized by (1) an increase in aromaticity with increasing PV and (2) greater variations in size-specific aromatic C content following redox oscillation processes and these changes became more prominent after 2nd RHC.

Molecular composition of the size-fractionated leachate samples was further elucidated through additional fluorescence indices and the PARAFAC analyses based on EEMs data. Fluorescence indices, including HIX, FIX, and BIX, along with component 3 (C3), component 5 (C5) and % protein-like fluorescence (component 8 + component 13) were used to characterize the molecular composition of size-fractionated OC (**Figure 3.6**). The oxic (control) column leachate samples had the highest HIX (0.74 ± 0.04), % C5 (3.91 ± 0.58) and % protein-like fluorescence (13.75 ± 1.97) values and the lowest BIX (0.59 ± 0.05), FI (1.53 ± 0.04), and % C3 (5.03 ± 1.73) values. Following the 2nd RHC, HIX (0.64 ± 0.04), % C5 (3.09 ± 0.38), and % protein-like fluorescence (10.55 ± 1.30) values gradually decreased and BIX (0.77 ± 0.05), FI (1.74 ± 0.03) and % C3 (10.35 ± 0.43) values increased. However, the fluorescent C components did not vary much in the size range between 2.3-450 nm but changed significantly at < 2.3 nm.

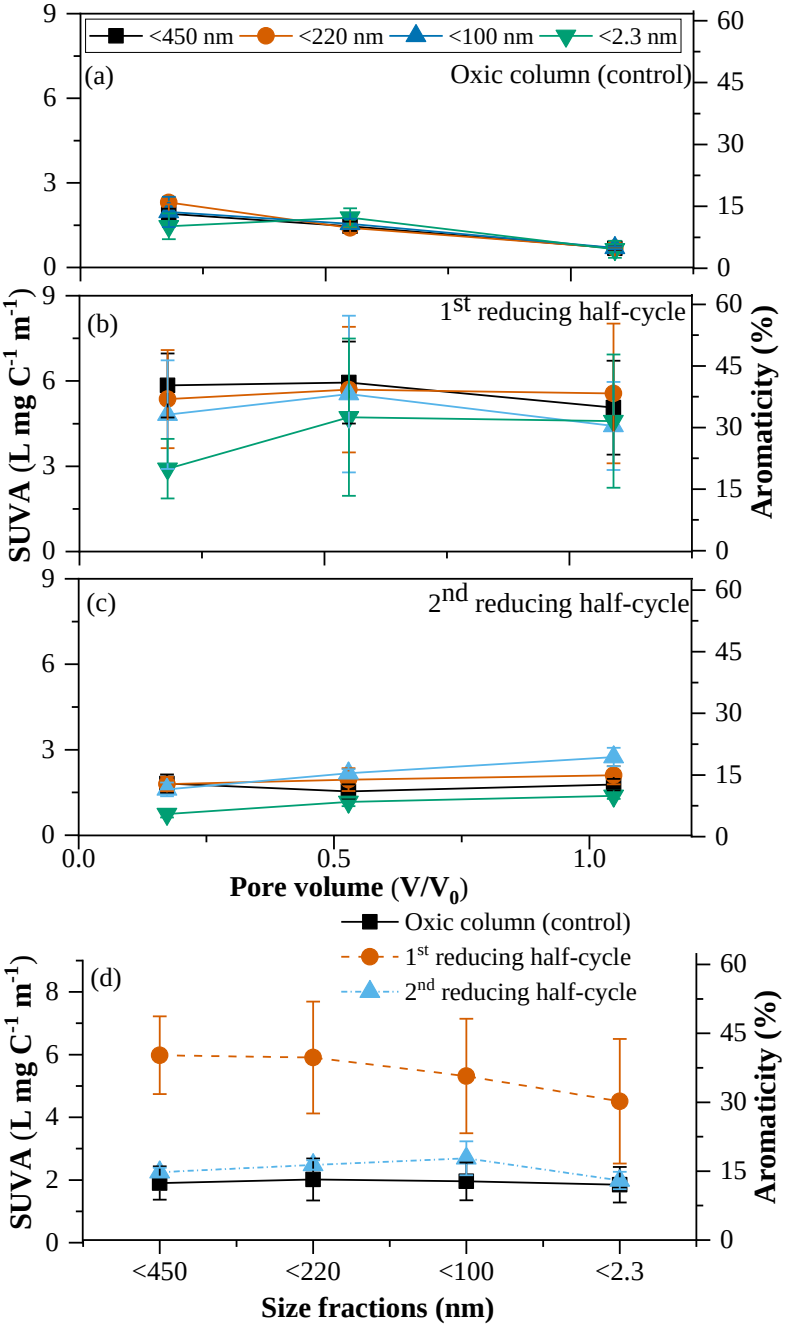

Figure 3.5: Changes in specific UV absorbance ($SUVA_{254}$, L mgC^{-1} m^{-1}) and % aromatic C content in leachate samples collected from soil columns subjected to (a) oxic column (control), (b) after 1st reducing half-cycle, and (c) after 2nd reducing half-cycle at 0.18, 0.55 and 1.09 PV (V/V_0). Fig. (d) shows the changes in SUVA and % aromaticity for < 450 nm, < 220 nm, < 100 nm, and < 2.3 nm.

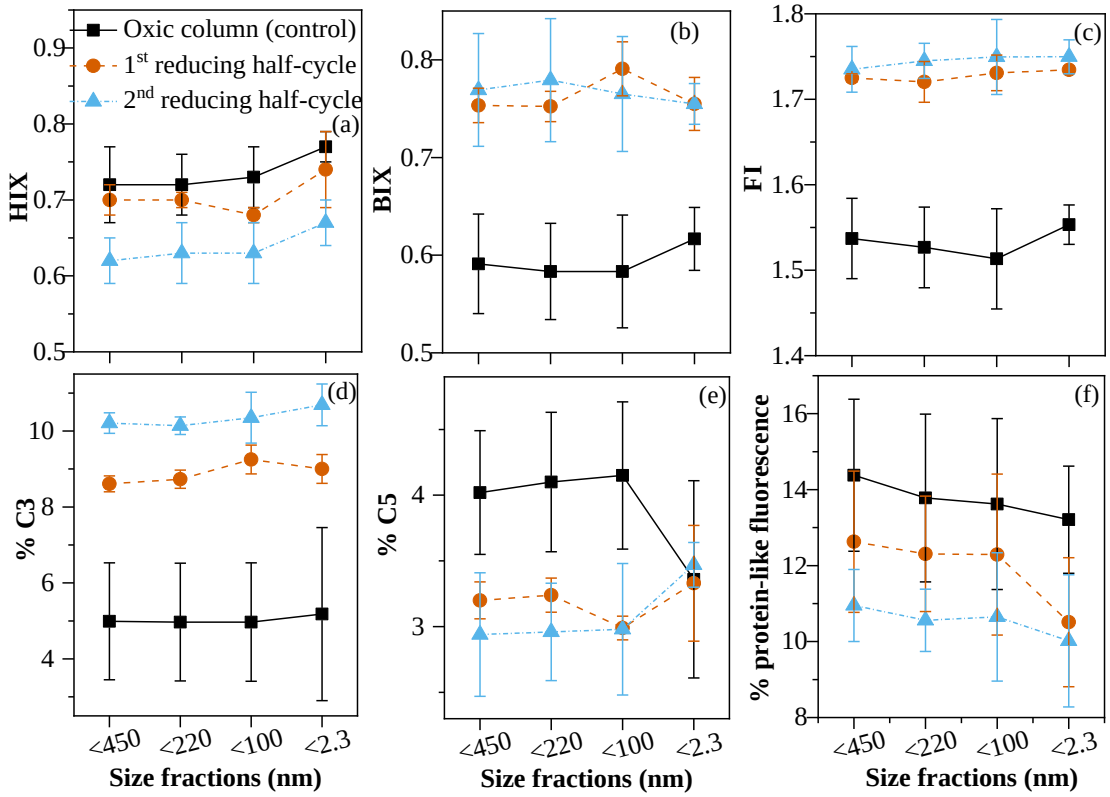

Figure 3.6: Changes in the fluorescence indices of the OC present in the column leachate samples. These indices include (a) humification index (HIX), (b) biological index (BIX) and (c) fluorescence index (FI), Cory and McKnight (2005) model components: (d) % C3, (e) % C5 and (f) % protein-like fluorescence. The error bars represent the standard deviations among different PVs of samples collected from duplicate soil columns.

3.3.3.2 Isotope Signature

The compositions of stable C and N ($\delta^{13}C$, $\delta^{15}N$) isotopes are summarized in **Figure 3.7**. Leachate samples collected after the 2nd RHC were significantly ($p < 0.001$) depleted in the heavier $\delta^{13}C$ (-28.55 ± 0.1 ‰) compared to the samples collected after the 1st RHC (-25.09 ± 0.29 ‰). An opposite trend was observed in N isotope values, while leachates were significantly ($p < 0.001$) enriched in the heavier $\delta^{15}N$ after the 2nd RHC. Like the OM fluorescent properties, wide variation in the

stable $\delta^{13}C$ values was observed between < 2.3 nm and 2.3-450 nm size fractions. In both the RHCs, kinetic fractionation of OC had relatively narrow size distribution within 2.3-450 nm. After 1st RHC, < 2.3 nm fraction was enriched in heavier ^{13}C isotope (-23.62 ± 0.5 ‰) than the larger size fractions. However, after 2nd RHC, < 2.3 nm fraction (-28.86 ± 0.2 ‰) was mostly depleted in heavier ^{13}C isotopes in contrast to larger particles. In comparison to the $\delta^{13}C$ values, opposite trend was observed in $\delta^{15}N$ values between 1st and 2nd RHC; OC was enriched in heavier ^{15}N isotopes after 2nd RHC than after 1st RHC.

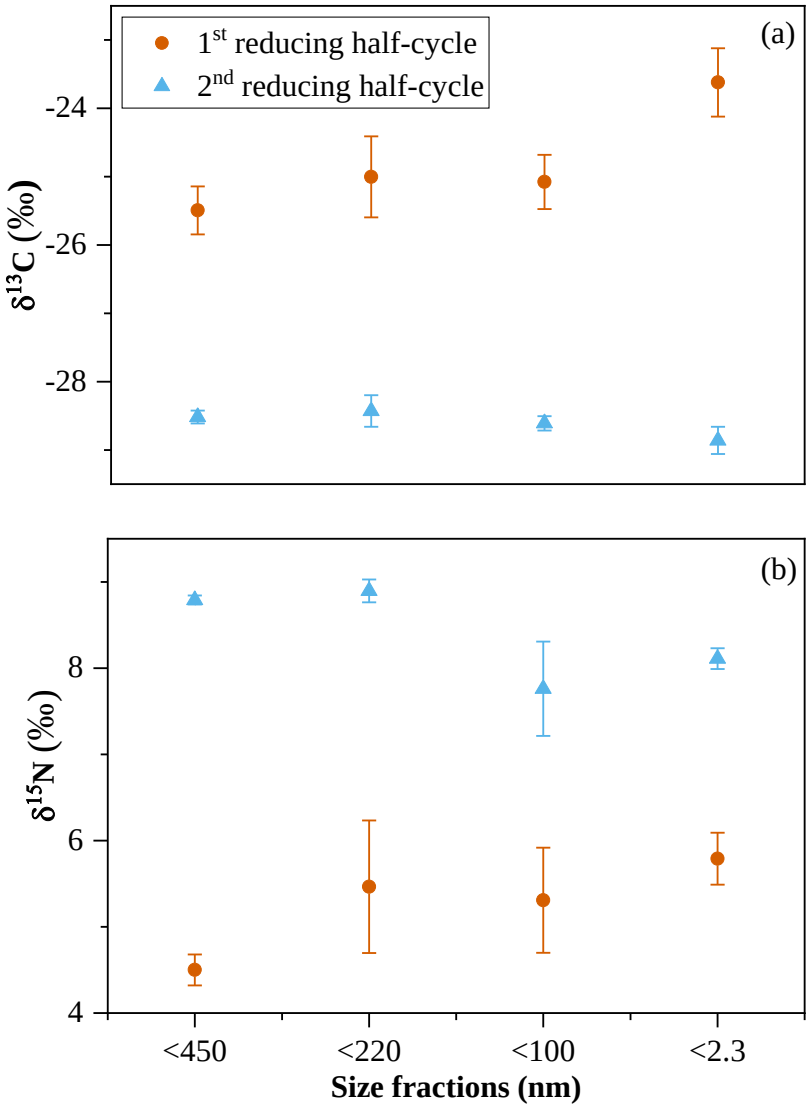

Figure 3.7: Distribution of stable (a) C ($\delta^{13}C$, ‰) and (b) N ($\delta^{15}N$, ‰) isotopes in different size-fractionated samples collected after 1st and 2nd RHC. The error bars represent the standard deviations in stable isotope values among different pore volumes as collected from duplicate soil columns.

3.4 DISCUSSION

3.4.1 Dynamic Response of Soil Colloids to Redox Oscillations

Changes in soil solution chemistry e.g., pH, pE, and IS can influence the release of soil colloids, nanoparticles, and associated OC (Ryan and Gschwend, 1994b; Thompson et al., 2006). **Figure 3.3** and **Table 3.2** show higher pE values, lower pH values, and lower Fe^{2+} concentrations after 2nd vs 1st RHC, indicating that the development of reducing condition was limited during 2nd RHC. This result is consistent with a recent report of Rapin et al. (2019), which showed similar trends in solution chemistry changes in sediments exposed to repeated redox fluctuations in dam reservoirs. The limited development of reducing condition during 2nd RHC may be attributed to the influence of alternate terminal electron acceptors, e.g., nitrate (NO_3^-) and to the limitation of decomposable OC. Nitrate can be produced during intermediate aerobic condition through ammonium oxidation ($NH_4^+ \rightarrow NO_2^- \rightarrow NO_3^-$), which can maintain higher pE values for longer time periods during 2nd RHC.

Reddy and Patrick (1975) reported that NO_3^- produced under prolonged intermediate aerobic conditions, which is comparable to the lapsed time between 1st and 2nd RHC in our study, prevented significant changes in redox potential values during successive reducing events. Release of less Fe^{2+} provides additional evidence for reduced microbial reductive dissolution of Fe minerals during 2nd RHC. I anticipated that such variations in solution chemistry may further affect the mobilization of colloids and transformation of associated OC as a function of redox oscillations.

I observed a strong positive correlation (Pearson's $r = 0.92$, $p < 0.001$) between pH and colloid concentration after the 1st RHC (**Figure 3.8**). This is because

consumption of protons during reduction reactions increased soil pH (Kirk, 2004), which can lead to mobilization of colloid-borne trace elements and OC (Grybos et al., 2009; Thompson et al., 2006). In a batch experiment, Thompson et al., (2006a) observed significant effects of pH on colloid (3 kDa-160 nm) dispersion during cumulative redox oscillation events. However, in our experiment, the strong correlation between increasing pH and colloid release was only significant after the 1st RHC and was not observed following the 2nd RHC. The differences in colloid and OC release between 1st and 2nd RHC are likely due to the variations in physico-chemical conditions between the two cycles.

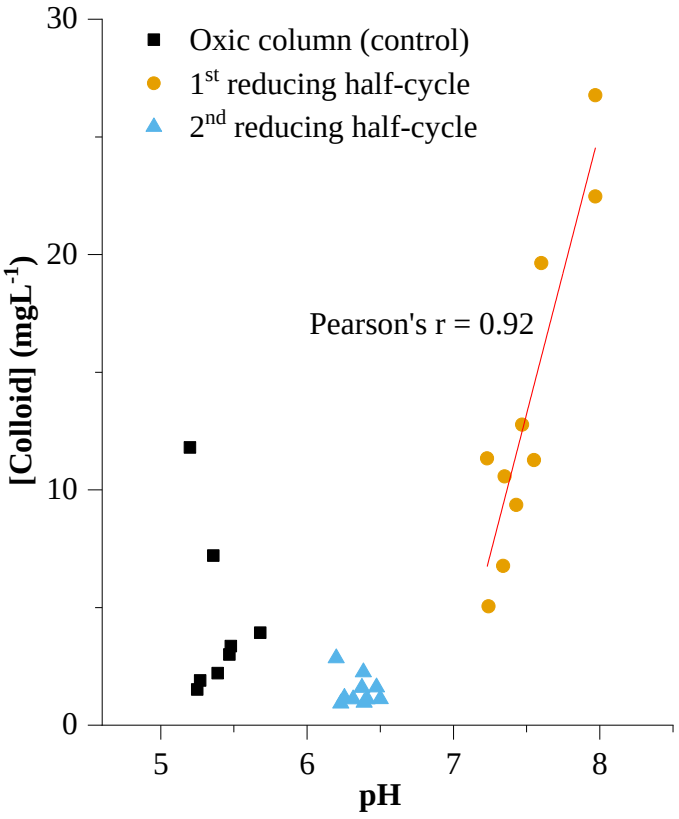

Figure 3.8: Correlation between colloid concentration [colloid] and pH of the column leachate samples.

Following the 2nd RHC, the small increase in pH and small drop in pE values, compared to during the 1st RHC, do not favor desorption of either colloids or OM due to less reductive dissolution of Fe minerals and less electrostatic repulsion between particles. Such difference might also be related to variations in molecular composition of the mineral-SOM complexes, as discussed below.

3.4.2 Dynamic response of soil OC to redox oscillations

The release of OC was significantly higher following redox oscillations in contrast to the oxic (control) column. The results are consistent with the observations from previous studies (Fiedler and Kalbitz, 2003; Grybos et al., 2009; Kögel-Knabner et al., 2010) and confirm that anoxic condition leads to greater mobilization of OC. The most interesting part of our study is that the relative contribution of size-fractionated samples to bulk OC content was different depending on whether the leachate samples were collected after 1st (single) or 2nd (cumulative) RHC. Dissolved and NNP fractions had the highest contributions to bulk OC content following the 1st RHC, while the proportions of these fractions decreased in favor of the fine colloid and particulate fractions following the 2nd RHC. Previous studies ascribed the greater mobilization of OC to the reductive dissolution of Fe-(oxyhydr) oxide (Kögel-Knabner et al., 2010) and/or to the accompanying increase in pH (Buettner et al., 2014; Grybos et al., 2009). However, most of the previous studies lumped fine colloid and NNP-C with dissolved phase using the cut-off size range of 450 nm for DOM. Here, I observed higher release of nano and dissolved OC fractions under high pH condition following the 1st RHC in contrast to larger size fractions. I also observed a significant correlation between C concentration and solution pH for NNP (Pearson's $r = 0.87$, $p < 0.01$) and dissolved (Pearson's $r = 0.93$, $p < 0.001$) size fractions (**Figure**

3.9). The point of zero charge (PZC) of SOM, defined as the pH at which particle has no net charge, is typically less than three (Perdue and Lytle, 1983; Tombacz and Meleg, 1990). Therefore, deprotonation of surface functional groups of SOM results in negative charges at solution pH above its PZC. An increase in pH diminished the positive surface charge of Fe and Al (hydr)oxides (PZC: ~ 6-9) and hence absorbed OC was released.

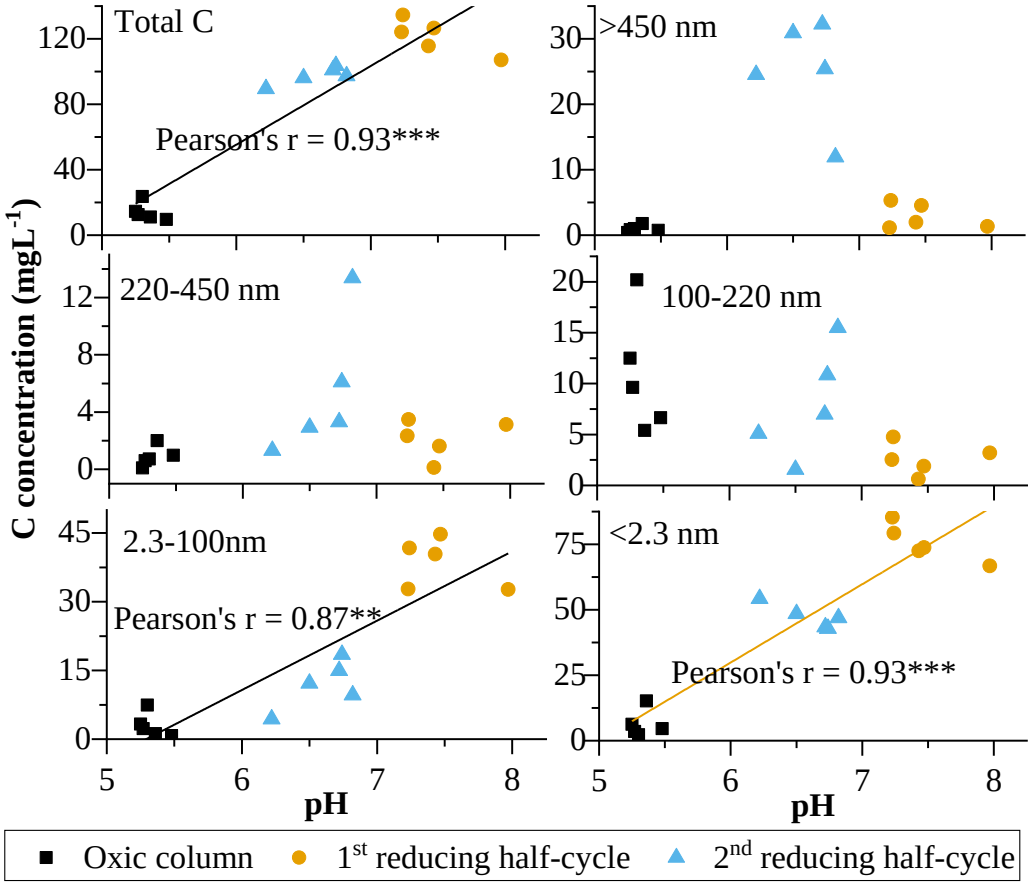

Figure 3.9: Correlation between C concentration (mgL^{-1}) in size-fractionated samples and solution pH. Pearson's r values significant at $p < 0.01$ and $p < 0.001$ are denoted as ** and *** respectively.

Following the 2nd RHC, fine colloid and particulate OC concentrations were higher than in the leachates after 1st RHC, despite very low bulk mineral colloid concentrations (**Figure 3.3e**). The low colloid concentration could be due to settling of the aggregates formed between the OC produced during the 2nd RHC with small particles through bridging. Based on the measured $SUVA_{254}$ and fluorescence indices, OC produced during 2nd RHC was mostly microbial-derived components. In contrast to plant-derived C, the less aromatic, microbial-processed OM (e.g., carbohydrates, cell wall components) has been previously confirmed to from stable nano and colloid-sized organo-mineral associations (Asano and Wagai, 2015) through bridging. Nano and colloid- sized organo-mineral associations, which can include both immobile solid phase and colloidally mobile phase (Buettner et al., 2014; Fritzsche et al., 2016), further act as composite building units of micro aggregates (Asano and Wagai, 2014; Kögel-Knabner et al., 2008a; Lehmann et al., 2007; Totsche et al., 2018). Colloidal aggregation resulting from the bridging effect of aquagenic biopolymers (e.g., carbohydrates) has also been reported in other water column studies (Hunter and White, 1987). In particular, Yan et al. (2016) observed decreases in colloid release under prolonged anaerobic incubation and ascribed the corresponding decrease to the bridging effect of dissolved organic fractions. They also found that release of colloids and OM upon changing redox conditions is a dynamic process and that OM with different molecular weights was released at different 'stages' of reduction. Thus, the distribution and nature of size-fractionated OC suggests that the types of organo-mineral associations may be different in response to redox change continuum. The results are particularly significant within the operationally defined DOM (< 450 nm)

size fraction, which contains NNPs that is very different in OC composition compared to the fine colloid sized organo-mineral associations.

3.4.3 Mineral-SOM interactions as a function of redox oscillations

Mobilization and transport of mineral-associated-organic carbon largely depends on electrostatic and chemisorption interactions between OM functional groups (e.g., carboxyl and hydroxyl groups) and the types of mineral surfaces (e.g., Al and Fe -(oxyhydr)oxides) (Edwards et al., 1996; Gu et al., 1994; Kaiser et al., 1997). Surface hydroxyl groups of Fe-oxyhydroxides and aluminosilicate minerals can strongly bind with the carboxylic and phenolic groups of aromatic OC substances. Being a function of aromaticity, a higher $SUVA_{254}$ value indicates the presence of more aromatic C in the OM (Weishaar et al., 2003). Therefore, the low $SUVA_{254}$ values in the oxic (control) column leachate samples reflect preferential release of less aromatic C and, correspondingly, suggest a greater affinity of aromatic OC to soil mineral surfaces. Such selective sorption has also been found in other studies, which reported that SOM having higher hydrophobicity and aromatic C content (35%) are preferentially removed from the solution and sorbed on soil mineral surfaces (Kaiser and Zech, 2000; Qualls and Haines, 1991; Ussiri and Johnson, 2004).

Interestingly, the release of soil OM having higher $SUVA_{254}$ and % aromatic C content following the 1st RHC confirms that this fraction became highly mobile under reduced condition. This finding is also in agreement with Rouwane et al. (2018), who worked with wetland soil and found that polar constituents in aromatic structures increased in the solubilized organic compounds during reducing conditions. Adhikari and Yang (2015) also observed higher release of aromatic C compounds upon abiotic reduction. The release of high aromatic C compounds following 1st RHC suggests a

greater contribution of lignin derivatives particularly from vascular plant materials (Engelhaupt and Bianchi, 2001). The molecular composition of the OC collected after the single (1^{st}) vs. cumulative (2^{nd}) RHC was very different. To elucidate the differences in the molecular composition of OC, I relied on spectrofluorometric indices. For example, % C3 is considered to represent microbial-derived C, while % C5 is assumed to indicate plant-derived C (Cory and McKnight, 2005). The FI values have been used to differentiate between terrestrial plant-derived C (FI: 1.3-1.4) and microbial-derived C (FI: 1.7-2.0) (McKnight et al., 2001). Following the 2^{nd} RHC, the mobile fraction became enriched in microbial-derived C (as suggested from the increase in % C3 components, BIX, and FI and decrease in HIX indices), and depleted in % aromatic C ($SUVA_{254}$). (Xu and Guo, 2017) reported that a decrease in HIX and an increase in BIX indicate the presence of freshly produced DOM, i.e., microbial-derived C. Similarly, several studies have also confirmed that microbial metabolites are often depleted in aromatic C (< 15%) (Chin et al., 1994; Weishaar et al., 2003).

At the end of 2^{nd} RHC, I observed an increase in microbial-derived, fine colloid and particulate OC in the mobile fraction, despite an overall decrease in colloid concentration. This general trend could also be attributed to the lower desorption of aromatic C components during 2^{nd} vs 1^{st} RHC due to the small changes in pH. Therefore, modeling downward cycling of soil OC should consider microbial processes and size-dependent mobilization of SOM in redox fluctuating environment. Molecular heterogeneity in the mobile OC fraction indicates that processes governing the accumulation and stabilization of SOM are different during single vs cumulative redox oscillations. An increase in microbial-derived C and decrease in bulk colloid concentration data are also in good agreement with the conceptual three-dimensional

functional view of C turnover dynamics as recently proposed by Kleber and Johnson (2010). In contrast to the two-dimensional concept (adsorbent; mineral surface – adsorbate; SOM), this later concept suggests that independent mineral-organic microstructures are formed around colloidal to sub-colloidal size organic matter, which are mostly microbial/fungal cell fragments. Extracellular glue-type materials, e.g., polysaccharides and proteins act as adhesives for aggregate formations. I infer that microbial-derived OC are forming colloid-sized organo-mineral associations through bridges with minerals during cumulative redox oscillation processes.

3.4.4 Stability of mineral-SOM complexes

The differences in OC molecular composition among size-fractionated samples and between single vs cumulative redox oscillations were further demonstrated through stable isotope analyses. After the 2nd RHC, leachate samples were more depleted in heavier ^{13}C isotopes compare to the 1st RHC. Kinetic isotope fractionation during microbial processing of SOM might be responsible for the shifts in stable isotope signatures. During 1st RHC, it is anticipated that microorganisms preferentially utilized lighter ^{12}C materials for their biomass formation that became strongly associated with soil minerals. As a result, C remaining in the solution phase (i.e., C in the column leachate samples) following the 1st RHC were more enriched in heavier ^{13}C isotopes. In a 40-day incubation study, Šantrůčková et al. (2000) also observed such enrichment of lighter ^{12}C isotopes or depletion of heavier ^{13}C isotopes in the microbial biomass C and postulated that under C limited conditions microorganisms synthesize storage materials which are enriched in lighter ^{12}C isotopes. However, this phenomenon contradicts with Dijkstra et al. (2006) who observed a consistent ^{13}C enrichment of the soil microbial biomass relative to the bulk soil C. The observed

isotopic fingerprint depends on the concentration and composition of OC present in the system, including more easily available C in lysed microbial cells, particularly during 2nd RHC due to the limitation of available C sources. Christ and David (1996) also reported that lysed microbial cells contribute significantly to the solubilized OC after cumulative redox oscillation processes. During 2nd RHC, limitation of available C sources results in the dependence of more-readily available C pool from lysed microbial cells. The observed higher pE and lower pH values after 2nd vs 1st RHC might also be due to the decrease in microbial activity resulting from cell lysis. Our results suggest that ^{13}C depleted microbial-derived C became highly susceptible to release from soil matrices and comprised a significant portion in the leachate samples. The depletion of ^{13}C isotopes and less aromatic nature of the C components following the 2nd RHC further indicate the release of less biologically reactive microbial components from soil column.

On the other hand, the heavier ^{15}N isotopes became enriched in all size-fractionated samples after the 2nd RHC in contrast to the 1st RHC. Under C limited condition, microorganisms utilize N containing SOM mostly as a source of C and energy and dissimilate excess N (organic N $\rightarrow$ NH_4^+ $\rightarrow$ NH_3) from the cell (Coyle et al., 2009; Dijkstra et al., 2008). During this process, kinetic isotopic fractionation preferentially removes the lighter ^{14}N from microbial cells. As a result, the microbial metabolites released after 2nd RHC tend to be enriched in heavier ^{15}N isotopes. Mounting evidences (Amelung et al., 2008; Gleixner, 2013; Kallenbach et al., 2016; Miltner et al., 2012) now support the idea that microbial-derived C components contribute significantly to the stable OM fractions in soil, However, how these microbial-derived SOM will response to redox oscillations was still unclear. Overall,

changes in stable C and N isotope signatures in our study indicate that the cumulative redox oscillations enhance the release of less biologically reactive, microbial-derived C from the soil columns.

3.5 CONCLUSIONS

Our study clearly demonstrates that redox oscillations can significantly alter size-dependent heterogeneity in both concentration and molecular composition of mobile soil OC. In contrast to a single RHC, cumulative redox oscillations facilitate the release of larger sized (fine colloid and particulate) organo-mineral associations that are composed of less aromatic microbial metabolites. Colloidal OC, which has different composition from dissolved fraction, could be a significant part of the global C pool under redox fluctuating environment. The size-dependent variations in OC concentration and composition during successive redox oscillations could have significant implications in the fate and transport of SOM to downstream ecosystems and to groundwater aquifers as well as in our understanding and accurate assessment of global C cycling. Our findings further suggest that mineral protection and stability of OC do not solely depend on the intrinsic properties of the SOM, supporting the ecosystem perspective view that persistence of SOM also depends strongly on environmental factors (Kleber et al., 2015; Schmidt et al., 2011). Knowledge gained from this study provides a baseline for the size-dependent heterogeneity in soil OC particularly within cut-off size ranges of traditional “dissolved” fraction. It will further help us better predict the environmental and ecological role of size-fractionated C in aquatic ecosystems as well as the effects of ongoing climate change on the turnover of soil OC in redox-sensitive environments such as wetlands.

Chapter 4

COLLOIDAL ORGANIC CARBON HAS A KEY BUT ACCOUNTED ROLE IN CARBON DYNAMICS IN A DEPRESSIONAL WETLAND

Abstract

Organo-mineral association is one of the most important stabilization mechanisms of soil organic matter. Such association becomes more significant in redox dynamic wetlands due to the onset of aerobic-anaerobic events. However, few studies have been conducted to assess the retention, transformation, and transport of colloids (1-1000 nm) and colloidal organic carbon (COC) in terrestrial environments. Given the particularly significant role of wetland soils in C storage and cycling, the dynamics of colloids and COC and their molecular composition remain a critical knowledge gap. In this study, I investigated the concentration and molecular composition of the dissolved (<2.3 nm), natural nanoparticle (NNP, 2.3-100 nm), fine colloid (100-450 nm) and particulate (450-1000 nm) fractions in pore-waters collected from a Delmarva bay depressional wetland located at Blackbird State Forest, Delaware, USA. Depending on the seasonal hydrologic condition, a transect was delineated from upland to wetland zones. Piezometers were installed at 50 cm, 100 cm, and 200 cm depths in each zone. Pore-water samples were collected from Feb 2018 to May 2019. Our results reveal that dissolved, NNP, fine colloid, and particulate fractions comprise 45 ± 4%, 38 ± 4%, 8 ± 3% and 7 ± 3% of the bulk organic C (OC) (< 1000 nm) concentration, respectively. Isotope ratio mass spectrometry (IRMS) analyses suggest enrichment of heavier $\delta^{13}C$ stable isotopes in the upland than in the

transition and wetland, while NNP was more $\delta^{13}C$ enriched than other larger size fractions. X-ray photoelectron spectroscopy (XPS) analyses of the surficial composition of the size-fractionated organo-mineral complexes further suggest that the NNP fraction has significantly higher atomic % of C ($p < 0.01$), N ($p < 0.01$), and Mg:Al ratios ($p < 0.05$) and lower atomic % of Al ($p < 0.01$) and Si ($p < 0.01$) than larger particles. The NNP fraction also has a higher proportion of mostly oxidized OC ($p < 0.05$), while the particulate fraction has more aliphatic/aromatic OC functional groups. Hence, my findings clearly demonstrate significant new insights into the differences in the concentration and molecular composition of size-fractionated COC, which imply the importance of taking into consideration of the NNP and fine colloid fractions separately (as opposed to combining them into the "dissolved" fraction following the conventional definition of 450 nm) when assessing the cycling and transport of various elements and associated organic C in depressional wetlands.

4.1 Introduction

Although wetlands cover only 5-8% of the world's land surface (Mitsch et al., 2013), they sequester an estimated 20-30% (450 Gt C) of the global carbon (C) stocks, which represents about a quarter of global soil OC inventory (Jokic et al., 2003; Lal, 2004). An improved understanding of stabilization, fluxes, and distribution of SOC in wetlands is essential as concerns for the impacts of climate change increase. Prolonged anaerobic periods in wetlands can facilitate C storage by slowing down the decomposition rate of soil organic matter (SOM) (Whiting and Chanton, 2001; Altor and Mitsch, 2008). Geomorphic depressional wetlands, which compose ~70% of all temperate forest wetlands in the US, are metabolically active ecosystems. These wetlands are mostly driven by precipitation and groundwater flow, while seasonal

wetting and drying creates biogeochemical “hotspots” for soil C cycling along a transect from upland-to-wetland as well as “hot moments” as the wetland hydrology changes seasonally. The ongoing climate change scenario additionally can alter the seasonal shifts in water balance by affecting the hydrologic conditions, which can modify the biogeochemical processes in such wetlands.

Redox-induced biogeochemical transformations are the key processes that control the stabilization of mineral-associated OC. The emerging concept of SOM stability as an ecosystem property suggests that the fate of SOM is not controlled by OM structure alone; rather, it is controlled by multiple environmental and biological factors (Schmidt et al., 2011). Among those factors, association between SOM and minerals has attracted increasing attention (Afsar et al., 2020; Barber et al., 2017; Hemingway et al., 2019; Lalonde et al., 2012). The association of OC with mineral phases, which involves physicochemical interactions between OC and the mineral matrix, depends on two main factors: 1) type and the specific surface area of the minerals and 2) the structural properties of SOM (Kalbitz et al., 2005; Mikutta et al., 2007).

In wetlands, oscillations between reduction and oxidation events impact mobilization of mineral colloids and biogeochemical C cycling through dissolution of Fe minerals and accompanying shifts in pH. Owing to their very large specific surface areas, high reactive site densities, and mobility, colloids (1-1000 nm) (Vold and Vold, 1983) can play an important role with respect to the binding of nutrients, contaminants, and SOM. Indeed, colloids are ubiquitous in different environments, e.g., marine, riverine (Orlandini et al., 1990), and groundwater (McCarthy and Zachara, 1989) ecosystems as well as in soil pore waters (Chin and Gschwend, 1991).

In uplands, Fe and Al (hydr)oxides protect OM from microbial decomposition, and thereby contribute to C storage for centuries to millennia. In flooded soils such as wetlands, however, reductive dissolution of Fe(III) oxides and pH changes can lead to the mobilization of previously mineral-bound OC (Grybos et al., 2009). During water table dropdown, Fe(II) is either leached out from the profile or re-oxidized to Fe(III) oxides upon re-oxygenation of the soil. Despite the significance of colloid particles in such associations, I have very limited understanding on the size-dependent composition of colloidal mineral-OC complexes and colloidal organic carbon (COC), and their influence on the mobilization of soil C. The use of an operational cut-off size range of dissolved organic matter (DOM; <450 nm) additionally hinders our ability to accurately assess C turnover rates due to the overestimation of the "dissolved" phase by including colloids of diameter < 450 nm (Yan et al., 2016; Afsar et al., 2020). This inaccurate differentiation of the colloids from the dissolved phase limits our ability to properly assess the biological functions and environmental fate and transport of colloid-associated-constituents such as OC.

Our knowledge about the isotopic and molecular composition of the size-fractionated COC in riverine and ocean ecosystems has been rapidly improving, however, very little is known for terrestrial ecosystems. In particular, owing to the more complex and dynamic redox features and high OC content, COC in depressional wetlands is expected to have distinctively different isotopic signatures and molecular composition at different size fractions. Under anaerobic conditions, soil microbes preferentially use more oxidized substrates thus tend to preserve OC in their reduced forms due to thermodynamic constraints (Boye et al., 2017). Therefore, knowledge of the size partitioning and molecular composition of COC could provide insights into

the fate, transport, bioavailability, and biogeochemical cycling of terrestrial SOM and other associated elements (Chen et al., 2004; Yin et al., 2014).

In this study, I have investigated the dynamics and molecular composition of the size-fractionated colloids and COC along the redox gradients in a depressional wetland. I have collected pore water samples along the transects delineated as upland, transition, and wetland zones from 50 cm, 100 cm, and 200 cm depths below the soil surface by maintaining *in situ* water chemistry conditions. The size-fractionated organo-mineral complexes, i.e., natural nanoparticles (NNP, 2.3-100 nm), fine colloid (100-450 nm), and particulate (450-1000 nm) fractions were analyzed using state-of-the-art spectroscopic techniques (e.g., isotope ratio mass spectrometry, IRMS; x-ray photoelectron spectroscopy, XPS). The goals of the study were to (1) quantify the size-dependent partitioning of COC within the colloidal size range and (2) determine the molecular composition of the size-fractionated COC.

4.2 Materials and Methods

4.2.1 Field Site Selection, Monitoring, and Sample Collection

4.2.1.1 Site Description

My study site is a freshwater depressional wetland located in Blackbird state forest (39°20'N 75°40'W), Delaware, USA. The peninsula is more than 183 miles in length and nearly 71 miles wide and comprises more than 17,000 bays. These bays are elliptical in shape, oriented NW to SE, with sandy rims and completely surrounded by uplands. Fenstermacher et al. (2014) discussed the distribution, morphology, and land-use patterns of Delmarva bays. The location of the study site and the transect delineated from the upland to the wetland are shown in **Figure 4.1**. Three zones were

established depending on the seasonal changes in the water table to monitor and collect pore water samples. Zone-1 is the wetland and is characterized by seasonal ponding during winter and early spring and then dried out sometime before or during the summer season. Zone-2 is a transitional zone with marked saturation, but not significant ponding. Zone-3 is in the upland area beyond the wetland boundary. Soils in wetland, transition, and upland zones are classified as fine, loamy, mixed, mesic Typic Umbraquults (Corsica soil series); fine, loamy, mixed, mesic Typic Endoaquults (Fallsington soil series); and fine, loamy, mixed, active, mesic Aquic Hapludults (Woodstown soil series), respectively, according to the U.S. Department of Agriculture (USDA) soil taxonomy (Soil Survey Staff, 2015). All the soil properties were described according to Schoeneberger et al. (2002). Daily rainfall amounts were recorded at a weather station located at the Blackbird State Forest office, ~ 200 m north of our study site. Soil profile characteristics in the wetland, transition, and upland zones are listed in **Table 4.1**.

4.2.1.2 Monitoring Well Installation

Standard monitoring wells (slotted PVC pipe, inner diameter = 5 cm) were installed to a depth of 95 cm below the soil surface in wetland and transition and 158 cm deep in upland. An additional well was placed in wetland zone with all but 15 cm of the screen above the soil to measure inundation. Wells were installed using a bucket auger with an outside diameter of 7.6 cm. Quartz sand (U.S. SILICA®) was placed around the well screen to promote water movement towards the well. At the soil surface, the riser was sealed with polyurethane-based insulating foam sealant to prevent water from running down the outside of the pipe to the well screen. The foam was used instead of bentonite sealant to prevent any additional colloids that could be

mobilized from bentonite to contaminate the samples. Detailed well installation procedure is shown schematically in **Figure 4.2**. Data recorders (Odyssey Capacitance Water Level Logger) were installed in each well to record water levels twice a day from November 20, 2016 to July 11, 2019. The automated water-level recorders were checked frequently for accuracy by comparison of automated readings to manual readings.

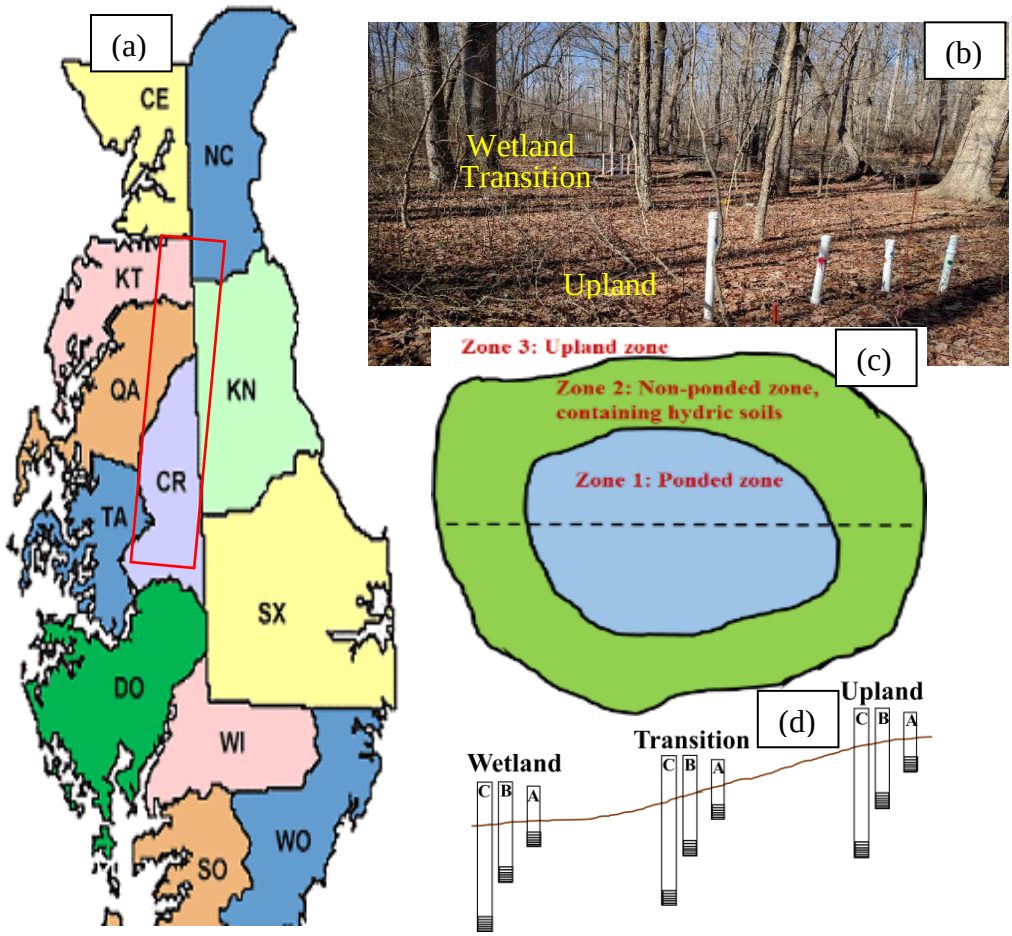

Figure 4.1: (a) Sampling site located in the Blackbird state forest, (b, c) schematic diagram showing three hydrological zones and a cross-section of the wetland instrumented with piezometers at different zones. Letter A, B and C indicates three piezometers installed at 50 cm, 100, cm and 200 cm at the wetland, transition, and upland zones.

Table 4.1: Characteristics of soil profile in wetland, transition, and upland zones in the depressional wetland.

Wetland zone					
Horizon	**Depth (cm)**	**Matrix**[†]	**Texture**[§]	**Structure**[¶]	**Organic C**[‡] **(%)**
A1	0-8	10YR2.5/1	CL	1, f, sbk	8.6
A2	8-28	10YR3/1	CL	1, f, sbk	6.8
ABtg1	28-36	10YR5/1	SiC	1, f, sbk	2.2
ABtg2	36-66	10YR5/1	SiC	M	1.5
BCg	66-76	6/N	SL	M	
2Cg1	76-86	6/N	SC		
2Cg2	84-94	6/N	CL		
2Cg3	94-107	10YR7/1	SCL		
3Cg1	107-132	10YR7/1	SL		
3Cg2	132-158	10YR7/1	LS		
3Cg3	183+	10YR7/1	FSL		
Transition zone					
A	0-22	10YR3/2	SCL	2, f, gr	2.7
EA	22-38	5YR5/1	SL	1, f, sbk	0.6
Eg1	38-46	7.5YR6/2	SL	2, m, sbk	
Eg2	46-58	10YR7/1	SL	2, m, sbk	
Btg	58-79	10YR7/1	SCL	3, m, sbk	
BCg	79-91	10YR7/1	SL	2, m sbk	
Cg1	91-112	10YR6/2	LS		
Cg2	112-137	10YR6/2	SL		
C1	137-150	10YR5/8	SL		
C2	183+	10YR6/6	SL		
Upland zone					
A	0-11	7.5YR3/1	SL	2, m, gr	3.87
Ap	11-25	7.5YR4/2	SL	1, f, gr	0.87
E	25-43	10YR6/3	LS	sg	
Eg1	43-66	2.5Y7/2	LS	sg	
Eg2	66-104	2.5Y7/2	LS	sg	
Btg1	104-117	10YR6/2	SL		
Btg2	117-127	10YR7/6	SL		
C1	127-145	10YR6/8	LS		
C2	145-168	10YR6/8	LS		
C3	183+	10YR6/6	LS		

[§]**Texture:** CL=clay loam, SiCL=silty clay loam, LS=loamy sand, SL=sandy loam, SCL=sandy clay loam, SiC=silty clay, FSL=fine sandy loam
[¶]**Structure:** 1=weak, 2=moderate, 3=strong, f=fine, m=medium, sg=single grain, M=massive, gr=granular, sbk=subangular blocky
[¶]**Organic C:** Loss on ignition

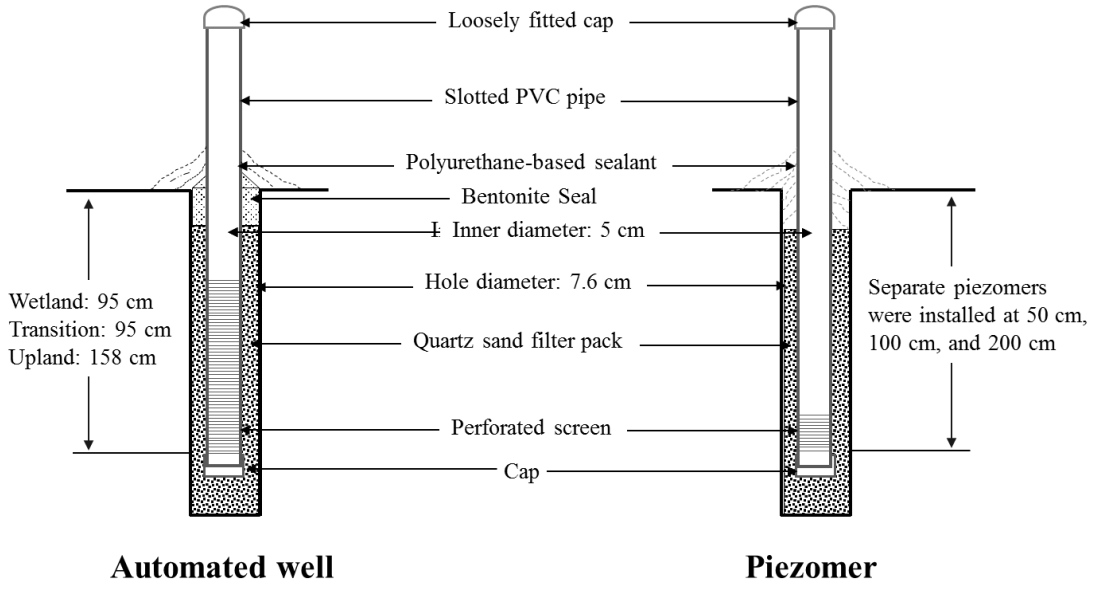

Figure 4.2: Schematic diagram of the monitoring wells and piezometers installed in the wetland, transition, and upland zones.

4.2.1.3 Piezometer Installation and Water Sample Collection

In each zone, three piezometers (PVC pipe, inner diameter: 5 cm) were installed separately at 50 cm, 100 cm, and 200 cm depths in Oct 2017 **(Figure 4.1D)**. Both the wells and piezometers were protected from potential contamination and rainfall using loosely fitted caps. I collected piezometer water samples from 2018 (Feb 21, Nov 20, and Dec 14) to 2019 (Feb 05, and May 01) to monitor changes in solution chemistry (pH, Eh, and IS) and dynamics of size-fractionated colloid and OC. Samples were collected under continuous purging with argon (Ar) gas to maintain the *in situ* water chemistry conditions using a peristaltic pump (Geotech, Denver) after discarding the first 3-well volumes of water. The well volume was calculated based on water height inside the piezometer. The pumping rate was maintained at ~100 ml min^{-1} to limit any interference from artificially suspended particles into the samples (Ryan and Gschwend, 1990). Depending on availability, 2-L purged water samples were

collected from each depth and stored in acid-washed polytetrafluoroethylene (PTFE) bottles. All samples were stored in ice and transported to the laboratory for immediate size fractionation.

4.2.2 Sample Preparation and Analyses

4.2.2.1 Sample Size Fractionation

All pore water samples were fractionated into < 1000 nm (10 min at 339×*g* rcf or 1250 rpm), < 450 nm (10 min at 1581×*g* rcf or 2700 rpm), and < 100 nm (30 min at 10628×*g* rcf or 7000 rpm) size fractions using a Thermo Scientific Sorvall Lynx 6000 centrifuge machine (Thermo Scientific) equipped with a fiber lite F9-6x1000 LEX rotor. The size-specific centrifugation speed and time was using the Stokes' law (Gimbert et al., 2005) assuming spherical particles and a particle density of 2.65 g cm^{-3}. Although these two assumptions are somewhat unrealistic and do not consider the heterogeneity of particle composition and size, I preferred using centrifugation over filtration for size fractionation (except <2.3 nm) as it avoids inaccuracies associated with the conventional filtration techniques. Membrane filters have been reported to remove more soil particles than the corresponding centrifugation procedure due to pore clogging, particle shapes, and interactions between colloid particles and membrane surface (Gimbert et al., 2005). However, I acknowledge that particles composed of mostly organic materials and thus having lower than 2.65 g cm^{-3} density, would preferentially remain in the supernatant than mineral particles with the same size and thus be underestimated. Finally, < 100 nm fraction was passed through an ultrafiltration system (Amicon® stirred cell) equipped with Ultracel® 10 kDa membrane ultrafiltration discs (EMD Millipore Corporation) to separate the dissolved

fraction. A 10 kDa membrane corresponds to a pore size of 2.3 nm (Guo and Santschi, 2007). All the size-fractionated filtrates, i.e., < 1000 nm, <450 nm, <100 nm, and <2.3 nm was immediately acidified with HCl to prevent precipitation of metal-OM complexes. The particulate, fine colloid, and NNP fractions were collected from the precipitates at each step and freeze-dried for further analyses. The weight of the size fractionated colloid particles was measured gravimetrically using a microbalance after freeze drying of the precipitates.

4.2.2.2 Sample Analyses

pH, Eh (pE), and EC of the pore water samples were measured using corresponding probes (Fisher Scientific, Hampton, NH). Ionic Strength (IS) was calculated as a function of the measured EC (Alva et al., 1991; Morrisson et al., 1990) using the equation: $IS = 0.013 \times EC$, where EC is the suspension electrical conductivity (ds m^{-1}). Iron (II) concentrations of the pore water samples were measured following the ferrozine method (Stookey, 1970) using UV-visible spectrophotometer (Agilent Technologies, Cary 60 UV-Vis). Total organic carbon (TOC) concentrations at < 2.3 nm, < 100 nm, < 450 nm, and < 1000 nm were measured using a TOC analyzer (Shimadzu TOC-L).

Stable $\delta^{13}C$ and $\delta^{15}N$ isotope values and total C and N concentrations of the freeze-dried, size-fractionated COC were determined using an IRMS (DELTA V plus, Thermo Fisher Scientific) equipped with an elemental analyzer (EA). Stable $\delta^{13}C$ or $\delta^{15}N$ values were calculated as $(R_{sample}/ R_{standard} -1) \times 1000$, where R is the ratio of heavier to lighter isotope ($^{13}C/^{12}C$, or $^{15}N/^{14}N$), and expressed in parts per thousand (‰) relative to their international standards Vienna-Pee Dee Belemnite (PDB) limestone and atmospheric N_2 standards. USGS-40 (L-glutamic acid, 40.8% C and

9.52% N) and USGS-41 (L-glutamic acid enriched in ^{13}C and ^{15}N, 41.9% C and 9.76% N) were used as reference materials.

The photoelectron spectra of the size-fractionated, freeze-dried samples were taken at the University of Delaware's Surface Analysis Facility using a Thermo Scientific K-alpha+ XPS (East Grinstead, United Kingdom). Samples were dispersed uniformly on double-sided conducting tapes and affixed to a stainless-steel plug. The samples were excited with a monochromated aluminum Kα radiation (E_{exc} = 1486.6 eV) at an incident angle of 57.2° with a spot size of 100 μm wide ellipse; charge neutralization was carried out with a low energy electron flood gun. A survey scanning was ran from 0 to 1200 eV using a 1 eV step size and 100 eV pass energy to measure the elemental composition of soil minerals and their associated OC. High-resolution scanning for every elements was obtained using a step size of 0.1 eV and pass energy of 20 eV. During the operation, vacuum was maintained at $< 3 \times 10^{-9}$ mbar. The chemical composition was revealed by deconvoluting C 1*s*, N 1*s*, Si 2*p*, Fe 2*p*3/2, Al 2*p*, Mn 2*p*, Mn 3*s*, O 1*s*, Mg 1*s*, Mg 2*p*, Ca 2*p*, Cl 2*p*, Na 1*s* peaks into sub-peaks by fitting Gaussian-Lorentzian functions and Shirley background correction of the XPS spectra using the CasaXPS version 2.3.16 (Teignmouth, UK). Molar fractions of the various elements were calculated from peak areas based on the acquisition parameters and atomic sensitivity factors calculated from the electronic cross-section of each element and orbital (Scofield, 1976).

A typical C spectrum obtained by XPS is deconvoluted into three components representing aliphatic and aromatic $C^{[0]}$ (C-C, C=C, C-H; at 284.6 eV), ether, alcohol, and amine C such as those in polysaccharides or amino acids, $C^{[+1]}$ (C-O, C-N; at 286.5 ± 0.2 eV), and carbonyl and carboxyl C, $C^{[+2]}$ (C=O, at 288.6 ± 0.2 eV),

depending on the specific bonding environments or oxidation states (Gerin et al., 2003; Mikutta et al., 2009). Though carbonyl/carboxyl C peaks are generally easily discerned, the effect of different counter ions (H, Na, K) and low concentration might shift the peak position. Therefore, a combined peak shape was used for the fitting. Weight % of surface C ($C_{surface}$) was calculated by multiplying the molecular weight of all elements with their measured atom % assuming that hydrogen has negligible contribution (Arnarson and Keil, 2001, 2007).

Freeze-dried size-fractionated particles were re-dissolved/isolated using ethanol for direct examination by transmission electron microscopy (TEM). The chemical composition of the individual particles was determined with an energy-dispersive X-ray spectroscopy (EDS) system.

4.3 Results

4.3.1 Changes in Water-table

Daily water table data from automated wells and monthly rainfall data from Nov 2016 to July 2019 are plotted in **Figure 4.3(a-b)**. In the wetland zone, the water table fluctuated seasonally from -50 cm to 25 cm from Nov. 2016 to Jan. 2018 followed by a continuous inundation of at least 20 cm of water. In the transition zone, the water table was -25 to -100 cm until Feb 2018 followed by an inundation up to 25 cm of water until June 2018. After June 2018, the drawdown of the water table started and reached -50 cm by Oct. 2018. The transition zone was inundated again by Nov 2018 reaching 50 cm of water. In the upland, the water table was entirely below the soil surface and fluctuated between -150 cm to -100 cm, -125 cm to -50 cm, and -100

cm to -25 cm from Nov 2016 to Dec 2017, Jan 2018 to Oct 2018, and Nov 2018 to July 2019, respectively.

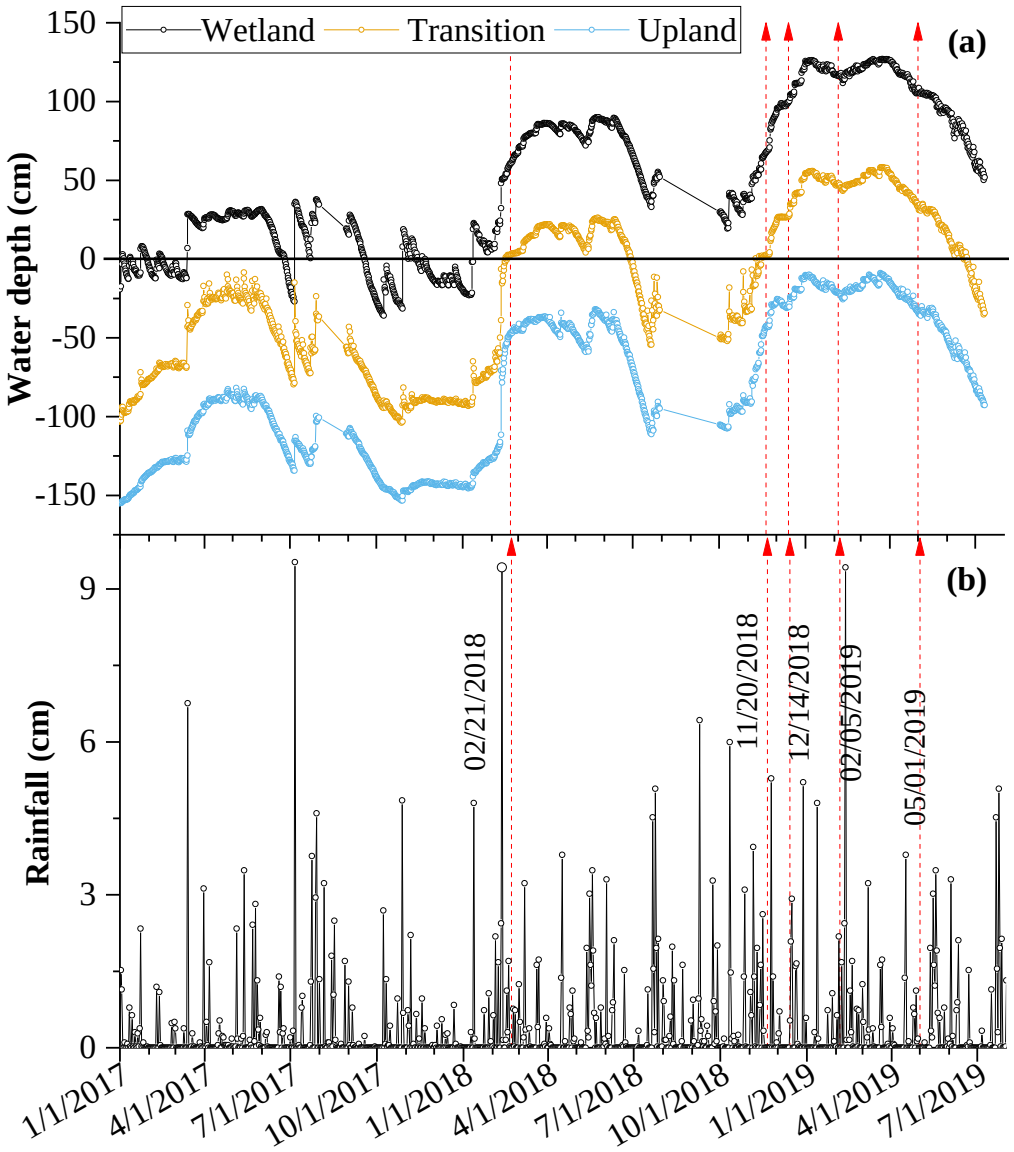

Figure 4.3: Seasonal dynamics of (a) daily average water table depth (cm) and (b) daily cumulative precipitation (cm) events for the hydrologic period between 2017 to 2019. Horizontal straight line indicates soil surface and vertical red dashed lines indicate sampling time.

4.3.2 Pore Water Chemistry

Fluctuations of water table level in the depressional wetland induced dynamic changes in physicochemical properties (e.g., pH, pE, and IS) of soil solution as summarized in **Figure 4.4**. Along the transect, the wetland zone had significantly the lowest ($p < 0.001$) and the least seasonal and vertical fluctuations in pH (5.10 ± 0.43) through the soil profile than the other two zones. The pH increased with depth from 5.67 ± 0.30 and 5.02 ± 0.64 at -50 cm depth to 6.18 ± 0.38 and 6.12 ± 0.27 at -200 cm depth, respectively, in the transition and upland zones. The calculated mean IS values ranged between 2.89 ± 1.26 mM to 3.10 ± 1.98 mM, 3.50 ± 0.30 mM to 5.25 ± 0.85 mM (except samples collected on Feb 2019), and 3.30 ± 1.33 mM to 7.11 ± 4.74 mM in the wetland, transition, and upland zones, respectively. Compare to the upland, Eh (pe) values were lower in the other two zones. Although the pourbaix Eh/pH diagram assumes complete equilibrium under idealized condition, it showed that shows that wetland pore water samples mostly fall below the Fe-reduction line in contrast to the transition and upland samples. The specific Eh/pH lines for oxygen and iron reduction are drawn by the respective Eh values at pH 7 of 350 mV and 120 mV, adjusted with a slope of -60 for each pH value less than 7 (Hurt, 2013). Additionally, most of the samples collected from the wetland and transition zones were located below the threshold limit of the anaerobic line, which is plotted following the equation: Eh = 595 – 60 (pH); commonly used to identify reducing conditions in soil (Vasilas and Vasilas, 2013). The more reduced condition in the wetland zone is supported by its higher aqueous Fe^{2+} concentrations compared to the transition and upland. Along the soil profile, Fe^{2+} concentrations were 103.17 ± 15.45 µM, 96.92 ± 21.64 µM and 40.90 ± 28.66 µM at -50 cm, -100 cm, and -200 cm depths in the wetland **(Figure 4.4d)**. Soluble Fe^{2+} concentrations were much lower (< 8 µM) in the other two zones.

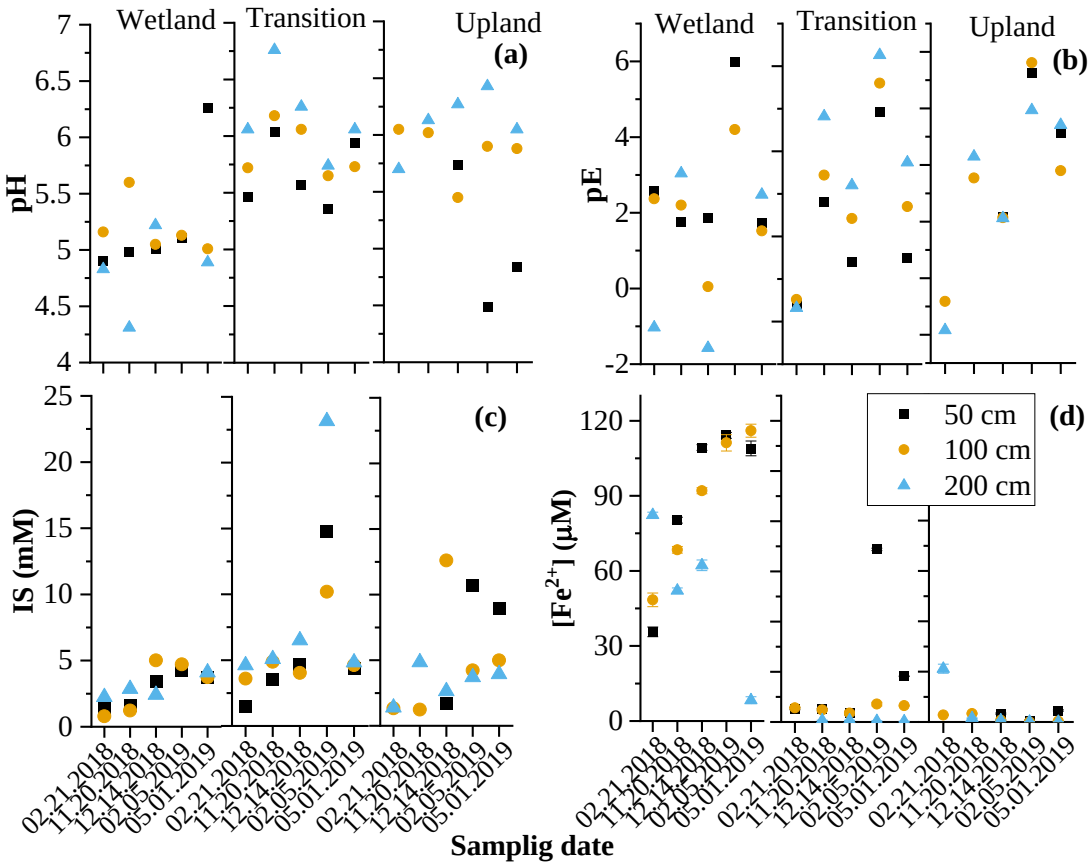

Figure 4.4: Changes in (a) pH, (b) pE, (c) IS and (d) Fe^{2+} concentration (µM) in pore water samples along the redox gradients from upland to wetland zones and at different soil depths.

4.3.1 Concentration of Soil Colloids in Pore Water

Total colloid (2.3-1000 nm) concentrations in pore water samples were significantly higher in the wetland ($p < 0.001$) than the transition and upland zones **(Figure 4.6)**. Colloid concentrations varied in concert with water table fluctuations, higher during the early water table rising phase and lower during static high and declining water table phases. Along the soil profile, colloid concentrations were significantly lower at -200 cm than at -50 cm depths in all three zones. Total colloid concentrations in NNP, fine colloid, and particulate fractions, determined using linear

regression analyses, were, respectively, 24%, 41%, and 33% of the total colloid present in the pore water samples **(Figure 4.7)**.

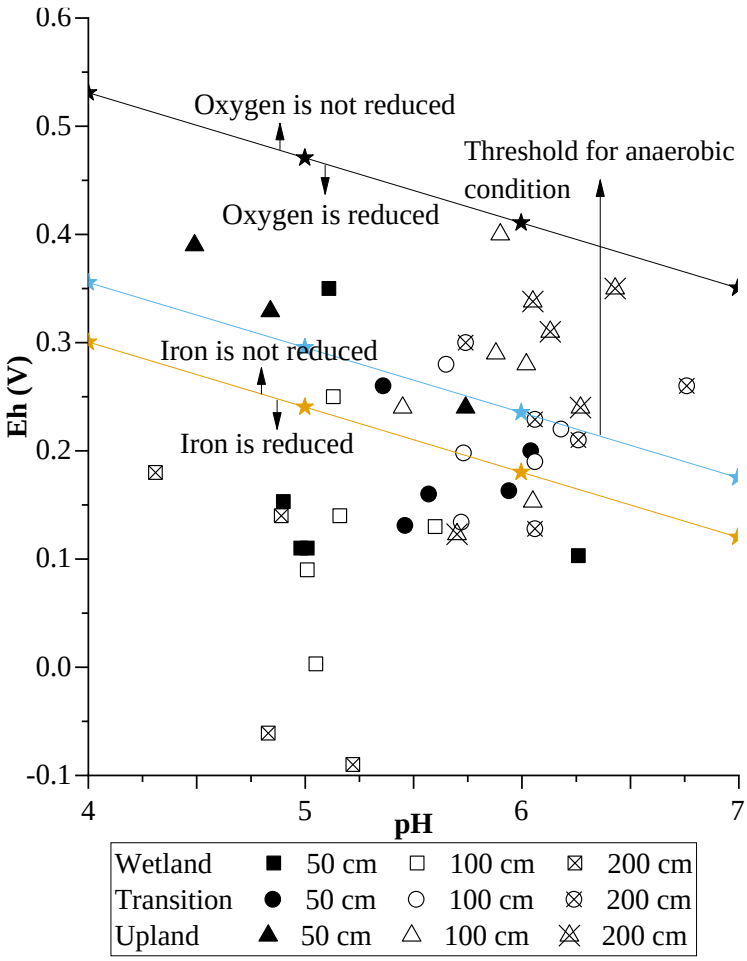

Figure 4.5: Distribution of Eh-pH values measured in pore water samples. Specific Eh/pH lines for oxygen and iron were drawn with the Eh values at pH 7 of + 0.35 V and + 0.12 V, respectively, adjusted with a slope of negative 60 for each pH value less than 7 (Hurt, 2013). The threshold limit for anaerobic condition was drawn as Eh = 595 – (60 x pH) (Vasilas and Vasilas, 2013).

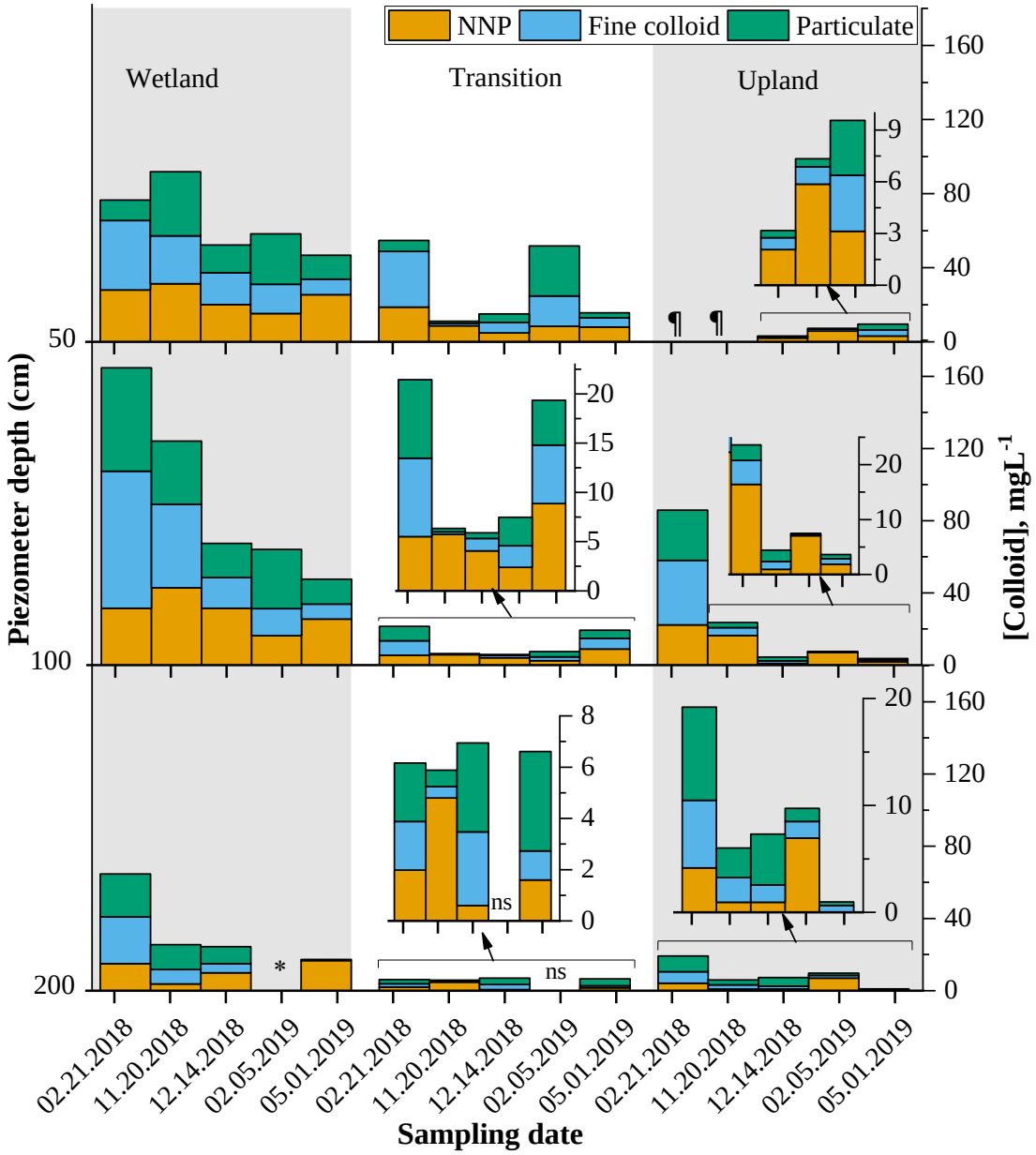

Figure 4.6: Colloid concentration in NNP, fine colloid, and particulate fractions. There was no water in the piezometer at 50 cm depth in upland during Feb 21 and Nov 20, 2018 as the water table was below that level (indicated by "¶"). On Feb 02, 2019, the riser of piezometer installed at 200 cm depth was below the standing water in wetland (indicated by "*"). Very negligible amount of size-fractionated colloids was present at 200 cm depth in transition zone on Feb 05, 2019.

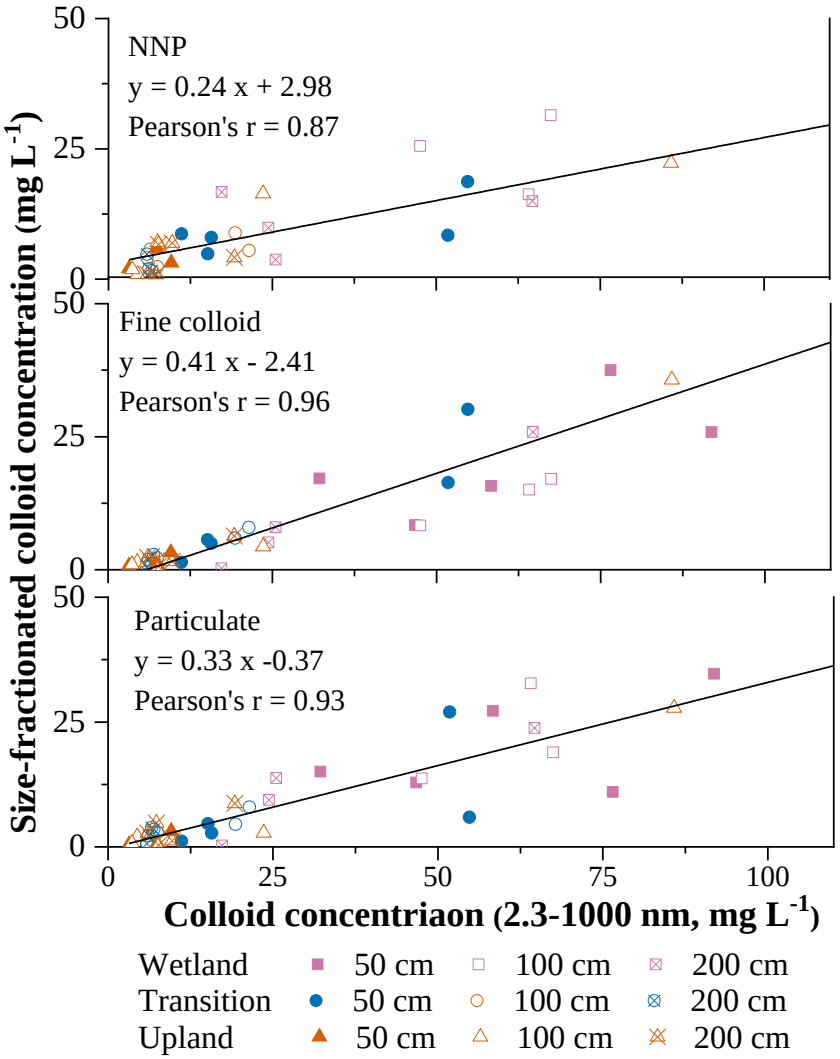

Figure 4.7: Linear relationship between size-fractionated colloid concentration to the total colloid concentration within 2.3-1000 nm range.

4.3.2 Size-fractionated SOC Concentrations in Pore Water

My measurements revealed significant increases ($p < 0.001$) in total OC concentration (<1000 nm, $TOC_{<1000}$) along the redox gradients from upland to wetland zones at all depths **(Figure 4.8)**. The average $TOC_{<1000}$ concentrations in the wetland were 34.77 ± 8.39 mg L^{-1}, 34.53 ± 11.03 mg L^{-1}, and 24.09 ± 7.55 mg L^{-1}, respectively at 50 cm, 100 cm, and 200 cm depth. Consistent with previous field studies (K.

Kalbitz et al., 2000; Michalzik et al., 2001), average $TOC_{<1000}$ concentrations were much lower at 200 cm depths in all the three zones. However, I did not see any significant changes in the $TOC_{<1000}$ concentration depending on the seasonal hydrologic condition except in the wetland and transition zone at the 100 cm depth. In all the three zones, the maximum $TOC_{<1000}$ concentration was observed at the early stage of the water table rising period (i.e., Feb and Nov 2018) followed by a decrease during the static high-water table condition (Feb 2019). However, $TOC_{<1000}$ concentration increased again when the water table dropped in May 2019.

I partitioned $TOC_{<1000}$ into four size classes: dissolved, NNP, fine colloid, and particulate fractions. Within the $TOC_{<1000}$ pool, I found that the distribution of pore water's OC content skewed mostly towards smaller size fractions. Dissolved and NNP fractions were the exclusive constituents among all the four size fractions, which comprised 47 ± 4% and 37 ± 4% of $TOC_{<1000}$ **(Figure 4.9)**, respectively. The other two size fractions, i.e., fine colloid and particulate fractions, each individually contributed ~8%. However, if I used the operationally defined "dissolved" fraction (<450 nm), the DOC comprised more than 90% of $TOC_{<1000}$ (**Figure 4.10**, $DOC_{<450} = 0.91 \pm 0.03 \times TOC_{<1000} - 0.18$), where the correlation coefficient is highly significant (Pearson correlation coefficient $r = 0.99$, $p < 0.001$).

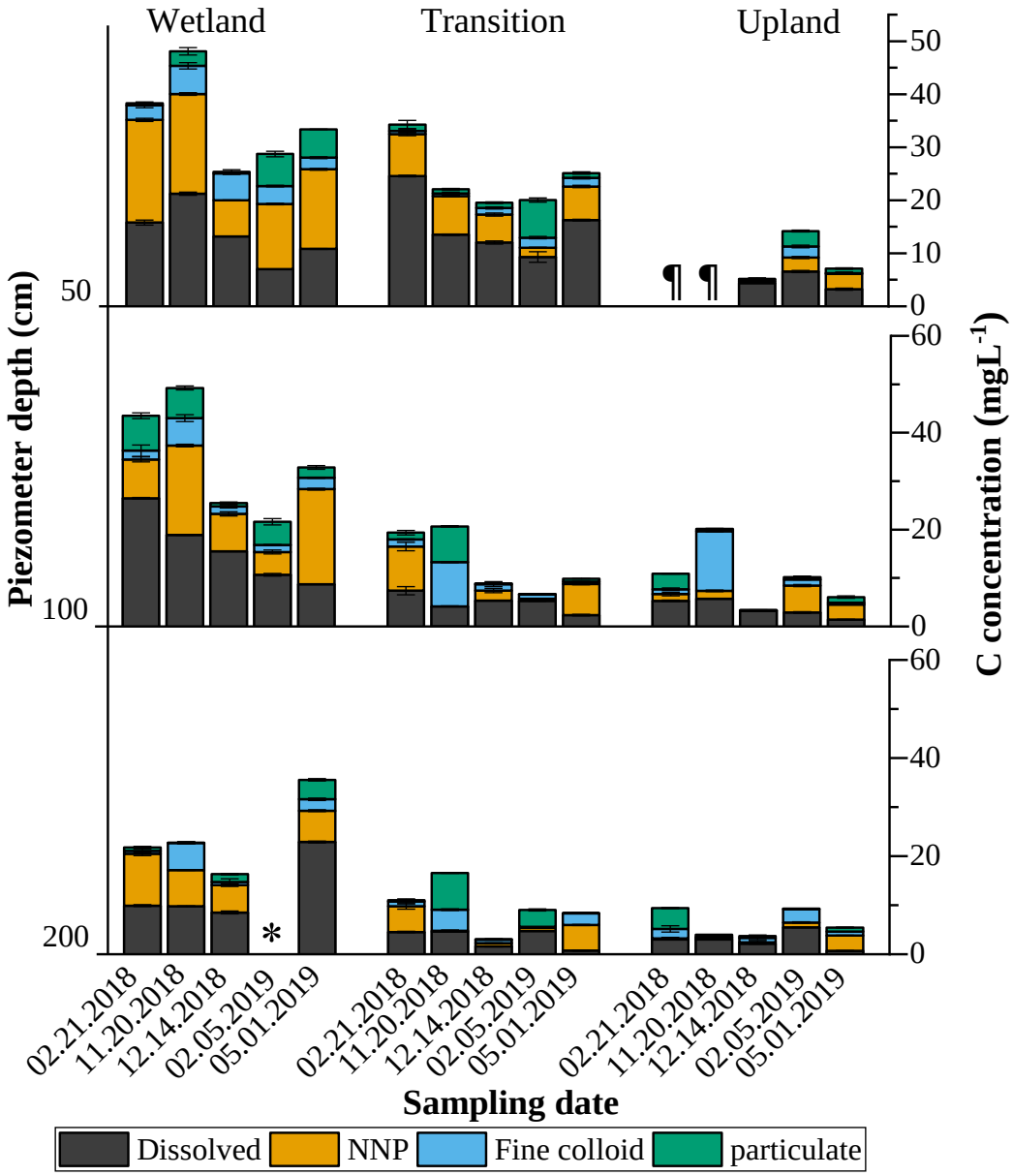

Figure 4.8: Organic C concentration in the dissolved, NNP, fine colloids, and particulate factions in pore water samples collected between Feb 21, 2018 to May 02, 2019 from wetland, transition and upland. There was no water in the piezometer at 50 cm depth in upland during Feb 21 and Nov 20, 2018 as the water table was below that level (indicated by "¶"). On Feb 02, 2019, the riser of piezometer installed at 200 cm depth was below the standing water in wetland (indicated by "*").

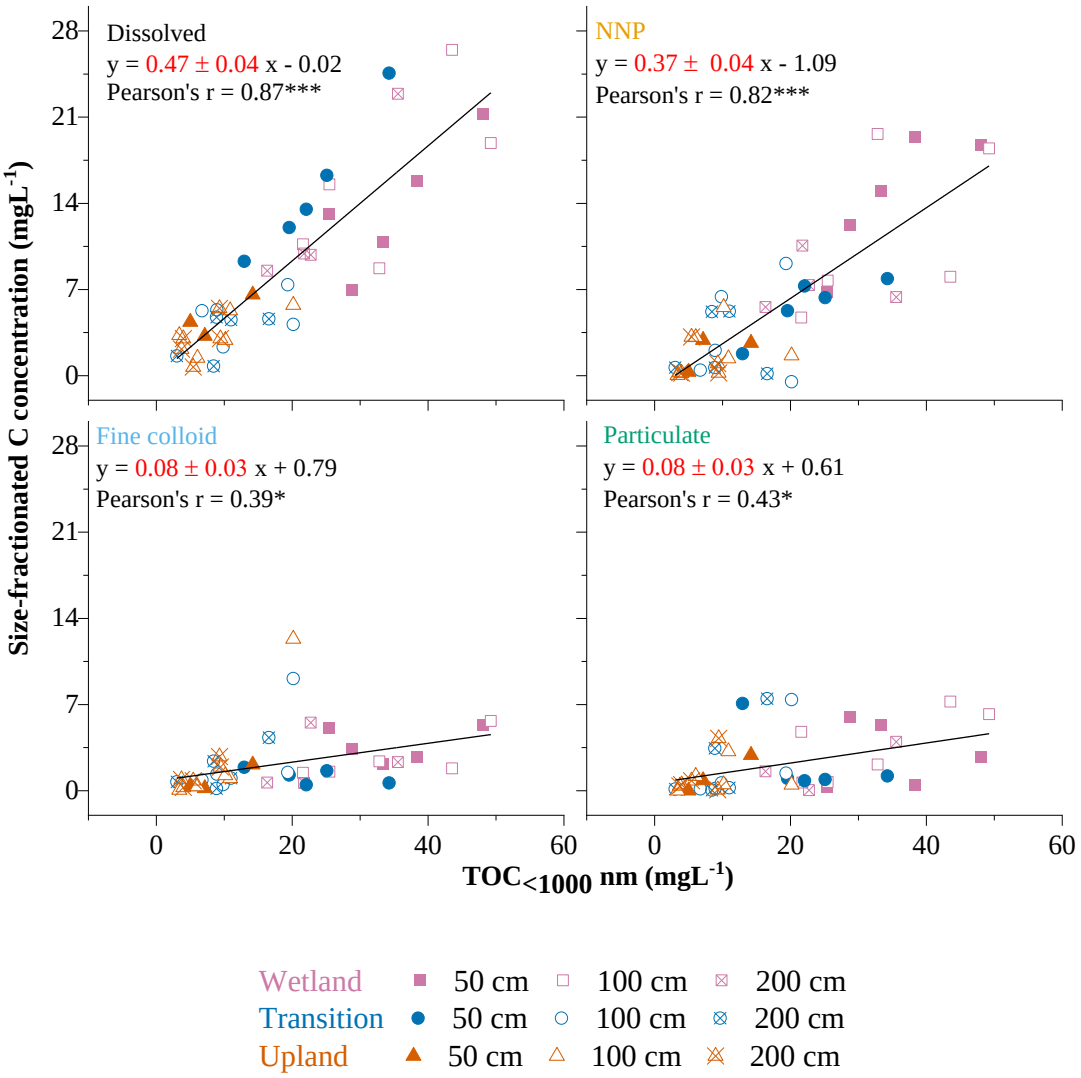

Figure 4.9: Linear regression analyses between size fractionated OC (dissolved, NNP, fine colloid, and particulate) and total OC ($TOC_{<1000}$). Level of significance: * $p < 0.05$, ** $p < 0.01$, *** $p < 0.001$. No asterisk indicates not significant.

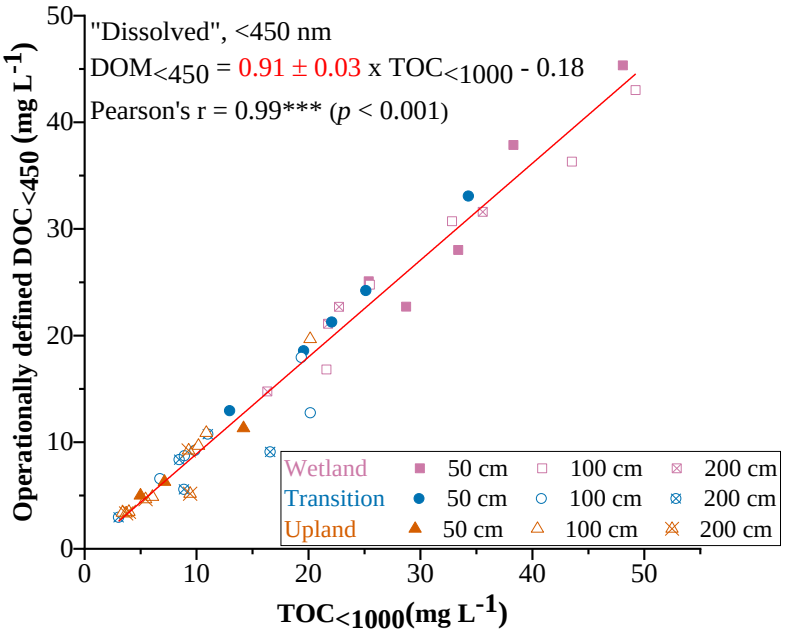

Figure 4.10: Relationship between operationally defined dissolved OC (<450 nm, $DOC_{<450}$) and total OC (<1000 nm, $TOC_{<1000}$).

Bulk C and N concentrations (C_{bulk} and N_{bulk}) of the freeze-dried, size-fractionated colloid particles collected on Feb 2018 were determined using IRMS. Among 3 size fractions (except dissolved), NNP fraction had the highest $[C]_{particle}$ and the values were 228.24 ± 10.28 g kg^{-1}, 108.68 ± 52.20 g kg^{-1}, and 50.78 ± 23.21 g kg^{-1}. On an average, the NNP fraction constituted 50-83% of total COC (2.3-1000 nm; **Figure 4.11** and **Table 4.2**) in the wetland, transition, and upland zones. Fine colloid and particulate fractions comprised, respectively, 11-28% and 7-27% of the COC. Similarly, deconvoluted XPS spectra showed that the NNP fraction had the highest surface C concentration ($C_{surface}$) compared to the other two larger size fractions (p < 0.01), while the C atom percentages were 33.50 ± 13.90 %, 13.22 ±3.97 %, and 14.86 ± 5.80 %, respectively, in NNP, fine colloid, and particulate size fractions **(Figure 4.12)**.

Table 4.2: Relative percentages of OC in the NNP, fine colloid, and particulate size fractions of samples collected on Feb. 2018 measured by using IRMS.

Zone	Depth (cm)	Relative OC %		
		NNP	Fine colloid	Particulate
Wetland	50	61.60 ± 0.84	16.93 ± 0.16	21.47 ± 0.69
	100	76.15 ± 0.26	11.72 ± 0.33	12.13 ± 0.59
	200	83.04 ± 0.49	10.07 ± 0.36	6.89 ± 0.13
Transition	50	54.09 ± 0.90	19.89 ± 0.27	26.02 ± 0.62
	100	50.99 ± 0.64	25.40 ± 0.92	23.61 ± 0.28
	200	53.86	19.63	26.51
Upland	50			
	100	50.20 ± 2.34	28.27 ± 1.03	21.53 ± 1.30
	200	62.21 ± 0.65	22.44 ± 2.24	15.35 ± 1.59

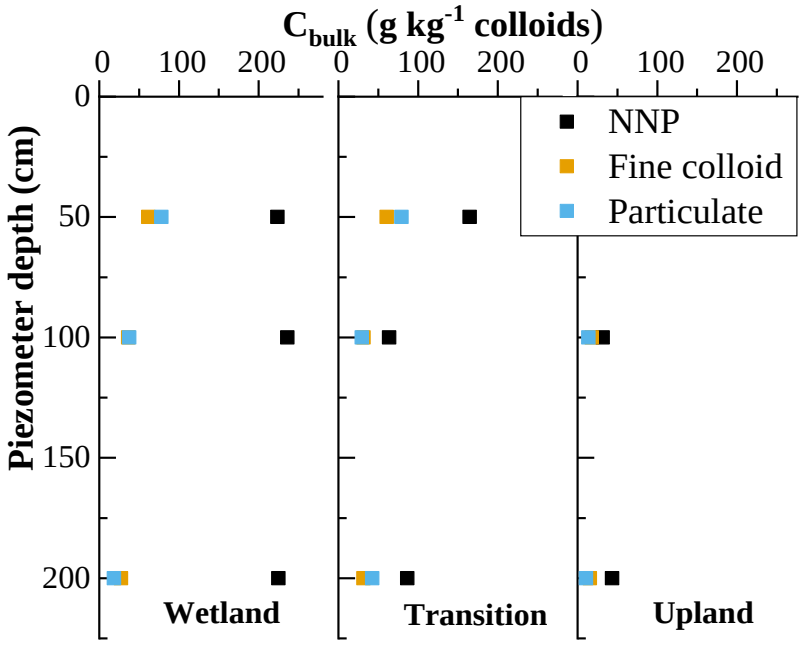

Figure 4.11: Bulk C concentration (C_{bulk})of the size-fractionated COC measured by using IRMS.

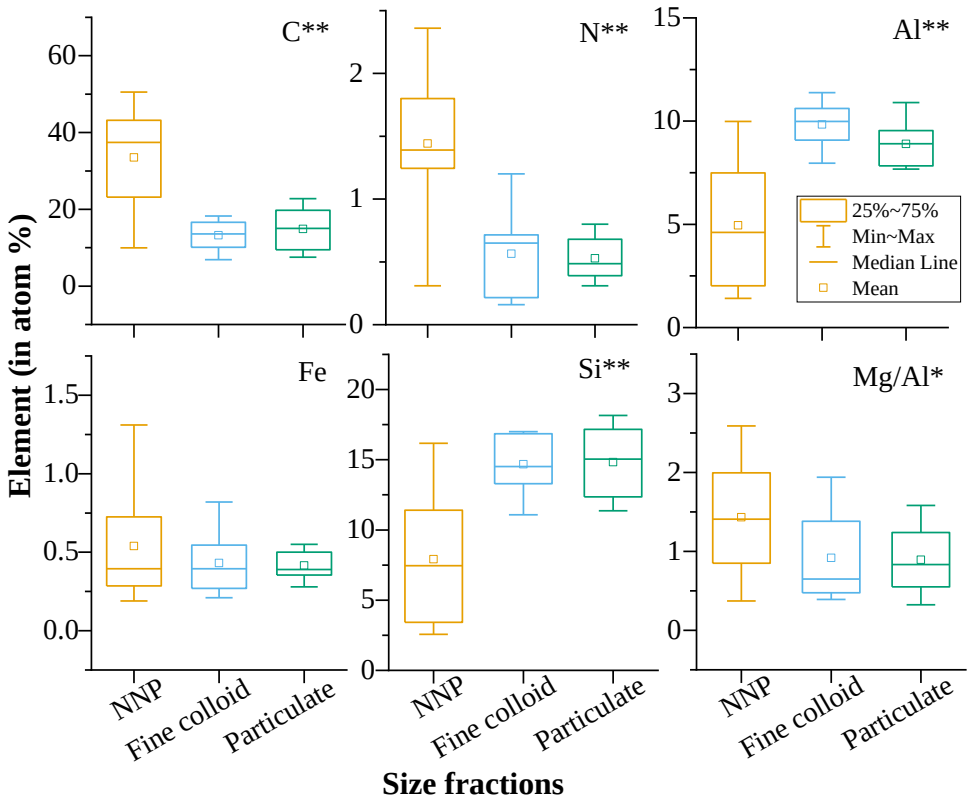

Figure 4.12: Surface atom percentages of different elements in size fractionated organo-mineral complexes as measured by XPS. Level of significance: * $p < 0.05$, ** $p < 0.01$, *** $p < 0.001$, no asterisk: not significant.

4.3.3 Surface and Bulk Molecular Composition of Size-fractionated Colloids and Associated COC

X-ray photoelectron spectroscopy analyses did not reveal any obvious trend in the atom percentages of different elements in the water samples collected from different zones and depths. However, among size-fractionated organo-mineral complexes, the NNP fraction had significantly higher surface C and N ($p < 0.01$) atom %, Mg:Al ratio ($p < 0.05$) and lower Al ($p < 0.01$) and Si atom % ($p < 0.01$) compare to the larger particle fractions **(Figure 4.12)**. The deconvoluted C 1s XPS spectra further confirmed a wide variation in the functional groups of surface OC among size-

fractionated particles. Carbon 1s spectra of the samples collected on Feb 2018 suggest that the reduced forms of C, e.g., aliphatic or aromatic $C^{[0]}$ (C-C, C-H), were selectively adsorbed to mineral surfaces over the oxidized $C^{[2+]}$ (C=O) carbonyl/carboxyl C functional groups ($p < 0.01$) regardless of particle size, redox gradient, and hydrologic condition **(Figure 4.13)**. Relative atom % of the C-C or C-H, C-O or C-N, and C=O were 49.82 ± 8.31 %, 33.22 ± 8.37 %, and 16.96 ± 4.48%, respectively. Consistent with the results from our previous redox oscillation microcosm study (Afsar et al., 2020), NNP fraction had significantly higher proportion of mostly oxidized OC ($p < 0.05$), while the particulate fraction had more aliphatic/aromatic OC functional groups on their surfaces.

The isotopic signature of the size-fractionated particles ($\delta^{13}C$, $\delta^{15}N$) revealed an enrichment of ^{13}C from wetland to upland **(Figure 4.14)**. Among different size fractions, NNP particles were more enriched in ^{13}C stable isotope than larger size fractions. A strong positive relationship between $[C]_{particle}$ and $[N]_{particle}$ as measured using the IRMS indicates that the C associated with soil colloids were mostly organic compounds **(Figure 4.15)**. Transmission electron microscopy and EDS data indicate that the size-fractionated particles differ in their elemental composition and concentration. In contrast to the fine colloid and particulate fractions, the NNP fraction had a weaker diffraction pattern, indicating minor crystallinity **(Figure 4.16)**. It makes sense to me as the amorphous is the 1st to form when metal oxides are created. However, the presence of lattice fringing in high-resolution images show the presence of some crystalline nanoparticles. Consistently with IRMS and XPS analyses, EDS data confirmed the highest C concentration at smaller size fractions. The atomic % of

C were 28%, 10%, and 5% respectively at NNP, fine colloid, and particulate size fractions.

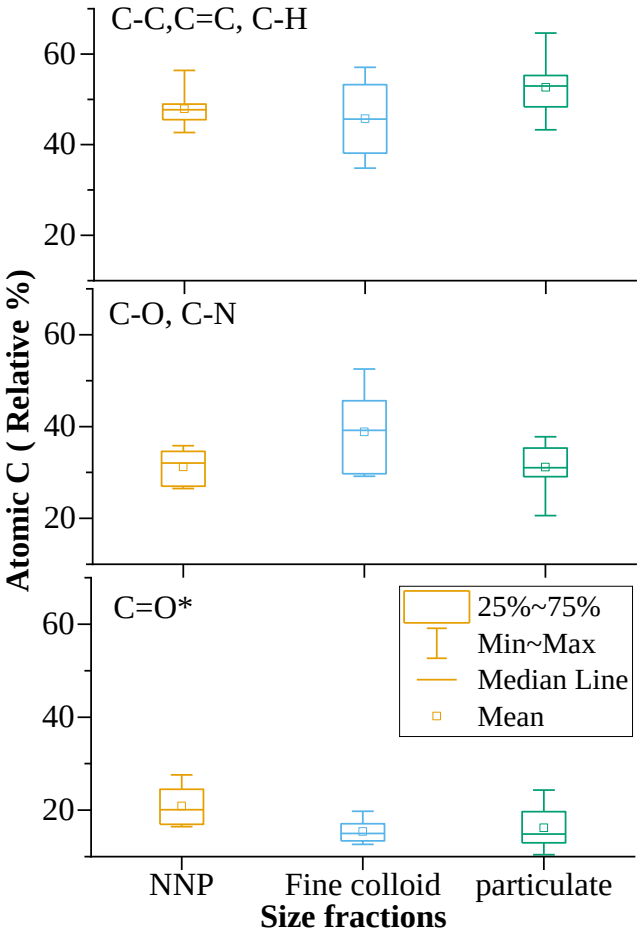

Figure 4.13: Relative atom percentages of carbon functional groups in pore water samples collected on Feb 2018 as de-convoluted from C 1s XPS spectra. (a) aliphatic or aromatic C (C-C, C=C, C-H; at 284.6 eV); (b) amines and/or alcohols like those in polysaccharides and amino acids (C-O, C-N, at 286.5 ± 0.2 eV); and (c) carbonyl/carboxyl C (C=O; 288.6 ± 0.2) each expressed as the relative atom percent of the total C in size fractionated organo-mineral complexes. Level of significance: * $p < 0.05$, ** $p < 0.01$, *** $p < 0.001$, no asterisk: not significant.

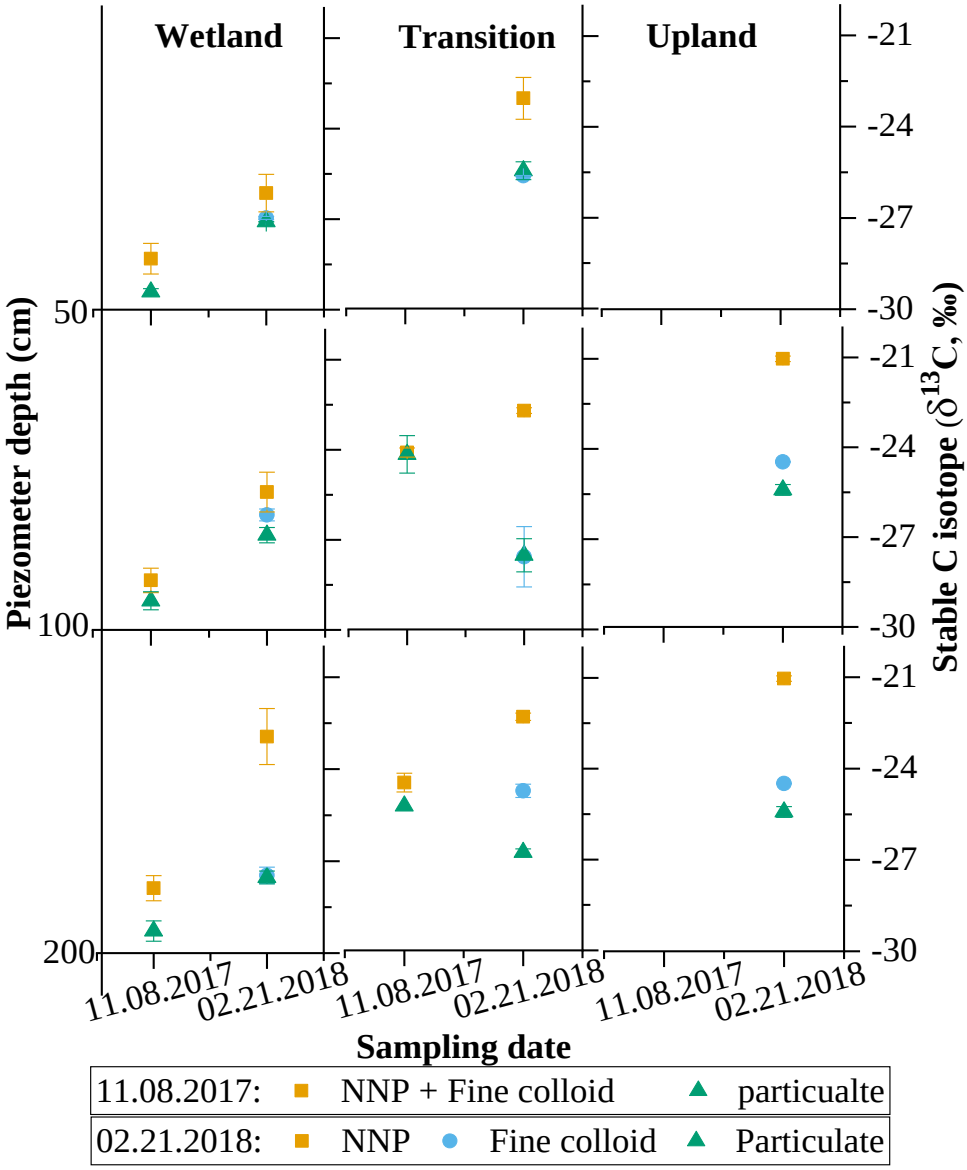

Figure 4.14: Variation in $\delta^{13}C$ in size-fractionated COC collected on 02.21.2018. The error bars represent standard deviations in stable isotope values among replicates.

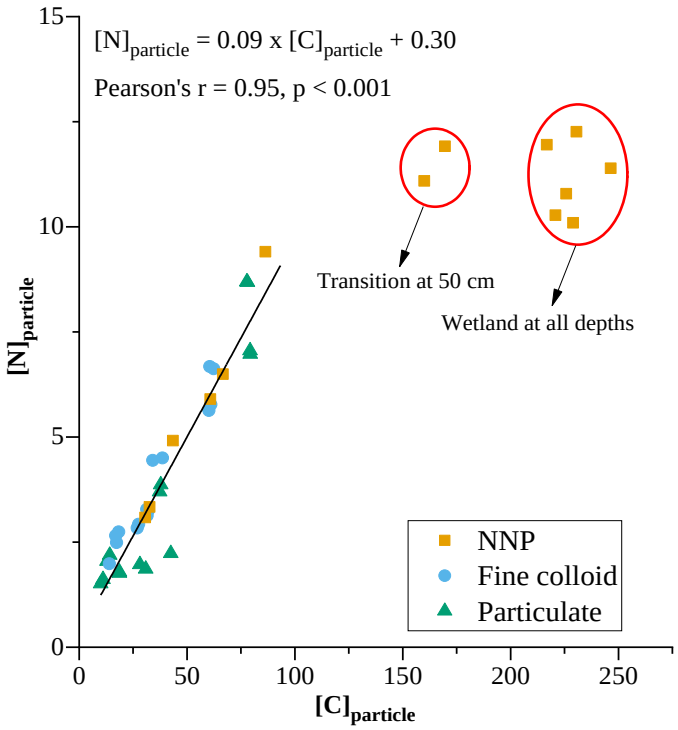

Figure 4.15: Linear relationship between bulk C ($[C]_{particle)}$) and N concentration ($[N]_{particle)}$) as measured by IRMS.

4.1 Discussion

4.1.1 Release of Soil Colloids and Associated OC

Along the redox gradients, the $TOC_{<1000}$ was significantly the highest in the wetland zone than that in other two zones. Increase in OC in terrestrial ecosystems is often attributed to the *in situ* formation of stable macromolecules from the condensation of low-molecular-weight constituents (Krom and Sholkovitz, 1977) and the partial and selective mineralization of particulate organic matter due to the biotic and abiotic reduction processes (Burdige, 2007; Santschi et al., 1990). Lower SOM decomposition rate resulting from the low pH and anaerobic conditions (Fellman et al., 2008; Hagedorn et al., 2001; Kögel-Knabner et al., 2010) might be another reason

for the high OC concentration in the wetland zone. Under reducing condition, reductive dissolution of Fe and Al (hydr)oxides can be resulted in the higher release of OC in the wetland zone (Hagedorn et al., 2001; Afsar et al., 2020). This phenomenon is often been observed in seasonally anoxic hypolimnion portion of the lakes (Tipping and Woof, 1983). Thermodynamic limitations under prolonged anaerobic conditions further prevent soil microorganisms from utilizing soluble OC under prevailing redox regimes (Boye et al., 2017; Jin and Bethke, 2005; LaRowe and van Cappellen, 2011). Several other studies have also reported wetlands as a potential source of DOM than that found in other surface waters (Aitkenhead-Peterson et al., 2005; Chin et al., 1998; Mulholland, 2003).

Mobilization of colloids and COC varied spatially along the redox gradients from upland to transition zone and to wetland as well as at different soil depths. We observed a strong correlation between the concentrations of COC and mineral colloids at NNP (Pearson's $r = 0.76$, $p < 0.001$) and particulate (Pearson's $r = 0.53$, $p < 0.001$) fractions **(Figure 4.17)**. Mobilization of colloids and COC is strongly influenced by solution pH, redox potential, IS, and ionic composition resulting from the oscillating reduction-oxidation events (Afsar et al., 2020; De-Campos et al., 2009b; Ryan and Gschwend, 1990; Thompson et al., 2006). In our study, concentrations of colloids ($p < 0.05$) and associated OC ($p < 0.05$) at NNP size fraction decreased, while colloid concentration at particulate ($p < 0.05$) size fraction increased with increasing pH. Dissolved OC concentration was negatively correlated with the solution pH. Enhanced mobilization of colloids and COC at low pHs as observed in the wetland is consistent with the findings in previous studies (Guggenberger et al., 1994), where the release of higher amount of metal-OC complexes was attributed to increased competition from

protons at low pHs. However, contradictory pH-DOM relationships have often been shown from laboratory and field studies as pH can control DOM release in different ways (Kalbitz et al., 2000).

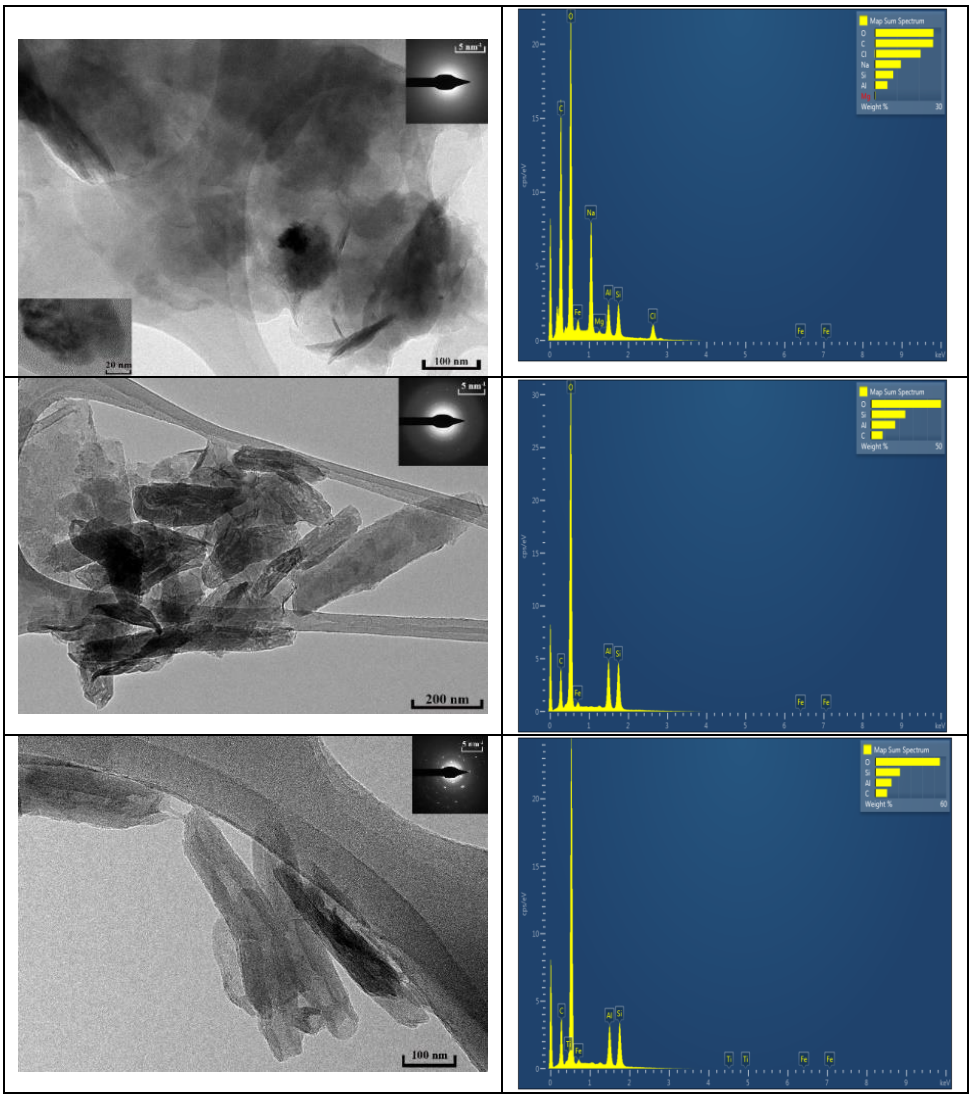

Figure 4.16: Transmission electron micrographs and energy dispersive X-ray spectroscopy of size-fractionated samples.

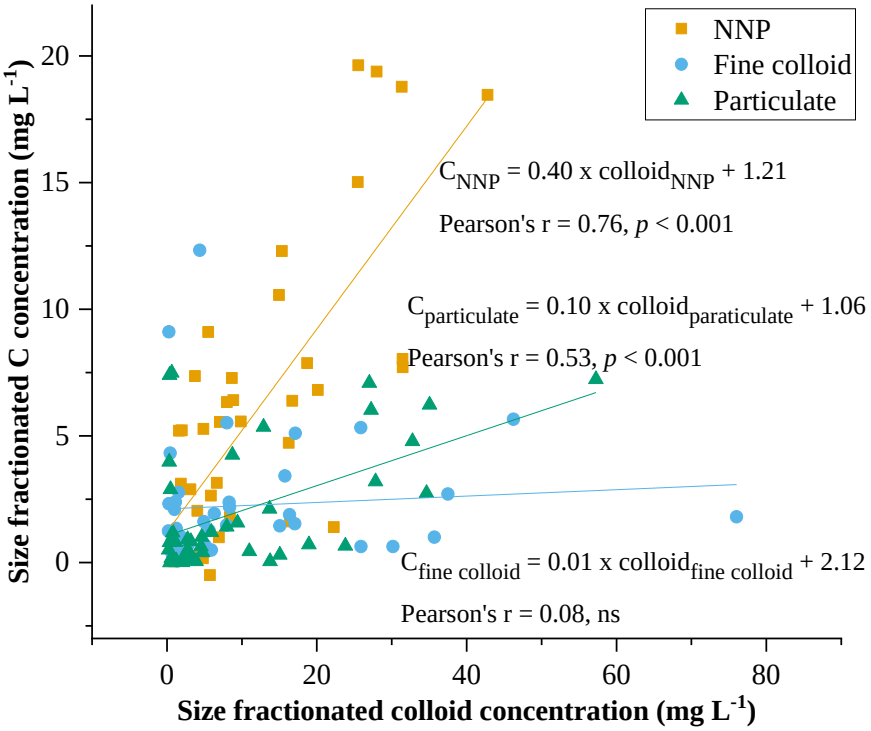

Figure 4.17: Linear relationship between the size-fractionated bulk C concentration (mg L^{-1}) to the colloid concentration (mg L^{-1}).

Both colloid and OC concentrations were negatively correlated with IS **(Table 4.3)**. The relationship between IS and colloid mobilization is consistent with the DLVO (Derjaguin-Landau-Verwey-Overbeek) theory, which predicts that a decrease in IS increases repulsive forces between colloid surfaces and facilitates colloid dispersion and mobilization (Khilar et al., 1990; Ryan and Gschwend, 1994b). Higher IS impedes solubilization of OC by reducing the charge density of organic substances, resulting in higher coagulation (Kalbitz et al., 2000; Tipping and Hurley, 1988). Rainfall events or snowmelts often lower the IS of pore waters due to the influx of dilute meteoric water. Heavy precipitation occurred immediately before sampling in Feb 21, 2018, which led to decreased IS in pore water samples, resulting in the higher concentrations of colloids and C observed in these samples. In Feb. 2019, IS was the

highest in the transition zone at 200-cm depth, which explains the insignificant presence of colloidal particles at this depth.

Table 4.3: Correlation (Pearson) between size-fractionated TOC concentration (ppm) and pH, pE, IS, soluble Fe^{2+} concentration of pore water samples (N = 42).

Size fractions (nm)	pH	pE	IS (µS/cm)	Fe (µM)
$C_{<450}$	-0.47**	-0.55***	-0.39**	0.57***
$C_{Dissolved}$	-0.45**	-0.57***	-0.25	0.39**
C_{NNP}	-0.43**	-0.44**	-0.37*	0.64***
$C_{Fine\ colloid}$	-0.01	-0.01	-0.25	0.17
$C_{Particulate}$	0.00	-0.10	0.13	0.32*
$Colloid_{NNP}$	-0.35*	-0.56**	-0.36*	0.63***
$Colloid_{Fine\ colloid}$	-0.33*	-0.50**	-0.29	0.38*
$Colloid_{Particulate}$	0.40*	-0.42**	0.18	0.65***

Level of significance: * $p < 0.05$, ** $p < 0.01$, *** $p < 0.001$, no asterisk: not significant.

The positive correlation between Fe reduction/release and increased concentrations of colloids and OC is consistent with the results reported in previous studies (Afsar et al., 2020; Kappler et al., 2004; Roden et al., 2010; Shimizu et al., 2013; Thompson et al., 2006). In the wetland zone, prolonged water-saturated conditions with higher soluble Fe^{2+} concentration points to the reductive dissolution of the Fe-oxides, acting as "cementing agents" between soil minerals and OC, that facilitates dispersion and release of soil colloids and associated OC (Ryan and Gschwend, 1990, 1992). Iron minerals, especially the nanoparticulate, short-ranged ordered (SRO) Fe phases are mostly susceptible to reductive dissolution (Bonneville et al., 2004). Indeed, De-Campos et al. (2009a) found that reducing conditions and associated reductive dissolution of Fe decreased soil aggregate stability to a greater extent than changes in solution pH alone. Reductive dissolution of structural Fe and

solubilization of Fe (hydr)oxide coatings can increase the cation exchange capacity (CEC) of long-term flooded soils (Favre et al., 2004; Kirk, 2004) that may additionally lead to enhanced soil disaggregation. The significance role that reductive dissolution of Fe could play in the release of colloids and associated OC is supported by their strong positive relationship observed in our study **(Table 4.3)**. The highest colloid and OC concentrations measured in the wetland's pore water samples is well explained by their position below the Fe reduction line in the Eh/pH pourbaix diagram **(Figure 4.5)**.

4.1.2 Significance of NNP and Fine Colloids

The detailed analyses of size-fractionated $TOC_{<1000}$ revealed that, if the operational definition of <0.45 μm were used for DOC, the contribution of COC, where the combined NNP and fine colloid fractions comprise 47 ± 20% of the DOC, would be greatly underestimated. Both IRMS and XPS analyses further demonstrated that the NNP and fine colloid-bound OC comprises a significant portion of the COC (2.3-1000 nm), which would otherwise be labeled as "dissolved", following the commonly used operational definition. Several previous studies have reported that colloidal OC comprises a significant portion of the operationally defined DOC fraction. For example, in marine environments, COC > 10 kDa and COC > 3 kDa makes up to 3-30% and 8-36% of the bulk DOC, respectively, depending on the ultrafiltration technique and sampling location (Guo and Santschi, 1997a and other references therein). In the Chesapeake Bay, the particulate (> 200 nm), colloidal (1 kDa – 200 nm), and dissolved (<1 kDa) fractions comprised, respectively, 39%, 32%, and 25% of the TOC concentration (Guo and Santschi, 1997a). Our findings clearly demonstrated the importance in assessing the COC concentrations in different size fractions, which could have significant implications in assessing the release and

transport of C under dynamic redox conditions. Typically, with decreasing particle size, colloidal particles have higher reactivity and shorter residence time (Benner and Amon, 2015; Moran and Buesseler, 1992). Therefore, it is reasonable to anticipate that the NNP and fine colloids can play an important yet mostly unclear role in the biogeochemical cycling of COC and other elements in the redox-sensitive wetlands (Afsar et al., 2020). However, these two size fractions are lumped with the "dissolved" fraction in the operational cutoff size range of DOM. As particle size decreases, the interactions between minerals and SOM are increasingly controlled by surface properties (e.g., specific surface area, electrical charge) rather than bulk properties (e.g., chemical composition) of the colloids. The very large specific surface area, high reactive site densities, and mobility associated with small colloids will dominate their environmental behavior, which could be very different from the behavior of larger particles for which the effects of gravitational force exceeds Brownian motion (Wilkinson and Lead, 2007).

4.1.3 Size-fractionated OC Concentration and Formation of Organo-mineral complexes

The strong correlation between $C_{surface}$ and C_{bulk} for samples collected on Feb 2018 (**Figure 4.18**, $C_{xps} = 1.20\ C_{IRMS} + 49.12$, Pearson's r = 0.92; $p < 0.001$) reflect the existence of COC as organo-mineral complexes in the pore water rather than being dispersed independently as a discrete component. Consistent with our previous microcosm study (Afsar et al., 2020), surface enrichment of C, i.e., the ratio of $C_{surface}$ to C_{bulk}, increased with increasing particle sizes from NNP (1.98 ± 0.68) to particulate fractions (2.97 ± 1.28). Arnarson and Keil (2001) and Jones and Singh (2014) also reported such increase in C-enrichment factor from lighter to heavier fractions and

argue that the later fraction is mostly mineral aggregates with increasing C concentration on the mineral surfaces relative to bulk C concentration.

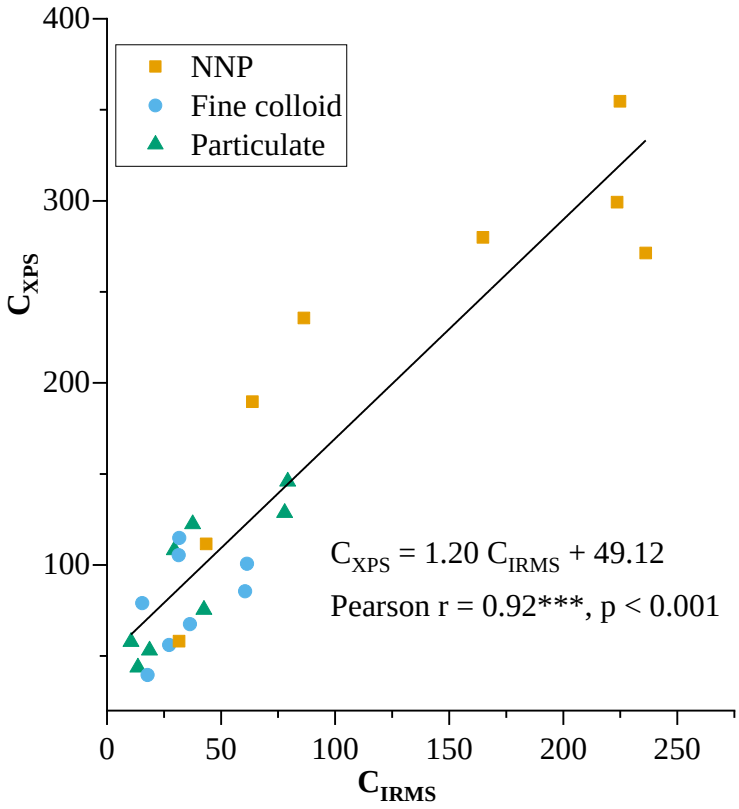

Figure 4.18: Relationship between bulk measured by IRMS (C_{IRMS}) and surface C concentration (C_{XPS}) measured by XPS of size-fractionated pore water samples collected on Feb 2018.

Variation in the chemical and molecular composition of the organo-mineral complexes influences their interactions, stability, and responses to the redox potential changes in the depressional wetland. Distinct elemental and OM functional groups associated with size-fractionated organo-mineral complexes could in part results in the differences in dominant binding mechanisms (Afsar et al., 2020; Jones and Singh, 2014). Along the redox gradients, the increase in stable $\delta^{13}C$ isotopes from wetland to

upland suggests the presence of more microbial biomass or metabolites in the well-aerated zones. Aerobic decomposition usually favors preferential release of lighter ^{12}C isotopes that may lead to an enrichment of heavier $\delta^{13}C$ in the remaining SOM in the upland zone (Agren et al., 1996; Nadelhoffer and Fry, 1988). During decomposition of SOM, microbes preferentially oxidize lighter ^{12}C enriched-C into CO_2 and H_2O, resulting in the assimilation of ^{13}C enriched-C as their cell components (Connin et al., 2001; Poage and Feng, 2004). Prolonged water saturation in the wetland zone leads to the formation of anaerobic conditions that limit microbial decomposition of SOM (Krull and Retallack 2000; Benner et al., 1987) and a decrease in the heavier $\delta^{13}C$ isotope signatures. For the same reason, I suggest that the NNP fraction is presumably more enriched in the microbial metabolites due to their higher $\delta^{13}C$ values in contrast to the larger size fractions. Significantly higher carbonyl/carboxyl C functional groups (C=O) indicates that the ligand exchange and/or H-boding with the mineral surfaces as the dominant binding mechanisms in the NNP fraction (Jones and Singh, 2014). Higher Mg: Al ratios (indicative of smectite minerals, **Figure 4.12**) in this fraction additionally suggests the presence of more phyllosilicate minerals that have a higher tendency to attach more OC on their surface (Bock and Mayer, 2000).

Interactions between soil organic matter and mineral matrices will depend on their size, shape, surface properties and functional groups, and have great implications for the stability of SOM because it can later significantly the turnover time of SOM. In my opinion, the size-fractionated continuum of the molecular composition of the organo-mineral complexes provide mechanistic insights into organo–mineral interactions, which could potentially inform land-carbon models that explicitly include mineral-bound C pools. Terrestrial C models that explicitly include mineral-bound

OC. Long residence times of soil organic matter have been attributed to reactive mineral surface sites that sorb organic species and cause inaccessibility due to physical isolation and chemical stabilization at the organic–mineral interface.

4.2 Conclusion

In this investigation, I have explored significance of the colloids and associated COC that are present within the operationally defined "dissolved" fraction at < 450 nm size range. It was revealed that the NNP and fine colloid fractions comprise ~ 38 ± 4% and 8 ± 3% of the bulk organic C (OC) (< 1000 nm) concentration, respectively. The NNP fraction is more $\delta^{13}C$ enriched and has higher proportion of oxidized C species than other larger size fractions. Hence, my findings clearly demonstrate significant new insights into the migration of size-fractionated COC in a redox-sensitive wetland.

Chapter 5

EFFECT OF METAL:CARBON RATIOS ON THE MOBILITY OF ORGANIC CARBON IN A DEPRESSIONAL WETLAND

Abstract

Understanding the mechanisms governing the mobility and stability of organo-mineral associations is critical to predicting the dynamics of soil organic matter (SOM) and the related global C cycling. Redox-induced biogeochemical transformations are the key processes that control the stabilization of SOC via association with metal oxides in terrestrial environments such as wetlands. Despite its high C content (20-30% of terrestrial C), size-dependent organo-mineral associations and their dynamic changes in the redox-dynamic wetlands are poorly understood. Here we present concentration of the trace elements in pore water samples from a depressional wetland located at the Delmarva Bay in Delaware, USA. The samples were collected on December 14, 2018 and May 01, 2019 from piezometers installed at multiple depths (50 cm, 100 cm, and 200 cm) and in three different zones (upland, transitional, and wetland). Four size fractions were analyzed: dissolved (<2.3 nm), natural nanoparticle (2.3-100 nm, NNP), fine colloid (100-450 nm), and particulate (450-100 nm) to measure the trace metals concentration using inductively coupled plasma mass spectrometry (ICP-MS). Our results revealed the presence of two main groups of elements in the pore water samples: (1) colloid bound elements (Al, Fe, V, Ga, Ti, and Zr) and (2) “truly” dissolved elements (Mn, Li, Na, K, Ca, Mg, Rb, Sr, Ba, and Co). The metal to organic C ratio increased with increasing size of the particles,

which might have influence on the sedimentation and aggregation of larger organo-mineral complexes in the pore water samples. This observation supports the idea that the vertical and later transport of size fractionated SOM might be different in the wetland.

5.1 Introduction

Colloids are defined as inorganic and organic particles with sizes ranging from 1-1000 nm (Buffle, 1990) and is considered both as a reservoir and source of particle aggregation and disaggregation. Wide variation in the physical and chemical composition of the colloids and associated organic C posits great challenges to the wetland hydrologists to assess the fate and transport of organo-mineral complexes within submicron size level. In natural ecosystems, the colloidal phase plays a major role in the fate and cycling of the fate and transport of the organic C, trace metals, radionuclides, bacteria, and viruses through the vadose zone (Afsar et al., 2020; de Jonge et al., 2004; Kjaergaard et al., 2004; Pédrot et al., 2008). However, while the elemental and molecular composition of size-fractionated colloids have been extensively studied in various aquatic ecosystems (Benoit and Rozan, 1999; Hilger et al., 1999; Rostad et al., 1997; Wilkinson and Lead, 2007), the data are largely scared in terrestrial ecosystems. The scarcity is mainly due to our current practices, where the chemical speciation largely relies on the operational definition of "dissolved" fraction. Operationally, the dissolved or solution phase has been defined as the filtrate that passes through 0.45 µm filter, while both colloidal and particulate phase are particles that will be retained on it. However, according to the size-based definition, the colloidal phase is a critical transition zone between the dissolved phase and particulate phase, while nanoparticles describe a subset of the colloidal particles ranging from 1-100 nm (Christian et al., 2008). In soil, clay-humic-metal complexation is more dominant within the size range of 10 -1000 nm. As a result, despite being an important vector, the fluxes and distribution of trace elements among different colloidal pools still remain poorly understood at submicron level.

Recent studies suggest that a large fraction of trace elements is closely associated with soil organic C (2-4, 12-23). Physicochemical properties of the terrestrial ecosystems such as pH, redox potential, temperature, pressure, and ionic strength (15, 24-27) can strongly influence mineral-organic C interactions. Redox induced biogeochemical transformations are the key processes that control such interactions and thus can regulate the amount and speciation of waterborne elements. Prolonged waterlogged condition in a wetland could lead to release large amount of organic C due to the reductive dissolution of Fe-oxyhydroxides and accompanying shifts in pH (Fiedler and Kalbitz, 2003; Grybos et al., 2009; Thompson et al., 2006). As a result, seasonal shifts in the water-table in a depressional wetland could exert a significant control on the biogeochemical cycling of soil OC and other trace elements. Pédrot et al. (2008) studied the colloid-mediated mobilization of trace elements in soil columns and characterized them into three groups: (1) "truly" dissolved elements (Li, B, K, Na, Rb, Si, Mg, Sr, Ca, Mn, Ba, and V), (2) intermediate groups (Cu, Cd, Co, and Ni), and (3) colloidal group (Al, Cr, U, Mo, Pb, Ti, Th, Fe, and rare earth elements).

In this chapter, I focus on how the colloids may influence the cycling of major and trace elements in a depressional wetlands. In particular, I attempt to constrain how colloidal entities may affect the speciation of different metals and I especially highlight the differences in elemental concentration among dissolved (< 2.3 nm), natural nano-particle (2.3-100 nm), fine colloid (100-450 nm), and particulate (450-1000 nm) fractions. I collected piezometer water samples from 50 cm, 100 cm, and 200 cm depths along the transect delineated as upland, transition, and wetland zones by maintaining *in situ* environmental conditions. Size- fractionated particles were

analyzed using inductively coupled plasma mass spectrometry (ICP-MS). The goals of the study were to (1) quantify the partitioning of trace elements into different size fractions, and (2) determine the changes in metal:OC ratios among different size fractions.

5.2 Materials and Methods

5.2.1 Study Site Description

Piezometer water samples were collected along the transect from the upland to the wetland zones in a freshwater depressional wetland located in the Blackbird state forest (39°20'N 75°40'W), Delaware, USA. For this study, I have collected water samples on Dec 14, 2018 and May 01, 2019. Detailed information about the study site and the transects are discussed more details in section 4.2.1.1. Initially, three zones were established along the transects depending on the seasonal changes in the water table to monitor and collect pore water samples. These are (1) wetland zone, which is usually ponded seasonally during winter and early spring and remained dry during summer, (2) transition zone, which does not have significant ponding and is between wetland and upland with marked saturation, and (3) upland zone, which is beyond the wetland boundary. Soils in the wetland, transition, and upland zones are classified as fine, loamy, mixed, mesic Typic Umbraquults (Corsica soil series); fine, loamy, mixed, mesic Typic Endoaquults (Fallsington soil series); and fine, loamy, mixed, active, mesic Aquic Hapludults (Woodstown soil series), respectively, according to the U.S. Department of Agriculture (USDA) soil taxonomy (Soil Survey Staff, 2015). All the soil properties were described according to Schoeneberger et al. (2002). Daily

rainfall amounts were recorded at a weather station located at the Blackbird State Forest office, 200 m north of our study site.

5.2.2 Monitoring Well and Piezometer Installation

The installation procedure for the monitoring wells and piezometers are discussed in section 4.2.1.2 and 4.2.1.1. Briefly, standard monitoring wells (slotted PVC pipe, inner diameter = 5 cm) were installed to a depth of 95 cm below the soil surface in wetland and transition and 158 cm deep in upland. Quartz sand (U.S. SILICA®) was placed around the well screen and the riser was sealed with polyurethane-based insulating foam at the soil surface. The foam sealant was used to prevent water from running down the outside of the pipe to the well screen. Automated data recorders (Odyssey Capacitance Water Level Logger) were installed in each well to record water levels twice a day from November 20, 2016 to July 11, 2019.

Three piezometers (PVC pipe, inner diameter: 5 cm) were installed in each zone separately at 50 cm, 100 cm, and 200 cm depths. I collected piezometer water samples during water-table rising and declining phases respectively on the Dec 14, 2018 and May 01, 2019 under continuous purging with argon (Ar) gas to maintain the *in situ* water chemistry conditions using a peristaltic pump (Geotech, Denver) after discarding the first 3-well volumes of water. All samples were stored in ice and transported to the laboratory for immediate size fractionation.

5.2.3 Sample Preparation and Analyses

Piezometer water samples were fractionated into < 1000 nm (10 min at 339×*g* rcf or 1250 rpm), < 450 nm (10 min at 1581×*g* rcf or 2700 rpm), and < 100 nm (30

min at 10628×*g* rcf or 7000 rpm) size fractions using Thermo Scientific Sorvall Lynx 6000 centrifuge (Thermo Scientific) with a fiber lite F9-6x1000 LEX rotor. The size-specific centrifugation speed and time was calculated from Stokes' law (Gimbert et al., 2005) assuming spherical particles and particle density of 2.65 g cm^{-3}. Finally, < 100 nm fraction was passed through an ultrafiltration system (Amicon® stirred cell) equipped with Ultracel® 10 kDa membrane ultrafiltration discs (EMD Millipore Corporation) to separate the dissolved fraction. The pH, Eh (pE), and EC of the pore water samples were measured *in situ* using corresponding probes (Fisher Scientific, Hampton, NH) and discussed in section 4.3.2. Iron (II) concentrations of the pore water samples were measured following the ferrozine method (Stookey, 1970) using UV-visible spectrophotometer (Agilent Technologies, Cary 60 UV-Vis). An aliquot of the size-fractionated filtrates, i.e., < 1000 nm, <450 nm, <100 nm, and <2.3 nm fractions were immediately acidified with 2% HCl (v/v) to prevent iron oxide or hydroxide precipitation for the Total organic carbon (TOC) analyses using TOC analyzer (Shimadzu TOC-L). Another portion of the size-fractionated filtrates were digested using the United States Environmental protection agency's (US-EPA) Method 3015A for the ICP-MS analyses. Forty-five ml aliquots and 5 ml trace-metal grade conc. HNO_3 were transferred to a Teflon digestion vessel and digested in a Mars 6 microwave digester (CEM Corporation). The temperature was raised to 170 ± 5 ^{0}C in approximately 10 min and remained at 170 ± 5 ^{0}C for another 10 min. After digestion, the acid fraction was decanted into another acid-washed tubes and was diluted to 2.5% acid for the inductively coupled plasma mass spectrometry (Thermo Scientific iCAP TQ ICP-MS) analysis.

In this study, Al, Fe, Mn, Li, Na, K, Ca, Mg, Rb, Sr, Ba, Co, V, Ga, Ti, and Zr concentrations were measured using the TQ ICP-MS system at the advanced material characterization lab at the University of Delaware. Quantitative analyses were carried out by external calibration by using mono- and multi-element standard solutions (Agilent Technologies). Indium was used as an internal standard at concentration of <100 µg L^{-1} in order to correct instrumental drift and matrix effects. The MilliQ distilled water blanks were digested, processed, and analyzed to monitor any potential contamination. The relative standard deviation (RSD) of the ICP-MS peak areas for triplicate measurements of a representative samples were 5.2% (Al), 1.5% (Fe), 7.8% (Mn), 4.9% (Li), 2.4% (Na), 1.7% (K), 2.3% (Ca), 3.5% (Mg), 8.1% (Rb), 6.75% (Sr), 4.2% (Ba), 4.1% (Co), 9.4% (V), 2.8% (Ga), 5.7% (Ti), and 2.1% (Zr). The limit of detection was 5.1 µg L^{-1} (Al), 0.02 µg L^{-1} (Fe), 0.01 µg L^{-1} (Mn), 0.04 µg L^{-1} (Li), 8.6 µg L^{-1} (Na), 5.0 µg L^{-1} (K), 10.2 µg L^{-1} (Ca), 11.8 µg L^{-1} (Mg), 0.02 µg L^{-1} (Rb), 1.5 µg L^{-1} (Sr), 1.0 µg L^{-1} (Ba), 0.02 µg L^{-1} (Co), 0.01 µg L^{-1} (V), 0.01 µg L^{-1} (Ga), 0.2 µg L^{-1} (Ti), and 0.03 µg L^{-1} (Zr).

5.2.4 Calculation of the Concentration and Partition Coefficient of Different Elements

The concentration of different elements in dissolved, NNP, fine colloid, and particulate fractions is calculated as follows:

$M_{dis} = M_{<2.3}$

$M_{NNP} = M_{<100} - M_{<2.3}$

$M_{fc} = M_{<450} - M_{<100}$

$M_{par} = M_{<1000} - M_{<450}$

$M_{tot} = M_{dis} + M_{NNP} + M_{fc} + M_{par}$

Where, M_{dis}, M_{NNP}, M_{fc}, and M_{par} are the metal concentration respectively in the dissolved, NNP, fine colloid, and particulate size fractions (µmol L^{-1}), M_{tot} is the total metal concentration (µmol L^{-1}) at <1000 nm size fractions, $M_{<2.3}$, $M_{<100}$, $M_{<450}$, and $M_{<1000}$ are the metal concentration in the <2.3 nm, <100 nm, <450 nm, and <1000 nm filtrates, respectively directly measured using the ICP-MS. Results and Discussion

5.2.5 Distribution of Elements in the Dissolved, NNP, Fine Colloid, and Particulate Fractions

The relative percentages (i.e., percentage of size-fractionated element concentration to the total concentration at <1000 nm size range) of different elements are illustrated in Figure 5.1-5.3. Here, All the elements can be divided into two main groups based on their distribution among four size classes as following:

Group 1: Colloid-bound elements

The relative percentages of Al, Fe, V, Ga, Ti, and Zr bound to the NNP and fine colloid fractions demonstrated substantial contribution of these two size fractions within operationally defined "dissolved" fraction. Therefore, they are classified as colloid-bound elements. On an average, the element percentages are 25-30%, 9-21%, 30-39% (Al); 10-40%, 26-29%, 18-27% (Fe); 14-55%, 16-24%, 17-29% (V); 10-40%, 11-22%, 28-33% (Ga); 41-51%, 9-14%, 20-26% (Ti); and 33-36%, 6-7%, 39-41% (Zr) at the dissolved, NNP and fine colloid fractions, respectively (Figure 5.1 and 5.2). Aluminum, Fe, and V showed very large variation in their concentration among different zones and depths, which might be due to their large sensitivity to the redox potential of the soil. Previous studies from shallow groundwater (Pourret et al., 2012) and soil column study (Pédrot et al., 2008) found significant amount of Al, Fe, and V in the colloidal fraction. Similarly, other studies also confirmed that the colloidal

phase plays a significant role in the transport and cycling of V (Dupré et al., 1999; Gaillardet et al., 2013; Lyvén et al., 2003). In this study, I did not see significant variations in Al, Fe, and V concentrations among different size fractions except Al at NNP ($p < 0.05$) and Mn at dissolved ($p < 0.001$) fractions. On the other hand, the percentages were significantly higher in the dissolved fraction ($p < 0.05$) during the water-table rising phase in Dec' 2018 than the water-table declining phase in May' 2019 and opposite trend was observed at > 2.3 nm size fractions. Figure 5.4 showed the concentration of Al, Fe, Mn, and V in different size fractions along the redox gradient from upland to wetland zones and at different depths. In the depressional wetland, Fe concentrations in the NNP, fine colloid, and particulate fractions over the dissolved fraction were 2.48 ± 1.11, 3.74 ± 2.73, and 6.92 ± 8.24 in May' 2019 and 1.32 ± 1.39, 0.86 ± 0.87, and 1.66 ± 4.02 in Dec' 2018, respectively. Vanadium exhibited similar trends and the ratios were 4-6 in May' 2019 and 1-2 in Dec' 2018.

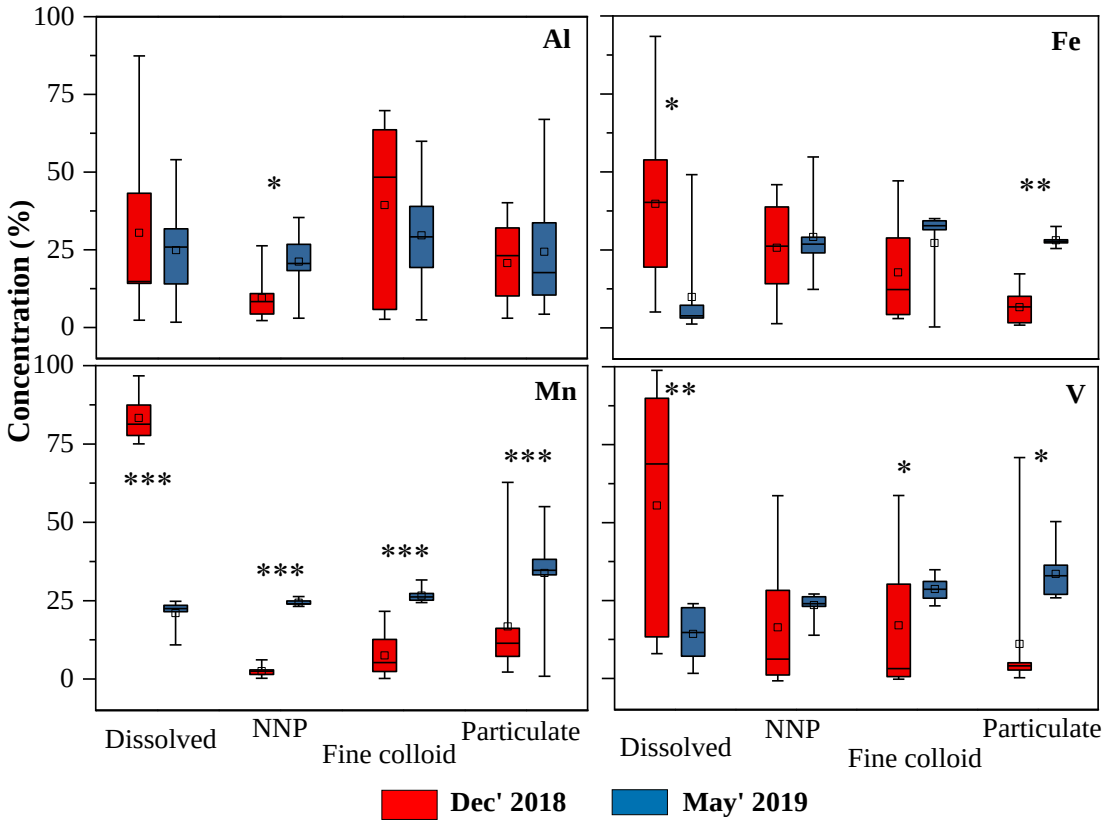

Figure 5.1: Box plot of the mean, median and 1st and 3rd quartiles (25 and 75%) of the Al, Fe, Mn, and V concentrations in the respective dissolved, NNP, fine colloid, and particulate fractions. Statistical differences between element concentration in samples collected on Dec' 2018 and May' 2019 are marked with *p < 0.05, **p < 0.01, and ***p < 0.001.

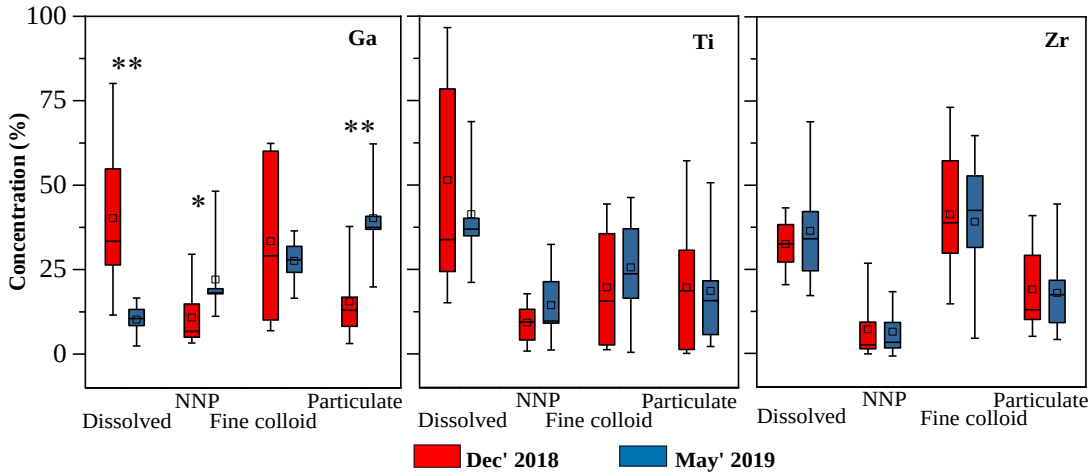

Figure 5.2: Box plot of the mean, median and 1st and 3rd quartiles (25 and 75%) of the Ga, Ti, and Zr concentrations in the respective dissolved, NNP, fine colloid, and particulate fractions. Statistical differences between element concentration in samples collected on Dec' 2018 and May' 2019 are marked with *p < 0.05, **p < 0.01, and ***p < 0.001.

Group 2: Truly dissolved elements

The concentration of Mn, Li, Na, K, Ca, Mg, Rb, Sr, Ba, and Co do not change significantly during the centrifugation and ultrafiltration processes and their dissolved fraction had the highest concentration (Figure 5.3). As a result, the colloidal fraction (> 2.3 nm) of these highly mobile elements decreased significantly in both the water-table rising and declining phases (Fig 5.3). Interestingly, the relative element percentages of the dissolved fraction significantly decreased during the water-table declining phase in May' 2019 than the water-table rising phase in Dec' 2018, while opposite trend was observed in colloidal (< 2.3 nm) fractions. For all these elements, molar concentrations in the NNP, fine colloid, and particulate fractions over the dissolved fraction were < 1. The alkaline and alkaline earth metal elements have been often described as truly dissolved elements in previous studies (Pokrovsky and Schott, 2002; Pourret et al., 2012). The highest concentration of dissolved Mn during the

water-table rising phase might be due to the high solubility of Mn^{2+} and the well-known slow oxidation kinetics of Mn^{2+} to insoluble Mn^{4+} (Davison, 1993; Diem and Stumm, 1984; Millero et al., 1987). It is interesting to see the differences in the partitioning of elements amongst different size fractions which can potentially influence the element distribution, biasing it towards higher proportions in the colloidal fractions during the water-table declining phase.

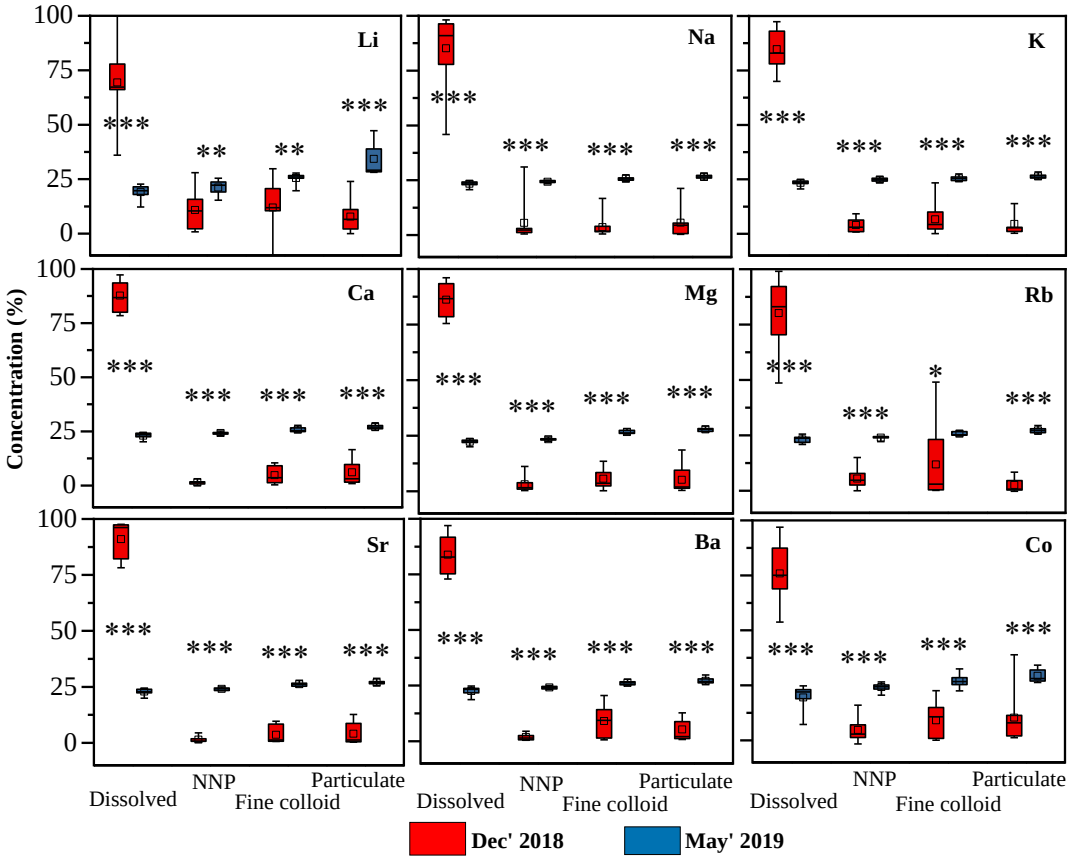

Figure 5.3: Box plot of the mean, median and 1st and 3rd quartiles (25 and 75%) of the Li, Na, K, Ca, Mg, Rb, Sr, Ba, and Co concentrations in the respective dissolved, NNP, fine colloid, and particulate fractions. Statistical differences between element concentration in samples collected on Dec' 2018 and May' 2019 are marked with *p < 0.05, **p < 0.01, and ***p < 0.001.

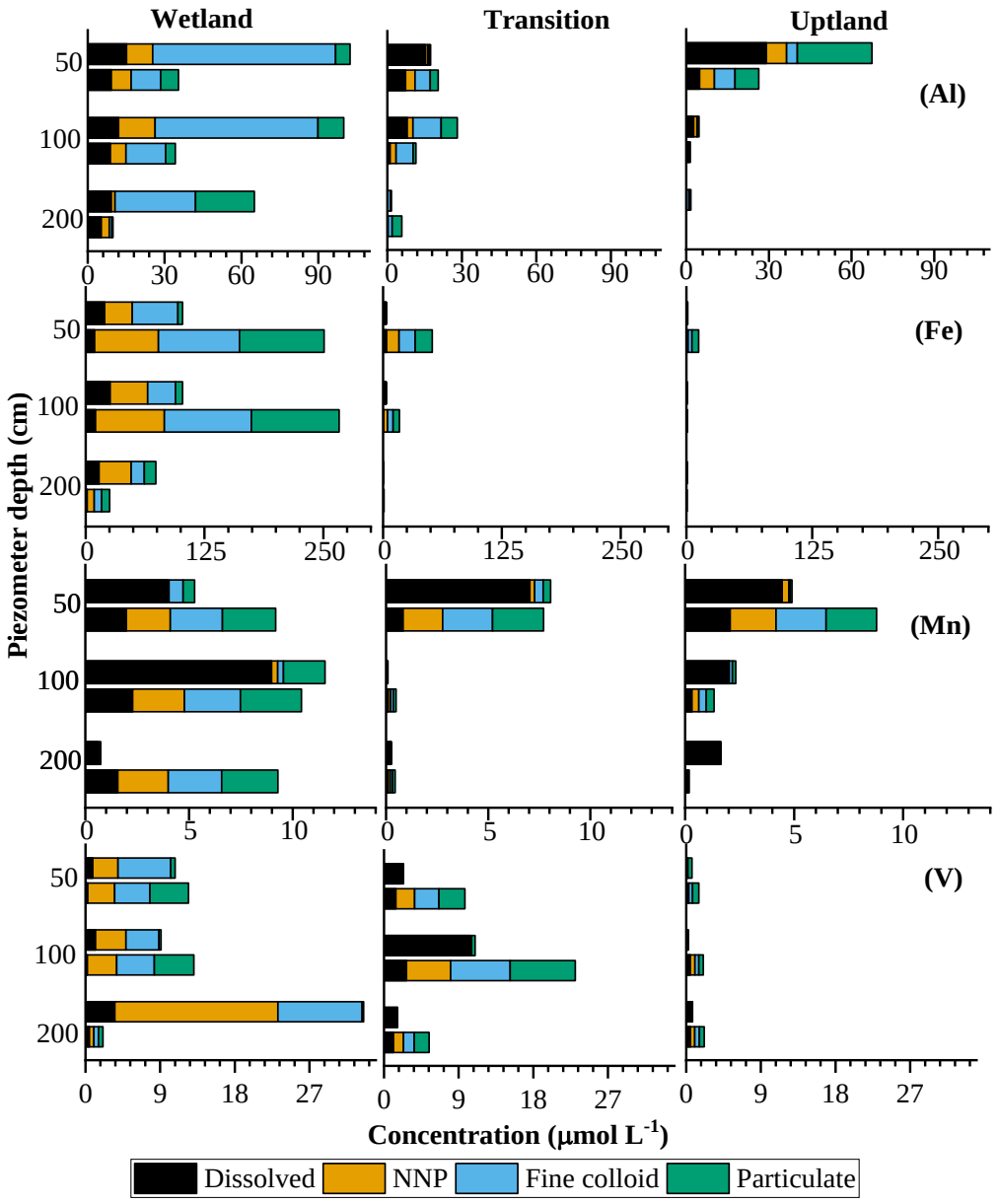

Figure 5.4: Distribution of Al, Fe, Mn, and V in the dissolved, NNP, fine colloid, and particulate fractions in different zones (wetland, transition, and upland zones) and at different depths (50 cm, 100 cm, and 200 cm). At each depth, the 1st and 2nd horizontal bars represent data for samples collected on Dec' 2018 and May' 2019, respectively.

5.2.6 Ratios of Metals (Al, Fe) to OC and mobilization of Size-fractionated Organo-mineral Complexes

The relative abundance of metals (Al, Fe) over organic C in soil pore water influences the structure and size of the organo-mineral complexes (Bazilevskaya et al., 2018). In this study, the metal to organic C ratios were 0.013 ± 0.018, 0.041 ± 0.095, 0.140 ± 0.188, and 0.159 ± 0.275 (Al:C) and 0.006 ± 0.007, 0.024 ± 0.027, 0.118 ± 0.156, and 0.095 ± 0.152 (Fe:C) in the dissolved, NNP, fine colloid, and particulate fractions, respectively.

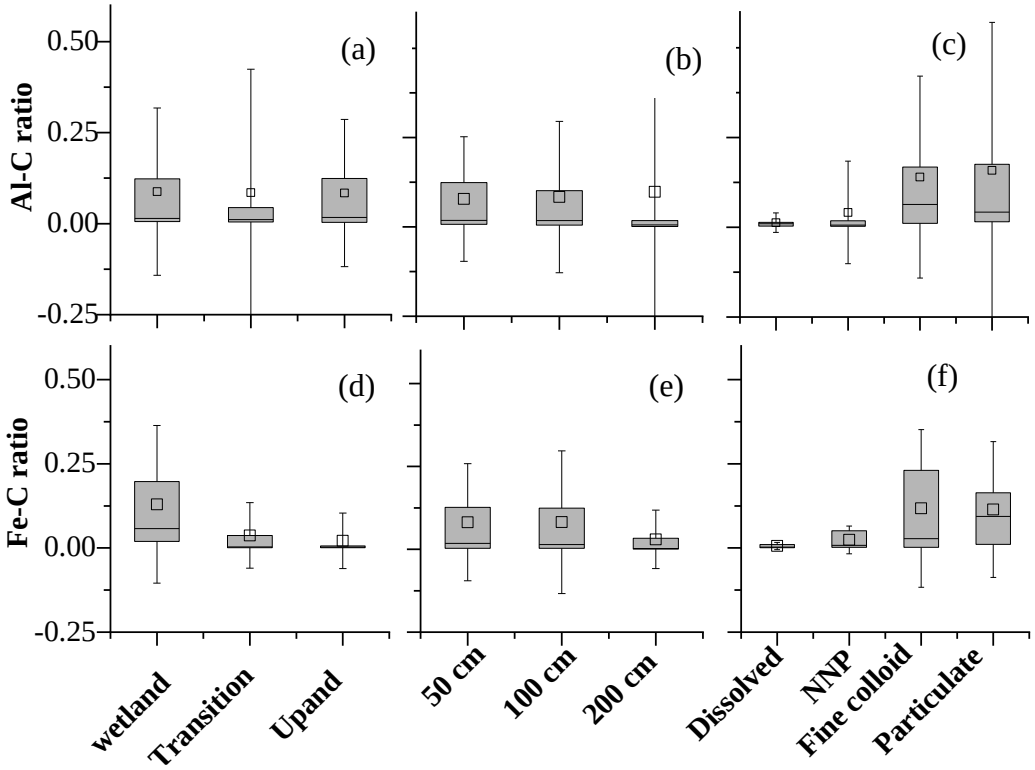

Figure 5.5: Box plot of the mean, median and 1st and 3rd quartiles (25 and 75%) of the Al-C and Fe-C ratios along the redox gradients from wetland-transition-upland zone (a, d), along the soil profile at 50 cm, 100 cm, and 200 cm depths (b, e), and in four different size fractions, i.e., dissolved, NNP, fine colloid, and particulate (c, f).

Negatively charged colloidal particles become neutralized at higher metal:C ratios in the organo-mineral complexes and therefore increase the polymerization, aggregation, and sedimentation of colloids. Riise et al (2000) observed an increased in the aggregation of the dissolved metal-organic C complexes at metal:C rations of ~0.03-0.04 to form colloids of > 450 nm in size.

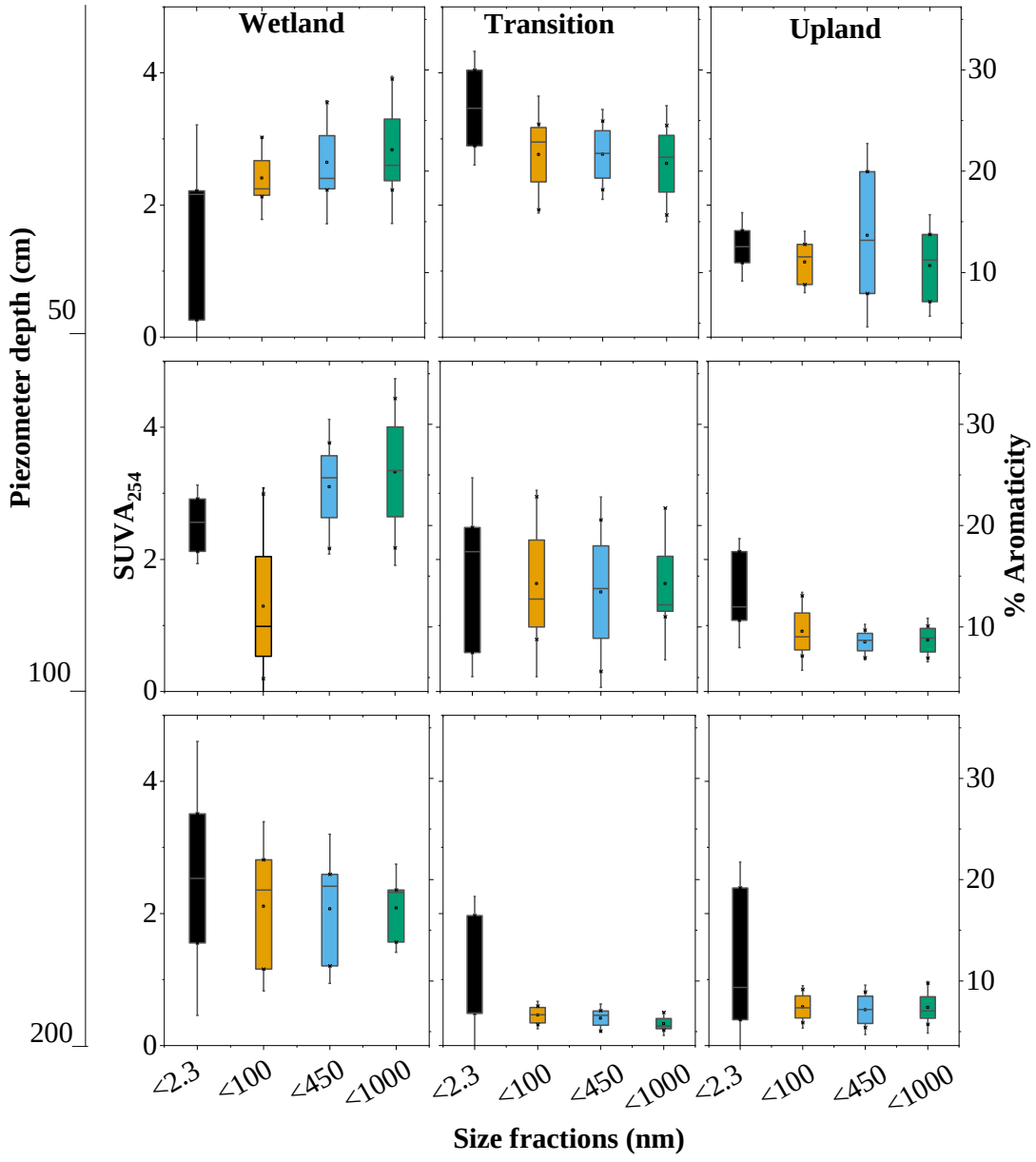

Figure 5.6: Box plot of the mean, median and 1st and 3rd quartiles (25 and 75%) of the specific UV absorbance at 254 nm ($SUVA_{254}$) and %Aromaticity for size fractionated samples

Chapter 6

CONCLUSIONS

6.1 Summary of Research

The research presented in this dissertation combined from the laboratory-based soil column and microcosm studies to the field observations, focusing on the (1) quantification of the Colloidal organic C (COC) load to the operationally defined "dissolved" pool, (2) identification of the molecular composition of colloids and associated OC in different size fractions, and (3) characterization of the influence on wetland hydrology on the concentration and composition of the organo-mineral complexes in the depressional wetland.

In Chapter 2, I discuss the dynamics of organo-mineral complexes within colloidal size range by conducting three consecutive 35-day redox (reduction-oxidation) oscillation experiments using a wetland soil. Molecular compositions of natural nanoparticle (NNP, 2.3-100 nm), fine colloid (100-450 nm), and particulate (450-1000 nm) fractions were measured using IRMS and XPS. My findings clearly demonstrate limitations of using the operationally defined "dissolved" fraction (<450 nm) to assess C cycling in ecosystems such as wetlands. Increase in colloid and OC concentrations and presence of more microbial-derived C in larger size fractions additionally imply that redox oscillations promote the formation of molecularly diverse sub-colloid sized organo-mineral associations. Being a composite unit of soil micro aggregates, organic-mineral associations can thus influence the overall stability of OC in wetland soils that undergo frequent redox oscillations.

In Chapter 3, I discuss the influence of redox oscillations on the mobilization of OC using soil columns in the laboratory. Results showed that bulk OC concentration increased by 425-1018% (121.55 ± 10.53 mg L^{-1}) and 311-830% (97.50 ± 5.36 mg L^{-1}) after respective 1st and 2nd reducing half-cycles (RHCs) in comparison to the oxic (control) soil column leachate (14.24 ± 5.43 mg L^{-1}) samples. Organic C released after the 1st RHC (i.e., single) had greater contributions from NNP and dissolved fractions, higher aromatic C content, and was more biologically reactive than the 2nd RHC (i.e., cumulative). In contrast, OC released after the 2nd RHC had higher contributions from fine colloid and particulate size fractions, and was less aromatic, less biologically reactive, microbial-derived components than the 1st RHC. The observed OC release as influenced by their molecular composition and redox fluctuations provides a baseline for the size continuum of soil OC and its potential ecological and environmental roles.

In Chapter 4, I show the concentration and molecular composition of the dissolved, NNP, fine colloid, and particulate fractions. The pore-waters samples were collected from a Delmarva bay depressional wetland located at Blackbird State Forest, Delaware, USA. Pore-water samples were collected from February 2018 to May 2019 from upland, transition, and wetland zones. Results reveal that (1) dissolved, NNP, fine colloid and particulate fractions comprise 45 ± 4%, 38 ± 4%, 8 ± 3% and 7 ± 3% of the bulk OC (< 1000 nm) concentration, respectively. (2) Organic C in the upland was more enriched in $\delta^{13}C$ stable isotopes than the transition and wetland zones, (2) the NNP was more enriched in $\delta^{13}C$ than other larger size fractions. (4) the NNP fraction has significantly higher has a higher proportion of mostly oxidized OC (p < 0.05), while the particulate fraction has more aliphatic/aromatic OC functional groups.

In chapter 5, I present results from the piezometer water samples from the Delmarva bay depressional wetlands for their major and trace-elements and DOC concentrations using inductively coupled plasma mass spectrometry (ICP-MS). The samples were collected during water-table rising (Dec. 14, 2018) and declining (May 01, 2019) phases. Our results revealed that the relative percentages of respective Al, Mn, and Fe were 47 ± 24%, 30 ± 22%, 50 ± 18% at 2.3-450 nm and 22 ± 16%, 17 ± 12%, 25 ± 19% at 450-1000 nm size fractions. Our findings clearly demonstrate significant new insights into the differences in the concentration and molecular composition of size-fractionated COC, which imply the importance of taking into consideration of the NNP and fine colloid fractions separately (as opposed to combining them into the "dissolved" fraction following the conventional definition of 450 nm) when assessing the cycling and transport of various elements and associated organic C in depressional wetlands.

6.2 Future Research

In natural ecosystem, there is an emerging paradigm emphasizing that extrinsic factors primarily control organic matter stability, while the interactions between minerals and SOM play a big role. My findings present a new framework for understanding the molecular composition and mobilization of the size-fractionated colloids and COC. In this field, the major challenge is the implication of the fine-scale processes and heterogeneity to the global scale. Moving forward requires utilization of more robust analytical techniques to study the image distribution of the OM coatings on the size-fractionated mineral surfaces. In addition, we require a much stronger focus on the molecular biomarkers of the size-fractionated organo-mineral

associations. The development of high-performance databases for the molecular SOM research will be necessary to better understand the response of SOM to the changing climatic conditions.

REFERENCES

Adhikari, D., and Yang, Y. (2015). Selective stabilization of aliphatic organic carbon by iron oxide. *Scientific Reports*, *5*, 1–7. https://doi.org/10.1038/srep11214

Afsar, M. Z., Hoque, S., and Osman, K. T. (2012a). A comparison of the Langmuir, Freundlich and Temkin equations to describe phosphate sorption characteristics of some representative soils of Bangladesh. *International Journal of Soil Science*, *7*(3), 91–99. http://scholar.google.com/scholar?hl=enandbtnG=Searchandq=intitle:No+Title#0

Afsar, M. Z., Hossain, M. E. (2012b). Characterization of some representative calcareous soils of Bangladesh with respect to soil phosphorus requirements. *International Jounral of Agricultural Research*. *7*(8), 388–397.

Afsar, M. Z., Hoque, S., and Osman, K. T. (2012c). Phosphate Desorption Characteristics of Some Representative Soils of Bangladesh: Effect of Exchangeable Anions, Water Molecules and Solution to Soil Ratios. *Open Journal of Soil Science*, *2*(3), 234–241. https://doi.org/10.4236/ojss.2012.23028

Afsar, M. Z., Goodwin, C., Beebe, T. P., Jaisi, D. P., and Jin, Y. (2020). Quantification and molecular characterization of organo-mineral associations as influenced by redox oscillations. *Science of the Total Environment*. 704, 1-10. https://doi.org/10.1016/j.scitotenv.2019.135454

Aitkenhead-Peterson, J. A., Alexander, J. E., and Clair, T. A. (2005). Dissolved organic carbon and dissolved organic nitrogen export from forested watersheds in Nova Scotia: Identifying controlling factors. *Global Biogeochemical Cycles*. 19, 1-8. https://doi.org/10.1029/2004GB002438

Altor, A. E., and Mitsch, W. J. (2008). Methane and carbon dioxide dynamics in wetland mesocosms: Effects of hydrology and soils. *Ecological Applications*. 18(5), 1307-1320. https://doi.org/10.1890/07-0009.1

Alva, A. K., Sumner, M. E., and Miller, W. P. (1991). Relationship between ionic strength and electrical conductivity for soil solutions. *Soil Science*. 152 (4), 239-242. https://doi.org/10.1097/00010694-199110000-00001

Amelung, W., Brodowski, S., Sandhage-Hofmann, A., and Bol, R. (2008). Chapter 6

Combining Biomarker with Stable Isotope Analyses for Assessing the Transformation and Turnover of Soil Organic Matter. In *Advances in Agronomy*. 100, 155-250. https://doi.org/10.1016/S0065-2113(08)00606-8

Arnarson, T. S., and Keil, R. G. (2001). Organic-mineral interactions in marine sediments studied using density fractionation and X-ray photoelectron spectroscopy. *Organic Geochemistry*, *32*(12), 1401–1415. https://doi.org/10.1016/S0146-6380(01)00114-0

Arnarson, T. S., and Keil, R. G. (2007). Changes in organic matter-mineral interactions for marine sediments with varying oxygen exposure times. *Geochimica et Cosmochimica Acta*, *71*(14), 3545–3556. https://doi.org/10.1016/j.gca.2007.04.027

Asano, M., and Wagai, R. (2014). Evidence of aggregate hierarchy at micro- to submicron scales in an allophanic andisol. *Geoderma*. 216, 62-74. https://doi.org/10.1016/j.geoderma.2013.10.005

Asano, M., and Wagai, R. (2015). Distinctive organic matter pools among particle-size fractions detected by solid-state 13C-NMR, δ13C and δ15N analyses only after strong dispersion in an allophanic andisol. *Soil Science and Plant Nutrition*. 61(2), 242-248. https://doi.org/10.1080/00380768.2014.982492

Avneri-Katz, S., Young, R. B., McKenna, A. M., Chen, H., Corilo, Y. E., Polubesova, T., Borch, T., and Chefetz, B. (2017). Adsorptive fractionation of dissolved organic matter (DOM) by mineral soil: Macroscale approach and molecular insight. *Organic Geochemistry*. 103, 113-124. https://doi.org/10.1016/j.orggeochem.2016.11.004

Baalousha, M., Lead, J. R., and Ju-Nam, Y. (2011). Natural Colloids and Manufactured Nanoparticles in Aquatic and Terrestrial Systems. In *Treatise on Water Science*. 3, 89-129. https://doi.org/10.1016/B978-0-444-53199-5.00053-1

Backhus, D. A., and Gschwend, P. M. (1990). Fluorescent Polycyciic Aromatic Hydrocarbons as Probes for Studying the Impact of Colloids on Pollutant Transport in Groundwater. *Environmental Science and Technology*. 24(8), 1214-1223. https://doi.org/10.1021/es00078a009

Baisden, W. T., Amundson, R., Cook, A. C., and Brenner, D. L. (2002). Turnover and storage of C and N in five density fractions from California annual grassland surface soils. *Global Biogeochemical Cycles*. 16(4), (1-16). https://doi.org/10.1029/2001gb001822

Baldock, J. A., and Skjemstad, J. O. (2000). Role of the soil matrix and minerals in

protecting natural organic materials against biological attack. *Organic Geochemistry*. 31(7-8), 697-710. https://doi.org/10.1016/S0146-6380(00)00049-8

Barber, A., Brandes, J., Leri, A., Lalonde, K., Balind, K., Wirick, S., Wang, J., and Gélinas, Y. (2017). Preservation of organic matter in marine sediments by inner-sphere interactions with reactive iron. *Scientific Reports*, *7*(1), 1–10. https://doi.org/10.1038/s41598-017-00494-0

Barr, T. L., Hoppe, E. E., Hardcastle, S., and Seal, S. (1999). X-ray photoelectron spectroscopy investigations of the chemistries of soils. *Journal of Vacuum Science and Technology A: Vacuum, Surfaces, and Films*. 17(4), 1079-1085. https://doi.org/10.1116/1.581778

Bartschat, B. M., Cabaniss, S. E., and Morel, F. M. M. (1992). Oligoelectrolyte Model for Cation Binding by Humic Substances. *Environmental Science and Technology*. 26(2), 284-294. https://doi.org/10.1021/es00026a007

Basile-Doelsch, I., Amundson, R., Stone, W. E. E., Borschneck, D., Bottero, J. Y., Moustier, S., Masin, F., and Colin, F. (2007). Mineral control of carbon pools in a volcanic soil horizon. *Geoderma*. 137(3-4), 477-489. https://doi.org/10.1016/j.geoderma.2006.10.006

Bazilevskaya, E., Archibald, D. D., and Martínez, C. E. (2018). Mineral colloids mediate organic carbon accumulation in a temperate forest Spodosol: depth-wise changes in pore water chemistry. *Biogeochemistry*, *141*(1), 75–94. https://doi.org/10.1007/s10533-018-0504-4

Benner, R., and Amon, R. M. W. (2015). The Size-Reactivity Continuum of Major Bioelements in the Ocean. *Annual Review of Marine Science*, *7*(1), 185–205. https://doi.org/10.1146/annurev-marine-010213-135126

Benoit, G., and Rozan, T. F. (1999). The influence of size distribution on the particle concentration effect and trace metal partitioning in rivers. *Geochimica et Cosmochimica Acta*. 63(1), 113-127. https://doi.org/10.1016/S0016-7037(98)00276-2

Bock, M. J., and Mayer, L. M. (2000). Mesodensity organo-clay associations in a near-shore sediment. *Marine Geology*. 163(1-4), 65-75. https://doi.org/10.1016/S0025-3227(99)00105-X

Bolan, N. S., Adriano, D. C., Kunhikrishnan, A., James, T., McDowell, R., and Senesi, N. (2011). Dissolved Organic Matter. Biogeochemistry, Dynamics, and Environmental Significance in Soils. In *Advances in Agronomy* (1st ed.), 110, 1-75. Elsevier Inc. https://doi.org/10.1016/B978-0-12-385531-2.00001-3

Bonneville, S., Van Cappellen, P., and Behrends, T. (2004). Microbial reduction of iron(III) oxyhydroxides: Effects of mineral solubility and availability. *Chemical Geology*. https://doi.org/10.1016/j.chemgeo.2004.08.015

Boye, K., Noël, V., Tfaily, M. M., Bone, S. E., Williams, K. H., Bargar, J. R., and Fendorf, S. (2017). Thermodynamically controlled preservation of organic carbon in floodplains. *Nature Geoscience*. 212(3-4), 255-268. https://doi.org/10.1038/ngeo2940

Buettner, S. W., Kramer, M. G., Chadwick, O. A., and Thompson, A. (2014). Mobilization of colloidal carbon during iron reduction in basaltic soils. *Geoderma, 221–222,* 139–145. https://doi.org/10.1016/j.geoderma.2014.01.012

Buffle, J. (1990). *Complexation reactions in aquatic systems*. Ellis Horwood, NY.

Bunn, R. A., Magelky, R. D., Ryan, J. N., and Elimelech, M. (2002). Mobilization of natural colloids from an iron oxide-coated sand aquifer: Effect of pH and ionic strength. *Environmental Science and Technology*. 36(3), 314-322 https://doi.org/10.1021/es0109141

Burdige, D. J. (2007). Preservation of organic matter in marine sediments: Controls, mechanisms, and an imbalance in sediment organic carbon budgets? *Chemical Reviews*, *107*(2), 467–485. https://doi.org/10.1021/cr050347q

Cabaniss, S. E., and Shuman, M. S. (1987). Synchronous fluorescence spectra of natural waters: tracing sources of dissolved organic matter. *Marine Chemistry*. 21(1), 37-50, https://doi.org/10.1016/0304-4203(87)90028-4

Chefet, B., Hadar, Y., and Chen, Y. (1998). Dissolved organic carbon fractions formed during composting of municipal solid waste: Properties and significance. *Acta Hydrochimica et Hydrobiologica*. 26(3), 172-179. https://doi.org/10.1002/(sici)1521-401x(199805)26:3<172::aid-aheh172>3.3.co;2-x

Chen, M., Wang, W. X., and Guo, L. (2004). Phase partitioning and solubility of iron in natural seawater controlled by dissolved organic matter. *Global Biogeochemical Cycles*. 18(4), 1-12. https://doi.org/10.1029/2003GB002160

Chen, Q., Shen, C., Sun, Y., Peng, S., Yi, W., Li, Z., and Jiang, M. (2005). Spatial and temporal distribution of carbon isotopes in soil organic matter at the Dinghushan Biosphere Reserve, South China. 273, 115-128 *Plant and Soil*. https://doi.org/10.1007/s11104-004-7245-y

Chin, Y. P., Alken, G., and O'Loughlin, E. (1994). Molecular Weight, Polydispersity,

and Spectroscopic Properties of Aquatic Humic Substances. *Environmental Science and Technology*. 28(11), 1853-1858. https://doi.org/10.1021/es00060a015

Chin, Y. P., Traina, S. J., Swank, C. R., and Backhus, D. (1998). Abundance and properties of dissolved organic matter in pore waters of a freshwater wetland. *Limnology and Oceanography*, *43*(6), 1287–1296. https://doi.org/10.4319/lo.1998.43.6.1287

Chin, Y. ping, and Gschwend, P. M. (1991). The abundance, distribution, and configuration of porewater organic colloids in recent sediments. *Geochimica et Cosmochimica Acta*. 55(5), 1309-1317. https://doi.org/10.1016/0016-7037(91)90309-S

Chiou, C. T., Malcolm, R. L., Brinton, T. I., and Kile, D. E. (1986). Water Solubility Enhancement of Some Organic Pollutants and Pesticides by Dissolved Humic and Fulvic Acids. *Environmental Science and Technology*. 20(5), 502-508. https://doi.org/10.1021/es00147a010

Christ, M. J., and David, M. B. (1996). Temperature and moisture effects on the production of dissolved organic carbon in a Spodosol. *Soil Biology and Biochemistry*. 28(9), 1191-1199. https://doi.org/10.1016/0038-0717(96)00120-4

Christian, P., Von Der Kammer, F., Baalousha, M., and Hofmann, T. (2008). Nanoparticles: Structure, properties, preparation and behaviour in environmental media. In *Ecotoxicology*. 17, 326-343. https://doi.org/10.1007/s10646-008-0213-1

Ciais, P., Sabine, C., Bala, G., Bopp, L., Brovkin, V., Canadell, J., Chhabra, A., DeFries, R., Galloway, J., Heimann, M., Jones, C., Quéré, C. Le, Myneni, R. B., Piao, S., and Thornton, P. (2013). The physical science basis. Contribution of working group I to the fifth assessment report of the intergovernmental panel on climate change. *Change, IPCC Climate*. https://doi.org/10.1017/CBO9781107415324.015

Connin, S. L., Feng, X., and Virginia, R. a. (2001). Isotopic discrimination during long-term decomposition in an arid land ecosystem. *Soil Biology and Biochemistry*, *33*(1), 41–51. https://doi.org/10.1016/S0038-0717(00)00113-9

Corrozi, M., Homsey, A., Kauffman, G., Farris, E., and Seymour, M. (2008). *White clay creek state of the watershed report, white clay creek wild and scenic river*.

Cory, R. M., and McKnight, D. M. (2005). Fluorescence spectroscopy reveals ubiquitous presence of oxidized and reduced quinones in dissolved organic

matter. *Environmental Science and Technology*. 39(21), 8142-8149. https://doi.org/10.1021/es0506962

Cotrufo, M. F., Wallenstein, M. D., Boot, C. M., Denef, K., and Paul, E. (2013). The Microbial Efficiency-Matrix Stabilization (MEMS) framework integrates plant litter decomposition with soil organic matter stabilization: Do labile plant inputs form stable soil organic matter? *Global Change Biology*. 19(4), 988-995. https://doi.org/10.1111/gcb.12113

Coyle, J. S., Dijkstra, P., Doucett, R. R., Schwartz, E., Hart, S. C., and Hungate, B. A. (2009). Relationships between C and N availability, substrate age, and natural abundance 13C and 15N signatures of soil microbial biomass in a semiarid climate. *Soil Biology and Biochemistry*. 41(8), 1605-1611. https://doi.org/10.1016/j.soilbio.2009.04.022

Crow, S. E., Swanston, C. W., Lajtha, K., Brooks, J. R., and Keirstead, H. (2007). Density fractionation of forest soils: Methodological questions and interpretation of incubation results and turnover time in an ecosystem context. 85, 69-90. *Biogeochemistry*. https://doi.org/10.1007/s10533-007-9100-8

Davidson, E. A., and Janssens, I. A. (2006). Temperature sensitivity of soil carbon decomposition and feedbacks to climate change. *Nature*, 440 (7081), 165–173. https://doi.org/10.1038/nature04514

Davison, W. (1993). Iron and manganese in lakes. *Earth Science Reviews*. 34 (2), 119-163. https://doi.org/10.1016/0012-8252(93)90029-7

De-Campos, A. B., Mamedov, A. I., and Huang, C. H. (2009). Short-term reducing conditions decrease soil aggregation. *Soil Science Society of America Journal*. 73 (2), 550-559. https://doi.org/10.2136/sssaj2007.0425

de Jonge, H. De, Jacobsen, O. H., Jonge, L. W. De, and Moldrup, P. (1998). Particle-Facilitated Transport of Prochloraz in Undisturbed Sandy Loam Soil Columns. *Journal of Environmental Quality*, 27, 1495–1503.

de Jonge, L. W., Kjaergaard, C., and Moldrup, P. (2004). Colloids and Colloid-Facilitated Transport of Contaminants in Soils: An Introduction. *Vadose Zone Joural*, 3, 321-325. https://doi.org/10.2136/vzj2004.0321

DeVilbiss, S. E., Zhou, Z., Klump, J. V., and Guo, L. (2016). Spatiotemporal variations in the abundance and composition of bulk and chromophoric dissolved organic matter in seasonally hypoxia-influenced Green Bay, Lake Michigan, USA. *Science of the Total Environment*. 565, 742-757. https://doi.org/10.1016/j.scitotenv.2016.05.015

Diem, D., and Stumm, W. (1984). Is dissolved Mn^{2+} being oxidized by O_2 in absence of Mn-bacteria or surface catalysts? *Geochimica et Cosmochimica Acta*. 48(7), 1571-1573. https://doi.org/10.1016/0016-7037(84)90413-7

Dijkstra, P., Ishizu, A., Doucett, R., Hart, S. C., Schwartz, E., Menyailo, O. V., and Hungate, B. A. (2006). ^{13}C and ^{15}N natural abundance of the soil microbial biomass. *Soil Biology and Biochemistry*. 38(11), 3257-3266. https://doi.org/10.1016/j.soilbio.2006.04.005

Dijkstra, P., Laviolette, C. M., Coyle, J. S., Doucett, R. R., Schwartz, E., Hart, S. C., and Hungate, B. A. (2008). ^{15}N enrichment as an integrator of the effects of C and N on microbial metabolism and ecosystem function. *Ecology Letters*. 11(4), 389-397. https://doi.org/10.1111/j.1461-0248.2008.01154.x

Doane, T. A., and Horwáth, W. R. (2010). Eliminating interference from iron(III) for ultraviolet absorbance measurements of dissolved organic matter. *Chemosphere*. 78(11), 1409-1415. https://doi.org/10.1016/j.chemosphere.2009.12.062

Docter, D., Westmeier, D., Markiewicz, M., Stolte, S., Knauer, S. K., and Stauber, R. H. (2015). The nanoparticle biomolecule corona: lessons learned - challenge accepted? *Chemical Society Reviews*. 44, 6094-6121. https://doi.org/10.1039/c5cs00217f

Doetterl, S., Stevens, A., Six, J., Merckx, R., Van Oost, K., Casanova Pinto, M., Casanova-Katny, A., Muñoz, C., Boudin, M., Zagal Venegas, E., and Boeckx, P. (2015). Soil carbon storage controlled by interactions between geochemistry and climate. *Nature Geoscience*. 8, 780-783. https://doi.org/10.1038/ngeo2516

Dupré, B., Viers, J., Dandurand, J. L., Polve, M., Bénézeth, P., Vervier, P., and Braun, J. J. (1999). Major and trace elements associated with colloids in organic-rich river waters: Ultrafiltration of natural and spiked solutions. *Chemical Geology*. 160(1-2), 63-80. https://doi.org/10.1016/S0009-2541(99)00060-1

Edwards, M., Benjamin, M. M., and Ryan, J. N. (1996). Role of organic acidity in sorption of natural organic matter (NOM) to oxide surfaces. *Colloids and Surfaces A: Physicochemical and Engineering Aspects*. 107, 297-307. https://doi.org/10.1016/0927-7757(95)03371-8

Ehleringer, J. R., Buchmann, N., and Flanagan, L. B. (2000). Carbon isotope ratios in belowground carbon cycle processes. In *Ecological Applications*. 10(2), 412-422. https://doi.org/10.1890/1051-0761(2000)010[0412:CIRIBC]2.0.CO;2

Emmerton, K. S., Callaghan, T. V., Jones, H. E., Leake, J. R., Michelsen, A., and Read, D. J. (2001). Assimilation and isotopic fractionation of nitrogen by

mycorrhizal fungi. *New Phytologist*. 151(2), 503-511. https://doi.org/10.1046/j.1469-8137.2001.00178.x

Engelhaupt, E., and Bianchi, T. S. (2001). Sources and composition of high-molecular-weight dissolved organic carbon in a southern Louisiana tidal stream (Bayou Trepagnier). *Limnology and Oceanography*. 46(4), 917-926 https://doi.org/10.4319/lo.2001.46.4.0917

Eusterhues, K., Hädrich, A., Neidhardt, J., Küsel, K., Keller, T. F., Jandt, K. D., and Totsche, K. U. (2014). Reduction of ferrihydrite with adsorbed and coprecipitated organic matter: Microbial reduction by Geobacter bremensis vs. abiotic reduction by Na-dithionite. *Biogeosciences*, *11*(18), 4953–4966. https://doi.org/10.5194/bg-11-4953-2014

Everett, D. H. (2019). Manual of Symbols and Terminology for Physicochemical Quantities and Units, Appendix II: Definitions, Terminology and Symbols in Colloid and Surface Chemistry. *Pure and Applied Chemistry*. https://doi.org/10.1351/pac197231040577

Favre, F., Jaunet, A. M., Pernes, M., Badraoui, M., Boivin, P., and Tessier, D. (2004). Changes in clay organization due to structural iron reduction in a flooded vertisol. *Clay Minerals*. https://doi.org/10.1180/0009855043920125

Fellman, J. B., D'Amore, D. V., Hood, E., and Boone, R. D. (2008). Fluorescence characteristics and biodegradability of dissolved organic matter in forest and wetland soils from coastal temperate watersheds in southeast Alaska. *Biogeochemistry*, *88*(2), 169–184. https://doi.org/10.1007/s10533-008-9203-x

Fenstermacher, D. E., Rabenhorst, M. C., Lang, M. W., McCarty, G. W., and Needelman, B. A. (2014). Distribution, Morphometry, and Land Use of Delmarva Bays. *Wetlands*. 34, 1219-1228. https://doi.org/10.1007/s13157-014-0583-5

Fiedler, S., and Kalbitz, K. (2003). Concentrations and properties of dissolved organic matter in forest soils as affected by the redox regime. *Soil Science*. https://doi.org/10.1097/01.ss.0000100471.96182.03

Fritzsche, A., Pagels, B., and Totsche, K. U. (2016). The composition of mobile matter in a floodplain topsoil: A comparative study with soil columns and field lysimeters. *Journal of Plant Nutrition and Soil Science*. 168, 793-801. https://doi.org/10.1002/jpln.201500169

Fry, B. (2006). Stable Isotope Ecology. In *Stable Isotope Ecology*. Springer.

Fuller, C. C., and Davis, J. A. (1987). Processes and kinetics of Cd^{2+} sorption by a calcareous aquifer sand. *Geochimica et Cosmochimica Acta*. 51(6), 1491-1502. https://doi.org/10.1016/0016-7037(87)90331-0

Gaillardet, J., Viers, J., and Dupré, B. (2013). Trace Elements in River Waters. In *Treatise on Geochemistry: 2nd ed*. 7, 195-235. https://doi.org/10.1016/B978-0-08-095975-7.00507-6

Gentsch, N., Mikutta, R., Shibistova, O., Wild, B., Schnecker, J., Richter, A., Urich, T., Gittel, A., Šantrůčková, H., Bárta, J., Lashchinskiy, N., Mueller, C. W., Fuß, R., and Guggenberger, G. (2015). Properties and bioavailability of particulate and mineral-associated organic matter in Arctic permafrost soils, Lower Kolyma Region, Russia. *European Journal of Soil Science*. 66, 722-734. https://doi.org/10.1111/ejss.12269

Gerin, P. A., Genet, M. J., Herbillon, A. J., and Delvaux, B. (2003). Surface analysis of soil material by X-ray photoelectron spectroscopy. *European Journal of Soil Science*. 54(3), 589-603. https://doi.org/10.1046/j.1365-2389.2003.00537.x

Gillabel, J., Cebrian-Lopez, B., Six, J., and Merckx, R. (2010). Experimental evidence for the attenuating effect of SOM protection on temperature sensitivity of SOM decomposition. *Global Change Biology*. 16(10), 2789-2798. https://doi.org/10.1111/j.1365-2486.2009.02132.x

Gimbert, L. J., Haygarth, P. M., Beckett, R., and Worsfold, P. J. (2005). Comparison of centrifugation and filtration techniques for the size fractionation of colloidal material in soil suspensions using sedimentation field-flow fractionation. *Environmental Science and Technology*. 39(6), 1731-1435. https://doi.org/10.1021/es049230u

Gleixner, G. (2013). Soil organic matter dynamics: A biological perspective derived from the use of compound-specific isotopes studies. *Ecological Research*. 28(3), 683-695. https://doi.org/10.1007/s11284-012-1022-9

Gleixner, G., Bol, R., and Balesdent, J. (1999). Molecular insight into soil carbon turnover. *Rapid Communications in Mass Spectrometry*. 13, 1278-1283. https://doi.org/10.1002/(SICI)1097-0231(19990715)13:13<1278::AID-RCM649>3.0.CO;2-N

Grandy, A. S., and Neff, J. C. (2008). Molecular C dynamics downstream: The biochemical decomposition sequence and its impact on soil organic matter structure and function. *Science of the Total Environment*, *404*(2–3), 297–307. https://doi.org/10.1016/j.scitotenv.2007.11.013

Green, S. A., and Blough, N. V. (1994). Optical absorption and fluorescence properties of chromophoric dissolved organic matter in natural waters. *Limnology and Oceanography*. 39(8), 1903-1916. https://doi.org/10.4319/lo.1994.39.8.1903

Grim, R. E. (1953). *Clay Mineralogy*. McGraw-Hill, New York, USA.

Grolimund, D., and Borkovec, M. (1999). Long-term release kinetics of colloidal particles from natural porous media. *Environmental Science and Technology*. 33(22), 4054-4060. https://doi.org/10.1021/es990194m

Grybos, M., Davranche, M., Gruau, G., Petitjean, P., and Pédrot, M. (2009). Increasing pH drives organic matter solubilization from wetland soils under reducing conditions. *Geoderma*. 154(1-2), 13-19. https://doi.org/10.1016/j.geoderma.2009.09.001

Gu, B., Schmitt, J., Chen, Z., Liang, L., and McCarthy, J. F. (1994). Adsorption and Desorption of Natural Organic Matter on Iron Oxide: Mechanisms and Models. *Environmental Science and Technology*. 28(1), 38-46. https://doi.org/10.1021/es00050a007

Guggenberger, G., Kaiser, K., and Zech, W. (1998). Organic Colloids in Forest Soils: 1. Biochemical Mobilization in the Forest Floor. *Physics and Chemistry of the Earth*. 23(2), 141-146. https://doi.org/10.1016/S0079-1946(98)00004-4

Guggenberger, Georg, Glaser, B., and Zech, W. (1994). Heavy metal binding by hydrophobic and hydrophilic dissolved organic carbon fractions in a Spodosol A and B horizon. *Water, Air, and Soil Pollution*. 23(2), 141-146. https://doi.org/10.1007/BF01257119

Guggenberger, Georg, and Kaiser, K. (2003). Dissolved organic matter in soil: Challenging the paradigm of sorptive preservation. *Geoderma*. 113(3-4), 293-310. https://doi.org/10.1016/S0016-7061(02)00366-X

Guggenberger, Georg, and Zech, W. (1994). Composition and dynamics of dissolved carbohydrates and lignin-degradation products in two coniferous forests, N.E. Bavaria, Germany. *Soil Biology and Biochemistry*. 26(1), 19-27. https://doi.org/10.1016/0038-0717(94)90191-0

Guo, L., and Macdonald, R. W. (2006). Source and transport of terrigenous organic matter in the upper Yukon River: Evidence from isotope ($\delta^{13}C$, $\Delta\ ^{14}C$, and $\delta^{15}N$) composition of dissolved, colloidal, and particulate phases. *Global Biogeochemical Cycles*. 20(2), 1-12. https://doi.org/10.1029/2005GB002593

Guo, L., and Santschi, P. H. (1997a). Composition and cycling of colloids in marine

environments. *Reviews of Geophysics*. 35(1), 17-40. https://doi.org/10.1029/96RG03195

Guo, L., and Santschi, P. H. (1997b). Isotopic and elemental characterization of colloidal organic matter from the Chesapeake Bay and Galveston Bay. *Marine Chemistry*, *59*(1–2), 1–15. https://doi.org/10.1016/S0304-4203(97)00072-8

Guo, L., and Santschi, P. H. (2007). Ultrafiltration and its Applications to Sampling and Characterisation of Aquatic Colloids. In K.J. Wilkinson and J. R. Lead (eds.), *Environmental Colloids and Particles: Behaviour, Separation and Characterisation* (pp. 159–221). Wiley. https://doi.org/10.1002/9780470024539.ch4

Gurwick, N. P., McCorkle, D. M., Groffman, P. M., Gold, A. J., Kellogg, D. Q., and Seitz-Rundlett, P. (2008). Mineralization of ancient carbon in the subsurface of riparian forests. *Journal of Geophysical Research: Biogeosciences*. 113, 1-13. https://doi.org/10.1029/2007JG000482

Hagedorn, F., Kaiser, K., Feyen, H., and Schleppi, P. (2000). Effects of Redox Conditions and Flow Processes on the Mobility of Dissolved Organic Carbon and Nitrogen in a Forest Soil. *Journal of Environmental Quality*. 29, 288-297. https://doi.org/10.2134/jeq2000.00472425002900010036x

Hagedorn, Frank, Bucher, J. B., and Schleppi, P. (2001). Contrasting dynamics of dissolved inorganic and organic nitrogen in soil and surface waters of forested catchments with Gleysols. *Geoderma*. 100(1-2), 173-192. https://doi.org/10.1016/S0016-7061(00)00085-9

Hatcher, P. G., Spiker, E. C., Szeverenyi, N. M., and Maciel, G. E. (1983). Selective preservation and origin of petroleum-forming aquatic kerogen. *Nature*. 305, 498-501. https://doi.org/10.1038/305498a0

Hedges, J. I., and Keil, R. G. (1995). Sedimentary organic matter preservation: an assessment and speculative synthesis. In *Marine Chemistry*. 49(2-3), 81-115. https://doi.org/10.1016/0304-4203(95)00008-F

Hedges, J. I., and Keil, R. G. (1999). Organic geochemical perspectives on estuarine processes: Sorption reactions and consequences. *Marine Chemistry*. 65(1-2), 55-65. https://doi.org/10.1016/S0304-4203(99)00010-9

Heil, D., and Sposito, G. (1993). Organic Matter Role in Illitic Soil Colloids Flocculation: I. Counter Ions and pH. *Soil Science Society of America Journal*. 57(5), 1241-1246. https://doi.org/10.2136/sssaj1993.03615995005700050014x

Heister, K., Höschen, C., Pronk, G. J., Mueller, C. W., and Kögel-Knabner, I. (2012). NanoSIMS as a tool for characterizing soil model compounds and organomineral associations in artificial soils. *Journal of Soils and Sediments*. 12, 35-47. https://doi.org/10.1007/s11368-011-0386-8

Hemingway, J. D., Rothman, D. H., Grant, K. E., Rosengard, S. Z., Eglinton, T. I., Derry, L. A., and Galy, V. V. (2019). Mineral protection regulates long-term global preservation of natural organic carbon. *Nature*, *570*(7760), 228–231. https://doi.org/10.1038/s41586-019-1280-6

Henderson, R., Kabengi, N., Mantripragada, N., Cabrera, M., Hassan, S., and Thompson, a. (2012). Anoxia-induced release of colloid- and nanoparticle-bound phosphorus in grassland soils. *Environmental Science and Technology*, *46*(21), 11727–11734. https://doi.org/10.1021/es302395r

Hilger, S., Sigg, L., and Barbieri, A. (1999). Size fractionation of phosphorus (dissolved, colloidal and particulate) in two tributaries to Lake Lugano. *Aquatic Sciences*. 61, 337-353. https://doi.org/10.1007/s000270050070

Hochella, M. F., Lower, S. K., Maurice, P. A., Penn, R. L., Sahai, N., Sparks, D. L., and Twining, B. S. (2008). Nanominerals, mineral nanoparticles, and earth systems. *Science*, *319*(5870), 1631–1635. https://doi.org/10.1126/science.1141134

Huang, Y., Eglinton, G., Van Der Hage, E. R. E., Boon, J. J., Bol, R., and Ineson, P. (1998). Dissolved organic matter and its parent organic matter in grass upland soil horizons studied by analytical pyrolysis techniques. *European Journal of Soil Science*. 49(1), 1-15. https://doi.org/10.1046/j.1365-2389.1998.00141.x

Hübner, H. (1986). Isotope effects of nitrogen in the soil and biosphere. In *The Terrestrial Environment, B*. pp 361-425.

Huygens, D., Denef, K., Vandeweyer, R., Godoy, R., Van Cleemput, O., and Boeckx, P. (2008). Do nitrogen isotope patterns reflect microbial colonization of soil organic matter fractions? *Biology and Fertility of Soils*. 44, 955-964. https://doi.org/10.1007/s00374-008-0280-8

Jepson, W. B. (1984). Kaolins: their properties and uses. *Philosophical Transactions of the Royal Society of London*. 311, 411-432. https://doi.org/10.1098/rsta.1984.0037

Jin, Q., and Bethke, C. M. (2005). Predicting the rate of microbial respiration in geochemical environments. *Geochimica et Cosmochimica Acta*. 69(5), 1133-1143. https://doi.org/10.1016/j.gca.2004.08.010

Jokic, A., Cutler, J. N., Ponomarenko, E., van der Kamp, G., and Anderson, D. W. (2003). Organic carbon and sulphur compounds in wetland soils: Insights on structure and transformation processes using K-edge XANES and NMR spectroscopy. *Geochimica et Cosmochimica Acta*. 67(14), 2585-2597. https://doi.org/10.1016/S0016-7037(03)00101-7

Jones, E., and Singh, B. (2014). Organo-mineral interactions in contrasting soils under natural vegetation. *Frontiers in Environmental Science*. 2(2), 1-15. https://doi.org/10.3389/fenvs.2014.00002

Kaiser, K., Guggenberger, G., Haumaier, L., and Zech, W. (1997). Dissolved organic matter sorption on subsoils and minerals studied by 13C-NMR and DRIFT spectroscopy. *European Journal of Soil Science*. 48(2), 301-310. https://doi.org/10.1111/j.1365-2389.1997.tb00550.x

Kaiser, K., and Zech, W. (2000). Sorption of dissolved organic nitrogen by acid subsoil horizons and individual mineral phases. *European Journal of Soil Science*. 51, 403-411. https://doi.org/10.1046/j.1365-2389.2000.00320.x

Kaiser, Klaus, Eusterhues, K., Rumpel, C., Guggenberger, G., and Kögel-Knabner, I. (2002). Stabilization of organic matter by soil minerals - Investigations of density and particle-size fractions from two acid forest soils. *Journal of Plant Nutrition and Soil Science*. 165, 451-459. https://doi.org/10.1002/1522-2624(200208)165:4<451::AID-JPLN451>3.0.CO;2-B

Kaiser, Klaus, Guggenberger, G., and Haumaier, L. (2004). Changes in dissolved lignin-derived phenols, neutral sugars, uronic acids, and amino sugars with depth in forested Haplic Arenosols and Rendzic Leptosols. *Biogeochemistry*. 70, 135-151. https://doi.org/10.1023/B:BIOG.0000049340.77963.18

Kaiser, Klaus, and Kalbitz, K. (2012). Cycling downwards - dissolved organic matter in soils. *Soil Biology and Biochemistry, 52*, 29–32. https://doi.org/10.1016/j.soilbio.2012.04.002

Kalbitz, K., Solinger, S., Park, J. H., Michalzik, B., and Matzner, E. (2000). Controls on the dynamics dissolved organic matter in soils: A review. *Soil Science*. 165(4), 277-304. https://doi.org/10.1097/00010694-200004000-00001

Kalbitz, Karsten, Schwesig, D., Rethemeyer, J., and Matzner, E. (2005). Stabilization of dissolved organic matter by sorption to the mineral soil. *Soil Biology and Biochemistry*, *37*(7), 1319–1331. https://doi.org/10.1016/j.soilbio.2004.11.028

Kallenbach, C. M., Frey, S. D., and Grandy, A. S. (2016). Direct evidence for microbial-derived soil organic matter formation and its ecophysiological controls.

Nature Communications. 7, 1-10. https://doi.org/10.1038/ncomms13630

Kappler, A., Benz, M., Schink, B., and Brune, A. (2004). Electron shuttling via humic acids in microbial iron(III) reduction in a freshwater sediment. *FEMS Microbiology Ecology*. 47(1), 85-92. https://doi.org/10.1016/S0168-6496(03)00245-9

Kellerman, A. M., Dittmar, T., Kothawala, D. N., and Tranvik, L. J. (2014). Chemodiversity of dissolved organic matter in lakes driven by climate and hydrology. *Nature Communications*. 5, 3804. https://doi.org/10.1038/ncomms4804

Kendall, C. (1998). Tracing Nitrogen Sources and Cycling in Catchments. In *Isotope Tracers in Catchment Hydrology*. Elsevier.

Khilar, K. C., and Fogler, H. S. (1984). The existence of a critical salt concentration for particle release. *Journal of Colloid And Interface Science*. 101(1), 214-224. https://doi.org/10.1016/0021-9797(84)90021-3

Khilar, Kartic C., Vaidya, R. N., and Fogler, H. S. (1990). Colloidally-induced fines release in porous media. *Journal of Petroleum Science and Engineering*. 4(3), 213-221. https://doi.org/10.1016/0920-4105(90)90011-Q

Kia, S. F., Fogler, H. S., and Reed, M. G. (1987). Effect of pH on colloidally induced fines migration. *Journal of Colloid And Interface Science*. 118(1), 158-168. https://doi.org/10.1016/0021-9797(87)90444-9

Kirk, G. (2004). The Biogeochemistry of Submerged Soils. In *The Biogeochemistry of Submerged Soils*.

Kjaergaard, C., Poulsen, T. G., Moldrup, P., and Jonge, L. W. De. (2004). *Colloid Mobilization and Transport in Undisturbed Soil Columns. I. Pore Structure Characterization and Tritium Transport*. *423*, 413–423.

Kleber, M., Sollins, P., and Sutton, R. (2007). A conceptual model of organo-mineral interactions in soils: Self-assembly of organic molecular fragments into zonal structures on mineral surfaces. *Biogeochemistry*. 85, 9-24. https://doi.org/10.1007/s10533-007-9103-5

Kleber, Markus, Eusterhues, K., Keiluweit, M., Mikutta, C., Mikutta, R., and Nico, P. S. (2015). Mineral-Organic Associations: Formation, Properties, and Relevance in Soil Environments. *Advances in Agronomy*. 130, 1-140. https://doi.org/10.1016/bs.agron.2014.10.005

Kleber, Markus, and Johnson, M. G. (2010). Advances in Understanding the Molecular Structure of Soil Organic Matter : Implications for Interactions in the Environment. In *Advances in Agronomy.* (106), 77-142. https://doi.org/10.1016/S0065-2113(10)06003-7

Knicker, H. (2011). Soil organic N - An under-rated player for C sequestration in soils? In *Soil Biology and Biochemistry*. 43(6), 1118-1129. https://doi.org/10.1016/j.soilbio.2011.02.020

Kögel-Knabner, I., Amelung, W., Cao, Z., Fiedler, S., Frenzel, P., Jahn, R., Kalbitz, K., Kölbl, A., and Schloter, M. (2010). Biogeochemistry of paddy soils. *Geoderma*, *157*(1–2), 1–14. https://doi.org/10.1016/j.geoderma.2010.03.009

Kögel-Knabner, I., Guggenberger, G., Kleber, M., Kandeler, E., Kalbitz, K., Scheu, S., Eusterhues, K., and Leinweber, P. (2008). Organo-mineral associations in temperate soils: Integrating biology, mineralogy, and organic matter chemistry. In *Journal of Plant Nutrition and Soil Science*. 171(1), 61-82. https://doi.org/10.1002/jpln.200700048

Kothawala, D. N., Roehm, C., Blodau, C., and Moore, T. R. (2012). Selective adsorption of dissolved organic matter to mineral soils. *Geoderma*. 189-190, 334-342. https://doi.org/10.1016/j.geoderma.2012.07.001

Kretzschmar, R., Borkovec, M., Grolimund, D., and Elimelech M., (1999). Mobile subsurface colloids their role in contaminant. *Advances in Agronomy*, 66, 121-193.

Krom, M. D., and Sholkovitz, E. R. (1977). Nature and reactions of dissolved organic matter in the interstitial waters of marine sediments. *Geochimica et Cosmochimica Acta*. 41(11), 1565-1574. https://doi.org/10.1016/0016-7037(77)90168-5

Lal, R. (2001). World cropland soils as a source or sink for atmospheric carbon. In *Advances in Agronomy*. 71, 145-191. https://doi.org/10.1016/s0065-2113(01)71014-0

Lal, R. (2004). Soil carbon sequestration impacts on global climate change and food security. *Science*, *304*(5677), 1623–1627. https://doi.org/10.1126/science.1097396

Lalonde, K., Mucci, A., Ouellet, A., and Gélinas, Y. (2012). Preservation of organic matter in sediments promoted by iron. *Nature*. 483, 198-200. https://doi.org/10.1038/nature10855

LaRowe, D. E., and Van Cappellen, P. (2011). Degradation of natural organic matter: A thermodynamic analysis. *Geochimica et Cosmochimica Acta*. 75(8), 2030-2042. https://doi.org/10.1016/j.gca.2011.01.020

Lehmann, J., Kinyangi, J., and Solomon, D. (2007). Organic matter stabilization in soil microaggregates: Implications from spatial heterogeneity of organic carbon contents and carbon forms. *Biogeochemistry*. 85, 45-57. https://doi.org/10.1007/s10533-007-9105-3

Lehmann, J., and Kleber, M. (2015). The contentious nature of soil organic matter. In *Nature*. 528, 60-68. https://doi.org/10.1038/nature16069

Liptzin, D., and Silver, W. L. (2009). Effects of carbon additions on iron reduction and phosphorus availability in a humid tropical forest soil. *Soil Biology and Biochemistry, 41*(8), 1696–1702. https://doi.org/10.1016/j.soilbio.2009.05.013

Lyvén, B., Hassellöv, M., Turner, D. R., Haraldsson, C., and Andersson, K. (2003). Competition between iron- and carbon-based colloidal carriers for trace metals in a freshwater assessed using flow field-flow fractionation coupled to ICPMS. *Geochimica et Cosmochimica Acta*. 67(20), 3791-3802. https://doi.org/10.1016/S0016-7037(03)00087-5

Magaritz, M., Amiel, A. J., Ronen, D., and Wells, M. C. (1990). Distribution of metals in a polluted aquifer: A comparison of aquifer suspended material to fine sediments of the adjacent environment. *Journal of Contaminant Hydrology*. 5(4), 333-347. https://doi.org/10.1016/0169-7722(90)90024-B

Marín-Spiotta, E., Gruley, K. E., Crawford, J., Atkinson, E. E., Miesel, J. R., Greene, S., Cardona-Correa, C., and Spencer, R. G. M. (2014). Paradigm shifts in soil organic matter research affect interpretations of aquatic carbon cycling: Transcending disciplinary and ecosystem boundaries. *Biogeochemistry*. 117, 279-297. https://doi.org/10.1007/s10533-013-9949-7

Mayer, L. M. (1994). Relationships between mineral surfaces and organic carbon concentrations in soils and sediments. *Chemical Geology*. 114(3-4), 347-363. https://doi.org/10.1016/0009-2541(94)90063-9

McCarthy, J. F., and Zachara, J. M. (1989). Subsurface transport of contaminants. *Environmental Science and Technology*. 23(5), 496-502. https://doi.org/10.1021/es00063a001

McGill, W. B., Cannon, K. R., Robertson, J. a., and D., C. F. (1986). Dynamics of soil microbial biomass and water-soluble organic C in BRETON L after 50 years of cropping to two rotations. *Canadian Jouranl of Soil Science*. 66, 1-19.

McKnight, D. M., Boyer, E. W., Westerhoff, P. K., Doran, P. T., Kulbe, T., and Andersen, D. T. (2001). Spectrofluorometric characterization of dissolved organic matter for indication of precursor organic material and aromaticity. *Limnology and Oceanography*. 46(1), 38-48. https://doi.org/10.4319/lo.2001.46.1.0038

Melillo, J. M., Terese, T. C. R., and W.Y., G. (2014). *Highlights of climate change impacts in the United States: The third national climate assessment*.

Michalzik, B., Kalbitz, K., Park, J. H., Solinger, S., and Matzner, E. (2001). Fluxes and concentrations of dissolved organic carbon and nitrogen - A synthesis for temperate forests. *Biogeochemistry*. 52, 173-205. https://doi.org/10.1023/A:1006441620810

Mikutta, R., Mikutta, C., Kalbitz, K., Scheel, T., Kaiser, K., and Jahn, R. (2007). Biodegradation of forest floor organic matter bound to minerals via different binding mechanisms. *Geochimica et Cosmochimica Acta*, *71*(10), 2569–2590. https://doi.org/10.1016/j.gca.2007.03.002

Mikutta, R., Schaumann, G. E., Gildemeister, D., Bonneville, S., Kramer, M. G., Chorover, J., Chadwick, O. A., and Guggenberger, G. (2009). Biogeochemistry of mineral-organic associations across a long-term mineralogical soil gradient (0.3-4100 kyr), Hawaiian Islands. *Geochimica et Cosmochimica Acta*. 73(7), 2034-2060. https://doi.org/10.1016/j.gca.2008.12.028

Millero, F. J., Sotolongo, S., and Izaguirre, M. (1987). The oxidation kinetics of Fe(II) in seawater. *Geochimica et Cosmochimica Acta*. 51(4), 793-801. https://doi.org/10.1016/0016-7037(87)90093-7

Miltner, A., Bombach, P., Schmidt-Brücken, B., and Kästner, M. (2012). SOM genesis: Microbial biomass as a significant source. *Biogeochemistry*. 111, 41-55 https://doi.org/10.1007/s10533-011-9658-z

Mitsch, W.J, and Gosselink, J. G. (2007). *Wetlands*. John Wiley and Sons Inc, New Jersey.

Mitsch, William J., Bernal, B., Nahlik, A. M., Mander, Ü., Zhang, L., Anderson, C. J., Jørgensen, S. E., and Brix, H. (2013). Wetlands, carbon, and climate change. *Landscape Ecology*. 28, 583-597. https://doi.org/10.1007/s10980-012-9758-8

Moran, S. B., and Buesseler, K. O. (1992). Short residence time of colloids in the upper ocean estimated from 238U-234Th disequilibria. *Nature*. 359, 221-223. https://doi.org/10.1038/359221a0

Morrisson, A. R., Park, J. S., and Sharp, B. L. (1990). Application of high-performance size-exclusion liquid chromatography to the study of copper speciation in waters extracted from sewage sludge treated soils. *The Analyst*, *115*(11), 1429–1433. https://doi.org/10.1039/an9901501429

Mortland, M. M. (1986). Mechanisms of adsoprtion of nonhumic organic species by clays. In P. M. Huang and M. Schnitzer (Eds.), *Interactions of Soil Minerals with Natural organics and Microbes*. Soil Science Society of America.

Muir, A., Anderson, B., and Stephen, I. (1957). Characteristics of some Tanganyika soils. *Journal of Soil Science*, *8*, 1–18.

Mulholland, P. J. (2003). Large-Scale Patterns in Dissolved Organic Carbon Concentration, Flux, and Sources. In *Aquatic Ecosystems*. 139-159. https://doi.org/10.1016/b978-012256371-3/50007-x

Murphy, D. M., Garbarino, J. R., Taylor, H. E., Hart, B. T., and Beckett, R. (1993). Determination of size and element composition distributions of complex colloids by sedimentation field-flow fractionation-inductively coupled plasma mass spectrometry. *Journal of Chromatography A*. 642(1-2), 459-467. https://doi.org/10.1016/0021-9673(93)80112-L

Oades, J. M. (1988). The retention of organic matter in soils. *Biogeochemistry*. 5, 35-70. https://doi.org/10.1007/BF02180317

Ohno, T. (2002). Fluorescence inner-filtering correction for determining the humification index of dissolved organic matter. *Environmental Science and Technology*, *36*(4), 742–746. https://doi.org/10.1021/es0155276

Olivie-Lauquet, G., Gruau, G., Dia, A., Riou, C., Jaffrezic, A., and Henin, O. (2001). Release of trace elements in wetlands: Role of seasonal variability. *Water Research*. 35(4), 943-952. https://doi.org/10.1016/S0043-1354(00)00328-6

Orlandini, K. A., Penrose, W. R., Harvey, B. R., Lovett, M. B., and Findlay, M. W. (1990). Colloidal Behavior of Actinides in an Oligotrophic Lake. *Environmental Science and Technology*. 24(5), 706-712. https://doi.org/10.1021/es00075a015

Osburn, C. L., Handsel, L. T., Mikan, M. P., Paerl, H. W., and Montgomery, M. T. (2012). Fluorescence tracking of dissolved and particulate organic matter quality in a river-dominated estuary. *Environmental Science and Technology*, *46*(16), 8628–8636. https://doi.org/10.1021/es3007723

Pantano, C. G., and Wittberg, T. N. (1990). XPS analysis of silane coupling agents and silane-treated E-glass fibers. *Surface and Interface Analysis*, *15*(8).

Pédrot, M., Dia, A., Davranche, M., Bouhnik-Le Coz, M., Henin, O., and Gruau, G. (2008). Insights into colloid-mediated trace element release at the soil/water interface. *Journal of Colloid and Interface Science*, *325*(1), 187–197. https://doi.org/10.1016/j.jcis.2008.05.019

Perdue, E. M., and Lytle, C. R. (1983). Distribution Model for Binding of Protons and Metal Ions by Humic Substances. *Environmental Science and Technology*. 17(11), 654-660. https://doi.org/10.1021/es00117a006

Poage, M. A., and Feng, X. (2004). A theoretical analysis of steady state δ13C profiles of soil organic matter. *Global Biogeochemical Cycles*. 18, 1-13. https://doi.org/10.1029/2003GB002195

Poulin, B. A., Ryan, J. N., and Aiken, G. R. (2014). Effects of iron on optical properties of dissolved organic matter. *Environmental Science and Technology*. 48(17), 10098-10106. https://doi.org/10.1021/es502670r

Pourret, O., Dia, A., Gruau, G., Davranche, M., and Bouhnik-Le Coz, M. (2012). Assessment of vanadium distribution in shallow groundwaters. *Chemical Geology*. 294-295, 89-102. https://doi.org/10.1016/j.chemgeo.2011.11.033

Proctor, A., and Sherwood, P. M. A. (1982). X-ray photoelectron spectroscopic studies of carbon fibre surfaces. III—Industrially treated fibres and the effect of heat and exposure to oxygen. *Surface and Interface Analysis*. 4(5), 212-219. https://doi.org/10.1002/sia.740040508

Pullin, M. J., and Cabaniss, S. E. (2003). The effects of pH, ionic strength, and iron-fulvic acid interactions on the kinetics of non-photochemical iron transformations. I. Iron(II) oxidation and iron(III) colloid formation. *Geochimica et Cosmochimica Acta*. 67(21), 4067-4077. https://doi.org/10.1016/S0016-7037(03)00366-1

Qualls, R. G., and Haines, B. L. (1991). Geochemistry of Dissolved Organic Nutrients in Water Percolating through a Forest Ecosystem. *Soil Science Society of America Journal*. 55, 1112-1123. https://doi.org/10.2136/sssaj1991.03615995005500040036x

Ransom, B., Bennett, R. H., Baerwald, R., and Shea, K. (1997). TEM study of in situ organic matter on continental margins: Occurrence and the "monolayer" hypothesis. *Marine Geology*. 138(1-2), 1-9. https://doi.org/10.1016/S0025-3227(97)00012-1

Rapin, A., Grybos, M., Rabiet, M., Mourier, B., and Deluchat, V. (2019). Phosphorus mobility in dam reservoir affected by redox oscillations: An experimental study.

Journal of Environmental Sciences (China). 77, 250-263. https://doi.org/10.1016/j.jes.2018.07.016

Reddy, K. R., and Patrick, W. H. (1975). Effect of alternate aerobic and anaerobic conditions on redox potential, organic matter decomposition and nitrogen loss in a flooded soil. *Soil Biology and Biochemistry*. 7(2), 87-94. https://doi.org/10.1016/0038-0717(75)90004-8

Rick, A. R., and Arai, Y. (2011). Role of Natural Nanoparticles in Phosphorus Transport Processes in Ultisols. *Soil Science Society of America Journal*, *75*(2), 335. 75(2), 335-347. https://doi.org/10.2136/sssaj2010.0124nps

Roden, E. E., Kappler, A., Bauer, I., Jiang, J., Paul, A., Stoesser, R., Konishi, H., and Xu, H. (2010). Extracellular electron transfer through microbial reduction of solid-phase humic substances. *Nature Geoscience*, *3*(6), 417–421. https://doi.org/10.1038/ngeo870

Rostad, C. E., Leenheer, J. A., and Daniel, S. R. (1997). Organic carbon and nitrogen content associated with colloids and suspended particulates from the Mississippi River and some of its tributaries. *Environmental Science and Technology*. 31(11), 3218-3225. https://doi.org/10.1021/es970196b

Rouwane, A., Grybos, M., Bourven, I., Rabiet, M., and Guibaud, G. (2018). Waterlogging and soil reduction affect the amount and apparent molecular weight distribution of dissolved organic matter in wetland soil: A laboratory study. *Soil Research*, *56*(1), 28–38. https://doi.org/10.1071/SR16308

Rumpel, C., and Kögel-Knabner, I. (2011). Deep soil organic matter-a key but poorly understood component of terrestrial C cycle. *Plant and Soil*, *338*(1), 143–158. https://doi.org/10.1007/s11104-010-0391-5

Ryan, J. N., and Elimelech, M. (1996). Colloid mobilization and transport in groundwater. *Colloids and Surfaces A: Physicochemical and Engineering Aspects*, *107*(95), 1–56. https://doi.org/10.1016/0927-7757(95)03384-X

Ryan, J. N., and Gschwend, P. M. (1990). Colloid mobilization in two Atlantic coastal plain aquifers: Field studies. *Water Resources Research*, *26*(2), 307–322. https://doi.org/10.1029/WR026i002p00307

Ryan, J. N., and Gschwend, P. M. (1992). Effect of iron diagenesis on the transport of colloidal clay in an unconfined sand aquifer. *Geochimica et Cosmochimica Acta*. 56(4), 1507-1521. https://doi.org/10.1016/0016-7037(92)90220-D

Ryan, J. N., and Gschwend, P. M. (1994a). Effect of Solution Chemistry on Clay

Colloid Release from an Iron Oxide-Coated Aquifer Sand. *Environmental Science and Technology*. 28(9), 1717-1726. https://doi.org/10.1021/es00058a025

Ryan, J. N., and Gschwend, P. M. (1994b). Effects of ionic strength and flow rate on colloid release: Relating kinetics to intersurface potential energy. *Journal of Colloid And Interface Science*. 164(1), 21-34. https://doi.org/10.1006/jcis.1994.1139

Sahagian, D., and Melack, J. (1998). Global Wetland Distribution and Functional Characterization: Trace Gases and the Hydrologic Cycle. The international geosphere-biosphere programme (IGBP), A study of Global Change Stockholm, Sweden.

Sainz Rozas, H. R., Echeverría, H. E., and Picone, L. I. (2001). Denitrification in maize under no-tillage: Effect of nitrogen rate and application time. *Soil Science Society of America Journal*. 65, 1314-1323. https://doi.org/10.2136/sssaj2001.6541314x

Šantrůčková, H., Bird, M. I., and Lloyd, J. (2000). Microbial processes and carbon-isotope fractionation in tropical and temperate grassland soils. *Functional Ecology*. 14, 108-114. https://doi.org/10.1046/j.1365-2435.2000.00402.x

Santschi, P., Höhener, P., Benoit, G., and Buchholtz-ten Brink, M. (1990). Chemical processes at the sediment-water interface. *Marine Chemistry*. 30, 269-315. https://doi.org/10.1016/0304-4203(90)90076-O

Schijf, J., and Zoll, A. M. (2011). When dissolved is not truly dissolved-The importance of colloids in studies of metal sorption on organic matter. *Journal of Colloid and Interface Science*. 261(1), 137-147. https://doi.org/10.1016/j.jcis.2011.05.029

Schmidt, M. W. I., Torn, M. S., Abiven, S., Dittmar, T., Guggenberger, G., Janssens, I. A., Kleber, M., Kögel-Knabner, I., Lehmann, J., Manning, D. A. C., Nannipieri, P., Rasse, D. P., Weiner, S., and Trumbore, S. E. (2011). Persistence of soil organic matter as an ecosystem property. *Nature*, *478*(7367), 49–56. https://doi.org/10.1038/nature10386

Schulten, H. R. (1999). Analytical pyrolysis and computational chemistry of aquatic humic substances and dissolved organic matter. *Journal of Analytical and Applied Pyrolysis*. 49(1-2), 385-415. https://doi.org/10.1016/S0165-2370(98)00137-5

Schulten, H. R., and Leinweber, P. (2000). New insights into organic-mineral particles: Composition, properties and models of molecular structure. In *Biology*

and Fertility of Soils. 30, 399-432. https://doi.org/10.1007/s003740050020

Scofield, J. H. (1976). Hartree-Slater subshell photoionization cross-sections at 1254 and 1487 eV. *Journal of Electron Spectroscopy and Related Phenomena*. 8(2), 129-137. https://doi.org/10.1016/0368-2048(76)80015-1

Shimizu, M., Zhou, J., Schröder, C., Obst, M., Kappler, A., and Borch, T. (2013). Dissimilatory reduction and transformation of ferrihydrite-humic acid coprecipitates. *Environmental Science and Technology*, *47*(23), 13375–13384. https://doi.org/10.1021/es402812j

Singh, P., and Kanwar, R. S. (1991). Preferential Solute Transport through Macropores in Large Undisturbed Saturated Soil Columns. *Journal of Environmental Quality*. 20, 295-300. https://doi.org/10.2134/jeq1991.00472425002000010048x

Soil Survey Staff. (2015). Illustrated Guide to Soil Taxonomy (version 2). In *United States Department of Agriculture*. U.S. Gov print office, Washington D.C.

Sollins, P., Homann, P., and Caldwell, B. A. (1996). Stabilization and destabilization of soil organic matter: Mechanisms and controls. *Geoderma*. 74(2), 65-105. https://doi.org/10.1016/S0016-7061(96)00036-5

Sollins, P., Kramer, M. G., Swanston, C., Lajtha, K., Filley, T., Aufdenkampe, A. K., Wagai, R., and Bowden, R. D. (2009). Sequential density fractionation across soils of contrasting mineralogy: Evidence for both microbial- and mineral-controlled soil organic matter stabilization. *Biogeochemistry*, *96*(1), 209–231. https://doi.org/10.1007/s10533-009-9359-z

Sollins, P., Swanston, C., Kleber, M., Filley, T., Kramer, M., Crow, S., Caldwell, B. A., Lajtha, K., and Bowden, R. (2006). Organic C and N stabilization in a forest soil: Evidence from sequential density fractionation. *Soil Biology and Biochemistry*. 38(11), 3313-3324. https://doi.org/10.1016/j.soilbio.2006.04.014

Sposito, G. (1989). *The chemistry of soils*. Oxford University Press, New York.

Sprague, L. A., Herman, J. S., Hornberger, G. M., and Mills, A. L. (2000). Atrazine Adsorption and Colloid-Facilitated Transport through the Unsaturated Zone. *Journal of Environmental Quality*. 29(5), 1632-1641. https://doi.org/10.2134/jeq2000.00472425002900050034x

Stefánsson, A. (2007). Iron(III) hydrolysis and solubility at 25°C. *Environmental Science and Technology*, *41*(17), 6117–6123. https://doi.org/10.1021/es070174h

Stookey, L. L. (1970). Ferrozine-A New Spectrophotometric Reagent for Iron. *Analytical Chemistry*. 42(7), 779-781. https://doi.org/10.1021/ac60289a016

Suarez, D. L., Rhoades, J. D., Lavado, R., and Grieve, C. M. (1984). Effect of pH on Saturated Hydraulic Conductivity and Soil Dispersion. *Soil Science Society of America Journal*. 48, 50-55. https://doi.org/10.2136/sssaj1984.03615995004800010009x

Sun, L., Perdue, E. M., Meyer, J. L., and Weis, J. (1997). Use of elemental composition to predict bioavailability of dissolved organic matter in a Georgia river. *Limnology and Oceanography*. 42(4), 714-721. https://doi.org/10.4319/lo.1997.42.4.0714

Taylor, H. E., Garbarino, J. R., Murphy, D. M., and Beckett, R. (1992). Inductively coupled plasma mass-spectrometry as an element-specific detector for field-flow fractionation particle separation. *Analytical Chemistry*, *64*, 2036–2041.

Team, R. C. (2016). R: A Language and Environment for Statistical Computing. In *R Foundation for Statistical Computing*.

Tfaily, M. M., Chu, R. K., Tolić, N., Roscioli, K. M., Anderton, C. R., Paša-Tolić, L., Robinson, E. W., and Hess, N. J. (2015). Advanced solvent based methods for molecular characterization of soil organic matter by high-resolution mass spectrometry. *Analytical Chemistry*. 87(10), 5206-5215. https://doi.org/10.1021/acs.analchem.5b00116

Thompson, A., Chadwick, O. A., Boman, S., and Chorover, J. (2006a). Colloid mobilization during soil iron redox oscillations. *Environmental Science and Technology*, *40*(18), 5743–5749.

Thompson, A., Chadwick, O. A., Rancourt, D. G., and Chorover, J. (2006b). Iron-oxide crystallinity increases during soil redox oscillations. *Geochimica et Cosmochimica Acta*. 70(7), 1710-1727. https://doi.org/10.1016/j.gca.2005.12.005

Thurman, E. M. (1985). Organic Geochemistry of Natural Waters. In *Organic Geochemistry of Natural Waters*. Springer.

Tipping, E., and Hurley, M. A. (1988). A model of solid-solution interactions in acid organic soils, based on the complexation properties of humic substances. *Journal of Soil Science*. 39(4), 505-519. https://doi.org/10.1111/j.1365-2389.1988.tb01235.x

Tipping, E., and Woof, C. (1983). Elevated concentrations of humic substances in a seasonally anoxic hypolimnion: Evidence for co-accumulation with iron. *Archiv*

Fur Hydrobiologie. 98, 137-145.

Tombacz, E., and Meleg, E. (1990). A theoretical explanation of the aggregation of humic substances as a function of pH and electrolyte concentration. *Organic Geochemistry*. 15(4), 375-381. https://doi.org/10.1016/0146-6380(90)90164-U

Torn, M. S., Trumbore, S. E., Chadwick, O. A., Vitousek, P. M., and Hendricks, D. M. (1997). Mineral control of soil organic carbon storage and turnover. *Nature*. 389, 170-173. https://doi.org/10.1038/38260

Totsche, K. U., Amelung, W., Gerzabek, M. H., Guggenberger, G., Klumpp, E., Knief, C., Lehndorff, E., Mikutta, R., Peth, S., Prechtel, A., Ray, N., and Kögel-Knabner, I. (2018). Microaggregates in soils. *Journal of Plant Nutrition and Soil Science*, *181*(1), 104–136. https://doi.org/10.1002/jpln.201600451

Tsao, T. M., Wang, Y. N., Chen, Y. M., Chou, Y. M., and Wang, M. K. (2013). Automated ultrafiltration device for environmental nanoparticle research and implications: A review. *Micromachines*. 4(2), 215-231. https://doi.org/10.3390/mi4020215

Ussiri, D. A. N., and Johnson, C. E. (2004). Sorption of Organic Carbon Fractions by Spodosol Mineral Horizons. *Soil Science Society of America Journal*. 68, 253-262. https://doi.org/10.2136/sssaj2004.2530

Vaidya, R. N., and Fogler, H. S. (1990). Formation damage due to colloidally induced fines migration. *Colloids and Surfaces*. 50, 215-229. https://doi.org/10.1016/0166-6622(90)80265-6

Van Oost, K., Verstraeten, G., Doetterl, S., Notebaert, B., Wiaux, F., Broothaerts, N., and Six, J. (2012). Legacy of human-induced C erosion and burial on soil-atmosphere C exchange. *Proceedings of the National Academy of Sciences of the United States of America*. 109(47), 19492-19497. https://doi.org/10.1073/pnas.1211162109

Vasilas, L. M. and B. L. Vasilas. 2013. Hydric soil identification techniques. *In* J. T. Anderson and C.A. Davis (eds.) Wetland Techniques Volume 1: Foundations. pp. 227-272. DOI 10.1007/978-94-007-6860-4 Springer Dordrecht Heidelberg New York London.

Villholth, K. G., Jarvis, N. J., Jacobsen, O. H., and Jonge, H. (2000). Field Investigations and Modeling of Particle-Facilitated Pesticide Transport in Macroporous Soil. *Journal of Environmental Quality*. 29(4), 1298-1309. https://doi.org/10.2134/jeq2000.00472425002900040037x

Viollier, E., Inglett, P. W., Hunter, K., Roychoudhury, A. N., and Van Cappellen, P. (2000). The ferrozine method revisited: Fe(II)/Fe(III) determination in natural waters. *Applied Geochemistry*. 15(6), 785-790. https://doi.org/10.1016/S0883-2927(99)00097-9

Vogel, C., Mueller, C. W., Höschen, C., Buegger, F., Heister, K., Schulz, S., Schloter, M., and Kögel-Knabner, I. (2014). Submicron structures provide preferential spots for carbon and nitrogen sequestration in soils. *Nature Communications, 5*, 1–7. https://doi.org/10.1038/ncomms3947

Vold, R. D., and Vold, M. J. (1983). *Colloid and interface chemistry*. Addison-Wesley.

Wagai, R., and Mayer, L. M. (2007). Sorptive stabilization of organic matter in soils by hydrous iron oxides. *Geochimica et Cosmochimica Acta*. 71(1), 25-35. https://doi.org/10.1016/j.gca.2006.08.047

Weishaar, J. L., Aiken, G. R., Bergamaschi, B. A., Fram, M. S., Fujii, R., and Mopper, K. (2003). Evaluation of specific ultraviolet absorbance as an indicator of the chemical composition and reactivity of dissolved organic carbon. *Environmental Science and Technology*, *37*(20), 4702–4708. https://doi.org/10.1021/es030360x

Weng, L. P., Koopal, L. K., Hiemstra, T., Meeussen, J. C. L., and Van Riemsdijk, W. H. (2005). Interactions of calcium and fulvic acid at the goethite-water interface. *Geochimica et Cosmochimica Acta*. 69(2), 325-339. https://doi.org/10.1016/j.gca.2004.07.002

Whiting, G. J., and Chanton, J. P. (2001). Greenhouse carbon balance of wetlands: methane emission versus carbon sequestration. *Tellus B*. 53, 521-528. https://doi.org/10.1034/j.1600-0889.2001.530501.x

Wilkinson, Kevin J., and Lead, J. R. (2007). Environmental Colloids and Particles: Behaviour, Separation and Characterisation. In *Environmental Colloids and Particles: Behaviour, Separation and Characterisation*. John Wiley & Sons Ltd. UK.

Woche, S. K., Goebel, M. O., Mikutta, R., Schurig, C., Kaestner, M., Guggenberger, G., and Bachmann, J. (2017). Soil wettability can be explained by the chemical composition of particle interfaces-An XPS study. *Scientific Reports*. 7, 42877. https://doi.org/10.1038/srep42877

Xu, H., and Guo, L. (2017). Molecular size-dependent abundance and composition of dissolved organic matter in river, lake and sea waters. *Water Research*, *117*, 115–126. https://doi.org/10.1016/j.watres.2017.04.006

Yan, J., Lazouskaya, V., and Jin, Y. (2016). Soil Colloid Release Affected by Dissolved Organic Matter and Redox Conditions. *Vadose Zone Journal*. 15(3), 1-10. https://doi.org/10.2136/vzj2015.02.0026

Yan, J., Manelski, R., Vasilas, B., and Jin, Y. (2018a). Mobile colloidal organic carbon: An underestimated carbon pool in global carbon cycles? *Frontiers in Environmental Science, 6*, 1–12. https://doi.org/10.3389/fenvs.2018.00148

Yan, J., Meng, X., and Jin, Y. (2017). Size-Dependent Turbidimetric Quantification of Suspended Soil Colloids. *Vadose Zone Journal*. 16(5), 1-8. https://doi.org/10.2136/vzj2016.10.0098

Yin, Y., Shen, M., Zhou, X., Yu, S., Chao, J., Liu, J., and Jiang, G. (2014). Photoreduction and stabilization capability of molecular weight fractionated natural organic matter in transformation of silver ion to metallic nanoparticle. *Environmental Science and Technology*. 48(16), 9366-9373. https://doi.org/10.1021/es502025e

Young, R. B., Avneri-Katz, S., McKenna, A. M., Chen, H., Bahureksa, W., Polubesova, T., Chefetz, B. 2, and Borch, T. (2018). Composition-Dependent Sorptive Fractionation of Anthropogenic Dissolved Organic Matter by Fe(III)-Montmorillonite. *Soil Systems*, *2*(1). 1-19.

Yousuf, T., Hossain, M. E., Afsar, M. Z., and Osman, K. T., (2018). Phosphate sorption indices as affected by the calcareousness of soil. Dhaka University Jounral of Biological Science. 28 (1), 93-110

Zsolnay, Á. (2003). Dissolved organic matter: Artefacts, definitions, and functions. *Geoderma*, *113*(3–4), 187–209. https://doi.org/10.1016/S0016-7061(02)00361-0

Appendix A

LIST OF SYMBOLS AND ABBREVIATIONS

COC- Colloidal organic carbon

DOM- Dissolved organic matter

ICP-MS- Inductively coupled plasma mass spectroscopy

IRMS- Isotope ratio mass spectrometry

OC- Organic carbon

OHC- Oxidizing half-cycle

NanoSIMS- Nano scale secondary ion mass spectrometry

NNP- Natural nanoparticles

POM- Particulate organic matter

PTFE- Polytetrafluoroethylene

RHC- Reducing half-cycle

SOC – Soil organic carbon

SOM- Soil organic matter

XPS- X-ray photoelectron spectroscopy

XRD- X-ray diffraction

Appendix B

CALCULATION OF CENTRIFUGATION TIME AND SPEED FOR DIFFERENTIAL CENTRIFUGATION

The settling time and rotation speed for each <1000, <450, and <100 nm size fractions were determined by using Stokes' law (Gimbert et al., 2005). This approach ideally assumes a homogeneous spherical geometry of the soil particle:

$$\omega = \left(\frac{2\pi}{60} . \text{rpm}\right)$$

$$t = \frac{18\eta \ln\left(\frac{R}{S}\right)}{\omega^2 d^2 \Delta\rho}$$

Where,

ω = angular velocity of the centrifuge (rad/s)

η = viscosity of water at 20^0C, 0.01 poise ($gcm^{-1}s^{-1}$)

t = settling time (s)

R = distance (cm) from the axis of rotation to the level from where the supernatant is decanted from the tube

S = distance (cm) from the axis of rotation to the surface of the suspension in the tube;

d = particle diameter (cm)

$\Delta\rho$ = the density difference between the particles and the water (gcm^{-3}) assuming that particle density is 2.65 gcm^{-3} and density of water is 0.997 gcm^{-3}.

References

Gimbert, L.J., Haygarth, P.M., Beckett, R., Worsfold, P.J., 2005. Comparison of centrifugation and filtration techniques for the size fractionation of colloidal material in soil suspensions using sedimentation field-flow fractionation. Environ. Sci. Technol. 39, 1731-1735.

Appendix C

DETERMINATION OF LAYER THICKNESS

The calculation considers a flat homogeneous surface of Si and Al and a homogeneous cover of OM patches of thickness t following the procedure outlined by Pantano and Wittberg (1990) and Woche et al. (2017). The layer thickness (t) was determined from the content of an element X occurring in the non-coated surface as well as in the underlying material of the coated surface. The content of X of the non-coated surface was derived from regression analysis with a photoelectrons (PE) with similar mean free path (λ) of an element Y occurring in the coating. The λ (nm) gives the distance a PE can travel through solid matter without losing its element-specific binding energy (BE).

The mean free path (λ) is,

$$\lambda = 0.087E_k^{0.5}$$

Ek = kinetic energy (eV)

The layer thickness (t) is,

$$t = -\lambda_x \ln\left(\frac{I_x}{I_{X^*}}\right)$$

I_x = content of element X determined for the coated surface (in atom%)

I_x^* = content of element X of the non-coated surface as determined from regression analysis with element Y (in atom %) as shown in **Figure 2.10**.

References

Pantano, C.G., Wittberg, T.N., 1990. XPS analysis of silane coupling agents and silane-treated E-glass fibers. Surf. Interface Anal. 15, 498-501.

Woche, S.K., Goebel, M.O., Mikutta, R., Schurig, C., Kaestner, M., Guggenberger, G., et al., 2017. Soil wettability can be explained by the chemical composition of particle interfaces - An XPS study. Sci. Rep. 7, 1-8

Appendix D

REPRINT PERMISSION LETTER

Permission letter to reprint “Afsar et al., 2020. Quantification and molecular characterization of organo-mineral associations as influenced by redox oscillations. Science of the Total Environment. 704: 135454 from Elsevier.”